Magnetic resonance imaging to identify a placental phenotype in hypertensive disorders and its association with clinical, ultrasound and biomarker variables

Ho, Alison

Awarding institution:
King's College London

Student Name: Alison Elizabeth Puiyun Ho
Student Number: 1761538

Magnetic Resonance Imaging to Identify a Placental Phenotype in Hypertensive Disorders and its Association with Clinical, Ultrasound and Biomarker Variables

Alison Elizabeth Puiyun Ho

Student Number 1761538

Thesis Submitted to King's College London for the Degree of Doctor Of Philosophy

Supervisors: Professor Lucy Chappell, Professor Mary Rutherford, Dr Lisa Story

Department of Women and Children's Health

King's Health Partners

Table of Contents

CHAPTER 1 INTRODUCTION 22

1.1 Hypertensive disorders of pregnancy 22

1.1.1 Definition of preeclampsia 22

1.1.2 Prevalence of preeclampsia 23

1.1.3 Definition of chronic hypertension in pregnancy 23

1.1.4 Prevalence of chronic hypertension in pregnancy 24

1.1.5 Adverse maternal and perinatal outcomes associated with chronic hypertension 24

1.1.6 Adverse maternal and perinatal outcomes associated with preeclampsia 25

1.2 Placental structure and function 26

1.2.1 Normal placental development 26

1.2.2 Placental dysfunction 27

1.2.2.1 Aetiology of hypertensive disorders of pregnancy 27

1.2.2.2 Fetal response 28

1.2.2.3 Maternal response 29

1.2.2.4 Fetal growth restriction and preeclampsia 29

1.3 Principles of magnetic resonance imaging 30

1.3.1 Atomic structure and spin 30

1.3.2 Applying a magnetic field 31

1.3.3 Application of a radiofrequency pulse and subsequent relaxation 31

1.3.3.1 T1 relaxation 31

1.3.3.2 T2 relaxation 32

1.3.4 Displaying an image 32

1.3.5 Diffusion weighted imaging 32

1.3.5.1 Diffusion tensor and derived measures 33

1.4 Safety of magnetic resonance imaging in pregnancy 34

1.4.1 Static magnetic field 35

1.4.2 Pulsed radiofrequency fields 36

1.4.3 Pulsed gradient magnetic fields 37

1.4.4 Positioning 38

1.4.5 Claustrophobia 39

1.5 Current applications of placental MRI 39

1.5.1 In clinical practice 39

1.5.1.1 Pregnancy outcomes in placenta accreta spectrum 40
1.5.1.2 Features of placenta accreta spectrum on MRI 40
1.5.1.3 Screening for placenta accreta spectrum 41
1.5.1.4 Role of magnetic resonance imaging in placenta accreta spectrum 41
1.5.2 In research 42
1.5.2.1 T2-weighted imaging 42
1.5.2.1.1 Simple visual analysis 43
1.5.2.1.2 Quantitative analysis using T2-weighted imaging 43
1.5.2.2 T2* relaxometry 45
1.5.2.2.1 Maternal hyperoxia 45
1.5.2.2.2 Interpreting T2* values 46
1.5.2.3 Diffusion 47
1.5.2.3.1 Intravoxel incoherent motion, IVIM 47

1.6 Placental biomarkers in hypertensive disorders of pregnancy 48
1.6.1 Placental growth factor, PlGF 48
1.6.1.1 PlGF concentrations in pregnancy 48
1.6.2 sFlt-1 49
1.6.3 Vascular cell adhesion molecule-1, VCAM-1 50
1.6.4 Hyaluronan 51
1.6.5 Placental biomarkers in this thesis 52

1.7 Summary 52

CHAPTER 2 HYPOTHESES, RESEARCH QUESTIONS AND OBJECTIVES 53

2.1 Hypotheses 53

2.2 Research questions and objectives 53
2.2.1 How can the placenta be optimally visually assessed *in vivo* using magnetic resonance imaging? 53
2.2.2 What are the acceptance and unexpected findings rates of magnetic resonance imaging in women with preeclampsia and chronic hypertension? 53
2.2.3 Can advanced techniques of T2* mapping and diffusion elucidate the underlying mechanisms of preeclampsia and chronic hypertension? 54
2.2.4 Do placental biomarkers further our understanding of placental changes observed in magnetic resonance imaging? 54

CHAPTER 3 OPTIMISATION OF METHODS 55

3.1 Practicalities of imaging women with hypertension in pregnancy 55
3.1.1 3T Philips Achieva scanner 55
3.1.2 1.5T Philips Ingenia 56
3.1.3 Maternal positioning 57
3.1.4 Recruitment 58
3.1.5 Claustrophobia and reasons for declining participation 60
3.1.6 Sample size 61

3.2 T2-weighted imaging 62
3.2.1 Image contrast in T2-weighted imaging 62
3.2.1.1 Echo time, TE 63
3.2.2 Field strength 64
3.2.3 Plane and field of view 65

3.3 T2 relaxometry 66
3.3.1 T2* map placenta segmentation 66
3.3.2 Quantitative assessment of T2* values in control group 67
3.3.2.1 Placental mean T2* 67
3.3.2.2 Measures of heterogeneity 69
3.3.2.2.1 Histogram Asymmetry Measure 69
3.3.2.2.2 Lacunarity 71
3.3.2.2.3 Skewness and kurtosis 73

3.4 Diffusion weighted imaging 74
3.4.1 Echo time, TE 76
3.4.2 Motion 76
3.4.3 Optimised diffusion protocol 77

3.5 Ultrasound 78

3.6 Histology 80
3.6.1 Placental histology in hypertensive disorders of pregnancy 80
3.6.2 Optimised histological examination protocol 81

CHAPTER 4 T2* PLACENTAL MAGNETIC RESONANCE IMAGING IN PRETERM PREECLAMPSIA: AN OBSERVATIONAL STUDY 82

4.1 Abstract 82

4.2 Introduction 82

4.3 Methods 83
4.3.1 Study Design 83
4.3.2 Magnetic Resonance Imaging 85
4.3.3 Placental growth factor, PlGF 86
4.3.4 Placental Histology 86
4.3.5 Statistical methods 87

4.4 Results 87

4.5 Discussion 100
4.5.1 Statement of principal findings 100
4.5.2 Strengths and weaknesses of the study 100
4.5.3 Strengths and weaknesses in relation to other studies 101
4.5.4 Meaning of the study 103
4.5.5 Unanswered questions and future research 103

4.6 Perspectives 104

4.7 Novelty and Significance 104
4.7.1 What Is New? 104
4.7.2 What Is Relevant? 105

4.8 Summary 105

4.9 Supplemental Data 106
4.9.1 Supplemental Tables 106
4.9.2 Supplemental Figures 108

CHAPTER 5 PLACENTAL MAGNETIC RESONANCE IMAGING IN CHRONIC HYPERTENSION: AN OBSERVATIONAL STUDY 110

5.1 Introduction 110

5.2 Materials and Methods 111
5.2.1 Study Design 111
5.2.2 Magnetic Resonance Imaging 112
5.2.3 Placental growth factor, PlGF 113
5.2.4 Ultrasound 114
5.2.5 Placental Histology 114
5.2.6 Statistical methods 114

5.3 Results 115

5.4 Discussion 127

5.4.1 Statement of principal findings 127

5.4.2 Strengths and weaknesses of the study 127

5.4.3 Strengths and weaknesses in relation to other studies 129

5.4.4 Meaning of the study 129

5.4.5 Unanswered questions and future research 130

5.5 Supplemental 131

CHAPTER 6 BIOMARKERS IN CHRONIC HYPERTENSION AND PREECLAMPSIA WITH IMAGING VARIABLES 138

6.1 Introduction 138

6.2 Methods 139

6.2.1 Assays 140

6.2.2 Magnetic Resonance Imaging 140

6.2.3 Statistical methods 140

6.3 Results 140

6.4 Discussion 160

6.4.1 Statement of principal findings 160

6.4.2 Strengths and weaknesses of the study 161

6.4.3 Strengths and weaknesses in relation to other studies 161

6.4.4 Meaning of the study 161

6.4.5 Unanswered questions and future research 162

CHAPTER 7 UNEXPECTED MATERNAL AND FETAL FINDINGS IN ANTENATAL FETAL MAGNETIC RESONANCE IMAGING 164

7.1 Introduction 164

7.2 Methods 165

7.3 Results 166

7.3.1 Fetal unexpected findings 168

7.3.2 Maternal unexpected findings 171

7.4 Discussion 173
7.4.1 Statement of principal findings 173
7.4.2 Strengths and weaknesses of the study 173
7.4.3 Strengths and weaknesses in relation to other studies 174
7.4.4 Meaning of the study 174
7.4.5 Unanswered questions and future research 175

CHAPTER 8 CONCLUSIONS AND FUTURE RESEARCH 177

8.1 Summary of key findings 177

8.2 Strengths and limitations of thesis 178
8.2.1 Imaging in women with preeclampsia and chronic hypertension 178
8.2.2 Use of 1.5T and 3T imaging 178
8.2.3 Methods optimisation 179

8.3 Meaning and clinical impact 179

8.4 Unanswered questions and future steps 180
8.4.1 Clinical groups 180
8.4.2 Mechanistic insights 181
8.4.3 Clinical application 181

LIST OF TABLES

Table 1.1: Diffusion measures as derivations of eigenvectors. 33
Table 3.1: Number of woman imaged using optimised protocols. 61
Table 4.1: Characteristics at booking and enrolment. 88
Table 4.2: Maternal and neonatal outcomes. 90
Table 4.3: Placental histology findings. 92
Table 5.1: Characteristics at booking and enrolment. 116
Table 5.2: Maternal and neonatal outcomes. 118
Table 6.1: Abnormal pregnancy outcome in the abnormal control group. 141
Table 6.2: Characteristics at booking and enrolment. 142
Table 6.3: Maternal and neonatal outcomes. 143
Table 7.1: Unexpected findings categories as listed by Abdullah, Dietz and Holm 2016 . 166
Table 7.2: Characteristics of women imaged and indication for imaging 167
Table 7.3: Fetal unexpected findings in uncomplicated low risk pregnancies, imaged as part of research studies. 169
Table 7.4: Maternal unexpected findings 171

LIST OF FIGURES

Figure 1.1: Definition of preeclampsia, as published by Brown et al., 2018 23
Figure 1.2: Proposed relationship among degree of oxidative stress and placental development in normal pregnancies, late-onset preeclampsia (PE), early-onset PE, and miscarriage. 30
Figure 1.3: Larmor equation 31
Figure 1.4: Blood oxygen level-dependent (BOLD) equation 32
Figure 1.5: Representation of a diffusion ellipsoid showing the eigenvectors, as published by (Neil 2008). 33
Figure 1.6: MRI safety checklist questions 36
Figure 1.7: Diagram showing accreta, increta and percreta villous tissue, as published by Jauniaux et al. 2018. 40
Figure 1.8: VEGF signalling and the role of sFlt-1 in maternal endothelial dysfunction as illustrated in Karumanchi et al. 2005 50
Figure 3.1: Laser cut plastic arch template of 3T scanner bore. 56
Figure 3.2: Participant flow chart for women with chronic hypertension from April 2017 – September 2017 inclusive. 59
Figure 3.3: Participant flow chart for women with preeclampsia from April 2017 – September 2017 inclusive. 59
Figure 3.4: Grannum grading system, as described by Grannum et al., 1979. 62
Figure 3.5: Proposed placenta grading system using T2-weighted MRI by Blaicher et al., 2006 63
Figure 3.6: Effect of echo time (TE) on contrast. (A) short TE. (B) long TE. 64
Figure 3.7: T2-weighted images taken on the same day of the same woman (A) 3T Achieva (B) 1.5T Ingenia 64
Figure 3.8: T2-weighted imaging at 1.5T with a high body mass index and posteriorly located placenta 65
Figure 3.9: Formula for calculating signal intensity. 66
Figure 3.10: T2-weighted imaging in coronal and sagittal plane (left) with T2* map in corresponding plane (right) in a woman with preeclampsia. 67
Figure 3.11: Placental mean T2* values against gestational age at imaging. (A) simple linear model (B) linear funnel model. Line in red represents 90th centile, grey 50th centile, yellow 10th centile and green 5th centile. 68

Figure 3.12: Scatterplot of mean T2* against gestational age imaged in the control group, with lines between points originating from the same woman from serial scans.....68
Figure 3.13: Scatterplot of Histogram Asymmetry Measure against gestational age at imaging.....70
Figure 3.14: Scatter plot of Histogram Asymmetry Measure against gestational age at imaging including those with preeclampsia......71
Figure 3.15: Illustrating influences of lacunarity.(A) Binary images of six spatial features (a) small gap pattern, (b) big gap patter, (c) small checker pattern, (d) big checker pattern, (e) small stripe patter, (f) random pattern. (B) Lacunarity curves of the six spatial features shown in (A). (Myint and Lam 2005).....72
Figure 3.16: Scatterplot of lacunarity measure against gestational age at imaging (box size 2.5cm x 2.5cm).....73
Figure 3.17: Illustration of skewness and kurtosis. (David, Marshall, and Zanna 2017).....73
Figure 3.18: Scatterplot of skewness in T2* placental data from uncomplcated pregnancies against gestational age at imaging.....74
Figure 3.19: Scatterplot of kurtosis in T2* placental data from uncomplicated pregnancies against gestational age at imaging.....74
Figure 3.20: Measuring water diffusion. RF = radiofrequency pulse. The gradients are both positive in the figure as the 180°pulse reverses the direction of precession. (Koh and Collins 2007).....75
Figure 3.21: Placental apparent diffusion coefficient (ADC) values (mm^2s^{-1}) in uncomplicated pregnancies at two different echo times......76
Figure 3.22: Apparent diffusion coefficient (ADC) map of a placenta (A) pre motion correction (B) post motion correction. Note the improvement in image quality......77
Figure 3.23: T2-diffusion sampling. (a) conventional T2-Diffusion sampling in separate scans together with the resulting delays. (b) joint T2*-Diffusion sampling. (c) transverse magnetization depicted schematically, showing the T2 decay in green and the T2* decay in orange......78
Figure 3.24: Consensus based definitions for early and late fetal growth restriction in the absence of congenital anomalies (Gordijn et al. 2016)......79
Figure 4.1: (A) Example T2-weighted placental imaging and T2* maps in coronal and sagittal planes across gestation. (B) Features of T2-weighted placental imaging in women with preeclampsia......93

Figure 4.2: Scatterplot of placental mean T2* against gestational age at imaging, lines representing 10th, 50th and 90th centiles. 94
Figure 4.3: (A) Scatterplot of lacunarity measure (derived from T2* mapping) against gestational age at imaging. (B) Scatterplot of Placental Growth Factor (sample taken within two weeks of magnetic resonance imaging) against placental mean T2* (derived from T2* mapping). 95
Figure 4.4: Scatterplot of placental volume (derived from T2* map segmentations) against gestational age at diagnosis of preeclampsia. 96
Figure 4.5: Scatterplot of placental volume (derived from T2* map segmentations) against birthweight in the preeclampsia group. 96
Figure 4.6: Scatterplot of placental volume (derived from T2* map segmentations) against birthweight centile in the preeclampsia group. 97
Figure 4.7: Scatterplot of lacunarity measure (derived from T2* mapping) against gestational age at diagnosis of preeclampsia. 97
Figure 4.8: Scatterplot of lacunarity measure (derived from T2* mapping) against birthweight in the preeclampsia group. 98
Figure 4.9: Scatterplot of lacunarity measure (derived from T2* mapping) against birthweight centile in the preeclampsia group. 98
Figure 4.10: Scatterplot of placental mean T2* against gestational age at imaging, categorised into umbilical artery pulsatility index <95th centile, >95th centile, absent end diastolic flow and intermittently reversed end diastolic flow. 99
Figure 4.11: Scatterplot of placental volume against gestational age at imaging. 100
Figure 5.1: Example T2-weighted placental imaging and T2* maps in coronal and sagittal planes across gestation. 120
Figure 5.2: Scatterplot of placental mean T2* against gestational age at imaging, subdivided by birthweight centile at subsequent delivery to show appropriate for gestational age (AGA) infants, and those small for gestational age (SGA), divided into 3rd-10th centile, and those <3rd centile (A) in uncomplicated control group and (B) in women with chronic hypertension. 121
Figure 5.3: Illustrative histogram plot of T2* values at the same gestation (27 weeks' gestation) for one woman from each of the following groups (A) the control group (B) with chronic hypertension (CHTN) and normal placental mean T2* (C) with chronic hypertension and a placental mean T2* less than the 10th centile for gestation (D) CHTN participant who developed superimposed preeclampsia (PE). 122

Figure 5.4: Scatterplot of histogram derived measures of (A) skewness at 3T imaging (B) skewness at 1.5T imaging (C) kurtosis at 3T imaging and (D) kurtosis at 1.5T imaging against gestational age at scan with i) chronic hypertension ii) chronic hypertension at enrolment who subsequently developed superimposed preeclampsia after imaging iii) controls iv) preeclampsia at enrolment. 123

Figure 5.5: Scatterplot results from combined diffusion-relaxometry acquisition sequence. 126

Figure 5.6: Scatterplot results of apparent diffusion coefficient (ADC) against gestational age from a diffusion sequence acquired during the initial methods development phase of the study and thus prior to acquisition of combined diffusion-relaxometry data. 126

Figure 5.7: Scatterplot of placental volume (from segmentations performed on T2* maps) against gestational age at imaging. 127

Figure 6.1: Quidel PlGF concentrations in each group (control, chronic hypertension, preeclampsia and abnormal control) 145

Figure 6.2: Roche PlGF concentrations in each group (control, chronic hypertension, preeclampsia and abnormal control) 146

Figure 6.3: Scatterplot of Quidel PlGF concentrations against Roche PlGF concentrations in the same plasma sample. 147

Figure 6.4: Roche sFlt-1 concentrations in each group (control, chronic hypertension, preeclampsia and abnormal control) 148

Figure 6.5: Roche sFlt-1/PlGF ratio in each group (control, chronic hypertension, preeclampsia and abnormal control) 149

Figure 6.6: Hyaluronan concentrations in each group (control, chronic hypertension, preeclampsia and abnormal control) 150

Figure 6.7: VCAM concentrations in each group (control, chronic hypertension, preeclampsia and abnormal control) 151

Figure 6.8: Scatterplot of (A) Quidel PlGF and (B) Roche PlGF against mean T2* values 152

Figure 6.9: Scatterplot of Roche sFlt-1 against mean T2* values 153

Figure 6.10: Scatterplot of Hyaluronan against mean T2* values 153

Figure 6.11: Scatterplot of VCAM against mean T2* values 154

Figure 6.12: Scatterplot of serum PlGF concentration against estimated fetal weight (by ultrasound scan) performed within 2 weeks of blood sample taken. 155

Figure 6.13: Scatterplot of serum PlGF concentration against estimated fetal weight (by ultrasound scan) performed within 2 weeks of blood sample taken. 155

Figure 6.14: Scatterplot of serum sFlt concentration against estimated fetal weight (by ultrasound scan) performed within 2 weeks of blood sample taken. 156
Figure 6.15: Scatterplot of serum VCAM concentration against estimated fetal weight (by ultrasound scan) performed within 2 weeks of blood sample taken.....156
Figure 6.16: Scatterplot of serum hyaluronan concentration against estimated fetal weight (by ultrasound scan) performed within 2 weeks of blood sample taken 157
Figure 6.17: Placental growth factor concentrations and placental mean T2* values in uncomplicated pregnancies and those with chronic hypertension, colour coded by pregnancy outcome. 158
Figure 6.18: Placental growth factor concentrations and placental mean T2* values in pregnancies complicated by chronic hypertension, colour coded by pregnancy outcome and grouped by gestational age at imaging. 159
Figure 6.19: Placental growth factor concentration and mean T2* as a predictor of adverse pregnancy outcome, divided into gestational age groups <28 and > 28 weeks' gestation 160

DEDICATION

To my parents; for their love, support and encouragement in both work and life.

ACKNOWLEDGEMENTS

I would like to especially thank my supervisors, Professor Lucy Chappell, Professor Mary Rutherford and Dr Lisa Story. A chance meeting with Professor Lucy Chappell in unusual circumstances inspired me to pursue research and embark on this PhD journey. Together with Professor Mary Rutherford and Dr Lisa Story, you have given me opportunities to develop professionally and been excellent role models in both clinical practice and research. You have all supported me through the countless challenges along the way and believed I could achieve what I thought was impossible at times.

I am privileged to have worked with some dedicated and enthusiastic researchers. I would particularly like to thank Professor Jo Hajnal, Dr Jana Hutter, Dr Laurence Jackson and Dr Paddy Slator (physicists who all welcomed an obstetrician into the imaging department), Emer Hughes, Joanna Allsop, Elaine Green, Kathleen Colford (radiographers), Laura Mccabe (Placenta imaging Project manager and senior research midwife), Dr Kate Wiles (ELISA tutor), Dr Carolyn Gill (Laboratory Technician), Anna Brockbank (Research Assistant), Paul Seed (Medical Statistician), Dr Mudher Al-Adnani, Dr Simi George, Dr Andreas Marnerides (histopathologists) and the research midwives who helped to chase pregnancy outcomes. I would also like to thank all the women who participated in the study, some of whom went to extraordinary lengths to take time out of their busy lives in order to do so.

Finally, I would like to thank Simon for being so supportive and my parents Victor and Catherine, to whom this work is dedicated.

STATEMENT OF OWN WORK

I wrote and led an application for an ethics amendment to include recruitment of a group of hypertensive women to the Placenta imaging Project. In addition to writing standard operating procedures for maternal blood sampling and processing, I created a study database using a REDCap platform, written following self-training through online resources and subsequent support from divisional personnel.

I approached the majority of the hypertensive women enrolled in this study in person. I was present at most magnetic resonance imaging scans and provided obstetric support. Post imaging, data processing and image analysis was performed with support from Jana Hutter, Laurence Jackson and Paddy Slator. Statistical analyses was performed with support from Paul Seed.

I processed the majority of the maternal blood samples and conducted all the enzyme-linked immunosorbent assays for vascular cell adhesion molecule (VCAM) and hyaluronan. I quantified the majority of plasma placental growth factor (PlGF) concentrations using the Triage PlGF Test (Quidel, San Diego, CA). I collected pregnancy outcomes for the hypertensive groups and some of the control group, performed data monitoring and data cleaning.

I wrote the first draft of the publication arising from Chapter 4, received comments from co-authors and submitted it to Hypertension journal. I wrote the first draft of the manuscript arising from Chapter 5 which was submitted to Placenta journal and subsequently accepted for publication. All chapters of this thesis were written by myself and subsequently reviewed by supervisors Professor Lucy Chappell, Professor Mary Rutherford and Dr Lisa Story. The work of others is appropriately referenced.

PRESENTATIONS AND PUBLICATIONS ARISING FROM THIS WORK

Publications arising directly from this thesis

Ho AEP, Hutter J, Jackson LH, Seed PT, Mccabe L, Al-Adnani M, Marnerides A, George S, Story L, Hajnal JV, Rutherford MA, Chappell LC. *T2* Placental Magnetic Resonance Imaging in Preterm Preeclampsia: An Observational Cohort Study.* Hypertension. 2020 Jun;75(6):1523-1531. doi: 10.1161/HYPERTENSIONAHA.120.14701.

Ho A, Hutter J, Slator P, Jackson L, Seed PT, McCabe L, Al-Adnani M, Marnerides A, George S, Story L, Hajnal JV, Rutherford M, and Chappell LC. *Placental magnetic resonance imaging in chronic hypertension: A case-control study*. Placenta. 2021 Jan; 104: 138-45. doi: 10.1016/j.placenta.2020.12.006

Submitted and revision requested

To Placenta:

Ho AEP, Chappell LCC, Story L, Al-Adnani M, Egloff A, Routledge E, Rutherford M, Hutter J. *Visual assessment of the placenta in antenatal magnetic resonance imaging.*

Publications related to this work to which I have contributed

Hutter J, Slator PJ, Jackson L, Gomes ADS, **Ho A**, Story L, O'Muircheartaigh J, Teixeira RPAG, Chappell LC, Alexander DC, Rutherford MA, Hajnal JV. *Multi-modal functional MRI to explore placental function over gestation.* Magn Reson Med. 2019 Feb;81(2):1191-1204. doi: 10.1002/mrm.27447.

Slator PJ, Hutter J, Palombo M, Jackson LH, **Ho A**, Panagiotaki E, Chappell LC, Rutherford MA, Hajnal JV, Alexander DC. *Combined diffusion-relaxometry MRI to identify dysfunction in the human placenta.* Magn Reson Med. 2019 Jul;82(1):95-106. doi: 10.1002/mrm.27733.

Hutter J, Harteveld AA, Jackson LH, Franklin S, Bos C, van Osch MJP, O'Muircheartaigh J, **Ho A**, Chappell L, Hajnal JV, Rutherford M, De Vita E. *Perfusion and apparent oxygenation in the human placenta (PERFOX).* Magn Reson Med. 2019 Aug 21. doi: 10.1002/mrm.27950.

Jackson, L. H., Price, A. N., Hutter, J. M., **Ho, A**. E. P., Roberts, T. A., Slator, P. J., Clough, J. R., Deprez, M., McCabe, L., Malik, S. J., Chappell, L. C., Rutherford, M. A. & Hajnal, J. V. *Respiration resolved imaging with continuous stable state 2D acquisition using linear frequency SWEEP*. Magn Reson Med. 2019 Nov;82(5):1631-1645. doi: 10.1002/mrm.27834.

Hutter J, Jackson L, **Ho A**, Pietsch M, Story L, Chappell L, Hajnal J, Rutherford M*. T2* relaxometry to characterize normal placental development over gestation in-vivo at 3T.* Wellcome Open Res 2019, 4:166 https://doi.org/10.12688/wellcomeopenres.15451.1

Steinweg JK, Hui GTY, Pietsch M, **Ho A,** van Poppel MP, Lloyd D, Colford K, Simpson JM, Razavi R, Pushparajah K, Rutherford M, Hutter J. *T2* placental MRI in pregnancies complicated with fetal congenital heart disease.* Placenta. 2021 Mar 9;108:23-31. doi: 10.1016/j.placenta.2021.02.015.

Story L, Zhang T, Uus A, Hutter J, Egloff A, Gibbons D, **Ho A**, Al-Adnani M, Knight CL, Theodoulou I, Deprez M, Seed PT, Tribe RM, Shennan AH, Rutherford M. *Antenatal thymus*

volumes in fetuses that delivered <32 weeks gestation: An MRI pilot study. Acta Obstet Gynecol Scand. 2020 Aug 31. doi: 10.1111/aogs.13983.

Accepted

Hutter J, **Ho A,** Jackson L, Slator PF, Chappell LC, Hajnal JV, Rutherford M. An efficient and combined placental T1-ADC acquisition in pregnancies with and without pre-eclampsia.Magn Reson Med. 2021 Mar. doi 10.1002/mrm.28809

Slator PJ, Hutter J, Marinescu RV, Palombo M, Jackson L, **Ho A**, Chappell LC, Rutherford M, Hajnal JV, Alexander DC. Data-Driven Multi-Contrast Spectral Microstructure Imaging with InSpect: INtegrated SPECTral Component Estimation and Mapping. Medical Image Analysis. 2021.

Submitted and accepted pending minor revisions

Story L, Knight CL, **Ho A**, Arulkumaran S, Matthew J, Lovell H, McCabe L, Byrne M, Egloff A, Jacques A, Carmichael J, Hajnal J, Shennan A, Rutherford M. *Maternal and fetal incidental findings detected on antenatal magnetic resonance imaging.* Pediatric Radiology

Oral presentations

T2 and T2* placenta magnetic resonance imaging in pregnancies complicated by chronic hypertension and preeclampsia.
International Society for Magnetic Resonance in Medicine Placental Workshop, Atlanta, February 2018.

T2 and T2* placental magnetic resonance imaging in chronic hypertension.
International Society for the Study of Hypertenion in Pregnancy, ISSHP, Lund 2nd-4th October 2019.

Poster presentations

Multi modal placental ex vivo MRI.
Placenta Imaging Workshop, CMIC (Centre for Medical Image Computing), University College London, April 2018.

T2 and T2* placental magnetic resonance imaging in preeclampsia.
Society for Reproductive Investigation, Paris, March 2019 and RCOG Annual Academic Meeting, London January 2019 *(First prize poster presentation).*

T2 and T2* placental magnetic resonance imaging in preeclampsia and chronic hypertension.
British Maternal Fetal Medicine Society, Edinburgh, March 2019.

T2 and T2* placental magnetic resonance imaging in chronic hypertension.
RCOG Annual Academic Meeting, London, February 2020.

ABREVIATIONS

AD	Axial diffusivity
ADC	Apprent diffusion coefficient
ARR	Absolute risk reduction
BOLD	Blood oxygen level dependent
CI	Confidence interval
dB	Decibel
DNA	Deoxyribonucleic acid
FA	Fractional anisotropy
FGR	Fetal growth restriction
HELLP	Haemolysis, Elevated Liver enzyme and Low Platelet
IQR	Interquartile range
IUD	Intrauterine death
kHz	Kilohertz
MCDA	Monochorionic diamniotic
MD	Mean diffusivity
MRI	Magnetic resonance imaging
NICE	National Institute for Health and Care Excellence
PlGF	Placental growth factor
RD	Radial diffusivity
RF	Radiofrequency
ROS	Reactive oxygen species
RR	Relative risk
SENSE	Sensitivity encoding
sFlt-1	Soluble fms-like tyrosine kinase 1
TE	Echo time
TR	Repetition time
UK	United Kingdom
VEGF	Vascular endothelial growth factor
VCAM	Vascular cell adhesion molecule

ABSTRACT

The aim of my thesis was to examine the use of placental magnetic resonance imaging in preeclampsia and chronic hypertension. Placental magnetic resonance imaging techniques are currently in development and there is a paucity of data for their use and application in hypertensive disorders of pregnancy.

The objectives of my research were to firstly optimise placental magnetic resonance imaging and associated measures in women with preeclampsia and chronic hypertension and to describe potential unexpected findings in magnetic resonance imaging performed for research during pregnancy. Secondly, I set out to provide an approach to visual assessment of the placenta in uncomplicated pregnancies using T2-weighted imaging. Thirdly I investigated placental changes in preeclampsia for an insight into the pathophysiology of preeclampsia and then investigated placental changes in chronic hypertension for an insight into the heterogeneity of pregnancy outcomes. Lastly, I explored changes in associated placental biomarkers Placental Growth Factor (PlGF), soluble fms-like tyrosine kinase 1 (sFlt-1), vascular adhesion molecule (VCAM) and hyaluronan in women with preeclampsia and chronic hypertension and described them in the context of placental T2* values obtained from magnetic resonance imaging.

These objectives were achieved through performing a prospective, observational study, embedded within the National Institutes of Health (NIH) funded Placenta imaging Project, which aimed to develop a novel magnetic resonance approach to assess growth and development of the human placenta in health and disease. The focus of my project related specifically to evaluating placental magnetic resonance imaging in women with chronic hypertension and preeclampsia.

In this thesis, the optimisation and application of advanced magnetic resonance imaging techniques have provided detailed placental imaging in women with preeclampsia and chronic hypertension. These techniques have enabled qualitative visual assessment and quantitative assessment of placental structure and function. Optimised T2-weighted imaging sequences have led to the development of a comprehensive approach to visual assessment of the placenta in uncomplicated pregnancies and are subsequently used as a reference for assessing women with preeclampsia and chronic hypertension. Quantitative assessment of the placenta has included the development of T2* mapping and diffusion sequences, culminating in an optimised combined diffusion-relaxometry sequence which provides regionally matched diffusion and T2* values in a reasonably fast and acceptable

scan time compared to conventional sequences. Methods assessing placental T2* maps to quantify the visual variation seen are explored and detect variability within such maps. These measures include lacunarity as well as histogram derived measures of kurtosis and skewness, in addition to mean T2*.

These advanced sequences of T2-weighted imaging, T2* mapping and diffusion weighted imaging have been applied to women with preeclampsia and chronic hypertension in order to explore the spectrum of placental phenotypes in these hypertensive disorders of pregnancy. In pregnancies complicated by preeclampsia, T2-weighted imaging showed substantial areas of low signal intensity, advanced lobularity and high granularity within lobules with a reduced entire placental mean T2* for gestational age and higher lacunarity values compared to uncomplicated pregnancies. In pregnancies complicated by chronic hypertension, T2-weighted imaging showed a varied visual appearance compared to gestation matched controls with some showing features similar to those with preeclampsia and some indistinguishable from those in the control group. Not all women with mean T2* values outside of the normal range developed adverse pregnancy outcomes and conversely not all women with normal mean T2* values had uncomplicated pregnancies. This suggest a more complex interaction between the placenta and maternal or fetal response, while the timing of imaging (in relation to delivery) may be crucial. Finally, T2* mapping was explored in conjunction with placental biomarkers of PlGF, sFlt-1, hyaluronan and VCAM to further elucidate mechanisms underlying preeclampsia and chronic hypertension. These biomarkers have been found to provide complementary mechanistic information of placental phenotypes seen with T2* mapping.

Chapter 1 INTRODUCTION

1.1 Hypertensive disorders of pregnancy

Hypertensive disorders complicate 10% of all pregnancies (Duley 2009) encompassing a spectrum of disease that includes chronic hypertension, gestational hypertension, preeclampsia and white coat hypertension (Brown et al. 2018). There is considerable overlap between the disorders; preeclampsia can occur either de novo or superimposed on chronic hypertension or as a progression in severity of gestational hypertension. They are all associated with an increase in adverse maternal and neonatal outcome. This work will focus on preeclampsia and chronic hypertension. The former is the most severe form of pregnancy hypertension and encompasses multi-organ features. Of necessity, the introduction covers a breadth of topics and therefore is not exhaustive on any single area.

1.1.1 Definition of preeclampsia

Many definitions of preeclampsia exist; however, they are centred around the measurements and thresholds of hypertension, maternal organ dysfunction and adverse fetal effects. The World Health Organisation acknowledges the varied definitions but reports that the general accepted definition includes the onset of a new hypertension during pregnancy (with persistent diastolic blood pressure >90mmHg) with the occurrence of substantial proteinuria (>0.3g/24 hours) (World Health Organisation 2011). A consensus definition allows for a unified approach into studying pregnancy outcomes, understanding the pathophysiology, stratifying management and interventions that may improve outcomes. However, the components of the definition represent clinical manifestations of end-organ disease, rather than upstream pathophysiology.

The International Society for the Study of Hypertension in Pregnancy have defined preeclampsia as follows:

Preeclampsia is gestational hypertension accompanied by ≥1 of the following new-onset conditions at or after 20 weeks' gestation:
Proteinuria
Other maternal organ dysfunction, including:
AKI (creatinine ≥90umol/L; 1 mg/dL)
Liver involvement (elevated transaminases, eg, alanine aminotransferase or aspartate aminotransferase >40 IU/L) with or without right upper quadrant or epigastric abdominal pain
Neurological complications (examples include eclampsia, altered mental status, blindness, stroke, clonus, severe headaches, and persistent visual scotomata)
Hematological complications (thrombocytopenia–platelet count <150 000/μL, disseminated intravascular coagulation, hemolysis)
Uteroplacental dysfunction (such as fetal growth restriction, abnormal umbilical artery [UA] Doppler wave form analysis, or stillbirth)

Figure 1.1: Definition of preeclampsia, as published by Brown et al., 2018

Fetal growth restriction with new-onset gestational hypertension and no other maternal features is classified as preeclampsia by the International Society for the Study of Hypertension in Pregnancy (ISSHP) definition (Brown et al. 2018) but not by the American College of Obstetricians and Gynecologists (ACOG) definition (Obstetricians and Gynecologists 2013). The current hypertension in pregnancy guidelines issued by the National Institute for Health and Care Excellence (National Institute for Health and Care Excellence 2019) define preeclampsia in line with the above definition proposed by The International Society for the Study of Hypertension in Pregnancy (Brown et al. 2018) and these were the definitions utilised.

1.1.2 Prevalence of preeclampsia

Preeclampsia is estimated to affect 2-8% of all pregnancies (Duley 2009). However, the prevalence of preeclampsia depends on the definition used, geographical location and population studied. In Northern Europe and Australia, rates have declined from 1997 to 2007 yet in Massachusetts they are reported to have increased (Roberts et al. 2011). A dataset of 61174 singleton pregnancies from three prospective screening studies with enrolment from February 2010 until December 2016 in the United Kingdom reported that 2.9% developed preeclampsia (Tan et al. 2018).

1.1.3 Definition of chronic hypertension in pregnancy

Chronic hypertension in pregnancy is defined by the International Society for the Study of Hypertension in Pregnancy as hypertension (systolic ≥140mmHg and/or diastolic blood

pressure ≥90mmHg) predating the pregnancy or recognised at less than 20 weeks' gestation (Brown et al. 2018). Prior to pregnancy, women may not have had their blood pressure measured within routine care and thus chronic hypertension may be diagnosed at their routine antenatal appointment. It is recommended that hypertension is confirmed with several readings and ideally with home blood pressure readings in order to distinguish between chronic hypertension and white coat hypertension (where blood pressure is normal outside of a clinical setting). The diagnosis has implications on antenatal management, as well as postnatal follow up, as women with confirmed chronic hypertension will require lifelong follow up and management of their cardiovascular risk factor. Although some international guidelines (Parati et al. 2008; Kario et al. 2019) recommend home or ambulatory blood pressure monitoring in women with hypertension prior to 20 weeks' gestation, the scarce evidence base in pregnancy behind this recommendation has meant that it has not been universally adopted, for example into UK national guidelines (National Institute for Health and Care Excellence 2019).

1.1.4 Prevalence of chronic hypertension in pregnancy

Chronic hypertension complicates an estimated 1-2% of pregnancies, but its prevalence is thought to be underestimated as studies often do not capture those women who are diagnosed with chronic hypertension in pregnancy (Roberts et al. 2008). The majority of women with chronic hypertension have primary hypertension rather than secondary hypertension (Bateman et al. 2012) and the prevalence has risen in recent years, suggested to be attributable to increasing maternal age and obesity in pregnancy.

1.1.5 Adverse maternal and perinatal outcomes associated with chronic hypertension

Adverse maternal pregnancy specific outcomes include superimposed preeclampsia amongst those with chronic hypertension (incidence 26%, RR 7.7 (95% CI 5.-10.1) when compared to pregnant controls in population studies in the United States (Bramham et al. 2014). Additionally, women with chronic hypertension have higher risks of end organ damage, caesarean section and placental abruption. Data from the United States revealed an abruption frequency of 1.6% in chronic hypertension versus 0.58% who were not hypertensive between 1995 and 2002 (relative risk 2.4; 95% confidence interval 2.3-2.5) (Ananth et al. 2007). This is consistent with previously reported data (Sibai et al. 1998) and a Swedish cohort (Zetterström et al. 2008).

Fetal growth restriction and preterm birth both contribute to adverse perinatal outcome in hypertensive disorders of pregnancy. Given the changing definition of fetal growth

restriction over time, these reported incidences are difficult to compare. However, a systematic review and meta-analysis reported pooled incidences of a birthweight less than 2500g to be 16.9% (95% confidence interval 21.0-31.5) and preterm delivery less than 37 weeks' gestation 28.1% (95% confidence interval 22.6-34.4) with neonatal unit admission 20.1% (95% confidence interval 15.7-26.4) in women with chronic hypertension (Bramham et al. 2014). Pooled incidence of perinatal death for women with chronic hypertension was 4.0% (Bramham et al. 2014).

1.1.6 Adverse maternal and perinatal outcomes associated with preeclampsia

In the context of hypertension in pregnancy, preeclampsia lies at one end of the spectrum with the highest associated maternal and neonatal morbidity and mortality. The impact of adverse maternal outcomes in pregnancy hypertension is highlighted by a reported 39.5% of obstetric admissions to 14 intensive care units in England being secondary to hypertensive disorders of pregnancy (Hazelgrove et al. 2001). Women are at increased risk of stroke, acute kidney injury, disseminated intravascular coagulopathy, hepatic failure, pulmonary oedema and cardiac complications (Mattar and Sibai 2000).

Preeclampsia has a higher prevalence of fetal growth restriction than those with isolated chronic hypertension (Srinivas et al. 2009). Placental abruption risk is higher compared to normotensive pregnancies and highest amongst those with pregnancies additionally complicated by fetal growth restriction, thus suggesting abruption as a manifestation of a chronic placental condition (Ananth et al. 1999; Ananth et al. 2007; Toivonen et al. 2002).

Hypertensive disorders are associated with maternal and perinatal mortality with variable incidences geographically. The proportion of maternal deaths from hypertensive disorders of pregnancy was 2% in the United Kingdom between 2015 and 2017 (Knight et al. 2019), 7.4% in the United States of America between 2011 and 2013 (Creanga et al. 2017) and 14% globally between 2003 to 2012 (Say et al. 2014). One in 20 stillbirths without congenital abnormality occur in women with preeclampsia (Cantwell et al. 2011).

Following pregnancy and delivery, there remains a lifetime adverse effect on maternal and infant health. Infants from pregnancies with preeclampsia have higher blood pressures in childhood (Tenhola et al. 2006) and increased risk of stroke during adulthood (Kajantie et al. 2009). In a systematic review and meta-analysis, women with preeclampsia had a subsequent increased risk of vascular disease, ischaemic heart disease, stroke and venous thromboembolism (Bellamy et al. 2007). Preeclampsia complicated by preterm delivery further increased the risk of death from cardiovascular causes compared to preeclampsia

without preterm delivery (Irgens et al. 2001). Furthermore, in some settings such as a contemporaneous South African cohort, only two-thirds of women with acute kidney injury in preeclampsia had confirmed renal recovery (Conti-Ramsden et al. 2019).

1.2 Placental structure and function

Elucidation of the processes involved in placental development have arisen through in vitro studies, histological examination and advances in imaging techniques *in vivo*. Initial in vitro studies provided crude simulation of the *in vivo* environment while histological studies were limited in examining early placental development and discerning causation and effect.

1.2.1 Normal placental development

Following fertilisation, the zygote undergoes rapid cell division and differentiation into a blastocyst. The blastocyst consists of an inner cell mass and outer trophoblastic layer. During implantation, underlying maternal endometrial glands support the growing conceptus. Through histotrophic nutrition, carbohydrate and lipid rich secretions as well as growth factors are delivered (Burton, Jauniaux, and Charnock-Jones 2007).

The trophoblast cells can be divided into two types: endovascular extravillous trophoblast cells and interstitial trophoblast cells. Endovascular extravillous trophoblast cells migrate down the lumens of spiral arteries while interstitial trophoblast cells migrate through the endometrial stroma, penetrating spiral arteries from the outside (Burton et al. 2009). The interstitial trophoblast cells reach the inner third of the myometrium (junctional zone) and transform into immotile giant cells by 14-15 weeks (Brosens, Pijnenborg, and Brosens 2002).

Trophoblastic invasion of spiral arteries is associated with spiral artery remodelling. In normal pregnancy during this process, a loss of smooth muscle cells and elastin from the arterial walls is replaced by fibrinoid material (Pijnenborg, Vercruysse, and Hanssens 2006). Spiral arteries become flaccid conduits of rich oxygenated blood and the terminal coils of spiral arteries dilate to 2-3mm in diameter (Harris and Ramsey 1966). As a result of this spiral artery remodelling, spiral arteries have a reduced capacity for vasoconstriction while the velocity and pulsatility of maternal flow into the placental intervillous space is reduced (Burton et al. 2009). It is thought that this occurs to avoid damage to the fragile trophoblastic villi (Brosens et al. 2010).

The invasion of spiral arteries by trophoblast cells is initially extensive, resulting in trophoblasts plugging the tips of the spiral arteries. This process can be demonstrated using *in vivo* contrast enhanced ultrasound (Roberts et al. 2017). The next stage of unplugging, to allow oxygenated maternal blood to flow freely into the intervillous space, completes by 18 weeks and starts peripherally, moving centrally. The fetoplacental unit therefore develops in a low oxygen environment in the first trimester and this is thought to protect the embryo from damaging reactive oxygen species and maintain stem cell potential (Burton and Jauniaux 2018).

While spiral artery remodelling occurs, there are also maternal adaptations. The arcuate and uterine arteries dilate and by 20 weeks' gestation, the diameter of arcuate arteries is equal to that of the uterine arteries (Burchell 1967). It has been proposed that mediators of this process include oestrogens, human chorionic gonadotrophin, placental growth factor and an increased nitric oxide production (Burton et al. 2009).

Trophoblastic villi undergo rapid branching in the first and second trimester to increase their surface area in contact with the maternal circulation. Maternal blood in spiral arteries enters the central cavity of a lobule that is free of villi, and then disperse radially between the villi. The existence of an oxygen concentration gradient across a lobule is supported by a high antioxidant enzyme activity in villous tissue sampled from the centre of the lobule compared to the periphery (Hempstock et al. 2003).

While maternal blood passes over the surface of placental villi, a complex exchange process occurs for fetal nutrient uptake, gas exchange, elimination of waste products, immunity and thermo-regulation. The maternal-fetal interface also has an endocrine function to orchestrate maternal adaptations to pregnancy (Burton and Jauniaux 2015).

1.2.2 Placental dysfunction

The placenta is central in the aetiology and disease progression of hypertensive disorders of pregnancy and its associated adverse outcomes (Brosens et al. 2011; Brosens, Pijnenborg, and Brosens 2002; Veerbeek et al. 2016).

1.2.2.1 Aetiology of hypertensive disorders of pregnancy

Inadequate spiral artery remodelling is thought to lead to a cascade of events resulting in placental dysfunction. The causes of deficient remodelling have been suggested to include inadequate histotrophic nutrition in the first few weeks, excessive apoptosis within the placental bed (and therefore failure of trophoblasts to invade spiral artery walls as

effectively) or an abnormal interaction with uterine natural killer cells (Burton and Jauniaux 2018).

Poorly remodelled spiral arteries have several characteristics and consequences. Maternal blood flow through them is pulsatile and of high velocity. This results in mechanical damage to the fragile placental villi. The vascular smooth muscle in the spiral arteries is retained and can vasoconstrict, therefore resulting in intermittent perfusion and ischaemia-reperfusion injury. Spiral arteries are also prone to acute atherotic changes with accumulation of foam cells and further narrowing of the lumen (Burton and Jauniaux 2018). Biopsies from pregnancies complicated by hypertensive disorders have absent trophoblastic invasion (Pijnenborg et al. 1991) with medial hyperplasia, fibrin deposition, endothelial vacuolation and thrombosis, thus supporting these putative mechanisms.

The timing and pattern of spiral artery unplugging across the placenta may also be crucial for placental perfusion. If this unplugging occurs too early, begins centrally (rather than peripherally) or extravillous trophoblast cells do not invade deep enough to form these plugs, then oxidative stress and a cascade of events leading to pregnancy failure and pre-eclampsia may occur (Pijnenborg, Vercruysse, and Hanssens 2006).

Altered placental perfusion is hypothesised to result in placental oxidative stress and excessive generation of reactive oxygen species (ROS). Reactive oxygen species can damage proteins, lipids and DNA, thus impairing cell function which can lead to apoptosis. This is demonstrated in placental explants where apoptosis and proinflammatory cytokines are released during exposure to hypoxia and reoxygenation *in vitro* (Hung et al. 2002).

1.2.2.2 Fetal response

Placental dysfunction results in metabolic and vascular changes in the fetus through a diminished oxygen and nutrient supply. This clinically manifests as fetal growth restriction, defined as the failure to reach growth potential.

Metabolic changes include a downregulation of insulin and the insulin-like growth factor-1 endocrine axis given the reduction in glucose delivery (Reece et al. 1994). Hepatic glucose metabolism falls and glycogenolysis occurs, reducing the size of fetal liver. There is an increased accumulation of lactate and ketone bodies. Other changes include altered protein and lipid metabolism, endocrine changes with upregulation of the adrenocortical axis and haematological adaptations. The fetal circulation adapts to a diminished oxygen and nutrient supply by preferentially redistributing umbilical venous blood to the

myocardium and brain (brain sparing effect). This can be detected clinically as a fall in the middle cerebral artery pulsatility index with a rise in the umbilical artery pulsatility index leading to absent or reversed end diastolic flow and a fall in the cerebroplacental ratio. Other indices of fetal growth restriction include an abdominal circumference or estimated fetal weight less than the third centile, a fall in growth velocity more than 2 quartiles on growth centiles (Gordijn et al. 2016) and an absent A-wave in the ductus venosus Doppler waveform (Lees et al. 2015).

1.2.2.3 Maternal response

In the presence of abnormal placentation, factors are released into the maternal circulation leading to the hypertensive maternal response and its complications. Factors contributing to this response include antiangiogenic soluble fms-like tyrosine kinase 1 (sFlt-1) as well as angiogenic factors vascular endothelial growth factor (VEGF) and placental growth factor (PlGF). Widespread maternal vascular endothelial dysfunction ensues and results in the maternal response that includes hypertension, glomerular endotheliosis (and thus proteinuria and renal insufficiency), cerebral oedema (clinically manifesting as headache and seizures) as well as HELLP syndrome (haemolysis elevated liver enzymes and low platelet count) (Karumanchi et al. 2005).

1.2.2.4 Fetal growth restriction and preeclampsia

Both fetal growth restriction and preeclampsia involve abnormal placentation; however, fetal growth restriction can occur in the absence of preeclampsia and vice versa. A proposed relationship between placental development and preeclampsia is outlined below (Figure 1.2).

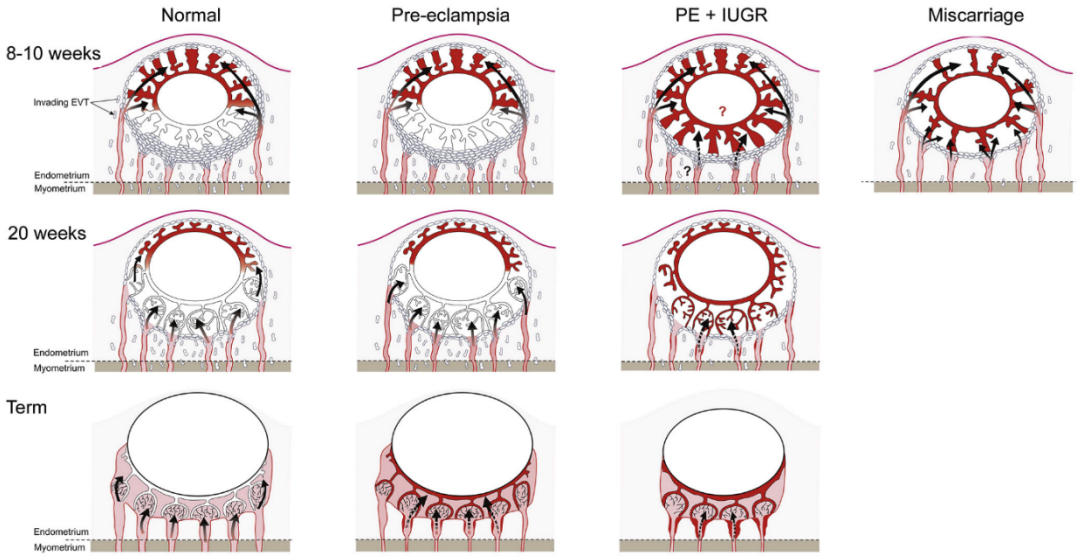

Figure 1.2: Proposed relationship among degree of oxidative stress and placental development in normal pregnancies, late-onset preeclampsia (PE), early-onset PE, and miscarriage.
In normal pregnancies onset of maternal circulation in periphery causes local oxidative stress, villous regression, and formation of chorion laeve. In miscarriage extravillous trophoblast (EVT) is severely deficient, leading to incomplete plugging of spiral arteries, premature and disorganized onset of blood flow, and overwhelming oxidative stress. Situation is intermediate in PE, being more severe in early-onset form of syndrome associated with fetal growth restriction (FGR). (Burton and Jauniaux 2004)

1.3 Principles of magnetic resonance imaging

Magnetic resonance imaging is based on the magnetisation properties of atomic nuclei. MRI scanners have a primary magnet, gradient coils (to generate second magnetic fields) and radiofrequency coils (to transmit radiofrequency pulses and receive signals).

1.3.1 Atomic structure and spin

Atoms consist of up to three components: electrons, neutrons and protons. Protons and neutrons are situated in a central atomic nucleus, while electrons orbit the nucleus. Electrons are negatively charged, protons are positively charged and neutrons have no charge. Different numbers of each of these components within an atom, give rise to different elements and isotopes.

When the number of protons equals the number of neutrons in an atomic nucleus, there is no net spin. In the case of hydrogen atoms, the nucleus consists of one proton without any neutrons. They therefore have a net spin. Given the presence of the proton's positive electrical charge and movement, a magnetic field is induced. This can be described as a vector. Without an external magnet, the protons will have their magnetic field vectors

pointing in random directions, such that a vector sum of a sample of protons equals zero. The hydrogen nucleus is used in magnetic resonance imaging as it is abundantly present in human tissue (mostly in water) and therefore a strong signal can be produced.

1.3.2 Applying a magnetic field

When an external magnet is applied to protons, the vectors of each proton will either align with the magnetic field or align opposite to the magnetic field but the net orientation vector is in the same direction as the external magnetic field. The external magnetic field also produces a secondary spin (or wobble) of the proton's axis around the magnetic field. The axis of the proton will spin around the long axis of the applied magnetic field (known as precession). The precession rate is called the Larmor frequency. When protons precess together, they are 'in phase.' When protons precess separately, they are 'out of phase.' The precession frequency is proportional to the magnetic field strength and also depends on the type of nucleus. It can be described by the Larmor equation. The strong static external magnetic field in an MRI scanner is termed B_0.

$$\omega = \gamma B_0$$

ω = precessional frequency
γ = gyromagnetic ratio
B_0= magnetic field strength

Figure 1.3: Larmor equation

1.3.3 Application of a radiofrequency pulse and subsequent relaxation

Once in the magnetic field, a radiofrequency (RF) pulse is applied. Protons will spin out of equilibrium against the pull of the magnetic field. After the radiofrequency field pulse, protons realign with the magnetic field. The realignment is termed relaxation, during which energy is emitted. The amount of energy released during relaxation and the time it takes to realign, depends on the environment and nature of the molecules.

1.3.3.1 T1 relaxation

T1 relaxation is the time it takes to restore the axis from perpendicular alignment to the magnetic field to a parallel alignment to the magnetic field. It therefore refers to the longitudinal relaxation or spin lattice relaxation. While T1 relaxation occurs, energy is dissipated into the lattice (the environment surrounding the nucleus). As a result, dark low signal areas on T1 weighted images correspond to areas with long T1 values such as water.

1.3.3.2 T2 relaxation

After the application of an radiofrequency pulse, all the spinning protons are in phase. They then lose coherence (dephase) as some spin slightly faster and others slower with energy exchange. This results in a reduction of the magnetic field vector. T2 relaxation measures how fast the spins lose their magnetisation through dephasing (i.e. decay) in a particular xy plane. It is also known as the transverse relaxation or spin-spin relaxation.

In reality, the spins dephase quicker than T2 because of inhomogeneities in the magnetic field. The inhomogeneity is because of intrinsic defects in the magnetic field or field distortions by the tissue itself. This is exploited to examine oxygenation in tissue as deoxyhaemoglobin is paramagnetic. The true T2 together with the magnetic field inhomogeneities is termed T2*. T2* weighted sequences can also be used in blood oxygen dependent imaging (BOLD) where the absolute BOLD signal is described as follows.

$$S \propto M_0 e^{(-TE/T2^*)}$$

S = absolute BOLD signal
M_0 = tissue equlibrium magnetisation
TE = echo time

Figure 1.4: Blood oxygen level-dependent (BOLD) equation

1.3.4 Displaying an image

The energy released through relaxation is picked up by a receiver coil in the MRI scanner, converted from an analogue signal to a digital signal, stored in the image space ('K space'), sent to a digital processor where Fourier transformation is applied. Fourier transformation deconstructs the input signal into its constituent sinusoids of different frequencies. This gives rise to an image displayed.

1.3.5 Diffusion weighted imaging

Diffusion measures the thermal microscopic translational motion of water molecules by applying magnetic field gradients. When water molecules move in the direction of the magnetic field gradient, the emitting signal drops. The displacement measured is in the order of five to ten μm.

Without any boundaries, water molecules move randomly and in no preferred direction (Brownian motion) and thus are equally spread throughout the medium. This is termed isotropic. Conversely, when there are boundaries (e.g. fibres, membranes), water preferentially moves parallel to these boundaries rather than perpendicular and this is termed anisotropic.

The magnitude of these movements can be characterised by the diffusion coefficient. The apparent diffusion coefficient (ADC) is principally used in imaging because it assumes a free diffusion model, when in reality movement is not isotropic due to the tissue properties present.

1.3.5.1 Diffusion tensor and derived measures

A diffusion tensor describes the movement of molecules using the x, y and z planes (Neil 2008). This is represented as a three-dimensional ellipse with three different eigenvectors λ_1, λ_2 and λ_3.

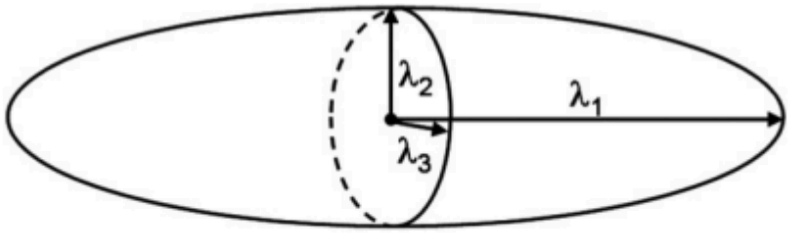

Figure 1.5: Representation of a diffusion ellipsoid showing the eigenvectors, as published by (Neil 2008).

To quantify the shape of the tensors within each voxel, several measures are used derived from the eigenvectors. These are the axial diffusivity (AD), radial diffusivity (RD), mean diffusivity (MD) and fractional anisotropy (FA).

Diffusion measure	Abbreviation	Equation
Axial diffusivity	AD	λ_1
Radial diffusivity	RD	$(\lambda_2 + \lambda_3) / 2$
Mean diffusivity	MD	$(\lambda_1 + \lambda_2 + \lambda_3) /3$
Fractional anisotropy	FA	$\sqrt{\frac{1}{2}}\frac{\sqrt{(\lambda_1-\lambda_2)^2+(\lambda_2-\lambda_3)^2+(\lambda_3-\lambda_1)^2}}{\sqrt{\lambda_1^2+\lambda_2^2+\lambda_3^2}}$

Table 1.1: Diffusion measures as derivations of eigenvectors.

Fractional anisotropy can be further described as the fraction of diffusion which is anisotropic.

1.4 Safety of magnetic resonance imaging in pregnancy

Magnetic resonance imaging does not utilise ionizing radiation and is considered a safe imaging modality (De Wilde, Rivers, and Price 2005). Several clinical practice guidelines state that it is considered safe at all trimesters of pregnancy without gadolinium administration (Jain 2019; Patenaude et al. 2014). Studies have shown that there are no alterations in fetal heart rate during magnetic resonance imaging (Michel et al. 2003; Poutamo et al. 1998; Vadeyar et al. 2000) or subsequent fetal growth post imaging (Myers et al. 1998). Furthermore, follow up studies show no increase in disease (Baker et al. 1994), functional or hearing impairment at preschool age (Bouyssi-Kobar et al. 2015). A study of 1737 children in Ontario, Canada up to 4 years of age between 2003 to 2015 also showed that magnetic resonance imaging in the first trimester was not associated with increased risk of harm (Ray et al. 2016).

On a cellular level, static magnetic fields have not been shown to affect cell growth (Miyakoshi 2005) even in the context of repeated exposure (Wiskirchen et al. 1999). In contrast, animal studies have been conflicting. Mice exposed to a magnetic field of 4Tesla for 9 hours on day 9 and/or day 12 post coitus showed no changes in fetal growth (Magin et al. 2000) while chicks exposed to 1.5Tesla for six hours and sacrificed on the sixth day of incubation showed a trend towards higher abnormality and mortality rate than controls (Yip et al. 1994). However, the duration of magnetic resonance exposure in these studies is much greater than those used during clinical imaging and the equivalent period in human development during exposure is early in the first trimester.

The safety of different magnetic field strengths in pregnancy has been limited by retrospective studies and a paucity of long term follow up data. In the largest retrospective study (Ray et al. 2016) where children were followed up until 4 years of age and there was no risk of harm demonstrated, the magnet strength was not documented although it is noted that most imaging was carried out at 1.5 Tesla. Outcomes examined included stillbirth, congenital anomalies, neoplasm, vision or hearing loss. Comparing imaging at 3 Tesla and 1.5 Tesla in terms of potential acoustic effects on fetal hearing, there were no clinically detectable hearing abnormalities found between the two groups (Jaimes et al. 2019). To date, no study has found a teratogenic effect at both 1.5Tesla and 3Tesla and there are no published studies investigating the safety of pregnancy at 7 Tesla.

In order to optimise and maintain the safety of pregnant women undergoing magnetic resonance imaging, the following potential risks must be considered (Dill 2008): the static

magnetic field, pulsed radiofrequency fields, pulsed gradient magnetic fields and maternal positioning in the scanner. Additionally, imaging may reveal unexpected findings that may cause anxiety for women or require further management. Protocols for unexpected findings must therefore be in place when imaging in order to ensure patient safety. Patients must also be informed of the potential for unexpected findings as part of the consent process in research studies.

1.4.1 Static magnetic field

The main safety risk of magnetic resonance imaging is the static magnetic field. Clinical MRI scanners are in the order of 1.5 Tesla or 3 Tesla and therefore any ferromagnetic objects nearby can move or accelerate towards the scanner magnet causing injury. By comparison, the Earth's magnetic field is 25-65 μTesla. Ferromagnetic objects may present themselves in the form of jewellery, surgical implants and clips or within clothing. In order to minimise this risk, a safety checklist is carried out twice on the day of imaging by two independent MRI trained staff. Women imaged also wear MRI safe hospital clothing.

Please answer the following questions carefully, with a **black pen** and ask if anything is not clear. All information is held in the strictest confidence.

Please tick your answer ☑	No	Yes	If yes, please comment
1. Do you have a heart pacemaker? **These may stop working near the MRI scanner.**	☐	☐	
2. Have you ever had any surgery on your heart?	☐	☐	
3. Have you ever had any surgery on your head, brain or eyes?	☐	☐	
4. Have you had any clinical procedure done in the past 6 months?	☐	☐	
5. Do you have any foreign bodies inside you? (e.g. implants, devices, shrapnel) Please list.	☐	☐	
6. Have you ever had any metal particles in your eyes? (e.g. from welding or metal work)	☐	☐	
7. Could you be pregnant?	☐	☐	
8. Do you wear dentures, a dental plate or a brace?	☐	☐	
9. Have you had blackouts, epilepsy or fits in the past 2 months?	☐	☐	
10. Do you have any tattoos or trans-dermal patches (medicated adhesive patches)?	☐	☐	
11. Are you wearing coloured contact lenses?	☐	☐	
12. An MRI contrast agent (dye) is often required to give us the best information from your MRI scan. Do you consent to an injection of contrast agent (dye) if required? If yes, please complete the Section B overleaf	☐	☐	
13. Do you suffer from any allergies (e.g. pet, food or drug allergies)?	☐	☐	
14. Before entering the MRI scan you must remove all metal objects, including coins, jewellery, body-piercings, hearing aids, dentures containing metal, clothing containing any metal, dental braces, artificial limbs or callipers. Will you remove all of the above before entering the MRI scan room?	☐	☐	
15. Is there anything else you think we should know about in relation to your MRI scan?	☐	☐	

Figure 1.6: MRI safety checklist questions

On a cellular level, static magnetic fields have not been shown to affect cell growth (Miyakoshi 2005) even in the context of repeated exposure (Wiskirchen et al. 1999). A survey completed by 1915 MRI workers (and therefore repeatedly exposed to static magnetic fields) showed no difference in reproductive outcomes of miscarriage, delayed conception, preterm delivery or low birthweight (Kanal et al. 1993).

1.4.2 Pulsed radiofrequency fields

Pulsed radiofrequency fields have a thermogenic effect that can adversely affect pregnancy. Organogenesis of the nervous system is particularly vulnerable and a rise in temperature can lead to neural tube defects, cranio-facial defects and microcephaly in animal models (Edwards, Saunders, and Shiota 2003). However, the threshold of temperature rise and duration of temperature rise vary between species (mouse, rat, rabbit, guinea-pig and hamster models) and different strains of the same species.

The degree of thermogenesis depends on the sequences deployed as well as patient characteristics. The heating potential can be expressed as the specific absorption rate (SAR), measured in watts per kilogram. The applied energy is absorbed by the body and converted into heat. Estimation of the specific absorption rate in utero of pregnant women has been achieved using anatomical models (Hand et al. 2006). International standards (IEC 60601) state that pulse sequences developed must not cause a body temperature to rise above 0.5°C for an MRI normal mode scan, 1°C for a controlled mode scan and 1°C in experimental mode. In the context of pregnancy, it is advised that the temperature of the woman does not rise by more than 0.5°C and the estimated temperature of the fetus should not exceed 38°C in order to avoid adverse fetal effects (Patenaude et al. 2014), accounting for fetal temperature being 0.5°C higher than that of the woman.

1.4.3 Pulsed gradient magnetic fields

Pulsed gradient magnetic fields have the potential to cause biological effects, acoustic noise damage, peripheral nerve stimulation, peripheral muscle stimulation, cardiac fibrillation and magnetophosphenes (De Wilde, Rivers, and Price 2005). Biological effects and acoustic noise are of relevance to the fetus when imaging in pregnancy. In terms of biological effects, studies have shown no measurable effect of magnetic resonance imaging on anxiety, spatial memory, long term memory, intelligence quotient, visual acuity, reaction time or acute changes in serum melatonin levels (Prato et al. 1992). Early studies were performed at 0.15 Tesla, assessing cognition at 3 months in 53 participants following exposure, with a sham and control group (Sweetland et al. 1987). Some animal studies did not replicate conditions in human imaging as exposure to magnetic fields was for greater than 24 hours.

Acoustic noise arises from the rapidly switching currents in the gradient coils within the magnetic field. Studies have suggested that high noise intensities greater than 99dB are associated with high frequency hearing loss in newborns, premature birth and fetal growth restriction (American Academy of Pediatrics 1997). However, these studies are mostly retrospectively conducted with self-reported noise exposure and noise may be a marker for other confounding risk factors.

Reassuringly, studies have shown that the acoustic noise of magnetic resonance imaging in the second and third trimester does not lead to substantial cochlear injury or hearing impairment in neonates (Reeves et al. 2010) and at three years no hearing deficit related to imaging was reported (Baker et al. 1994). The fetus is somewhat protected from

environmental noise by attenuation from surrounding amniotic fluid and maternal tissue. An estimation of such attenuation has been achieved from a hydrophone swallowed by a volunteer, where a 30dB attenuation in intensity was recorded (Glover et al. 1995). It is noted that this was not an accurate simulation of an in-utero environment. A recent study quantifying the in utero acoustic transmission using a sheep model showed that frequency contents above the 10kHz are transmitted into the amniotic sac and that some frequencies are attenuated by as little as 3dB (Gélat et al. 2019).

In view of the potential adverse effects of acoustic noise, the imaging protocols used in this study do not exceed 110dB. This cut off is derived from the Occupational Safety and Health recommendation of a maximum noise exposure of 90dB for 4 hours a day in the workplace (Śliwińska-Kowalska and Zaborowski 2017) and accounts for a 30dB attenuation from amniotic fluid and maternal tissue. The maternal hearing is protected using earplugs and noise cancelling headphones.

1.4.4 Positioning

Routine obstetric ultrasound imaging and conventional imaging of non-pregnant patients occurs in the supine position. This can be challenging in pregnant women due to supine hypotensive syndrome which clinically manifests with symptoms of dizziness, sweating, nausea and signs of pallor, tachycardia and hypotension (Kinsella and Lohmann 1994). It is thought to occur secondary to aortocaval compression by the gravid uterus (Lees et al. 1967); however, recent magnetic resonance imaging has illustrated that it is mainly inferior vena cava compression (and not aorta compression) that occurs when lying supine (Higuchi et al. 2015).

The spinal venous plexus and ascending lumbar veins act as collateral pathways to maintain vascular homeostasis in pregnant women lying supine (Hughes et al. 2021; Humphries, Stone, and Mirjalili 2017). Other studies have shown a reduction in fetal heart rate variability in the supine position (Stone et al. 2017) and a fall in global perfusion with increasing gestational age in healthy pregnancies when lying supine that is not seen when lying in left lateral (Zun et al. 2017). This effect may be as a result of a fall in cardiac output and aortic blood flow when supine (Humphries, Stone, and Mirjalili 2017; Humphries et al. 2019). Using a combined diffusion weighted imaging and T2 relaxometry technique, a study has shown that supine position resulted in a fall in oxygen transfer to the fetus and reduction in fetal oxygen saturation that was not statistically significant (Couper et al. 2020). There remain no studies of whether these short-term reversible changes have an

impact on neonatal outcome. In addition, positioning a woman in left lateral tilt for a short period followed by rotation to supine has been found to increase venous return in the inferior vena cava and spinal venous plexus, suggested in part due to a smaller proportion of the uterus on the right side of the abdomen (Hughes et al. 2021). Thus, the suggested changes seen in supine imaging may be mitigated by placing a woman in left lateral tilt prior to rotation to supine for imaging.

Concerns regarding the supine position have been raised aside from reversible symptomatic discomfort. It has been suggested that the supine maternal sleep position is an additional risk factor for late pregnancy stillbirth in an already compromised fetus (Gordon et al. 2015). In a prospective case control study carried out in 41 maternity units, the supine going to sleep after 28 weeks' gestation had an increased risk of late stillbirth compared with the left side (adjusted odds ratio (aOR) 2.31, 95% CI 1.04-5.11) (Heazell et al. 2018). An individual-level participant data meta-analysis showed that the supine going-to-sleep position was associated with increased odds of late stillbirth (aOR 2.63, 95% CI 1.72-4.04) compared with left side (Cronin et al. 2019). However, the duration of remaining supine during sleep is notably longer than that of imaging and the retrospective study is subject to bias and reverse causation. Other studies have shown a reduction in fetal heart rate variability in the supine position (Stone et al. 2017) and a fall in global perfusion with increasing gestational age in healthy pregnancies when lying supine that is not seen when lying in left lateral (Zun et al. 2017). There remain no studies of whether these short-term reversible changes have an impact on neonatal outcome.

1.4.5 Claustrophobia

Claustrophobia presents a challenge in magnetic resonance imaging. In 939 adult patients requiring clinically indicated brain imaging, a reported 14.3% required sedation in order to tolerate imaging (Murphy and Brunberg 1997). When imaging pregnant women, the effect of claustrophobia can be minimised by entering the magnet bore feet first and the use of prism glasses that allowing the woman to see outside the scanner into the console room behind the magnet bore.

1.5 Current applications of placental MRI

1.5.1 In clinical practice

The clinical use of placental MRI remains principally as an investigative tool in the suspicion of the placenta accreta spectrum disorder. In this pregnancy complication, there is a

disruption in the endometrial-myometrial interface leading to failure of normal decidualisation, usually in an area of a uterine scar occurring secondary to a previous caesarean section (Jauniaux and Bhide 2017). Trophoblast and villous tissue invade the myometrium and surrounding pelvic organs. On placental histology, there is complete or partial absence of the decidua basalis. The degree of invasion can be divided into placenta creta, increta and percreta.

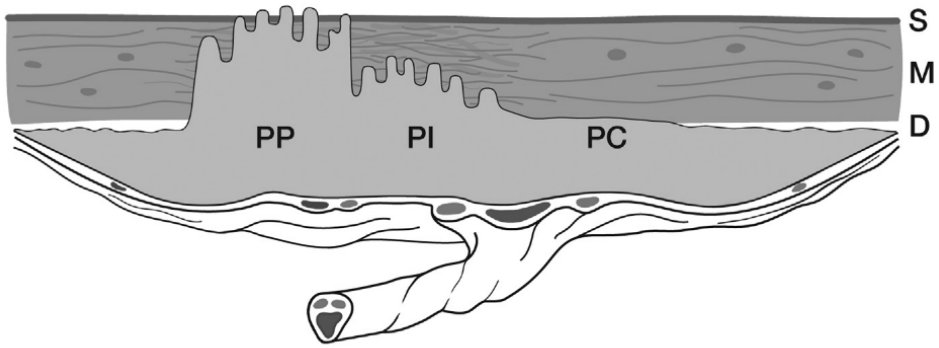

Anterior placenta previa accreta combining areas of abnormal adherence and invasion to the uterine wall: creta, increta, and percreta.

D, decidua; *M*, myometrium; *PC*, placenta creta; *PI*, placenta increta; *PP*, placenta percreta; *S*, serosa.

Figure 1.7: Diagram showing accreta, increta and percreta villous tissue, as published by Jauniaux et al. 2018.

1.5.1.1 Pregnancy outcomes in placenta accreta spectrum

Placenta accreta spectrum is associated with adverse maternal and fetal outcomes. Maternal risks include life-threatening obstetric haemorrhage, uterine rupture, hysterectomy, damage to the urinary tract and admission to intensive care (Balayla and Bondarenko 2013). Fetal risks include preterm birth, low birth weight (Balayla and Bondarenko 2013) and admission to the neonatal intensive care unit (Farquhar et al. 2017). Early accurate antenatal diagnosis enables optimisation of clinical management especially with respect to delivery. A planned co-ordinated delivery by elective caesarean section before the onset of labor is advised, as it is associated with a reduction in morbidity (Jauniaux et al. 2019). Outcomes are further improved if delivery occurs in a multidisciplinary setting in a specialist centre with expertise in complex pelvic surgery as well as diagnosing and managing invasive placentation (Shamshirsaz et al. 2015).

1.5.1.2 Features of placenta accreta spectrum on MRI

Several studies have assessed the predictive value of MRI features in determining placenta accreta spectrum. T2-weighted images are often performed in three planes (axial, sagittal

and coronal) with at least a partially filled bladder in order to assess bladder involvement in placenta percreta. A study where two expert MRI readers (masked to clinical outcome) assessed MRI scans from 20 patients, half of whom had a diagnosis of placenta accreta spectrum following delivery (Lax et al. 2007) was performed. Features of uterine bulging, heterogenous signal intensity within the placenta and dark intraplacental bands were found to be the most useful in determining those with and those without placental invasion. Other suggested imaging findings include focal interruptions in the myometrial wall, tenting of bladder and direct visualisation of the invasion of pelvic structures by placental tissue (Baughman, Corteville, and Shah 2008). Assessment of images from 42 women suspected of having placenta accreta spectrum by MRI readers masked to clinical outcome reported uterine bulging as the feature with the best positive predictive value and its combination with the presence of dark intraplacental bands further improving the predictive value (Riteau et al. 2014).

1.5.1.3 Screening for placenta accreta spectrum

In the United Kingdom, all pregnant women are offered an obstetric ultrasound scan as part of the National Health Service Fetal Anomaly Screening Programme between 18 to 20+6 weeks' gestation (Public Health England 2018) Within this ultrasound scan, the placental site is reported. Current clinical guidelines from the Royal College of Obstetrician and Gynaecologists advise that those with a previous history of placenta accreta spectrum or a previous caesarean section with an anterior low-lying placenta (defined as less than 20mm from the internal cervical os) or placenta praevia should have a specialist ultrasound scan for placenta accreta spectrum. Ultrasound features of placenta accreta spectrum have been standardised by the European Working Group on Abnormally Invasive Placenta (Collins et al. 2016) and a proforma protocol produced by the international Abnormally Invasive Placenta Expert Group (Alfirevic et al. 2016).

1.5.1.4 Role of magnetic resonance imaging in placenta accreta spectrum

The use of magnetic resonance imaging in placenta accreta spectrum is controversial and operator dependent as it is considered that it does not improve the diagnosis compared to ultrasound alone when performed by experts. Systematic reviews and meta-analyses comparing the two imaging modalities show similar detection rates of placenta accreta spectrum (D'Antonio et al. 2014; Meng, Xie, and Song 2013). These studies may be limited by selection bias as MRI is often only performed when there is already suspicion of placenta accreta spectrum from ultrasound. Gadolinium contrast during magnetic resonance imaging may improve the detection rate, especially amongst those with limited

experience interpreting imaging; however, there are limited gadolinium safety data and it is rarely used (Millischer et al. 2017).

The benefits of magnetic resonance imaging as an imaging modality compared to ultrasound include a larger field of view and better soft tissue contrast. In addition, the impact of body mass index and placenta location do not have as much as an adverse effect on image quality. However, magnetic resonance imaging is currently more costly and available only in expert centres with clinical expertise in interpreting imaging. It must also be noted that not all women can undergo magnetic resonance imaging due to claustrophobia, a restricted scanner bore size or failure of the metal safety checklist, commonly due to previous surgical implants or clips.

In view of the above, the current advice from the Royal College of Obstetrician and Gynaecologists is that magnetic resonance imaging may be used to complement ultrasound imaging in order to assess depth of invasion and lateral extension of myometrial invasion, especially with posterior placentation and or ultrasound signs suggesting parametrial invasion (Jauniaux et al. 2019). This is especially useful in surgical planning. Visualising the placental margins along with the whole placenta within the same field of view can facilitate decisions regarding the abdominal and uterine incision, the latter should avoid the placenta often requiring a nontraditional incision. Magnetic resonance imaging can also assist in the decision for inserting ureteric stents preoperatively to risk of urinary tract injury and at ureteric stent placement, cystoscopic assessment can assess for bladder invasion by the placenta (Allen et al. 2018). This advice is in line with the American College of Obstetricians and Gynecologists (ACOG 2018).

1.5.2 In research

1.5.2.1 T2-weighted imaging

T2-weighted imaging allows for visualisation of the placental structure *in vivo* within a large field of view. The boundary between the amniotic fluid and placenta can be easily visualised while the delineation between the placenta and uterine wall is not as clear. Mapping the vascular tree *in vivo* may assist surgical planning of laser division in twin-twin transfusion syndrome (Aughwane et al. 2020). Multislice sets of images can be taken for the quantification of placental structure using measures such as placental volume, thickness and shape. Despite the challenges presented by interslice motion, varying placental location, size, shape and signal intensities in pathology, acquisition and

processing techniques have been automated, thus removing the need for time consuming manual segmentation (Wang et al. 2016; Wang et al. 2019).

1.5.2.1.1 Simple visual analysis

The placenta, with its associated large volume of blood, has a low signal intensity on T1 weighted images and high signal intensity on T2-weighted imaged (Gowland 2005). In uncomplicated pregnancies, with advancing gestation, the placenta appears more heterogenous with an increasing lobularity and a reduction in the ratio of placental and amniotic fluid signal intensity on T2-weighted imaging (Blaicher et al. 2006). In pregnancies complicated by fetal growth restriction, simple visual analysis revealed a thickened globular appearance (Damodaram et al. 2010). Other visual features seen on T2-weighted imaging include placental haemorrhages (retroplacental haematomas, intervillous thrombi and subchorionic haematomas) and ischaemic lesions (Linduska et al. 2009). These have been found to correlate with placental histology findings performed postnatally with a median of seven days between imaging and delivery (Linduska et al. 2009). However, small macroscopic changes associated with perivillous fibrin deposition were not visually detected on magnetic resonance imaging in this study, noted to be performed on a 1.5T scanner.

1.5.2.1.2 Quantitative analysis using T2-weighted imaging

Placental volume and thickness have been explored in several studies, mostly in uncomplicated pregnancies and pregnancies complicated by fetal growth restriction. Longitudinal data involving women with uncomplicated pregnancies scanned at four-weekly intervals, showed a linear placental growth throughout the second and third trimester (Langhoff et al. 2017). In contrast, examination of 20 pregnancies complicated by fetal growth restriction (mean gestation at imaging 26.96, standard deviation 3.6) found a reduced placental volume and a high placenta thickness to volume ratio (Damodaram et al. 2010). In addition to these findings, an abnormal signal intensity consistent with placental pathology was found to predict fetal or neonatal death. These findings were consistent with another study (Ohgiya et al. 2016) which additionally found that the size of flow voids between the uterus and placenta were associated with growth restricted fetuses in a group of 50 singleton pregnancies.

The large field of view in magnetic resonance imaging encompasses the fetal brain which may additionally inform prognosis. Placental, global and regional brain volumes were calculated in pregnancies complicated by fetal growth restriction (Andescavage et al. 2017).

These volumes increased with advancing gestational age but were smaller compared to controls. Brain volumes were found to be smallest in growth restricted fetuses with abnormal umbilical artery dopplers yet interestingly, brainstem volume remained preserved.

The advent of machine learning has led to the prediction of fetal growth restriction and birthweight using placental shape and textural features (Dahdouh et al. 2018). Shape features included placental volume, thickness and elongation while textural features included mean, variance, kurtosis and skewness of placental grey levels. The T2-weighted images were further assessed using gray level co-occurrence and run-length matrices to characterise placental homogeneity, symmetry and coarseness. The framework was able to distinguish growth restricted fetuses from those normally grown and predict birthweight in both groups.

T2 relaxation times have been calculated in various studies and shown to fall linearly with advancing gestation (Derwig, Barker, et al. 2013; Gowland et al. 1998; Wright et al. 2011). In one study, 10 out of 14 compromised pregnancies (defined as those complicated by fetal growth restriction or preeclampsia) were found to have T2 relaxation times lower than the normal linear regression line (Gowland et al. 1998). Only two of these pregnancies were complicated by preeclampsia and imaging was performed beyond 35 weeks' gestation in both, thus perhaps representing a less severe clinical phenotype of preeclampsia. A further study (Derwig, Barker, et al. 2013) illustrated a decreased T2 relaxation time in small for gestational age fetuses that was additionally associated with raised uterine artery pulsatility index and lower birthweight percentiles.

Interpreting the biological correlate of the T2 relaxation time has involved histological analysis. Histological analysis of placentae from women imaged within a week of delivery found a positive correlation between fibrin volume density, ratio of fibrin:villlous volume densities and T2 relaxation times (Wright et al. 2011). In a mouse model, loss of placental blood flow abolished T2 contrast thereby suggesting that T2-weighted imaging may detect changes in placental vasculature (Moore et al. 2008).

Long T2 values occur in tissues with a high intracellular non-membrane bound lipid content (Cameron, Ord, and Fullerton 1984). Short T2 values occur in tissues with a greater overall surface area that originates from cellular membranes, intracellular or extracellular fibrillar macromolecules. The extracellular fluid volume fraction can also influence the T2

relaxation time. The reduction in T2 relaxation times with advancing gestational age in uncomplicated pregnancies is therefore thought to occur secondary to villous branching.

1.5.2.2 T2* relaxometry

Studies have shown a linear reduction in placental mean T2* values in uncomplicated pregnancies with increasing gestation (Hutter, Jackson, et al. 2019; Sørensen et al. 2013; Sørensen et al. 2020). There remains a paucity of literature examining T2* values in hypertensive disorders of pregnancy as most studies have focussed on fetal growth restriction.

Lower mean T2* values have been reported in placentae of pregnancies complicated by fetal growth restriction, thus suggesting its clinical application as an indicator of placental dysfunction (Ingram et al. 2017; Sinding, Peters, Frøkjaer, et al. 2016). Results of four cases of fetal growth restriction at a gestational age range from 25 to 31 weeks (Sinding, Peters, Frøkjaer, et al. 2016) were consistent with a larger case-control study (Ingram et al. 2017) including 23 cases of fetal growth restriction (gestational age range from 23 to 35 weeks).

A small study in which T2* values were examined in four women with fetal growth restriction, included one woman with co-existing preeclampsia (Sinding, Peters, Frøkjaer, et al. 2016). Another study also examined T2* in a mixed cohort of 33 women (reported as R2* = 1/T2*) at earlier gestations (prior to 24 weeks' gestation) included two women with fetal growth restriction and one with preeclampsia (Armstrong et al. 2019). Mean R2* values in women with fetal growth restriction were similar to those with uncomplicated pregnancies. However, these women were imaged during early second trimester and all delivered at term thus perhaps suggesting a different disease mechanism in preterm preeclampsia, term preeclampsia, early and late fetal growth restriction. R2* may additionally remain normal at early second trimester with changes becoming apparent only later in pregnancy.

1.5.2.2.1 Maternal hyperoxia

In uncomplicated pregnancies, the BOLD signal has been seen to increase and become more homogenous within the placenta with maternal hyperoxia (Sørensen et al. 2013). This effect is more marked on the fetal side of the placenta. This is consistent with another study where R2* (1/T2*) was reported to decrease with hyperoxia (Huen et al. 2013); however, interestingly gestational age did not affect R2* changes in these 14 women.

The placental response to maternal hyperoxia has been investigated as a potential tool to explore placental dysfunction in cases of fetal growth restriction. Animal studies have been conflicting. One study showed that ΔT2* increased in cases of fetal growth restriction during hyperoxia (Collinot et al. 2018) while another study showed that ΔT2* reduced with hyperoxia (Chalouhi and Salomon 2014). In human studies, 13 women with placental dysfunction (defined as birthweight <10th centile or pathology consistent vascular malperfusion) were imaged with a group of 49 controls (Sinding et al. 2018). Those with placental dysfunction had lower baseline T2* values and a high hyperoxic BOLD response. The time to plateau during maternal hyperoxia may be of relevance as a study in monochorionic twins showed that mean placental time to plateau positively correlated with placental pathology (Luo et al. 2017).

Given the interest in T2* changes in pregnancies complicated by fetal growth restriction, the clinical utility in predicting birthweight has been explored in two studies. Firstly, the combination of $\Delta P0_2$, baseline R1 and baseline R2* was found to have high predictive value in identifying fetal growth restriction (Ingram et al. 2017). Secondly, the area under the receiver operating characteristic curve was higher when using T2* to predict low birthweight compared to uterine artery pulsatility index (Sinding et al. 2017).

1.5.2.2.2 Interpreting T2* values

T2* values probe placental oxygenation as the paramagnetic properties of deoxyhaemoglobin cause magnetic field distortions and a faster T2* decay (i.e. reduced transverse relaxation time) than oxyhaemoglobin. Hypoxic tissues therefore have a reduced T2* value (Blood Oxygen Level Dependency effect). This is supported by the change in T2* values seen with maternal hyperoxia. Although the T2* relaxation time is thought to be an indicative measure of oxygenation, it can also be influenced by villous density, calcium and the distribution of oxygenated blood. Placental pathological findings have been found to be closely related to T2* values (Sinding, Peters, Frøkjaer, et al. 2016).

Regional differences in T2* values can also be found within the placenta and this must be considered when interpreting studies. Contrast enhanced imaging in Rhesus macaques has shown local areas of high T2* values in T2* maps correlating with spiral arteries (Schabel et al. 2016); a slow spread of signal intensity enhancement from a spiral artery across lobule to periphery has been shown in a naturally occurring Rhesus macaque model of fetal growth restriction (Lo et al. 2018). Calculations of T2* values should therefore ideally encompass the whole placental volume or at least an average of several slices

encompassing both the maternal and fetal placental interface. Uterine contractions have been found to reduce T2* values (Sinding, Peters, Frøkjær, et al. 2016). T2* values are also inherently affected by magnetic field strength and there remains a lack of literature reporting mean T2* in uncomplicated pregnancies at 3 Tesla.

1.5.2.3 Diffusion

Measures of diffusivity have also been mainly studied in pregnancies complicated by fetal growth restriction rather than in hypertensive disorders. Reduced placental apparent diffusion coefficient (ADC) values in growth restriction have implicated a phenotype with restricted diffusion (Bonel et al. 2010) in a retrospective cohort of 102 singleton pregnancies, of whom 33 were classified as having placental insuffiency by ultrasound imaging. Another study (Javor et al. 2013) showed maximum diffusivity, mean diffusivity and fractional anisotropy values reduced in 14 cases of fetal growth restriction, imaged between 22 to 35 weeks gestation. Phase contrast angiography in six cases of preeclampsia showed higher mean velocity with a wider range of velocities compaired to controls, suggesting the presence of resistance in the fetal villous circulation or altered villous branching and villous tone (Dellschaft et al. 2020).

The effect of gestational age and sampling site has been explored in a study examining only uncomplicated pregnancies (Capuani et al. 2017). ADC values were negatively correlated with gestational age but only after 30 weeks' gestation in the peripheral placenta. Prior to 30 weeks' gestation the ADC was not dependent on gestational age. There was also a positive linear correlation between perfusion fraction and gestational age in the central and peripheral placenta after 30 weeks. In a more recent study (Siauve et al. 2019), ADC values had a quadratic correlation with gestational age; ADC increased between 16-22 weeks' gestation, remained stable and then decreased after 28 weeks' gestation. These results perhaps reflect parenchymal changes with initial placental angiogenesis in the first and second trimester, followed by villi maturation, calcium deposition and fibrosis in the third trimester. Techniques coupling diffusion with T2 relaxometry (Melbourne et al. 2019; Slator et al. 2019) may help to further probe the underlying biological processes.

1.5.2.3.1 Intravoxel incoherent motion, IVIM

The placenta is highly vascularised and by varying the gradient fields applied, imaging can be sensitive to the microcirculation of blood in the capillary network. With strong gradients, the signal loss is due to diffusion, while with weak gradients, the signal loss can be secondary to the microcirculation of blood in the capillary network. Intravoxel

incoherent motion (IVIM) is a technique which is sensitive to the microscopic movement of water due to diffusion as well as capillary perfusion. Studies have shown pregnancies complicated by fetal growth restriction have a reduction in IVIM measures of perfusing fraction (Derwig, Lythgoe, et al. 2013; Moore et al. 2000; Siauve et al. 2019)

There are a few studies using IVIM as a technique in women with preeclampsia. One study found a reduced fraction of moving blood at the basal plate in those with preeclampsia (Moore et al. 2000). Given this area is within the region of spiral arteries, it is suggested that this reduction may be secondary to inadequate spiral artery remodelling (and thus narrow spiral artery lumen) or fewer spiral arteries transformed. However, early and late onset preeclampsia may have a different disease aetiology. In those with early preeclampsia, there was a smaller placental perfusion while those with late preeclampsia had a larger perfusion fraction compared to normal controls (Sohlberg et al. 2014).

1.6 Placental biomarkers in hypertensive disorders of pregnancy

1.6.1 Placental growth factor, PlGF

PlGF is a proangiogenic factor and member of the vascular endothelial growth factor (VEGF) family of signalling proteins (De Falco 2012) . This family of proteins is involved in angiogenesis and all share biochemical and functional features. During pregnancy, PlGF is predominantly expressed in the vasculosyncytial membrane of the villous trophoblast (Khaliq et al. 1996), thus suggesting its integral role in placental angiogenesis during invasion of the trophoblast into the maternal decidua. Under normal physiological conditions, PlGF is expressed in low levels in the heart, lung, thyroid, skeletal muscle and adipose tissue (Persico, Vincenti, and DiPalma 1999; Viglietto et al. 1995; Voros et al. 2005).

PlGF is encoded by the PlGF gene on chromosome 14 (Maglione et al. 1993) and alternative splicing gives rise to four different isoforms, PlGF 1-4. PlGF-1 and PlGF-3 are non-heparin diffusible isoforms while in contrast, PlGF-2 and PlGF-4 have heparin binding domains and are membrane associated (Yang et al. 2003). PlGF exerts its proangiogenic, anticoagulant and vasodilatory activity through binding to fms-like tyrosine kinase 1 receptor (flt-1, also known as VEGFR-1) on trophoblast membranes (Shore et al. 1997).

1.6.1.1 PlGF concentrations in pregnancy

In normal uncomplicated pregnancies, PlGF concentrations in the maternal circulation increase until 29-32 weeks and then subsequently decline until delivery (Levine et al. 2004;

Romero et al. 2008; Saffer et al. 2013). Given the hypothesized role of PlGF in placentation, PlGF concentrations in women with preeclampsia and their potential clinical utility have been investigated. Studies have shown low maternal concentrations of PlGF in preeclampsia (Livingston et al. 2000; Staff et al. 2013; Wikström et al. 2007) including cases of preeclampsia with a background of chronic kidney disease and chronic hypertension (Bramham et al. 2016). Reduced PlGF concentrations predict the subsequent development of preeclampsia (Levine et al. 2004) and in women presenting with suspected preeclampsia, there is high sensitivity and negative predictive value for the development of preeclampsia requiring delivery within 14 days (Chappell et al. 2013). The clinical utility of PlGF testing has been shown to reduce time to diagnosis of preeclampsia and suggested to reduce incidence of maternal adverse outcomes through targeted enhanced surveillance with knowledge of PlGF result (Duhig et al. 2019).

In the context of preeclampsia, factors which may influence PlGF concentrations include hypoxia and sFlt-1. The prominent expression of PlGF in cultured trophoblast cells can be down regulated by hypoxia (Shore et al. 1997). It therefore suggests that low oxygen levels or fluctuations in oxygen may lead to low PlGF production by trophoblast and altered release into the maternal circulation. In preeclampsia, this hypoxia is thought to originate through abnormal placentation. In addition to flt-1 receptors on the trophoblast membrane, PlGF can bind to circulating sFlt-1 which is a soluble variant of flt-1 receptor.

1.6.2 sFlt-1

In preeclampsia, it has been suggested that excess placental sFlt-1 binds to circulating PlGF (as well as VEGF), resulting in a reduction in the bioavailability of PlGF binding to Flt-1 membrane receptor. Animal studies have shown that administering sFlt-1 to pregnant rats induces a preeclamptic phenotype with hypertension, proteinuria and glomerular endotheliosis (Maynard et al. 2003). In human studies (Hertig et al. 2004; Levine et al. 2004), increasing levels of sFlt-1 can be found five weeks prior to the onset of clinical preeclampsia. This is accompanied by a decrease in concentrations of free PlGF and VEGF.

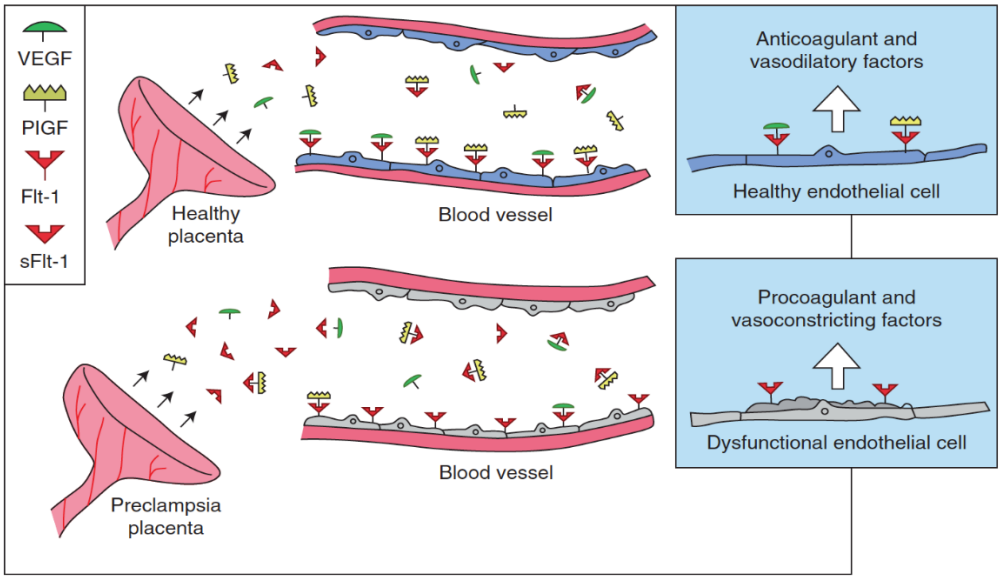

Figure 1.8: VEGF signalling and the role of sFlt-1 in maternal endothelial dysfunction as illustrated in Karumanchi et al. 2005

The clinical utility of sFlt-1 in combination with PlGF, in women suspected of having preeclampsia has been explored in several studies. A high sFlt-1/PlGF ratio in women presenting at less than 34 weeks' gestation with suspected preeclampsia, predicted adverse maternal and perinatal outcomes and correlated with duration of pregnancy (Rana et al. 2012). The sFlt-1/PlGF ratio had a better performance than either sFlt-1 or PlGF alone. A prospective multicentre observational study in a large cohort of 500 women suspected of preeclampsia, found that an sFlt-1/PlGF ratio of 38 or lower could predict short term absence of preeclampsia (Zeisler et al. 2016).

1.6.3 Vascular cell adhesion molecule-1, VCAM-1

The vascular endothelium is lined by a protective layer termed the endothelial glycocalyx. This layer affects blood cell to vessel wall interactions and acts as a gatekeeper between the endothelial cell surface and blood flow, thus influencing vascular permeability (Reitsma et al. 2007). The endothelial glycocalyx incorporates soluble molecules (which are either plasma or endothelium derived) to modulate function. Vascular cellular adhesion molecule, VCAM-1, is one such molecule and therefore a component of the endothelial glycocalyx.

The function of VCAM-1 is to mediate leukocyte endothelial adhesion. A study including non-pregnant women has shown that the concentrations do not differ from those with normal uncomplicated pregnancies (Austgulen et al. 1997). There is also no change in VCAM-1 concentration over gestation in those with normal pregnancies (Austgulen et al. 1997; Krauss et al. 1997).

High plasma concentrations of VCAM-1 are hypothesized to represent damage to the endothelial glycocalyx. Given the underlying pathology of preeclampsia is thought to involve endothelial cell damage, several studies have examined VCAM-1 as a biomarker for preeclampsia. These have consistently shown that VCAM-1 concentrations are higher in women with preeclampsia (Austgulen et al. 1997; Chaiworapongsa et al. 2002; Kim et al. 2004; Krauss et al. 1997). Plasma VCAM-1 can additionally distinguish superimposed preeclampsia from those without superimposed preeclampsia in women with chronic kidney disease (Wiles et al. 2019). Longitudinal profiles showed high levels of VCAM-1 in women 5-15 weeks prior to a clinical diagnosis of pre-eclampsia, thus suggesting a role in prediction (Krauss et al. 1997). However, this incorporates a large range of time and further studies are currently lacking.

1.6.4 Hyaluronan

Hyaluronan is a linear polysaccharide with high water binding capacity. It is another component of the endothelial glycocalyx where it can be bound to receptor CD44 (Nandi, Estess, and Siegelman 2000). Hyaluronan-hyaluronan complexes are thought to have a role in stabilising the luminal glycocalyx (Scott and Heatley 1999). In addition, hyaluronan has a role in motility, cell-cell and cell-matrix adhesion. Fibroblasts produce hyaluronan as a component of the extracellular matrix.

High plasma hyaluronan concentrations can be found in sepsis, thus indicating a role in inflammation (Berg 1997). This relationship is further strengthened by the observation that hyaluronan concentrations correlate with sepsis severity and prognosis. It remains uncertain whether the high concentrations are secondary to increased production or reduced clearance by lymph nodes and liver or both.

Given the hypothesized roles of this biomarker, hyaluronan in the context of pregnancy and hypertensive disorders have been explored. Hyaluronan can be found in mesenchymal villi, especially in the first trimester, where the angiogenic, proliferative and differentiative processes take place (Marzioni et al. 2001). High concentrations of hyaluronan have been found in women with preeclampsia (Matejevic et al. 1999; Berg et al. 2001) and in uncomplicated pregnancies hyaluronan has not been found to be gestational dependent (Osmers et al. 1998). Interestingly, high concentrations of hyaluronan did not differ between early or late onset preeclampsia (Kornacki, Wirstlein, and Wender-Ozegowska 2019) but could differentiate women with preeclampsia from women with gestational hypertension (Romão et al. 2014). A recent study showed that hyaluronan was higher in

women with preeclampsia superimposed on chronic kidney disease compared to women with chronic kidney disease and no superimposed preeclampsia (Wiles et al. 2019). Hyaluronan therefore has the potential to help distinguish those women with preeclampsia in groups where diagnosis may be unclear clinically.

1.6.5 Placental biomarkers in this thesis

Angiogenesis related biomarkers PlGF and sFlt-1 and endothelial glycocalyx related biomarkers VCAM and hyaluronan have shown promise in their use as a predictive and diagnostic test for preterm preeclampsia. Measurement of angiogenic and anti-angiogenic factors remain the leading commercially available test to aid the short term diagnosis of preeclampsia requiring delivery within two weeks (McCarthy, Ryan, and Chappell 2018). Additionally, both PlGF and sFlt-1 as a single angiogenesis-related biomarker were found to be a useful diagnostic test for women presenting with suspected preterm preeclampsia when compared to 47 biomarkers (Duckworth et al. 2016).

In this exploratory study, VCAM and hyaluronan were additionally measured as the development of superimposed preeclampsia in women with chronic hypertension was of interest. Both VCAM and hyaluronan distinguished women with chronic kidney disease and superimposed preeclampsia from those without superimposed preeclampsia when compared with other plasma biomarkers derived from the endothelial glycocalyx (intercellular adhesion molecule, P-selectin, E-selectin) and those derived from complement activation (C3a, C5a, complement factor H, C5b-9) (Wiles et al. 2019). The literature on superimposed preeclampsia is sparse. Biological plausibility was therefore applied to examine the best performing biomarkers, whilst acknowledging that chronic kidney disease may have a different pathophysiological pathway compared to chronic hypertension.

1.7 Summary

Preeclampsia and chronic hypertension are both associated with adverse pregnancy outcome. MRI offers potential for non-invasive high resolution multimodal direct *in vivo* assessment of the placenta. MRI measures of structure and function may help to understand disease aetiology. In combination with placental biomarkers, this may increase our understanding of pathophysiological mechanisms.

Chapter 2 HYPOTHESES, RESEARCH QUESTIONS AND OBJECTIVES

The subject of this thesis is the use of placental magnetic resonance imaging in preeclampsia and chronic hypertension. The hypotheses, research questions and objectives for each workstream are outlined below.

2.1 Hypotheses

- Placental magnetic resonance imaging in pregnancy, including imaging those with chronic hypertension and preeclampsia, requires bespoke protocols.

- Visual assessment of magnetic resonance imaging provides an insight into gross placental structure and aids the development of quantitative analysis.

- In women with preeclampsia and chronic hypertension, magnetic resonance imaging identifies a placental phenotype that assists in identification of women and fetuses at risk of adverse pregnancy outcome.

- Biomarkers in chronic hypertension and preeclampsia aid understanding of placental magnetic resonance imaging measures.

2.2 Research questions and objectives

2.2.1 How can the placenta be optimally visually assessed *in vivo* using magnetic resonance imaging?

Objective: To optimise magnetic resonance imaging and associated measures in women with preeclampsia and chronic hypertension (Chapter 3)

2.2.2 What are the acceptance and unexpected findings rates of magnetic resonance imaging in women with preeclampsia and chronic hypertension?

Objectives: To determine the acceptance rate of magnetic resonance imaging in women with preeclampsia and chronic hypertension (Chapter 3) and to describe potential unexpected findings in MRI performed for research during pregnancy (Chapter 7).

2.2.3 Can advanced techniques of T2* mapping and diffusion elucidate the underlying mechanisms of preeclampsia and chronic hypertension?

Objectives: To investigate cross-sectional placental changes in preeclampsia and thus provide an insight into the pathophysiology of preeclampsia (Chapter 4) compared to controls and to investigate cross-sectional placental changes in chronic hypertension and thus provide an insight into the heterogeneity of pregnancy outcomes (Chapter 5) compared to controls.

2.2.4 Do placental biomarkers further our understanding of placental changes observed in magnetic resonance imaging?

Objective: To explore changes in associated placental biomarkers PlGF, sFlt-1, VCAM and hyaluronan in women with preeclampsia and chronic hypertension and to describe them in the context of placental T2* values obtained from magnetic resonance imaging (Chapter 6).

Chapter 3 OPTIMISATION OF METHODS

This prospective, observational study was embedded within the National Institutes of Health (NIH) funded Placenta imaging Project (Structure and function of the placenta from implantation to delivery: a next generation MRI approach). The aim of the Placenta imaging Project is to develop a novel magnetic resonance approach to assess growth and development of the human placenta in health and disease. The project is currently recruiting until late 2020 and therefore imaging techniques were continually being optimised during this study and remain in development.

Work for this study commenced in April 2017 with specific ethics approval for the main Placental Imaging Project. I led an application for an ethics amendment to include recruitment of a group of hypertensive women to the Placenta imaging Project, in addition to writing standard operating procedures for maternal blood sampling and processing. I created a study database using a REDCap platform for the Placental Imaging Project, written following self-training through online resources, and with subsequent support from divisional personnel. Variables recorded included maternal characteristics at enrolment, pregnancy outcome variables, safety monitoring documentation (maternal blood pressure, temperature pre and post imaging), barcodes for blood samples and imaging specific data which could be piped into scripts for automatic processing.

3.1 Practicalities of imaging women with hypertension in pregnancy

Two research scanners were available for this study: a 1.5T Philips Ingenia (with a magnet bore size of 70cm) and a 3T Phillips Achieva scanner (with a magnet bore size of 60cm).

3.1.1 3T Philips Achieva scanner

Initial optimisation was started on the 3T Phillips Achieva scanner as the high field strength confers a greater signal-to-noise ratio. This occurs because the signal generated is proportional to the square of the static field strength while noise increases linearly with increasing field strength. Generating a signal from gradient-echo sequences used in diffusion are especially difficult, thus the higher field strength is especially advantageous.

The 3T Phillips Achieva scanner in our unit is limited by a bore size of 60 cm and a maximum body mass index of 30kg/m^2. The body mass index was therefore used as a screening tool to assess participant comfort and suitability in the scanner, however; it became evident that a high body mass index could have a varied body mass distribution

and thus not necessarily reflect abdominal girth contribution. Some women with a body mass index greater than 30kg/m^2 could therefore be imaged, especially up until the early second trimester and if lying supine rather than in left lateral tilt position. I therefore designed and constructed a plastic arch to model the size of the scanner bore. It was subsequently used when approaching women for the study in the antenatal clinic and antenatal ward to assess suitability for the scanner when women were supine. The arch also gave women an idea of what to expect in terms of space within the scanner bore.

Figure 3.1: Laser cut plastic arch template of 3T scanner bore.

3.1.2 1.5T Philips Ingenia

Although imaging on the 1.5T Ingenia scanner increases potential applicability by including women of a higher body mass index and advanced gestation, there are several factors to consider when comparing to imaging at 3T. The reduced field strength of 1.5T results in a reduced signal-to-noise ratio. In addition, the increased body habitus introduces noise and reduces radiofrequency depth penetration with the receiver coils at an increased distance to the placenta, further reducing the signal-to-noise ratio.

The high signal-to-noise ratio in 3T imaging is exploited to improve image quality (through increased in plane resolution) or reduce scan time by reducing slice thickness. However, artefacts from maternal respiration and fetal motion may be more prominent in 3T imaging and therefore the reduction in signal-to-noise ratio at 1.5T may confer an advantage. 1.5T imaging has the additional advantage of a reduced specific absorption rate (as it is proportional to the static field squared) and a reduction in acoustic noise with less intense gradient switching.

3.1.3 Maternal positioning

In this study, we chose to image women supine rather than in left lateral tilt (see 1.4.4 regarding safety considerations). MRI scanners, along with their anterior receiver coils, were designed for supine imaging to improve the signal to noise ratio and homogeneity of signal. Supine imaging therefore confers an advantage in that it enables an improved proximity of the receiver coil to the large field of view given by the gravid uterus, and therefore an improvement in signal detection compared to left lateral tilt imaging. A high signal-to-noise ratio is also advantageous in women with high body mass index and posterior placentas as the distance between the placenta and receiver coil are greater. The limited bore size can also better accommodate women in the supine rather than left lateral tilt position and consistency in sequence planning is more easily achieved compared to inconsistent tilt angles when placing a woman in left lateral. A short period of lying left lateral prior to slowly rotating to supine position for imaging can successfully shift the fetal position to minimise inferior vena cava compression (Hughes et al. 2016; Hughes et al. 2021).

In anticipation of potential effects of lying supine, from both a symptomatic and clinical perspective in terms of blood pressure, all women were imaged with the presence and support of either a midwife or obstetrician. In addition, women were placed in a left lateral tilt prior to rotation to supine for imaging. A blood pressure was taken every 10 minutes during imaging with concomitant heart rate and oxygen saturation monitoring. Any fall in blood pressure was assessed in conjunction with maternal heart rate and repeated to ensure no further clinically significant fall. Verbal communication with the woman was maintained throughout and assessed for symptoms on direct questioning. If the blood pressure remained stable and the woman reported that she was asymptomatic then scanning continued.

The effect of lying supine on blood pressure was evaluated. Upon lying supine, the systolic blood pressure fell from a mean of 105mmHg (95% CI 101-109) to 98mmHg (95% CI 97-101) in the control group, 139mmHg (95% CI 136-142) to 128 (95%CI 125-132) in the preeclamptic group and 125mmHg (95% CI 121-129) to 112mmHg (95%CI 109-115) in the chronic hypertensive group. The diastolic blood pressure fell by a smaller degree: from 64mmHg (95% CI 60-67) to 59mmHg (95%CI 57-61) in the control group, 88mmHg (95%CI 82-93) to 83mmHg (95%CI 79-86) in the preeclamptic group and 78mmHg (95%CI 75-82) to 71mmHg (68-74) in the chronic hypertensive group. These findings were consistent with clinical variance seen in 24-hour ambulatory blood pressure monitoring of women with

hypertensive disorders of pregnancy on treatment (Shawkat et al. 2018) and the variance seen in home versus clinic blood pressure readings (Kalafat et al. 2018).

In order to assess stability of blood pressure during imaging, the standard deviation of systolic and diastolic blood pressure readings during imaging were compared between groups. The systolic blood pressure was 49% more variable in the preeclamptic group versus controls (geometric mean ratio 1.49) and 24% more variable in the chronic hypertensive group versus controls (geometric mean ratio 1.24). The diastolic geometric mean ratio in the preeclamptic group versus controls was 0.95 and in the chronic hypertensive group versus controls 1.02. Maternal lie supine or left lateral, 30 and 7 cases respectively, had no significant effect on mean T2* values in our control group (Fisher's exact tests, $p = 0.44$).

3.1.4 Recruitment

Women were eligible for inclusion in the study if they had a singleton pregnancy, were at or over 16 years of age and able to give informed consent. Exclusion criteria were as follows: under 16 years of age, contraindication for magnetic resonance imaging (e.g. implanted electric and electronic devices), intracranial metal clips, metallic bodies in the eyes, surgery in the preceding 12 weeks and claustrophobia. Maternity notes were screened for eligibility before being approached for the study.

Women with preeclampsia and chronic hypertension were imaged when clinically stable and at a time which minimised disruption from clinical care. In this unit, all women with preeclampsia are admitted to the antenatal ward until delivery. They were therefore approached in person on the antenatal ward. The optimal time to image them was therefore in the late morning following administration of antihypertensive medication, cardiotocography monitoring and review by the attending consultant.

Women with chronic hypertension are seen in a specialist hypertension clinic at St Thomas' Hospital. Given the frequency of antenatal clinic appointments required for management of women with chronic hypertension, these women were often imaged on the same day as their antenatal clinic appointment in order to avoid repeated travel to and from the hospital.

Participant flow charts for the first six months of recruitment (April 2017 until September 2017) are shown below (Figure 3.2, Figure 3.3). Initial optimisation work occurred on the 3T Philips Achieva. 15 women with chronic hypertension and 4 women with preeclampsia

were imaged during this time period. Reasons for a failed metal check included past surgical histories of a gastric sleeve operation, patent ductus arteriosus occlude insertion, aneurysm coil insertion following renal nephrectomy, orbit reconstruction and clips from laparoscopic cholecystectomies. Common reasons for declining the study included claustrophobia, duration of imaging, potential for unexpected findings, difficulties in taking time off work or finding childcare.

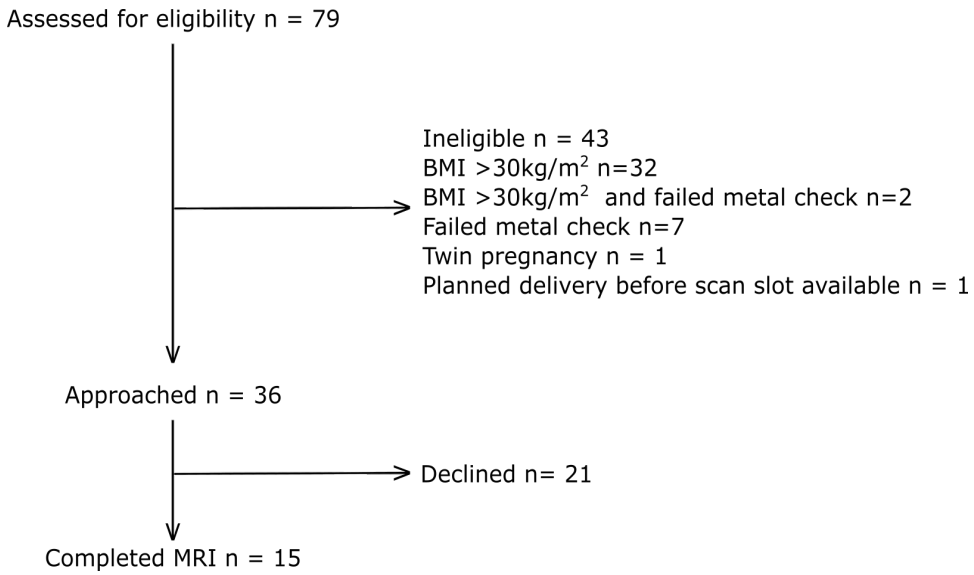

Figure 3.2: Participant flow chart for women with chronic hypertension from April 2017 – September 2017 inclusive.

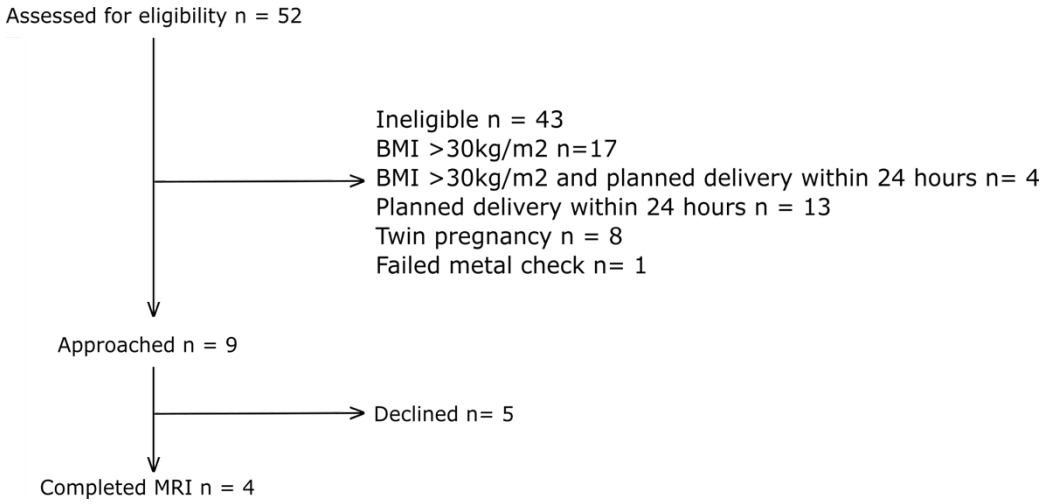

Figure 3.3: Participant flow chart for women with preeclampsia from April 2017 – September 2017 inclusive.

After initial optimisation work on the 3T Philips Achieva, optimisation work on the 1.5T Philips Ingenia followed. The scanner was required given the high prevalence of obesity in women with preeclampsia and chronic hypertension. Obesity is an additional risk factor for adverse pregnancy outcomes such as preeclampsia, stillbirth and neonatal death (Chu et al. 2007; Heslehurst et al. 2007) and therefore including these women in the study was of particular interest. The larger bore size of the 1.5T Ingenia scanner enabled imaging of women with a higher body mass index, greater abdominal girth and at later gestations more comfortably. In addition, the Ingenia had a field strength of 1.5T which is more widely available in the clinical setting amongst other obstetric units (thus enabling reproducibility and applicability) while a variety of implanted devices are compatible in a 1.5T scanner but not 3T. The impact of imaging at different field strengths on data produced is discussed in 0.

3.1.5 Claustrophobia and reasons for declining participation

In this study, 10 out of 49 women (20%) who gave a reason for declining participation cited claustrophobia. A video link demonstrating a pregnant woman undergoing magnetic resonance imaging was sent to all women who were approached for participation in the study and therefore helped to anticipate those with claustrophobia. One out of 62 women (2%) in the hypertensive group and five out of 86 women (6%) in the control group were unable to complete the imaging protocol due to claustrophobia. Claustrophobia was apparent within minutes of trying to enter the magnet bore in all cases. As heart rate and blood pressure monitoring was documented at ten-minute intervals and women left the scanner when they became claustrophobic, there are no data on potential heart rate or blood pressure changes in women with claustrophobia. The woman in the hypertensive group, returned as a participant in the study in a subsequent pregnancy a year later. Following her previous feedback we implemented additional measures which included additional time scheduled for entering the scanner and breaks, removal of pillow, minimised padding inside bore, increased communication from radiographer and own music playing prior to commencing the imaging protocol. The participant found the new measures made the scanning procedure acceptable and was able to complete the imaging protocol at 28 weeks and 33 weeks.

Other reasons for declining participation included 16 women (33%) under the impression that they had too many clinic and scan appointments already, 11 women (22%) who declined participation in all research (regardless of the study presented), 5 women (10%) who were concerned about the safety of magnetic resonance imaging, 3 women (6%) who

felt that the appointment for imaging was too long, 2 women (4%) who were concerned about the noise of the scanner and 2 women (4%) who were concerned that imaging would reveal an unexpected finding.

3.1.6 Sample size

No formal sample size was calculated for power of outcome variables as this was an exploratory study describing a novel technique in technology development application. However, using an optimised protocol, we aimed to enrol 20 women with preeclampsia, 40 women with chronic hypertension and 60 women as healthy controls as previous studies in the literature have used a similar sample size (Damodaram et al. 2010).

The use of the 1.5T Ingenia commenced in January 2018 and enrolment continued using both scanners until April 2019. A total of 55 women with chronic hypertension, 24 with preeclampsia and 100 uncomplicated pregnancies were enrolled (Table 3.1). The last woman in the study delivered in August 2019.

Table 3.1: Number of woman imaged using optimised protocols.

	Chronic hypertension	**Preeclampsia**	**Control**
Optimised 3T T2-weighted and T2* mapping protocol	30	14	70
Optimised 1.5T T2-weighted and T2* mapping protocol	13	5	16
Optimised 3T diffusion protocol	7	3	21

The following sections will now describe placental imaging techniques currently in development. As this is an exploratory study that includes optimisation of scanning protocols and processing, not all techniques were performed on all women. However, all women had a basic core of anatomical T2-weighted imaging of the fetal brain that was suitable for clinical reporting and made available to the clinical team.

3.2 T2-weighted imaging

T2-weighted imaging, the core of most antenatal imaging examinations, was optimised to improve visual analysis for this study. T2-weighted imaging is achieved through a spin echo sequence. In a spin-echo sequence, a pair of radiofrequency pules are applied – a 90° radiofrequency pulse followed by 180° radiofrequency pulse. The signal therefore decays initially but then has a partial recovery ('echo') after the 180° radiofrequency pulse. A 2D Turbo Spin Echo (TSE) sequence was chosen for this study as it is fast and the 2D nature of the sequence freezes motion during acquisition, thus minimising the effect of fetal and maternal breathing motion. Other factors taken into account for the T2-weighted imaging sequence parameters were the image contrast, signal-to noise ratio, time taken for image acquisition, safety limits and ease of placental localisation post imaging.

3.2.1 Image contrast in T2-weighted imaging

In vivo features of placental maturation have been described using ultrasound and MRI. Ultrasound assessment of the placenta using the Grannum grading system (Grannum, Berkowitz, and Hobbins 1979) correlates weakly with adverse perinatal outcome and has poor interobserver agreement (Sau, Seed, and Langford 2004) but is described as follows (Figure 3.4).

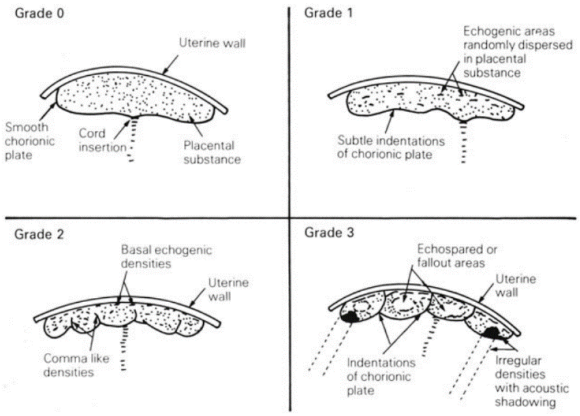

Figure 3.4: Grannum grading system, as described by Grannum et al., 1979.

A similar grading system using T2-weighted magnetic resonance imaging at 1.5T has been proposed but its application to pregnancy complications and adverse pregnancy outcomes warrant further investigation (Blaicher et al. 2006)(Figure 3.5).

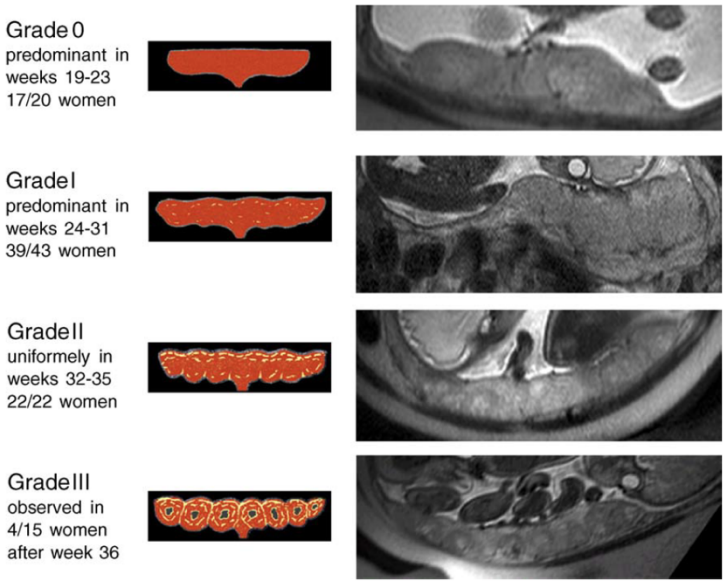

Figure 3.5: Proposed placenta grading system using T2-weighted MRI by Blaicher et al., 2006

Given these descriptors of placental maturation, a T2-weighted imaging sequence was modified to provide appropriate contrast sensitive to granularity, lobularity and signal intensity heterogeneity within the placenta. This process was undertaken initially at 3T and subsequently at 1.5T.

3.2.1.1 Echo time, TE

The time between the radiofrequency excitation pulse and when the signal was measured (TE, echo time) influences the contrast. The T2 decay time is inherent to the placental tissue and thus an appropriate echo time must be chosen to optimise contrast within the placenta. Images obtained at longer echo times have a better contrast than images obtained at shorter times, which do not allow as much time for T2 decay differences to appear. A further constraint of short echo times is that in order to achieve shorter echo times, the image acquisition (specifically the read-out) must be accelerated using techniques such as SENSE (sensitivity encoding). Their use can in turn reduce the signal-to-noise ratio.

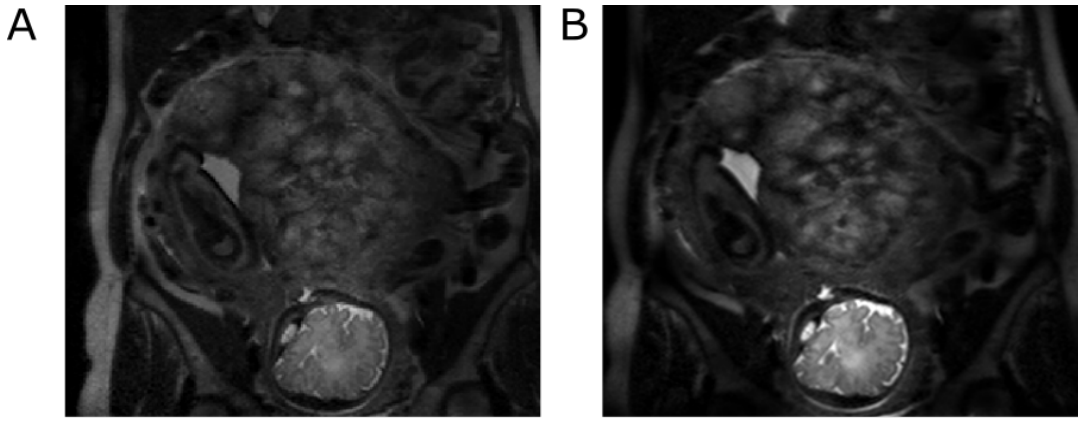

**Figure 3.6: Effect of echo time (TE) on contrast. (A) short TE. (B) long TE.
Note the influence of the higher acceleration factor (SENSE factor) for (A) leading to reduced signal-to-noise ratio.**

3.2.2 Field strength

A small number of women were imaged on both scanners to assess whether data quality was comparable and to document any systematic differences. Imaging was performed on the same day. The T2-weighted images taken on the 1.5T and 3T have comparable image quality (Figure 3.7). In both sets of images, placental lobularity, signal intensity homogeneity and granularity are visually similar. However, there is a higher signal-to-noise ratio and resolution at 3T. In order to achieve imaging on both scanners in the same woman, the body mass index was less than 30kg/m^2, and thus the impact of signal-to-noise ratio at 1.5T may not be as marked in these examples.

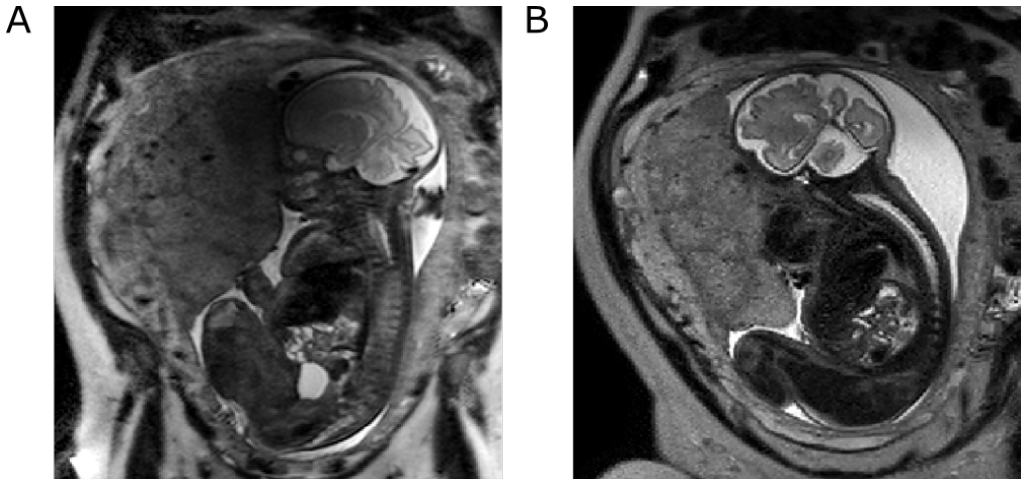

Figure 3.7: T2-weighted images taken on the same day of the same woman (A) 3T Achieva (B) 1.5T Ingenia

Figure 3.8 further illustrates the image quality in T2-weighted imaging at 1.5T. Despite a high body mass index of 34kg/m^2 and a posteriorly located placenta (the latter of which further reduces the signal-to-noise ratio), placental lobularity, granularity and signal intensity homogeneity can be visualised. However, the reduction in signal-to-noise ratio is more evident in comparison Figure 3.7 (B).

Figure 3.8: T2-weighted imaging at 1.5T with a high body mass index and posteriorly located placenta

Final parameters chosen were TE = 190ms, TR = 16s, SENSE 2.5, partial Fourier 0.625 for imaging on the 3T Phillips Achieva scanner.

3.2.3 Plane and field of view

Conventional acquisition protocols use an approach in which slices are positioned according to the region of interest. T2-weighted imaging was initially performed parallel to the basal plate but was challenging due to varying placental positions which included lateral and fundal in addition to posterior and anterior. This resulted in an increase in scan times to incorporate image acquisition planning for individual women.

In order to overcome this, T2-weighted imaging of the whole uterus was acquired both in the sagittal and coronal plane, orientated to maternal position and not placental site. A consistent maternal-centric approach, rather than placenta centric approach, allowed for swift ease of planning and accommodated all placenta locations. Capturing the whole uterus in the field of view, ensured that the whole placenta was efficiently visualised. The development of motion corrected image reconstruction methods, such as Slice-to-Volume

(SVR) (Kuklisova-Murgasova et al. 2012), do not require in-plane acquisitions and thus this maternal-centric approach provided data suitable for potential 3D reconstructive purposes.

3.3 T2 relaxometry

Gradient-echo sequences (in contrast to spin-echo sequences) have a single radiofrequency pulse, followed by a gradient to rephase the spins. The gradient does not refocus field inhomogeneities and therefore gradient-echo sequences are inherently T2* weighted.

The sequence chosen to achieve T2* maps of the placenta was a multi-echo, gradient echo, echo planar imaging sequence (MEGE EPI). By acquiring subsequent images at increasing echo times, the signal decay is sampled and can be consequently fitted to a mono-exponential decay model as it is assumed that T2* decay occurs mono exponentially. The signal intensity can be derived as follows (Figure 3.9).

$$S(TE) = S_0 e^{-(TE/T2^*)}$$

S = signal intensity
TE = echo time
S_0 = signal at TE=0

Figure 3.9: Formula for calculating signal intensity.

Echo planar imaging acquires data quickly by obtaining the data required for an entire slice within <100ms. This effectively freezes motion within the slice and thus minimizes inconsistency effects from motion. The inter-echo spacing was chosen as the optimum balance between the need for short acquisition times and safe acoustic noise limits (see 1.4.3). In order to reduce the effect of inhomogeneities in the magnetic field, an in-house image based shimming technique was used after acquiring a B0 map.

In the optimised protocol for 3T scanning, 5 echo times were used: 13.81ms/ 70.40ms/ 127.00ms/ 183.60ms/ 240.2ms, TR=3s, SENSE=3, halfscan=0.6 at 3mm^3 resolution with the whole placenta covered within 60 slices. For 1.5T scanning, 5 echo times were used: 11.376ms / 57.313ms / 103.249ms / 149.186ms / 195.122ms, TR=14s, no SENSE, no halfscan at 2.5mm^3 resolution with the whole placenta covered within 90 slices.

3.3.1 T2* map placenta segmentation

Studies in the literature using T2* relaxometry have calculated mean T2* within the placenta either in a slice, the average of several slices or the whole placenta volume

(Armstrong et al. 2019; Hutter, Slator, et al. 2019; Ingram et al. 2017; Sinding, Peters, Frøkjaer, et al. 2016).

Our optimised protocol provided full placental coverage to ensure that the derived T2* values encompassed the whole placental volume and therefore accounted for the inherent heterogeneity within the placenta. This was especially advantageous as upon visual inspection of T2* maps, T2* values varied across the placenta both in the coronal and sagittal planes (Figure 3.10).

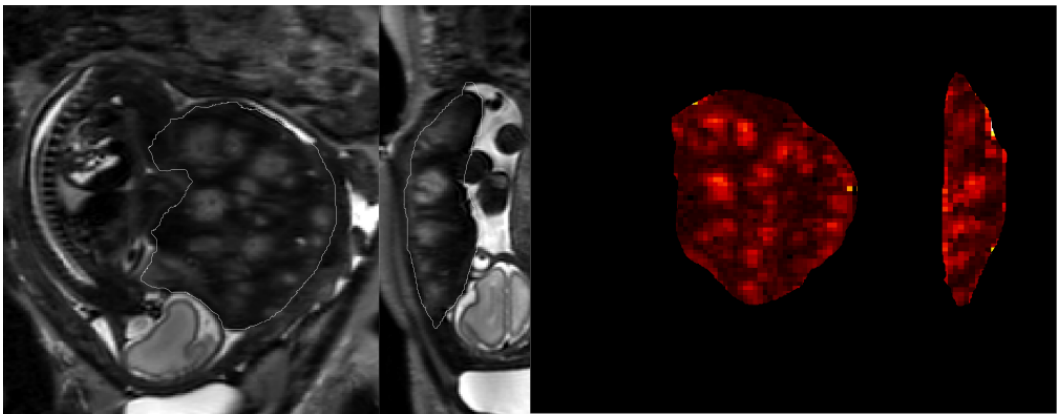

Figure 3.10: T2-weighted imaging in coronal and sagittal plane (left) with T2* map in corresponding plane (right) in a woman with preeclampsia.

To produce a T2* map of the placenta , it was initially segmented manually in MRtrix3 using the assistance of T2-weighted imaging to confirm placenta location. It was segmented conservatively, to ensure that only placental tissue was sampled without including amniotic fluid or maternal uterine wall. Non-physiological values of >200ms at 3T imaging (and >300ms at 1.5T imaging) were excluded to refine the masks. The dice coefficient of the first 84 T2* map segmentations was 0.86 between myself and Dr. Jana Hutter, a post doctoral researcher in placental imaging. In 10 randomly selected T2* maps, the intra rater variability had a dice coefficient of 0.87.

3.3.2 Quantitative assessment of T2* values in control group

3.3.2.1 Placental mean T2*

Prior to assessing values in the preeclamptic and chronic hypertensive groups, we assessed T2* data obtained from 68 women with normal pregnancy and outcome in order to explore the most appropriate modelling. Previous studies have shown a linear reduction in placental mean T2* values in uncomplicated pregnancies with increasing gestation (Sørensen et al. 2020). In this study, following pregnancy outcome data collection, normal

uncomplicated pregnancies were defined as those women who had no co-morbidities or pregnancy complications, delivering a neonate at term with a normal birthweight centile. The placental mean T2* was plotted against gestational age at imaging and a range of possible models were explored using the STATA command –xriml- to produce gestation-adjusted reference ranges. A simple linear model gave a final deviance of 612 while a linear funnel model a final deviance of 560 (Figure 3.11). The simple linear model was chosen despite a larger final deviance as data from women who were scanned twice during their pregnancy in the normal group had parallel reductions in mean T2* values with gestation (Figure 3.12).

A B

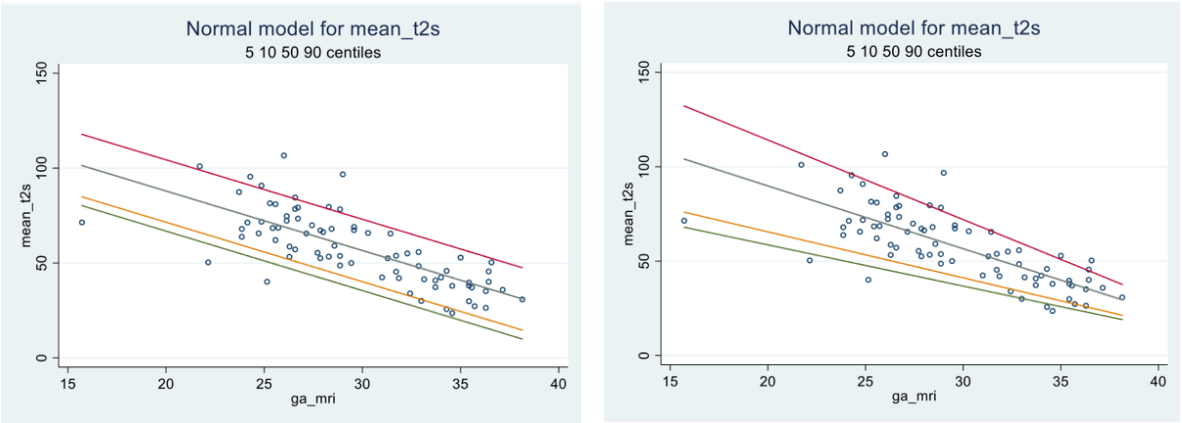

Figure 3.11: Placental mean T2* values against gestational age at imaging. (A) simple linear model (B) linear funnel model. Line in red represents 90th centile, grey 50th centile, yellow 10th centile and green 5th centile.

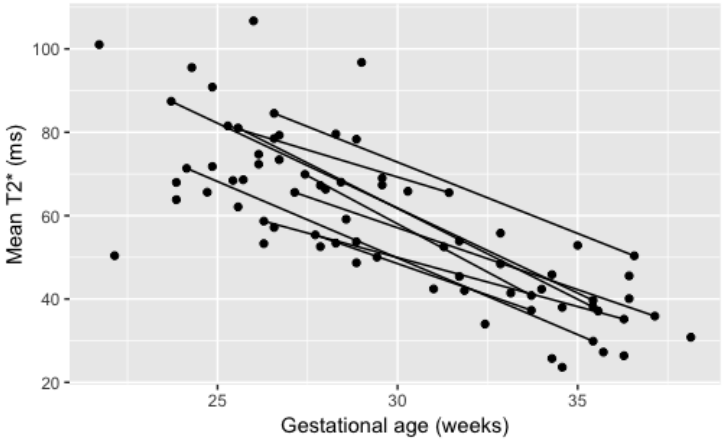

Figure 3.12: Scatterplot of mean T2* against gestational age imaged in the control group, with lines between points originating from the same woman from serial scans

T2* values are inherently affected by magnetic field strength. Given the different field strengths of the two scanners in this study, gestation adjusted reference ranges of mean T2* values were calculated for each scanner. Similar findings were noted of a linear reduction in mean T2* values with increasing gestation from 1.5T imaging, consistent with existing literature.

3.3.2.2 Measures of heterogeneity

Given visual assessment of T2* maps showed that T2* values did not uniformly decrease across the whole placenta, quantitative objective values were sought that also included measures of heterogeneity. Furthermore, as data were acquired at two different field strengths (1.5T and 3T), resulting in differences in absolute values at any given gestation (see above figures), field-strength independent parameters (and thus not absolute T2* values) were required to allow for comparisons between women despite being imaged on different scanners.

3.3.2.2.1 Histogram Asymmetry Measure

To examine the distribution of T2* values within the whole placenta, the fraction of voxels greater than 0.9 of the maximum T2* value was calculated and termed 'Histogram Asymmetry Measure.' In uncomplicated pregnancies, a scatterplot of Histogram Asymmetry Measure values against gestational age at imaging showed values close to 1 until the third trimester, followed by a decline in values (Figure 3.13). This may illustrate the biological theory that fetal demand exceeds placental supply in the third trimester and after a threshold is reached, labour is initiated.

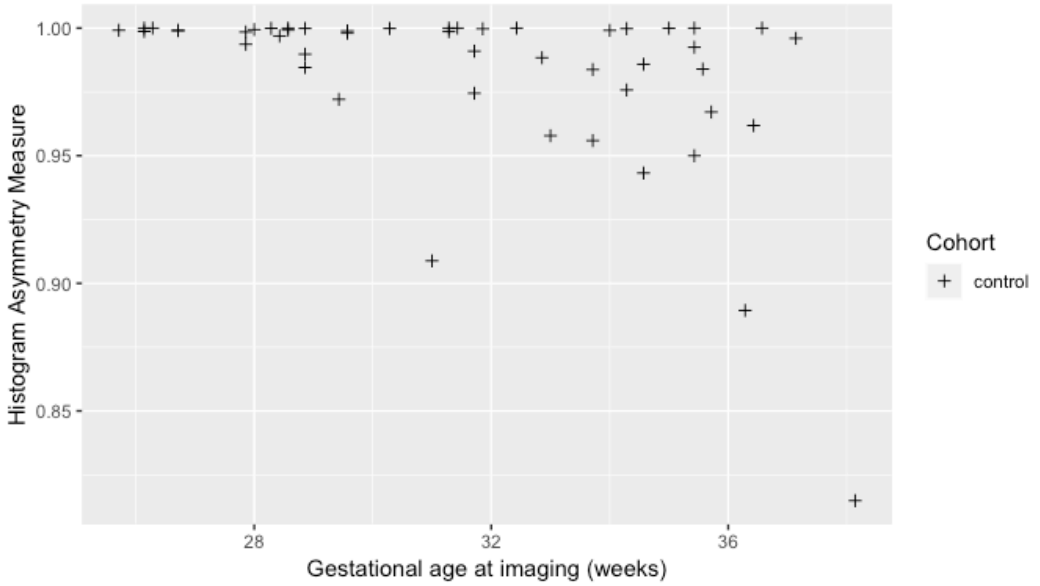

Figure 3.13: Scatterplot of Histogram Asymmetry Measure against gestational age at imaging

To explore the utlity of Histogram Asymmetry Measure further, we assessed its discriminatory utlity in a wider group of women including those with preeclampsia (Figure 3.14). An arbitrary cut off of less than 0.9 was taken as a low Histogram Asymmetry Measure Value. Ten out of 16 scans in women with preeclampsia had Histogram Asymmetry Measure values less than 0.9 and lower than gestation matched controls. In the women with preeclampsia, the time from imaging to delivery was 12 days (IQR 5-20) in those with a low Histogram Asymmetry Measure value compared to 9 days (IQR 7-20) in those with a high Histogram Asymmetry Measure value. The birthweight centile was 6 (IQR 2-26) in the low Histogram Asymmetry Measure group and also 6 (IQR 2-17) in the high Histogram Asymmetry Measure group. Co-morbidities of chronic hypertension and gestational diabetes occurred in both groups. The longer interval to delivery time in the low Histogram Asymmetry Measure group therefore did not reflect the suggestion that values reflect the interplay between fetal demand and placental supply prompting delivery. However, the contribution of potential compensatory mechanisms and the maternal response to placental dysfunction are not measured and thus these results, in a small sample size, were interpreted with caution.

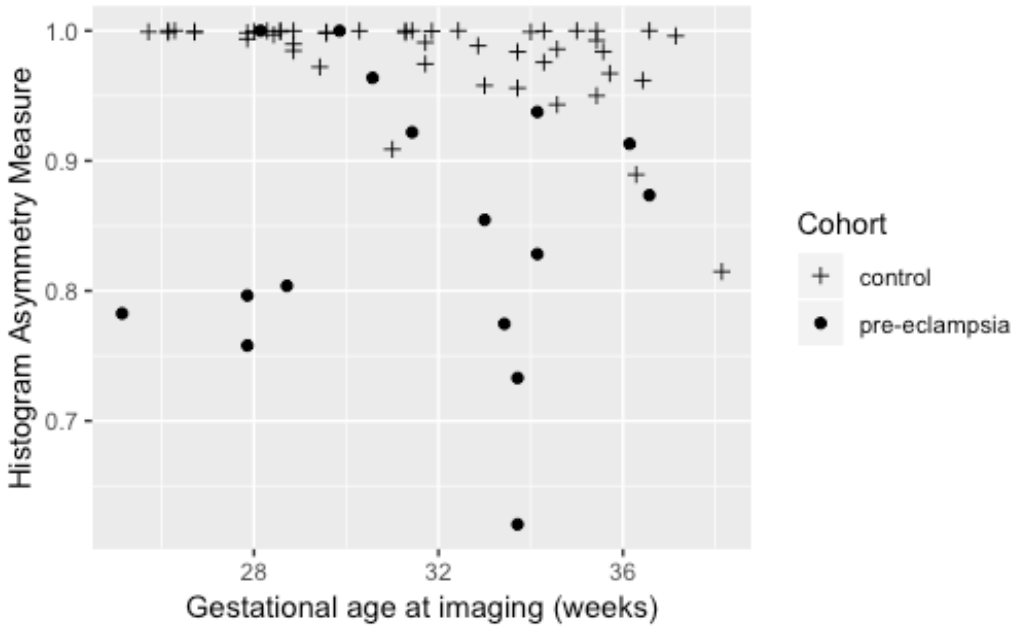

Figure 3.14: Scatter plot of Histogram Asymmetry Measure against gestational age at imaging including those with preeclampsia.

3.3.2.2.2 Lacunarity

Lacunarity reflects the spatial distribution of 'gaps' of a specific size across a region of interest and it is often described as a measure of visual texture. Low lacunarity values reflect a homogenous image with similarly sized gaps which, when rotated, do not visually change (i.e. little rotational variance). In contrast, high lacunarity reflects a heterogenous image with many differently sized gaps and high rotational variance (Karperien and Jelinek 2015)(**Figure 3.15**). Lacunarity values are calculated by gliding a box of a given size across the region of interest and therefore are influenced by box size chosen. In this study, the box size chosen was based on the expected size of a lobule in placentas from uncomplicated pregnancies, which was 2.5-3cm in diameter.

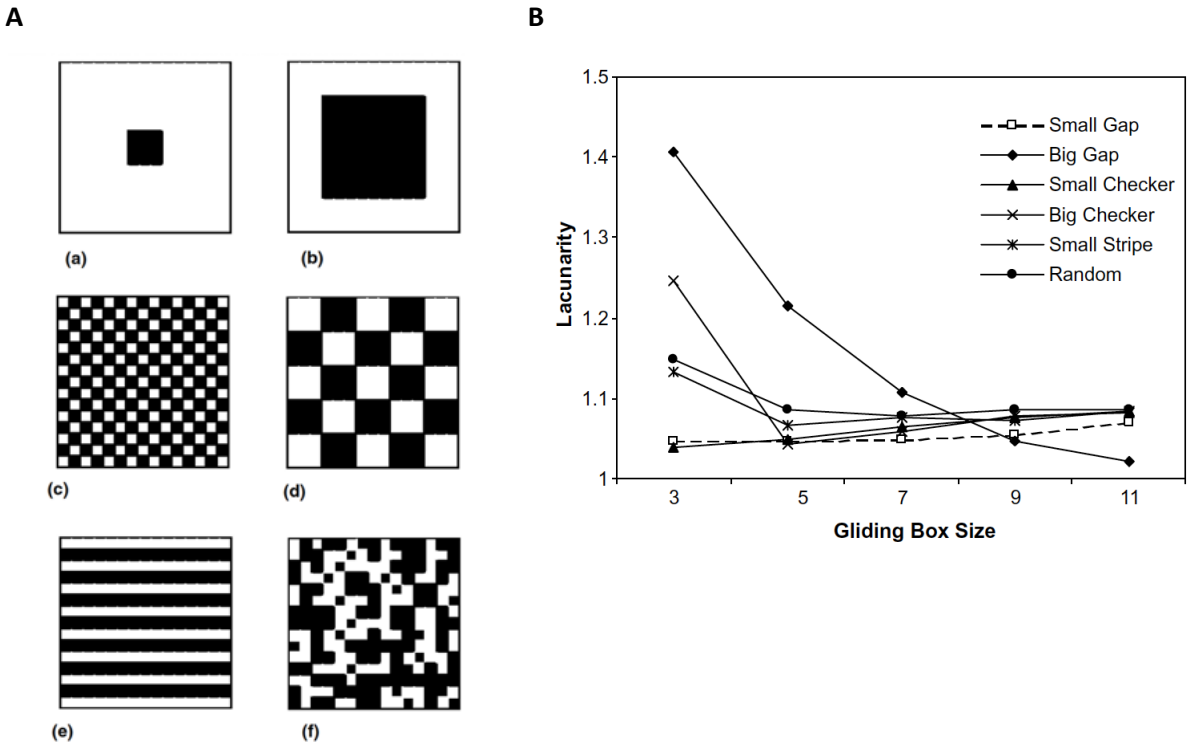

Figure 3.15: Illustrating influences of lacunarity.(A) Binary images of six spatial features (a) small gap pattern, (b) big gap patter, (c) small checker pattern, (d) big checker pattern, (e) small stripe patter, (f) random pattern. (B) Lacunarity curves of the six spatial features shown in (A). (Myint and Lam 2005)

Lacunarity values increased with advancing gestation in uncomplicated pregnancies (Figure 3.16). This is likely to reflect the lobularity seen on T2-weighted imaging with advancing lobularity.

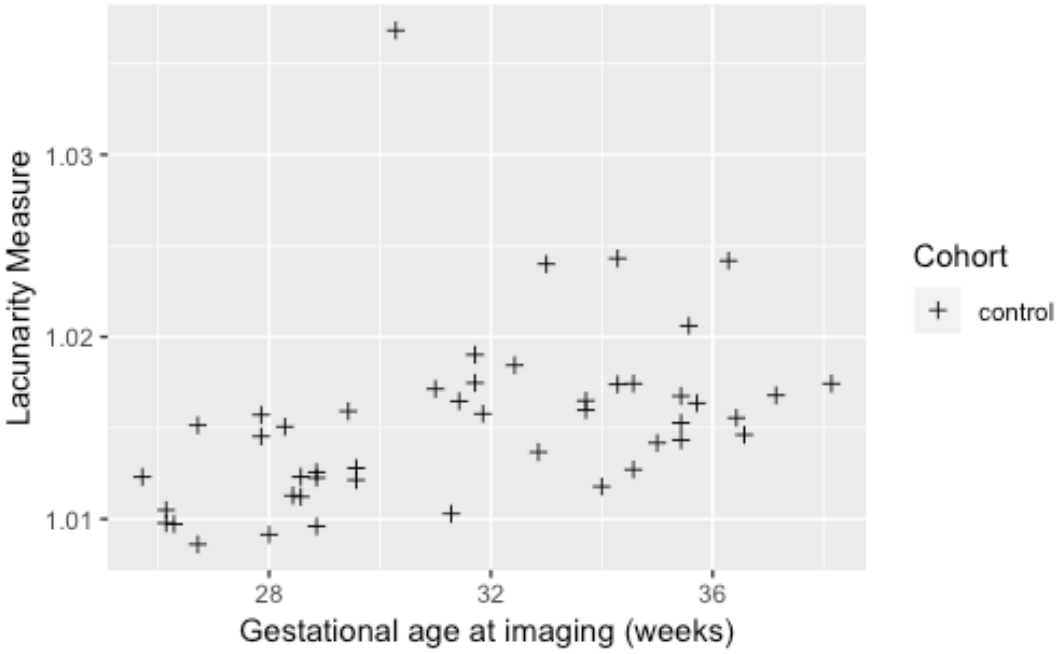

Figure 3.16: Scatterplot of lacunarity measure against gestational age at imaging (box size 2.5cm x 2.5cm)

3.3.2.2.3 Skewness and kurtosis

Skewness and kurtosis of T2* values were explored given the potential variety in illustrative histogram shape. Skewness is a measure of the degree of symmetry in the frequency distribution while kurtosis measures whether the frequency distribution is heavy-tailed or light-tailed relative to a normal distribution.

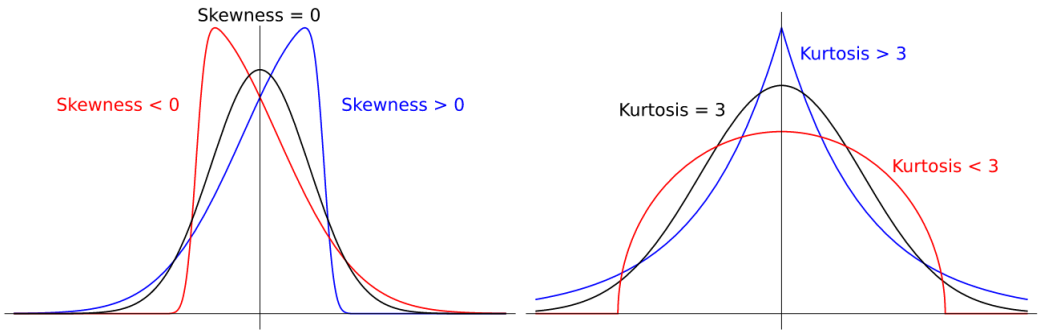

Fig. 1. *Left*: examples of positively skewed (*red*) and negatively skewed (*blue*) distributions compared with a normal distribution (*black*). *Right*: examples of leptokurtic (*red*), kurtosis greater than three, and platykurtic (*blue*), kurtosis less than three, distributions compared with a normal distribution with a kurtosis of three (*black*). All distributions shown have a mean of 0 and a standard deviation of 1. (For interpretation of the references to colour in this figure legend, the reader is referred to the web version of this article.)

Figure 3.17: Illustration of skewness and kurtosis. (David, Marshall, and Zanna 2017)

In T2* weighted placental imaging from uncomplicated pregnancies, skewness increased with advancing gestation (Figure 3.18) while kurtosis did not (Figure 3.19).

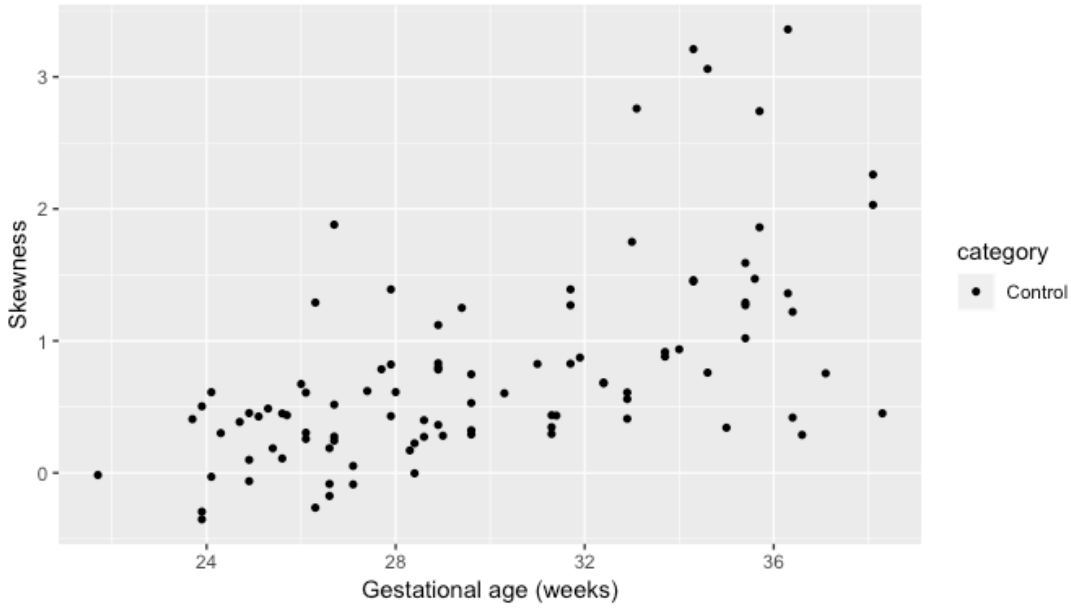

Figure 3.18: Scatterplot of skewness in T2* placental data from uncomplcated pregnancies against gestational age at imaging

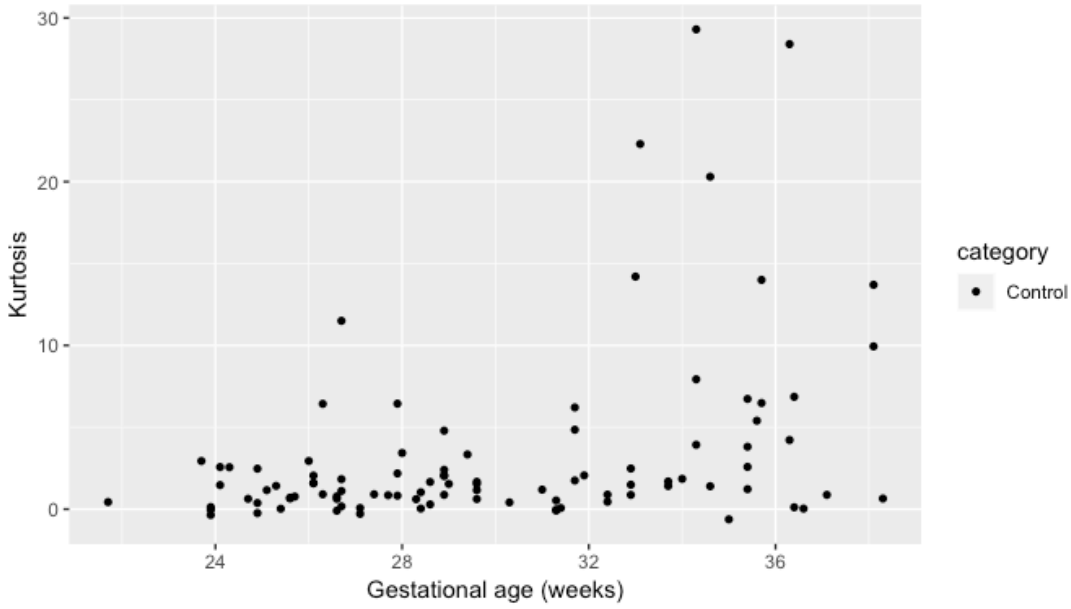

Figure 3.19: Scatterplot of kurtosis in T2* placental data from uncomplicated pregnancies against gestational age at imaging

3.4 Diffusion weighted imaging

Diffusion weighted imaging was considered potentially useful to investigate the hypothesis that the placenta in hypertensive disorders of pregnancy demonstrates inefficient spiral

artery remodelling and altered placental perfusion. Optimisation of diffusion weighted imaging for the placenta was therefore performed.

Diffusion weighted imaging is based on a conventional T2-weighted spin-echo sequence. In diffusion weighted imaging, two strong magnetic gradients are applied either side of a 180° radiofrequency pulse. These gradients are both equal but opposite polarity. The first gradient dephases the hydrogen spins while the second gradient rephases the spins. If the spins do not move, there is no net phase shift but if the spins do move, there is a net phase shift. Apparent diffusion coefficient (ADC) maps are calculated from a minimum of two sets of images - the first set of images is from the spin-echo sequence without the diffusion gradients (effectively a T2-weighted image) and the second set from the spin-echo with the diffusion gradients.

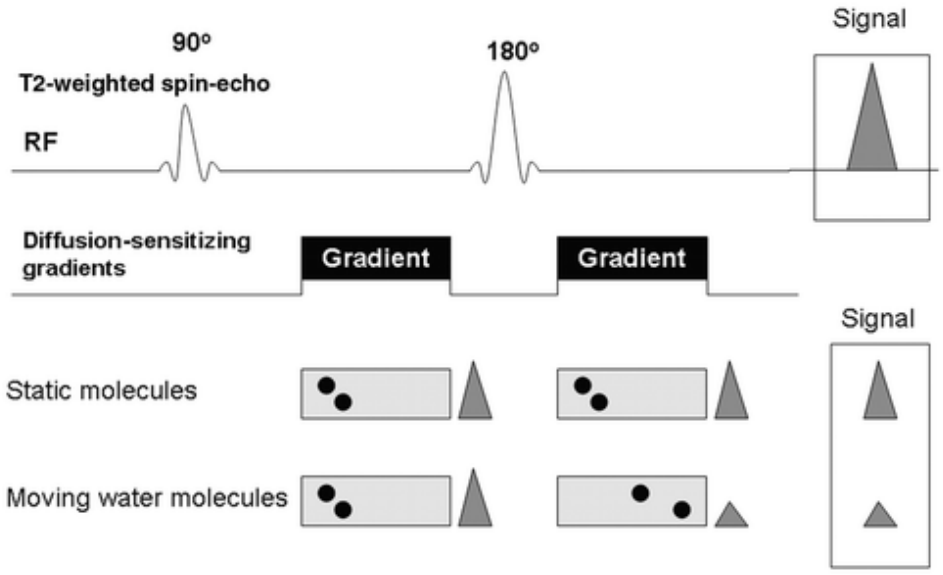

Figure 3.20: Measuring water diffusion. RF = radiofrequency pulse. The gradients are both positive in the figure as the 180°pulse reverses the direction of precession. (Koh and Collins 2007)

There are several variables that can affect the sensitivity of the sequence to molecular motion. These include the time between applying the two gradients, the duration of applying the gradient and the amplitude of the gradient. The strength and duration of the diffusion gradient is denoted by the 'b value.' With higher b values, differences in a tissue's apparent diffusion coefficient value can be exaggerated i.e. greater contrast (Chilla et al. 2015).

3.4.1 Echo time, TE

The echo time is ideally as short as possible to measure the resultant signal but is limited by time taken up by the diffusion gradient applied following the 180° radiofrequency pulse. The effect of echo time on apparent diffusion coefficient values is demonstrated in Figure 3.21 whereby the second echo time is longer than the first.

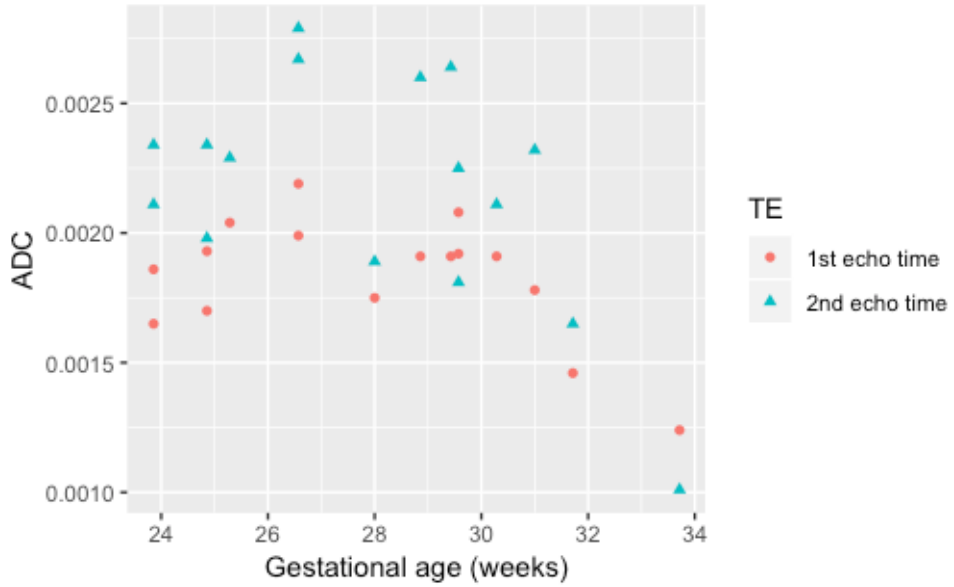

Figure 3.21: Placental apparent diffusion coefficient (ADC) values (mm^2s^{-1}) in uncomplicated pregnancies at two different echo times.

3.4.2 Motion

Diffusion measures the thermal microscopic translational motion of water molecules; therefore, sequences are ideally fast in order to minimise the effect of macroscopic motion. Motion correction can be achieved post acquisition to further accurately probe the inherent diffusion properties. This is demonstrated in Figure 3.22 where motion correction also substantially improves image quality which in turn, improves ease of manual segmentation for quantitative values within the placenta. Work on motion correction remains ongoing as part of the wider Placenta imaging Project.

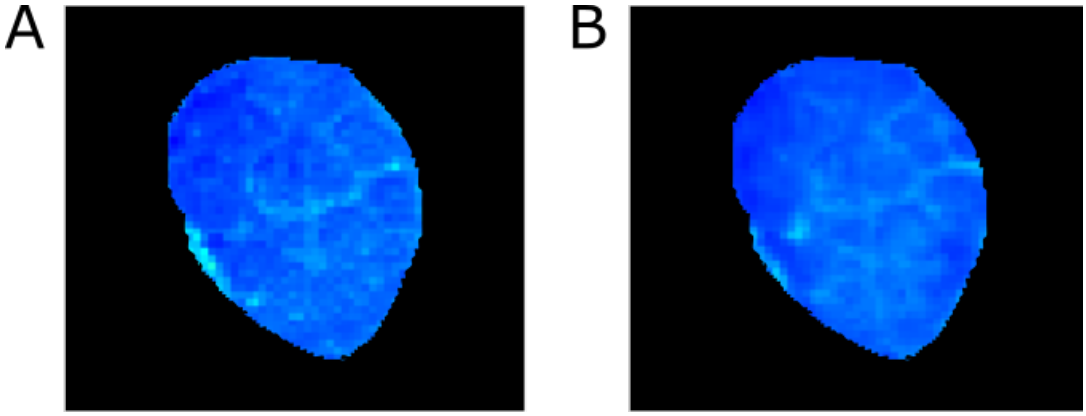

Figure 3.22: Apparent diffusion coefficient (ADC) map of a placenta (A) pre motion correction (B) post motion correction. Note the improvement in image quality.

3.4.3 Optimised diffusion protocol

The molecular motion that occurs during a diffusion sequence is also affected by T2 decay and T2*. To reduce this effect, diffusion measures (such as apparent diffusion coefficient) are often calculated from a series of different b values that have been applied.

During the course of this study, a novel combined diffusion-relaxometry magnetic resonance acquisition sequence was designed to further overcome this. In the novel sequence, a spin-echo with subsequent gradient echoes are used (Figure 3.23). The integrated approach gives a more specific measure of diffusion properties and T2* in a reasonably fast scan time within the same imaging space (Hutter et al. 2018; Slator et al. 2019). This is especially useful when trying to elucidate underlying mechanisms of placental dysfunction where T2* values vary across an individual placenta, with gestation and with pregnancy complications.

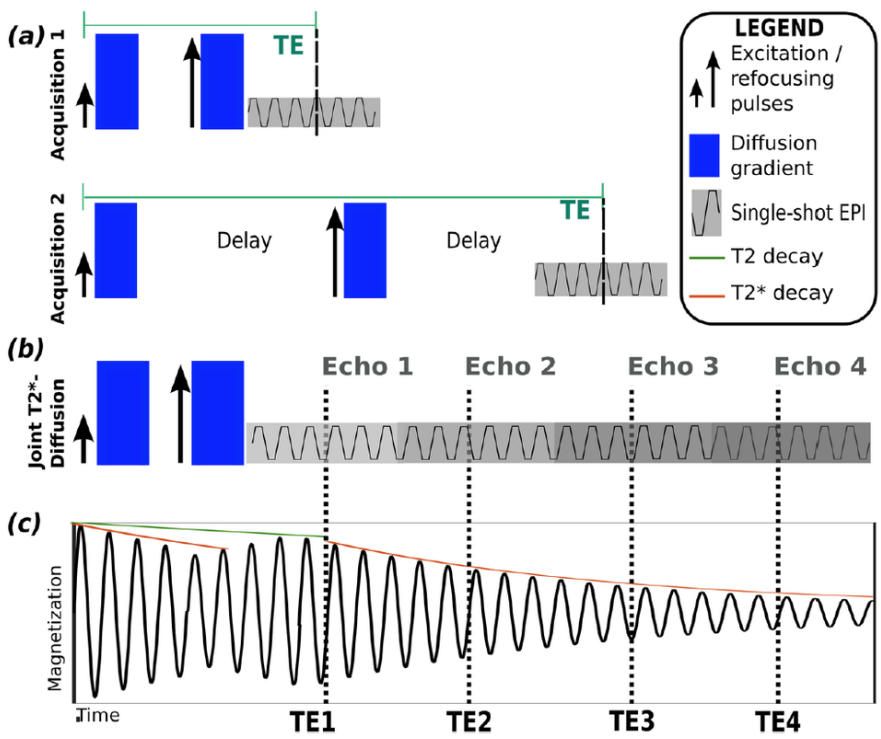

Figure 3.23: T2-diffusion sampling. (a) conventional T2-Diffusion sampling in separate scans together with the resulting delays. (b) joint T2*-Diffusion sampling. (c) transverse magnetization depicted schematically, showing the T2 decay in green and the T2* decay in orange.

3.5 Ultrasound

Ultrasound scans were performed on the same day as magnetic resonance imaging wherever possible, or at a maximum within two weeks. Women with pre-eclampsia or chronic hypertension had a clinically indicated ultrasound scans performed in line with national guidelines (National Institute for Health and Care Excellence 2019). In the control group, ultrasound scans were performed on a Philips EPIQ V7 by sonographers following a clinical protocol. Fetal measurements included biparietal diameter, head circumference, femur length and abdominal circumference which were used to derive an estimated fetal weight using the Hadlock formula, umbilical artery Doppler pulsatility index (PI), amniotic fluid index and maternal uterine artery pulsatility index. The presence of fetal growth restriction was established by ultrasonographic assessment using accepted international definitions (Gordijn et al. 2016) (Figure 3.24).

Early FGR: *GA < 32 weeks, in absence of congenital anomalies*	*Late FGR:* *GA ≥ 32 weeks, in absence of congenital anomalies*
AC/EFW < 3rd centile *or* UA-AEDF	AC/EFW < 3rd centile
Or 1. AC/EFW < 10th centile *combined with* 2. UtA-PI > 95th centile *and/or* 3. UA-PI > 95th centile	*Or at least two out of three of the following* 1. AC/EFW < 10th centile 2. AC/EFW crossing centiles >2 quartiles on growth centiles* 3. CPR < 5th centile *or* UA-PI > 95th centile

*Growth centiles are non-customized centiles. AC, fetal abdominal circumference; AEDF, absent end-diastolic flow; CPR, cerebroplacental ratio; EFW, estimated fetal weight; GA, gestational age; PI, pulsatility index; UA, umbilical artery; UtA, uterine artery.

Figure 3.24: Consensus based definitions for early and late fetal growth restriction in the absence of congenital anomalies (Gordijn et al. 2016).

In line with national guidelines, women with chronic hypertension and preeclampsia had ultrasound scans performed in the clinical setting. In women with chronic hypertension, this was carried out at 28, 32 and 36 weeks' gestation (National Institute for Health and Care Excellence 2019) and included fetal growth and amniotic fluid volume assessment, and umbilical artery Doppler velocimetry. In women with preeclampsia, this was carried out at the time of diagnosis and every two weeks. Subsequent surveillance and monitoring were determined by the findings of these scans. Due to the frequency of ultrasound scans performed in both the chronic hypertension and preeclamptic group, additional ultrasounds were not performed on the day of magnetic resonance imaging in order to minimise additional appointment times for the women, especially as some women declined participation in the study due their heavy existing clinical schedules. As this was not primarily a study in fetal growth restriction, placental magnetic resonance imaging was not timed in accordance with any ultrasound findings indicating fetal growth restriction, although this warrants further investigation in future studies.

Where available, ultrasound findings in women with either chronic hypertension or preeclampsia had lower estimated fetal weight centiles. In the control group, median estimated fetal weight centile was 54 (IQR 41-70) compared to 48 (IQR 27-70) in the chronic hypertensive group and 6 (IQR 3-21) in the preeclamptic group. The umbilical artery Doppler pulsatility index was less than the 95th centile in women with chronic hypertension while five women with preeclampsia (26%) had values greater than the 95th centile. Additionally, one woman with preeclampsia had intermittently reversed end diastolic flow in the umbilical artery and two had absent end diastolic flow. An estimated fetal weight derived from magnetic resonance imaging values was not investigated as this study primarily focussed on placental imaging and optimisation in women with pregnancy hypertension. Further work may address this, examining estimated fetal weight centiles

derived from magnetic resonance imaging and comparing them with ultrasound derived values.

3.6 Histology

Histological examination of the placenta post delivery can yield insight into aetiology of adverse pregnancy outcomes. Current clinical indications for placental histology reporting at St Thomas' Hospital are stillbirth, late miscarriage under 20 weeks' gestation, unexpected admission to the neonatal unit, birthweight under the 3rd centile, preterm delivery under 34 weeks' gestation, suspected placental abruption and request by the fetal medicine unit following an ultrasound scan.

The initial placental histological examination for all placentae, regardless of group, occurred in line with local protocols at the Cellular Pathology Department, St Thomas' Hospital. Following delivery, placentae were collected within 48 hours and fixed in 10% buffered formalin. The umbilical cord and membranes were trimmed before weighing the placenta. The following areas were sampled and then embedded in paraffin: 2 transverse sections of the umbilical cord, one roll of membranes (including rupture site), 2 to 3 full-thickness blocks of the parenchyma away from the placental edge (including fetal and maternal surfaces). Paraffin-embedded tissue sections were then cut into 4-micron sections, deparaffinized and stained with hematoxylin and eosin before histological examination. A clinical report for all placentas submitted was issued, in accordance with local hospital reporting guidelines. Clinically relevant findings were reported by histopathologists and thus the absence of a mention of a feature, did not confirm the absence or presence of that feature.

3.6.1 Placental histology in hypertensive disorders of pregnancy

Studies have shown an association of maternal vascular malperfusion lesions with hypertensive disorders of pregnancy. Maternal vascular malperfusion lesions were highest in women with chronic hypertension and preeclampsia compared to those with gestational hypertension or no hypertensive disorder of pregnancy (Kovo et al. 2017). Villous features included increased syncytial knots, villous agglutination, increased intervillous fibrin deposition and villous infarcts. Placental vascular lesions have been shown to be greater in those with preeclampsia diagnosed before 34 weeks' gestation compared to those diagnosed after 34 weeks' gestation (Nelson et al. 2014) thus suggesting a difference in aetiology between early and late onset preeclampsia.

Maternal vascular malperfusion features have been reported to be more specific to preeclampsia compared to other hypertensive disorders of pregnancy (Bustamante Helfrich et al. 2017). In a large study examining 3074 placentae, the adjusted odds ratio of maternal vascular malperfusion lesions was highest in those with preeclampsia complicated by haemolysis, elevated liver enzymes, low platelet count (HELLP) (aOR 4.90, 95% CI 2.22-10.83), followed by those with preeclampsia alone (aOR 2.51, 95% CI 2-3.16), then preeclampsia superimposed on a background of chronic hypertension (aOR 2.00, 95% CI 1.38-2.92). Those with chronic hypertension in isolation were not associated with maternal vascular malperfusion lesions (aOR 094, 95% CI 0.62-1.41). Although a large study, histopathologists were not masked to clinical outcome.

3.6.2 Optimised histological examination protocol

Histopathologists that provided a second report of the tissue in this study were masked to pregnancy outcome and clinical history in order to reduce bias. There is a reported overlap in histological features between uncomplicated and hypertensive pregnancies (Bustamante Helfrich et al. 2017; Herman et al. 2020; Kovo et al. 2017). Frequencies of such features were smaller in studies masked to clinical history (Falco et al. 2017).

A second report (in addition to clinical reporting) was issued with assessment of a predefined collection of features in this study by histopathologists for consistent reporting. Placental features for classification incorporated the 2014 Amsterdam Placental Workshop Group criteria (Redline 2015) for a systematic approach in reporting the absence or presence of a feature. Three main categories were chosen based on classifications suggested by the Perinatal Section of the Society for Pediatric Pathology workshop, who considered these categories the most important pathologic processes (Redline et al. 2005). These categories were placental features consistent with a) maternal vascular malperfusion, b) fetal vascular malperfusion and c) chorioamnionitis. In view of the hypertensive group studied that could have co-existing fetal growth restriction, the categories of maternal and fetal vascular malperfusion were of particular interest.

In this study, ex vivo histopathological placental examination was performed by histopathologists masked to clinical history and pregnancy outcome, and also reported using the above three categories. This reduced bias and provided systematic reporting and thus enabled both visual assessment of placental imaging and quantitative imaging derived values to be examined in conjunction with histopathological findings to further understand potential changes seen.

Chapter 4 T2* PLACENTAL MAGNETIC RESONANCE IMAGING IN PRETERM PREECLAMPSIA: AN OBSERVATIONAL STUDY

4.1 Abstract

Placental dysfunction underlies the aetiology of pregnancies complicated by preeclampsia. The use of placental magnetic resonance imaging (MRI) to provide an insight into the pathophysiology of preeclampsia and thus assess its potential use to inform prognosis and clinical management was explored. In this prospective observational study, 14 women with preterm preeclampsia and 48 gestation-matched controls at median of 31.6 weeks (interquartile range (IQR) 28.6-34.6) and 32.2 weeks (IQR 28.6-33.8) respectively were imaged using 3-Tesla MRI. The acquired data included T2-weighted images and T2* maps of the placenta, the latter an indicative measure of placental oxygenation. Placentae in women with preeclampsia demonstrated advanced lobulation, varied lobule sizes, high granularity and substantial areas of low signal intensity on T2-weighted imaging, with reduced entire placental mean T2* values for gestational age (two sample t-test, t=7.49) which correlated with a reduction in maternal placental growth factor concentrations (PlGF, Spearman's rank correlation coefficient 0.76) and increased lacunarity values (t=3.26). Median mean T2* reduced from 67ms (IQR 54-73) at 26.0-29.8 weeks' gestation to 38ms (IQR 28-40) at 34.0-37.9 weeks' gestation in the control group. In women with preeclampsia, median T2* was 23ms (IQR 20-23) at 26.0-29.8 weeks' gestation and remained low at 22ms (IQR 20-26) at 34.0-37.8 weeks' gestation). Histological features of maternal vascular malperfusion were only found in placentae from women with preeclampsia. Placental volume did not differ between the control group and women with preeclampsia. Placental MRI allows both objective quantification of placental function *in vivo* and some elucidation of the complex mechanisms underlying preeclampsia development.

4.2 Introduction

Preeclampsia affects approximately 3% of all pregnancies (Hutcheon, Lisonkova, and Joseph 2011) with associated maternal complications of renal injury, hepatic injury, stroke, haemorrhage and eclampsia as well as fetal complications including growth restriction and stillbirth. Half of women with severe preeclampsia deliver preterm and one in twenty stillbirths without congenital abnormality occur in women with preeclampsia (Cantwell et al. 2011).

Placental dysfunction underlies the aetiology of pregnancies complicated by preeclampsia and their associated adverse pregnancy outcomes (Hod, Cerdeira, and Karumanchi 2015; Kingdom et al. 2018). *In vivo* assessment of placental function in clinical practice is currently limited to indirect assessments as a proxy for placental function including measures of fetal growth, and Doppler umbilical artery velocimetry.

Objective *in vivo* assessment of placental structure and quantification of function may help elucidate the pathophysiology in those pregnancies with established preeclampsia and provide a potential tool to inform prognosis. Quantitative non-invasive *in vivo* assessment of the placenta can be achieved with magnetic resonance imaging (MRI). T2* mapping probes placental oxygenation as the paramagnetic properties of deoxyhaemoglobin cause magnetic field distortions and a faster T2* decay (i.e. reduced transverse relaxation time) than oxyhaemoglobin. Hypoxic tissues therefore have a reduced T2* value (Blood Oxygen Level Dependency effect). In addition to oxygenation, T2* values are also affected by lipid content, calcium content, extracellular fluid volume and surface area, the latter contributed by cellular membranes, intracellular or extracellular macromolecules (Cameron, Ord, and Fullerton 1984). Studies have shown a linear reduction in mean T2* values in uncomplicated pregnancies with increasing gestation (Hutter, Slator, et al. 2019) and an increase in placental T2* with maternal hyperoxia (Huen et al. 2013; Sørensen et al. 2013). Lower mean T2* values have been found in placentae of pregnancies complicated by fetal growth restriction (Ingram et al. 2017; Sinding, Peters, Frøkjaer, et al. 2016); however, to our knowledge, no published study has reported T2* evaluation in women with preeclampsia.

The aim of this study was to explore the use of placental magnetic resonance imaging to provide an insight into the pathophysiology of preeclampsia and thus assess its potential use to inform prognosis and clinical management.

4.3 Methods

The acquisition and processing pipeline for T2* mapping has been published and is freely available (Hutter, Slator, et al. 2019).

4.3.1 Study Design

This prospective observational study was undertaken at St Thomas' Hospital, London, a tertiary level maternity unit. Women with preeclampsia were approached in person

antenatally. Women in the control group were recruited at their routine 20-week anomaly scan or self-referred to take part in the study. All women in the study gave written informed consent.

Follow up was until delivery. Prospectively specified data collection included baseline demographic characteristics, maternal and neonatal outcomes.

Women were considered for inclusion in the study if they had a singleton pregnancy, were clinically stable, over 16 years of age, not claustrophobic with no contraindication for magnetic resonance imaging. They were assessed for our Philips 3T Achieva scanner; given the 60cm scanner bore size, women also had to have a body mass index less than 30kg/m^2 and abdominal girth less than 130cm.

Preeclampsia was prospectively defined using the international consensus definition (Brown et al. 2018). This was women who developed gestational hypertension accompanied by one or more of the following new-onset conditions at or after 20 weeks' gestation: proteinuria, acute kidney injury, liver involvement, neurological complications, haematological complications and uteroplacental dysfunction. Preeclampsia superimposed on chronic hypertension was defined as the additional presence of maternal organ dysfunction consistent with preeclampsia. PlGF was not used as part of the clinical or research definition. Clinical management of hypertensive women were according to national guidelines (National Institute for Health and Care Excellence 2019) with responsibility under the attending consultant.

Women in the control group fulfilled the following criteria: no diagnosis of a hypertensive disorder at enrolment and until delivery, no significant past medical history, no pregnancy complications (including gestational diabetes), delivery at term with birthweight between the 3rd and 97th centile (calculated using INTERGROWTH-21st, version 1.3.5)(Villar et al. 2014) thus excluding potential confounders of placental change (Desoye and Hauguel-de Mouzon 2007; Llurba et al. 2014; Salafia et al. 1995). These women were gestation matched to women with preeclampsia and selected from a research study (Placenta Imaging Project, REC 16/LO/1573, IRAS 201609), the primary objective of which is to develop a novel magnetic resonance approach to assess growth and development of the human placenta. Gestation matching was achieved masked to values derived from magnetic resonance imaging so that three women with uncomplicated pregnancies with imaging within two weeks of the gestation at which each woman with preeclampsia was imaged were chosen for comparison.

No formal sample size was calculated for power of outcome variables as this was an exploratory study describing a novel technique in technology development application. The study was approved by Fulham Research Ethics Committee, REC 16/LO/1573.

4.3.2 Magnetic Resonance Imaging

Magnetic resonance imaging was performed on a clinical Philips 3T Achieva with a 32-channel cardiac coil. Women underwent magnetic resonance imaging on up to two occasions, a minimum of two weeks apart and at any time point between their clinically routine anomaly ultrasound scan (at around 18-22 weeks' gestation) and delivery. Imaging was performed supine with supported lower limbs and shoulders after a period of three minutes in left lateral. Total imaging time did not exceed one hour, and women were offered a break of under 30 minutes halfway through the scan. Maternal assessments during imaging included blood pressure measurements every 10 minutes with continuous maternal heart rate and oxygen saturation monitoring. All scans had an obstetrician or specialist midwife present throughout. No pharmacological sedation was used.

Image based shimming was achieved using an in-house tool, after acquiring a B0 map, in order to reduce the effect of inhomogeneities in the magnetic field. Multi-echo gradient echo, echo planar imaging at $3mm^3$ resolution was performed with free breathing and took less than one minute, with the whole placenta covered within 60 slices (5 echo times: 13.81ms/70.40ms/127.00ms/183.60ms/240.2ms, TR=3s, SENSE=3, halfscan=0.6). One scan was performed at $2mm^3$ resolution. Echo times result from the chosen EPI train characteristics. Thereby, the intra-echo spacing was chosen to minimize acoustic noise and the inter-echo spacing as the minimal possible spacing. Parameters were kept constant between women with preeclampsia and the control group.

A long TE (180ms) T2-weighted single shot turbo spin echo sequence of the whole uterus (thereby including placenta) was acquired in coronal and sagittal planes to the woman with TR = 16s, SENSE = 2.5 and partial Fourier 0.625. In-plane resolution was 1.5 mm x 1.5mm, slice thickness 2.5mm with an overlap of 0.5mm. The field of view was 300 x 360 x [100-200] mm (coronal) and 300 x 300 x 340 mm (sagittal) in the FH x RL x AP directions respectively. Structural images of the fetal brain were reported and available to the clinical team. Data quality was assessed to exclude sequences with uterine contractions. Visual analysis examined the signal intensity across the placenta and whether the presence of placental lobules and septae were visually apparent. The signal intensity within lobules was

visually assessed for granularity with high granularity defined as the presence of both high and low signal intensity within individual lobules.

An in-house Python script by JH produced T2* maps. The placenta was manually segmented by an experienced observer [AH] using ITK-SNAP. A further processing step calculated mean placental T2*and lacunarity. Lacunarity values reflect the spatial distribution of gaps of a specific size within lobules. The acquisition and processing pipeline for T2* imaging has been described previously and shown to have good reproducibility with a high Dice coefficient between observers who segmented the placenta (Hutter, Slator, et al. 2019; Hutter, Jackson, et al. 2019).

4.3.3 Placental growth factor, PlGF

Venepuncture blood sampling was performed as close to magnetic resonance imaging as feasible, usually on the same day (in 32 out of 43 available samples). Six millilitres of blood were drawn into a bottle containing ethylenediamine tetra-acetic acid, transported to the laboratory within 1 hour and underwent centrifugation at 1400 x g (rcf) for 10 minutes at 4˚C. PlGF was quantified using the Triage PlGF Test (Alere, San Diego, CA) according to the manufacturer's instructions while masked to both group and clinical outcome. The clinical team did not receive the result; however, in five women with preeclampsia PlGF was performed as part of their clinical care as diagnostic workup (National Institute for Health and Care Excellence 2019) when preeclampsia was suspected.

4.3.4 Placental Histology

Following delivery and where available, placentas underwent histological examination according to local protocols at the Cellular Pathology Department, St Thomas' Hospital. Placentas were fixed in 10% buffered formalin and trimmed of both umbilical cord and membranes for placenta weight. The following areas were sampled and then embedded in paraffin: two transverse sections of the umbilical cord, one roll of membranes (including rupture site), two to three full thickness blocks of the placental parenchyma away from the placental edge (including fetal and maternal surfaces). Additional areas were sampled depending on macroscopic findings. Paraffin embedded tissue sections were then cut into four-micron sections, deparaffinized and stained with haemotoxylin and eosin prior to histological examination. A clinical report for all placentas submitted was issued, in accordance with local hospital reporting guidelines. Histological slides were then re-examined for features of maternal vascular malperfusion, fetal vascular malperfusion and acute chorioamnionitis by histopathologists who were masked to the pregnancy outcome;

features were identified and classified using guidelines from the International Placental Pathology Consensus Meeting, Amsterdam 2014 (Redline et al. 2005). Any discrepancies between reporting histopathologists were re-examined (again masked to the pregnancy outcome) and a consensus opinion was reached.

4.3.5 Statistical methods

In uncomplicated pregnancies, gestation-adjusted reference ranges for placental mean T2* and lacunarity values were established after examining a range of possible models using the Stata command -xriml- (Wright and Royston 1996), and 10% to 90% reference range established. A two sample t-test was used to compare placental mean T2* and lacunarity (z scores) between these groups, using robust standard errors to allow for clustering given two women were imaged twice in the preeclamptic group. Multiple regression, adjusting for gestation, was used to compare placental volume between uncomplicated pregnancies and those with preeclampsia.

Spearman's rank correlation coefficient was calculated to evaluate the relationship between Placental Growth Factor and placental mean T2*. Women who declined venepuncture were not included in the analysis. Birthweight centiles were calculated using INTERGROWTH-21st version 1.3.5 (Villar et al. 2014). Pregnancy outcome data was available for all women in both groups. Statistical analysis was performed using Stata version 15.1 (StataCorp, College Station, Texas).

4.4 Results

Enrolment was between May 2017 and April 2019. Of the 14 women with preeclampsia who were recruited, all 14 women were imaged (none of whom had uterine contractions during imaging) with 48 gestation-matched controls. Five of 14 women (36%) had superimposed preeclampsia on a background of chronic hypertension (Table 4.1). Women with preeclampsia had higher blood pressures both prior and during imaging and had lower placental growth factor concentrations (Table 4.1). Of women with available data on haemoglobin concentrations, the median haemoglobin at booking was 123g/L (interquartile range 121-131) and at 28 weeks' gestation was 117g/L (interquartile range 113-122; n=37 women). In women with preeclampsia, the median haemoglobin at booking was 124g/L (interquartile range 120-131) and at 28 weeks' gestation was 120g/L (interquartile range 110-137; n=10 women). The median number of days between diagnosis of preeclampsia and placental magnetic resonance imaging was 6 (IQR 3-15). Out

of the 14 women with preeclampsia, 11 (79%) were diagnosed before 34 weeks' gestation and 3 (21%) after 34 weeks' gestation.

Table 4.1: Characteristics at booking and enrolment.

Booking and enrolment characteristics	Control n=48	Preeclampsia n=14
At booking		
Maternal age, y, median (IQR)	33 (32-36)	32 (26-37)
Gestational age on day of MRI, wk, median (IQR)	31.6 (28.6-34.6)	32.2 (28.6-33.8)
Body mass index, kg/m^2, median (IQR)	22 (21-24)	25 (23-25)
Nulliparous	24 (50)	6 (43)
White ethnicity	44 (92)	8 (57)
Black ethnicity	1 (2)	3 (21)
Asian ethnicity	2 (4)	0
Chinese	0	3 (21)
Mixed ethnicity	1 (2)	0
Current smoking	1 (2)	0
Quit smoking before pregnancy	4 (8)	4 (29)
Never smoked	43 (90)	10 (71)
Previous preeclampsia	0	3 (21)
Chronic hypertension	0	5 (36)
Gestational diabetes	0	2 (14)
Inflammatory bowel disease	0	2 (14)

Values given as a number (percentage) unles stated otherwise.

Table 4.1 (cont)	**Control n=48**	**Preeclampsia n=14**
Intrahepatic cholestasis of pregnancy	0	1 (7)
At enrolment on day of MRI		
Aspirin	4 (8)	8 (57)
No oral antihypertensive agent	48 (100)	2 (14)
1 oral antihypertensive agent	0	5 (36)
2 or more oral antihypertensive agents	0	7 (50)
Placental Growth Factor, pg/mL, median (IQR)	419 (102-815)	<12(<12-<12))
Placental growth factor <100 pg/mL	7/29 (24)	14/14 (100)
Placental growth factor <12 pg/mL	0	12/14 (86)
Sitting blood pressure on day of MRI		
Systolic, mmHg, median (IQR)	103 (99-111)	141 (138-145)
Diastolic, mmHg, median (IQR)	61 (55-64)	91 (87-98)
Mean Arterial Pressure, mmHg, median (IQR)	75 (70-80)	108 (104-113)
Supine blood pressure during MRI		
Systolic, mmHg, median of individual's median (IQR)	98 (91-103)	127 (124-130)
Diastolic, mmHg, median of individual's medians (IQR)	58 (54-64)	80 (77-87)
Mean Arterial Pressure, mmHg, median of individual's medians (IQR)	72 (67-76)	94 (93-100)

Values given as a number (percentage) unless stated otherwise.

Time from magnetic resonance imaging to delivery was shorter in women with preeclampsia (Table 4.2) In the preeclamptic group, 11 women delivered preterm with seven prior to 34 weeks' gestation (Table 4.2, Supplemental Table S1) while all women in the control group delivered after 37 weeks' gestation. 21 placentae from the control group and 12 placentae from the preeclamptic group underwent histological examination, with double reading by two histopathologists to standardised protocols, masked to clinical outcome (Table 4.3). On assessment, there were no features of maternal vascular malperfusion on placental histological examination in the control group whilst ten of twelve placentae examined from women with preeclampsia did (Table 4.3). In the two placentae from preeclamptic women with no features of maternal vascular malperfusion, delivery occurred after 37 weeks' gestation with normal birthweight centiles. There were no features of fetal vascular malperfusion on placental histopathological examination in either group.

Table 4.2: Maternal and neonatal outcomes.

Maternal and neonatal outcome variables	**Control n=48**	**Preeclampsia n=14**
Time from MRI to delivery, days, median (IQR)	65 (37-84)	10 (6-19)
Onset of delivery		
Spontaneous	31 (65)	0
Induction	9 (19)	8 (57)
Pre labour caesarean	8 (17)	6 (43)
Primary reason for induction or prelabour caesarean*		
Maternal indication	4/17 (24)	7/14 (50)
Fetal indication	13/17 (76)	7/14 (50)
Delivery		
Livebirth	48 (100)	14 (100)
Gestational age at delivery, weeks, median, IQR	40.4 (39.2-41.1)	34.0 (30.0-36.5)

Table 4.2 (cont)	**Control n=48**	**Preeclampsia n=14**
Spontaneous vaginal delivery	24 (50)	1 (7)
Assisted vaginal delivery	9 (19)	1 (7)
Elective pre-labour caesarean section	7 (15)	0
Urgent caesarean section	8 (17)	12 (86)
Preterm birth <37/40	0	11 (79)
Preterm birth < 34/40	0	7 (50)
Birthweight, g, median (IQR)	3460 (3109-3726)	1635 (926-2157)
Birthweight centile, centile, median (IQR)	65 (32-80)	7 (3-17)
5 minute APGAR score ≥7	47 (98)	13 (93)
Respiratory support required in delivery room	4 (8)	6 (43)
Number admitted to neonatal unit for >=48 hours	1 (2)	12 (86)
Length of stay in intensive care, day, median, IQR	0	8 (1-10)
Length of stay in high dependency, day, median, IQR	0	1 (0-4)
Length of stay in special care, day, median, IQR	3	7 (2-16)
Primary indication for neonatal unit admission		
Prematurity	0	7/12 (58)
Fetal growth restriction/small for gestational age	0	2/12 (17)
Respiratory disease	0	1/12 (8)
Suspected sepsis	0	1/12 (8)
Hypoglycaemia	0	1/12 (8)

Values given as a number (percentage) unless stated otherwise. *Full details given in Supplemental Table S1. (at end of chapter)

Table 4.3: Placental histology findings.

Placental histology characteristics	Control	Preeclampsia
Number of placentae assessed	21	12
Placental weight, g, median (IQR)	454 (403-562)	346 (188-458)
Fetal-placental birthweight ratio, median (IQR)	7.4 (7.1-7.7)	5.6 (4.8-5.9)
Maternal vascular malperfusion features	0	10 (83)*
Fetal vascular malperfusion features	0	0
Chorioamnionitis features	10 (48)	2 (17)

Values given as a number (percentage) unless stated otherwise. *2 of the 12 placentas in the preeclamptic group did not have maternal vascular malperfusion features and delivered at term.

Example T2-weighted images from the control and preeclamptic groups are shown in Figure 4.1, with areas of high signal on T2-weighted imaging corresponding to long T2* and low signal on T2-weighted imaging corresponding to short T2* values. In the control group, placental lobularity (the visual presence of lobules, i.e. presumed functional units) was more apparent with increasing gestational age at imaging. The placental lobules were of low granularity (i.e. consistent signal intensity within each lobule). Compared to gestation-matched controls, the placentae in women with preeclampsia showed more marked lobularity (Figure 4.1, with numerical data given in Supplemental Table S2), variable lobule size and high granularity with a decline in T2* towards lobule periphery. In addition, the placentae in women with preeclampsia had substantial additional areas of low signal intensity (Figure 4.1).

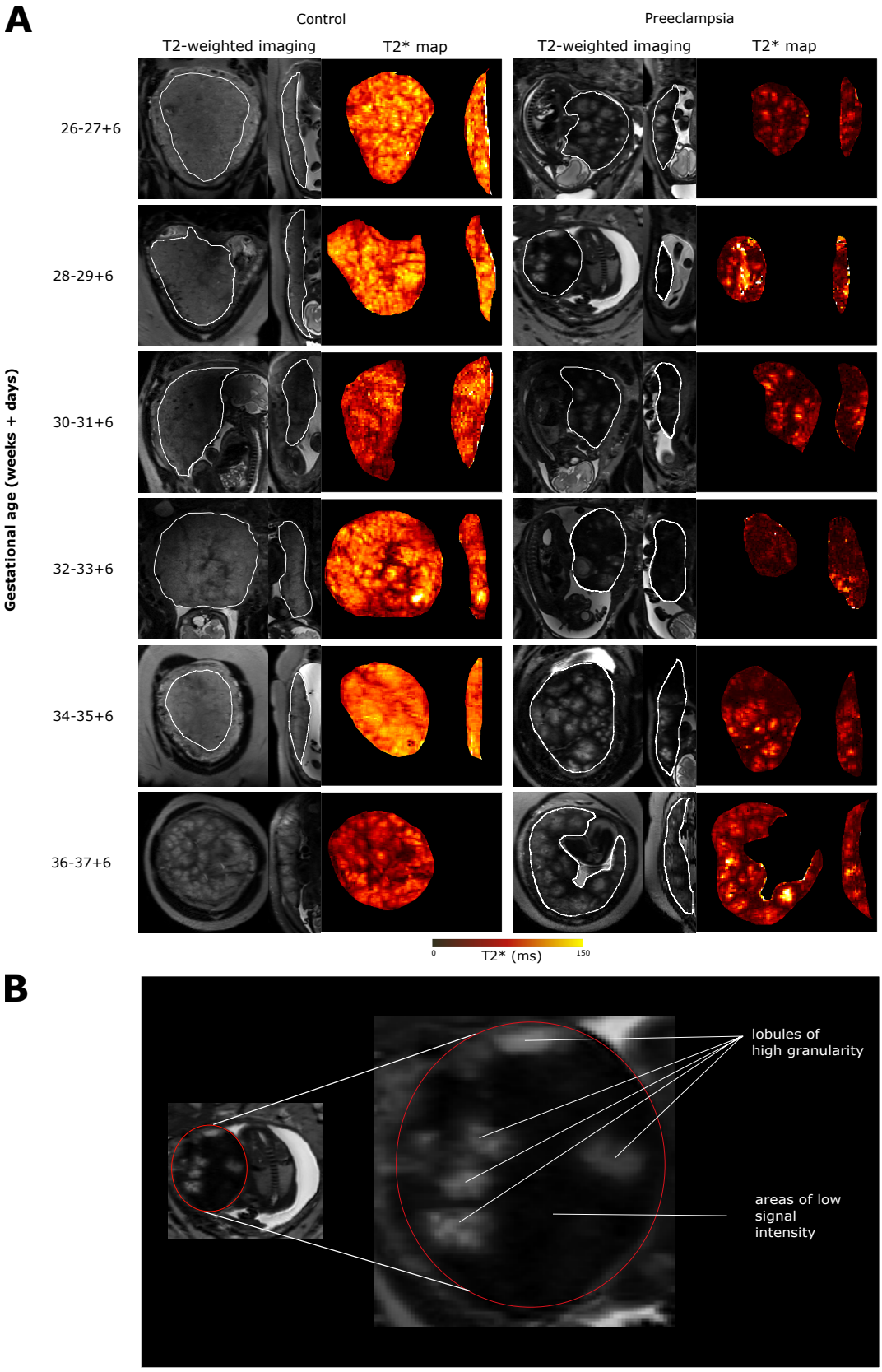

Figure 4.1: (A) Example T2-weighted placental imaging and T2* maps in coronal and sagittal planes across gestation. (B) Features of T2-weighted placental imaging in women with preeclampsia.

With increasing gestation, placental mean T2* values decreased linearly in the control group (Figure 4.2, Supplemental Table S2). In women with preeclampsia, 13 of 14 cases had placental mean T2* values lower than the 10th centile of normal values derived from the gestation-matched control group (two sample t-test, t=7.49 vs controls). One woman with preeclampsia and placental mean T2* value within normal range delivered a baby of normal birthweight centile at 37 weeks' gestation, with normal placental histological examination. Women with preeclampsia had higher placental lacunarity values (two sample t-test, t=3.83) on T2* and in the control group, lacunarity increased with increasing gestation (Figure 4.3A, Supplemental Table S2). Placental mean T2* positively correlated (Spearman's rank correlation coefficient of 0.76) with placental growth factor concentration (Figure 4.3B). Placental volume did not differ significantly between women in the control group and women with preeclampsia (Supplemental Figure S1). Two women with preeclampsia were imaged twice, two weeks apart (as indicated in the participant flow diagram in Supplemental Figure S2 at end of chapter).

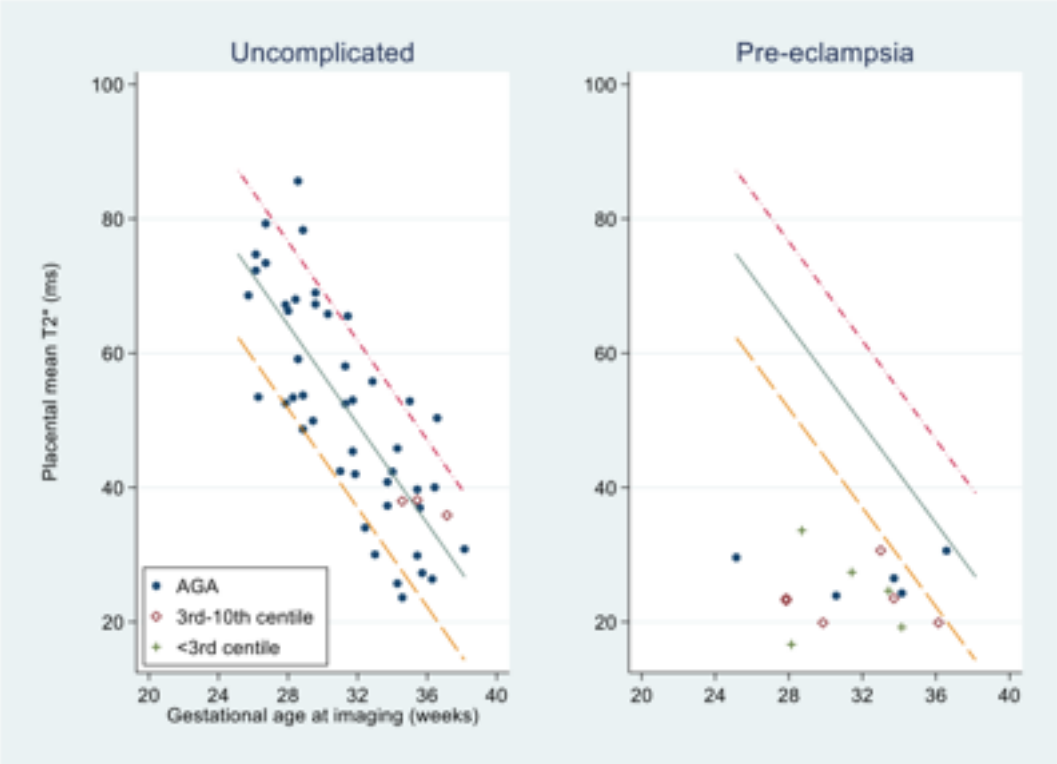

Figure 4.2: Scatterplot of placental mean T2* against gestational age at imaging, lines representing 10th, 50th and 90th centiles.
Actual placental mean T2* values given in Supplemental Table S2.

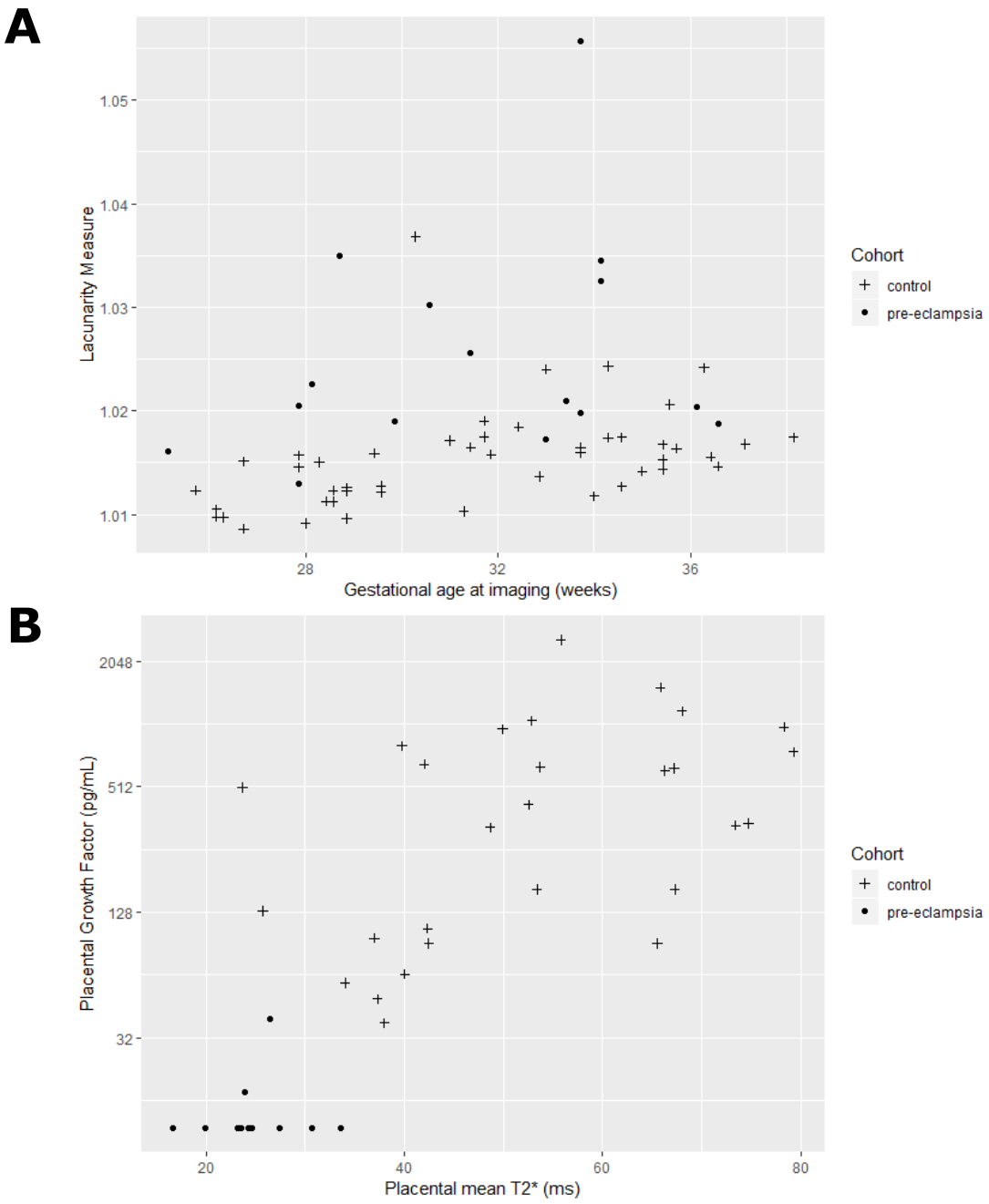

Figure 4.3: (A) Scatterplot of lacunarity measure (derived from T2* mapping) against gestational age at imaging. (B) Scatterplot of Placental Growth Factor (sample taken within two weeks of magnetic resonance imaging) against placental mean T2* (derived from T2* mapping).

In the preeclampsia group, there was no clear trend between placental volume and gestational age at diagnosis of preeclampsia, birthweight or birthweight centile (Figures 4.4, 4.5 and 4.6). The control group were not included in the scatterplots as the interval between imaging and delivery would render such data comparisons as uninformative.

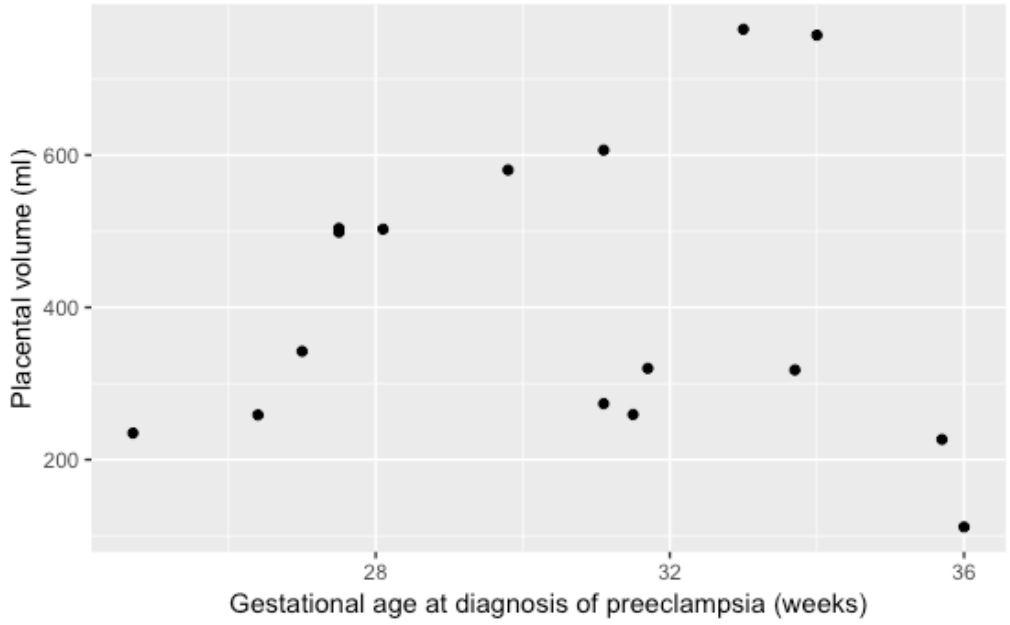

Figure 4.4: Scatterplot of placental volume (derived from T2* map segmentations) against gestational age at diagnosis of preeclampsia.

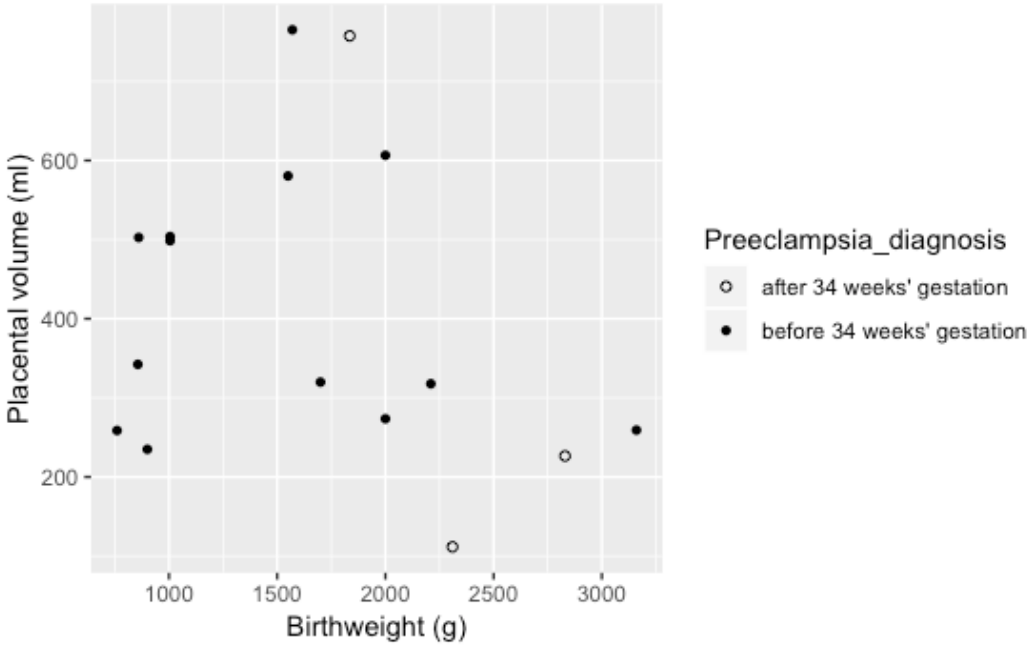

Figure 4.5: Scatterplot of placental volume (derived from T2* map segmentations) against birthweight in the preeclampsia group.

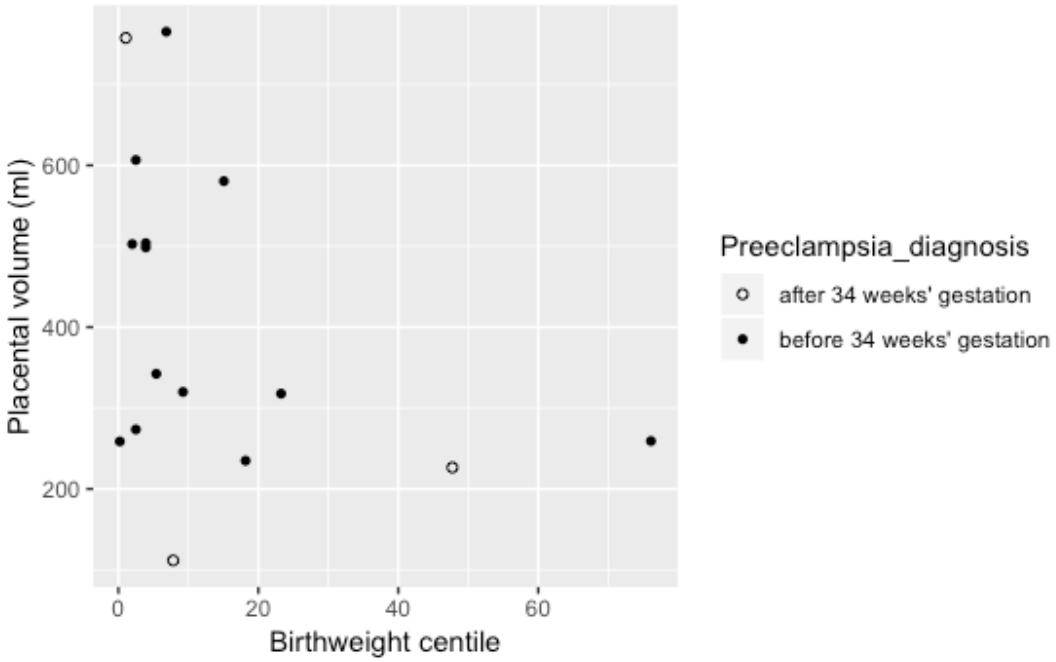

Figure 4.6: Scatterplot of placental volume (derived from T2* map segmentations) against birthweight centile in the preeclampsia group.

In the preeclampsia group, there was no clear trend between lacunarity values and gestational age at diagnosis of preeclampsia, birthweight or birthweight centile (Figures 4.7, 4.8 and 4.9).

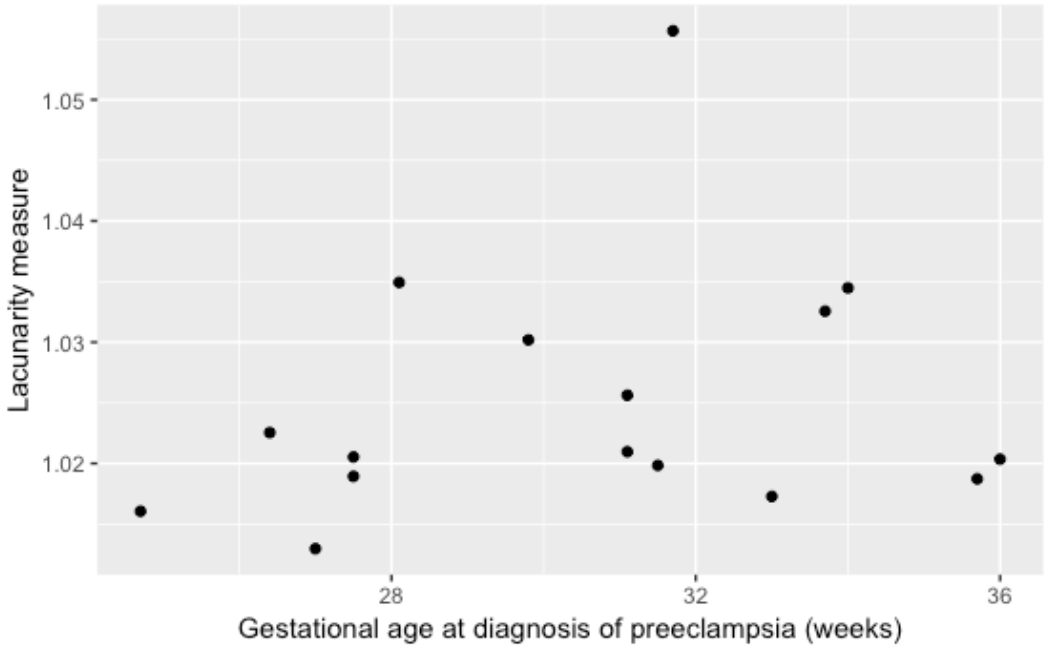

Figure 4.7: Scatterplot of lacunarity measure (derived from T2* mapping) against gestational age at diagnosis of preeclampsia.

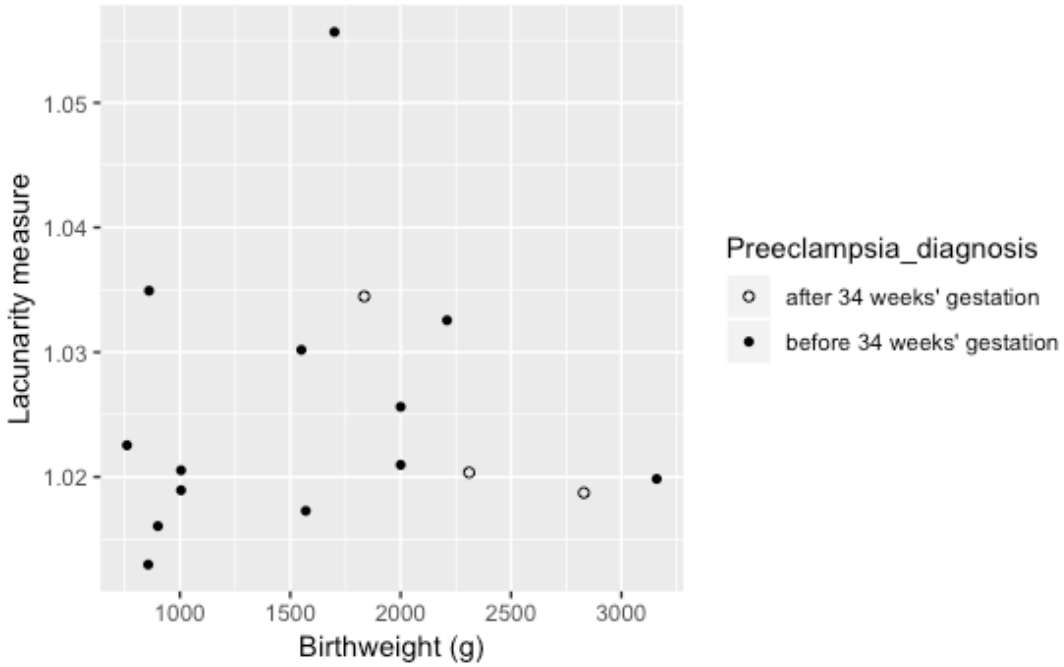

Figure 4.8: Scatterplot of lacunarity measure (derived from T2* mapping) against birthweight in the preeclampsia group.

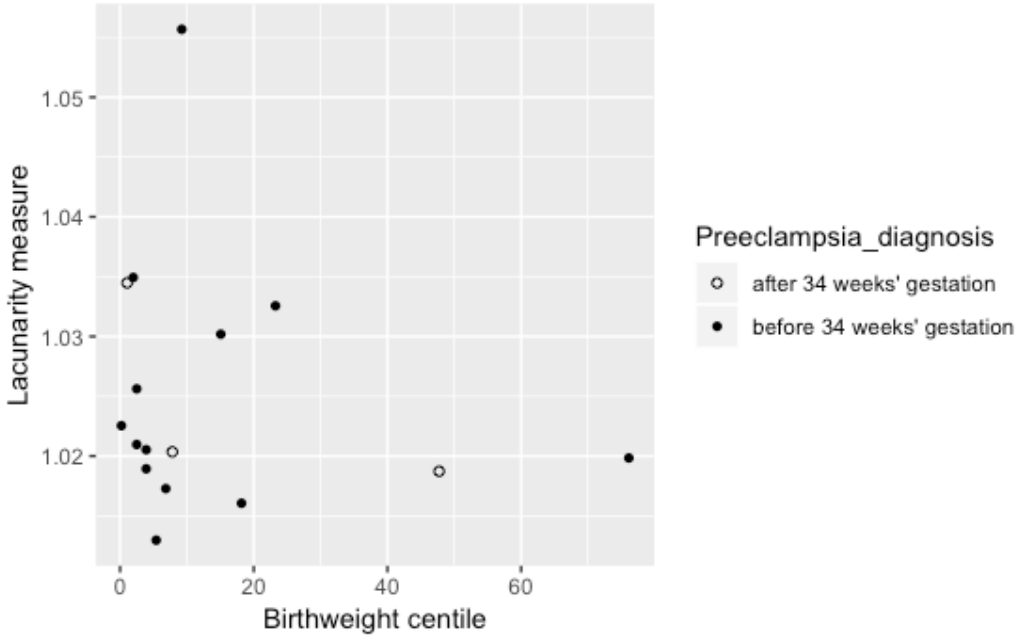

Figure 4.9: Scatterplot of lacunarity measure (derived from T2* mapping) against birthweight centile in the preeclampsia group.

In the preeclampsia group, the umbilical artery pulsatility index (categorised into <95th centile, >95th centile, absent end diastolic flow and intermittently reversed end diastolic flow) did not show a clear relationship with placental mean T2* values (Figure 4.10). For

consistency with birthweight centiles, we have used INTERGROWTH umbilical artery centiles but this is provided in table form only which allows for categorisation.

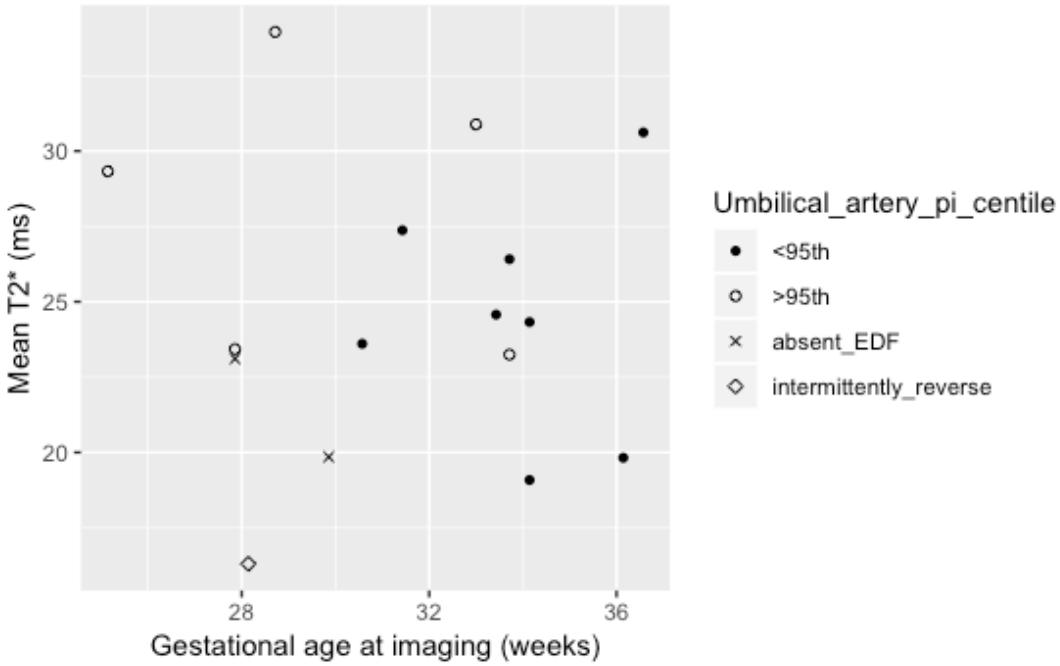

Figure 4.10: Scatterplot of placental mean T2* against gestational age at imaging, categorised into umbilical artery pulsatility index <95th centile, >95th centile, absent end diastolic flow and intermittently reversed end diastolic flow.

Placental volume did not differ significantly between women in the control group and women with preeclampsia (Figure 4.11).

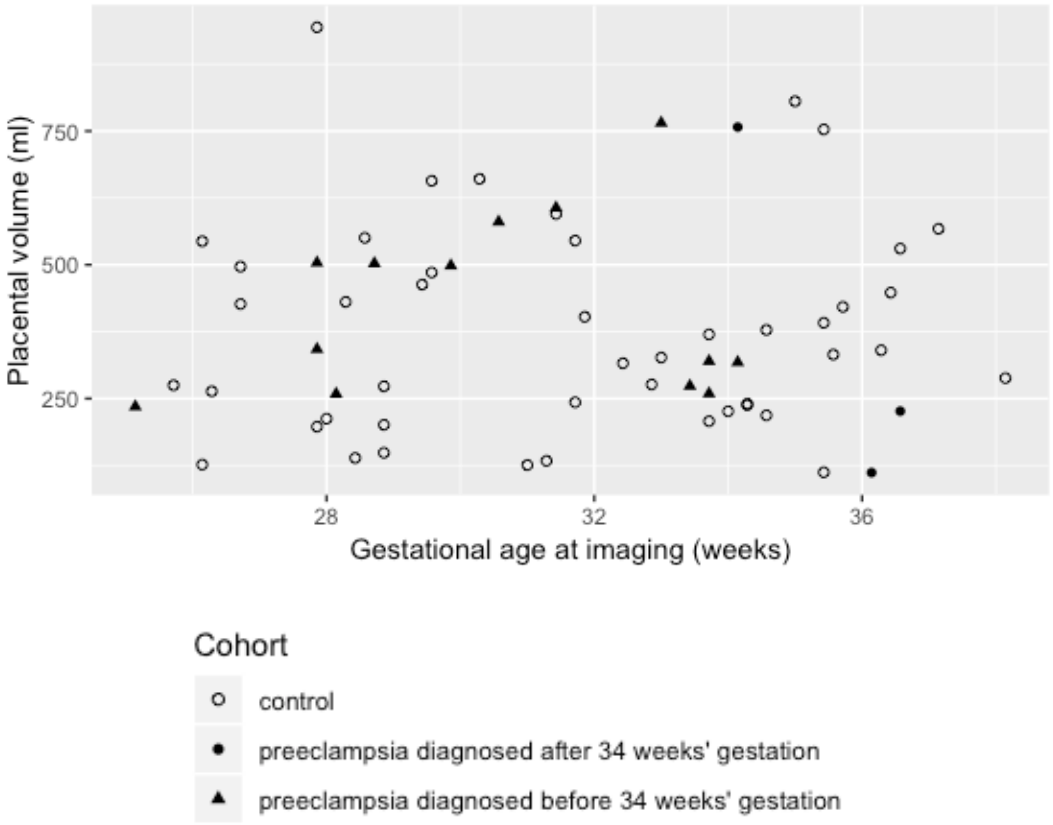

Figure 4.11: Scatterplot of placental volume against gestational age at imaging.

4.5 Discussion

4.5.1 Statement of principal findings

Using a well-tolerated optimised magnetic resonance imaging protocol (Hutter, Jackson, et al. 2019) this study has provided a magnetic resonance whole placental phenotype in pregnancies complicated by preeclampsia and these findings have been compared to a gestation-matched control group.

On visual inspection of T2-weighted imaging, placentae from women with preeclampsia showed substantial areas of low signal intensity, advanced lobularity and high granularity within lobules. Objective magnetic resonance quantification of these placentae also showed a reduced entire placental mean T2* for gestational age, with higher lacunarity values compared with controls. The placental volumes in the preeclamptic group were not significantly different to those in the control group.

4.5.2 Strengths and weaknesses of the study

A major strength of this study is the novelty of the imaging undertaken in women with preeclampsia, particularly assessing placental mean T2* with a measure of texture

(lacunarity values) in a group of women with preeclampsia. Visual analysis can be easily adopted in clinical practice, without the need for further processing of imaging data. However, whilst simple visual analysis of T2-weighted images alone showed characteristic features of the placenta in women with preeclampsia, T2* information obtained objective quantifiable information allowing comparisons between women, amongst which the whole placental mean T2* was the most discriminatory in identifying women with preeclampsia. Rapid acquisition of T2* images (in less than one minute) increases potential for clinical applicability and used a technique which has been previously demonstrated to be reproducible (Hutter, Jackson, et al. 2019). Multi-Echo acquisition was chosen as it freezes motion per slice. All data required for the T2* fit per slice was acquired in less than 250ms. The motion occurring between slices does not influence the fitting process.

Our robust safety approach included blood pressure monitoring with continuous maternal heart rate and oxygen saturation during imaging. A strength of this study is that we have imaged women at a range of gestations (25-37 weeks) in our preeclamptic group with anticipated complications, including fetal growth restriction, iatrogenic preterm delivery, neonatal unit admission and low birthweight centiles. Limitations included being unable to image women with a body mass index greater than 30kg/m^2 due to size limitations of our 3T Achieva scanner bore; however, we have been able to image across the third trimester, thus increasing applicability to a clinical context.

In the scatterplot of placental mean T2* against gestational age at imaging, those women who delivered <3rd birthweight centile have an overlap of T2* values with those women who delivered >3rd birthweight centile. Given the evolution of fetal growth restriction over time and the time points of preeclampsia diagnosis, imaging and delivery, it is challenging to dichotomise the preeclampsia group into those with and those without fetal growth restriction. Additionally, no estimated fetal weight or indices of fetal growth restriction were derived from magnetic resonance imaging. Future research may examine whether the co-existence of fetal growth restriction in women with preeclampsia affect magnetic resonance imaging derived values.

4.5.3 Strengths and weaknesses in relation to other studies

In uncomplicated pregnancies T2-weighted visual analysis shows increasing lobulation with widening of the low signal intensity septal areas around lobules. This and previous studies have shown that this visual maturation corresponds to a reduction in mean T2* values across the placenta (Sinding, Peters, Frøkjaer, et al. 2016; Armstrong et al. 2019; Sinding et

al. 2017). Mean T2* values are consistent with previously reported studies; however, values are inherently affected by magnetic field strength and there remains a lack of literature reporting mean T2* in uncomplicated pregnancies at 3 Tesla (Sørensen et al. 2020). The placental volume is derived from a conservative manual segmentation of the T2* maps to ensure only placental tissue sampled, and thus is smaller than previously reported in the literature where volume is derived from T2-weighted imaging (Andescavage et al. 2017; Langhoff et al. 2017). The conservative method of segmentation presents a limitation. Further studies may address this by using T2 weighted imaging and 3D reconstruction techniques that can further aid placental volume segmentation with clearer placental boundaries. However, T2* values may provide a more informative functional value compared to placental volume.

Our findings of low placental mean T2* values in pregnancies complicated by preeclampsia are consistent with a previous smaller study (Sinding, Peters, Frøkjaer, et al. 2016) in which T2* values were examined in four women with fetal growth restriction, one of whom had co-existing preeclampsia. Another study also examined T2* in a mixed cohort of 33 women (reported as R2* = 1/T2*) at earlier gestations (prior to 24 weeks' gestation) including two women with fetal growth restriction and one with preeclampsia (Armstrong et al. 2019). Mean R2* values in women with fetal growth restriction were similar to uncomplicated pregnancies. However, these women were imaged during early second trimester and all delivered at term thus perhaps suggesting a different disease mechanism in preterm preeclampsia and term preeclampsia. In our study, albeit a small sample size, co-existing fetal growth restriction in women with preeclampsia did not appear to further impact placental mean T2* values. Recent *in vivo* magnetic resonance imaging in women with preeclampsia using a different imaging parameter of placental perfusion fraction (rather than T2* mapping) showed a difference between early and late-onset preeclampsia and a decreased fraction with increasing gestation in controls correlating to maternal biomarkers (Sohlberg et al. 2014; Sohlberg et al. 2015).

Contrast enhanced imaging in Rhesus macaques, has previously demonstrated a slow spread of signal intensity enhancement from a spiral artery across lobule to periphery in a naturally occurring fetal growth restriction case (Lo et al. 2018). No contrast was used in our study; however, we demonstrated a fall in signal intensity from the centre to the periphery of lobules in women with preeclampsia. Previous studies have not included maternal biomarker analysis, while we have shown that all women with a placental growth factor <12pg/mL had a mean T2* lower than gestation-matched controls.

4.5.4 Meaning of the study

The striking visual differences between women with preeclampsia and our control group on T2-weighted imaging and quantitative T2* values provide a magnetic resonance placental phenotype in preeclampsia. Marked widening of low signal septal areas and accelerated maturation of lobules in the placentae of women with preeclampsia suggests areas of non-functioning or poorly functioning tissue. This is supported by detailed histological analysis which showed that ten of twelve placentae from women with preeclampsia had evidence of maternal vascular malperfusion. Areas of low signal intensity on T2-weighted imaging therefore likely reflect a poorly perfused and poorly oxygenated placenta with a corresponding short T2*, also reflected in low maternal placental growth factor concentrations. In a healthy placenta, these low signal intensity areas are consistently between lobules and likely to represent normal septae with low oxygenation. In abnormal placentae, the areas of low signal intensity on T2 are different in distribution, size and shape, suggesting poorly oxygenated areas extending beyond the normal septae. More detailed histology to selectively sample these areas would further elucidate any structural differences. All women had haemoglobin concentrations within normal limits and thus this is unlikely to have substantially affected T2* values. Within lobules, there are regional T2* differences with a marked decline in T2* towards the lobule periphery in preeclampsia. This could be explained by a reduction in perfusion of the lobule periphery with oxygenated blood following ischaemic reperfusion injury from high pressure flow in poorly remodelled spiral arteries. The peripheral areas of lobules may be more vulnerable to damage, giving rise to the areas of short T2* distal from central arteries. High lacunarity values in women with preeclampsia further support the visual phenotype seen on both T2-weighted imaging and T2* maps where there is high granularity within individual lobules and heterogeneity across the placenta.

4.5.5 Unanswered questions and future research

More detailed placental histology, biomarkers relating to placental oxygenation and diffusion magnetic resonance imaging may yield further insight into the pathophysiology of preeclampsia in conjunction with placental T2* mapping. While the relationship between concentration of deoxygenated haemoglobin and T2* values is well established (BOLD effect), it does not allow absolute quantification of oxygen concentration. T2* depends additionally on geometry, saturation, haemoglobin concentration.

A larger sample size of women with preeclampsia encompassing those with and without co-existing fetal growth restriction and those with early and late onset would be beneficial

to examine potential differing mechanisms that result in additional fetal morbidity. Placental magnetic resonance imaging may demonstrate different phenotypes in these sub-groups, aligned with different placental histological findings, and require further elucidation. Further characteristics of interest would include the presence of other co-morbidities, use of antihypertensive medication and aspirin usage. It would be advantageous to image using a wide bore scanner at 3 Tesla to encompass those women in whom a high body mass index and girth is more prevalent. Further studies could be useful to investigate the potential role of placental growth factor (and other maternal serum biomarkers of placental function, alongside conventional ultrasound parameters) for triage of clinically higher risk women in whom placental magnetic resonance imaging may be beneficial. However, the two modalities (biomarkers and magnetic resonance imaging) may be providing complementary predictive and mechanistic information.

4.6 Perspectives

Our study using T2-weighted imaging, T2* mapping and maternal placental growth factor concentrations has quantitatively demonstrated a placental phenotype in preeclampsia that has helped to support prevailing theories of complex mechanisms underlying placental dysfunction in preeclampsia. Further studies to determine whether there is a potential role for predicting the subsequent development of preterm preeclampsia in high risk groups (for example those with chronic hypertension, gestational hypertension) or women undergoing a fetal magnetic resonance imaging for other indications (such as fetal congenital cardiac abnormalities or fetal growth restriction) would be of interest. Future applications of T2* mapping may include monitoring of high-risk pregnancies to aid clinical management decisions or measuring effectiveness of new therapies in preeclampsia that aim to target underlying oxidative mechanisms.

4.7 Novelty and Significance

4.7.1 What Is New?

- Using *in vivo* magnetic resonance imaging to quantify placental function, we have evaluated and demonstrated a placental phenotype in women with pregnancies complicated by preeclampsia.
- Techniques include T2* mapping as an indicative measure of placental oxygenation and the use of lacunarity to quantify the spatial distribution of gaps of a given size across a region of interest.
- The placentae of women with preeclampsia have low mean T2* and high lacunarity values.

4.7.2 What Is Relevant?

- Preeclampsia is a hypertensive disorder of pregnancy associated with adverse pregnancy outcome.
- Placental dysfunction underlies the aetiology of these pregnancies.
- MRI provides objective quantification of placental function *in vivo* and elucidation of complex mechanisms underlying preeclampsia development, thus has potential to inform prognosis and clinical management.

4.8 Summary

This prospective observational study has used T2-weighted imaging, T2* mapping and maternal placental growth factor concentrations to quantitatively demonstrate a placental phenotype in preeclampsia.

4.9 Supplemental Data

4.9.1 Supplemental Tables

Supplemental Table S1: Primary reason for induction or prelabour caesarean (taken from clinical notes).

Primary reason for induction or prelabour caesarean	Control n = 17	Preeclampsia n=14
Fetal growth restriction	0	5 (36)
Preeclampsia and reached 37/40	0	3 (21)
Difficult blood pressure control	0	3 (21)
Abnormal cardiotocogram	1 (6)	2 (14)
Randomised to planned delivery within trial	0	1 (7)
Prelabour rupture of membranes	5 (29)	0
Post dates	4 (24)	0
Previous caesarean/uterine surgery	2 (12)	0
Fetal presentation not cephalic	2 (12)	0
Maternal request	2 (12)	0
Placenta praevia	1 (6)	0

Values given as a number (percentage) unless stated otherwise

Supplemental Table S2: Actual placental mean T2*, lacunarity and volume values.

Placental imaging variables	**26-29+6 weeks**	**30-33+6 weeks**	**34-37+6 weeks**
Preeclampsia			
Mean T2*, ms, median (IQR)	23 (20-23)	26 (24-27)	22 (20-26)
Lacunarity, median (IQR)	1.021 (1.019-1.023)	1.023 (1.020-1.029)	1.026 (1.020-1.033)
Placental volume, ml, median (IQR)	499 (342-503)	450 (285-600)	272 (197-428)
Control			
Placental volume, ml, median (IQR)	427 (201-497)	321 (234-438)	385 (263-510)
Mean T2*, ms, median (IQR)	67 (54-73)	45 (41-56)	38 (28-40)
Lacunarity, median (IQR)	1.012 (1.010-1.014)	1.017 (1.016-1.019)	1.017 (1.015-1.017)

4.9.2 Supplemental Figures

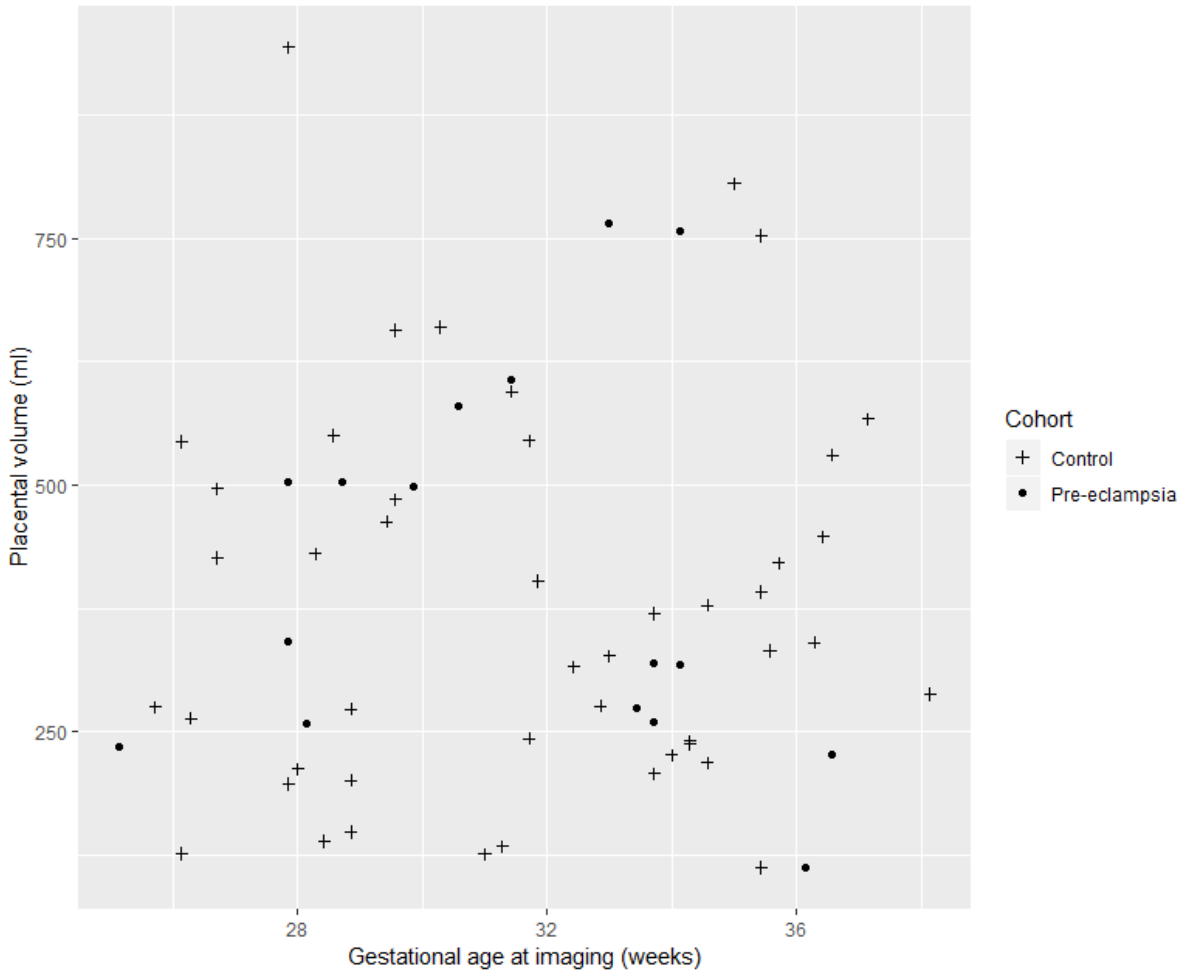

Supplemental Figure S1: Scatterplot of placental volume against gestational age at imaging.

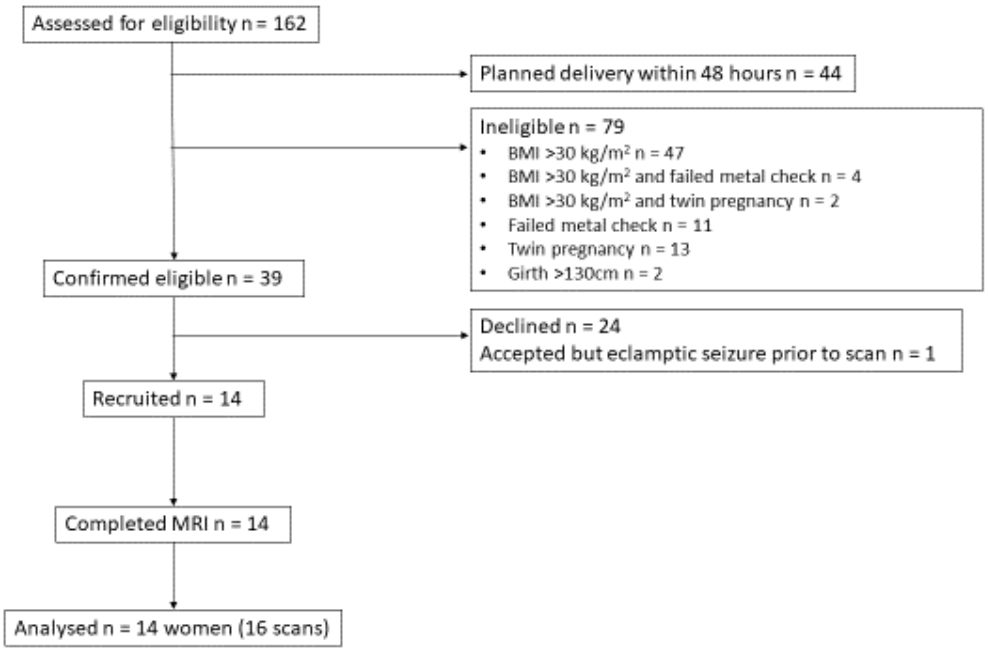

Supplemental Figure S2: Flow diagram of participants with preeclampsia.

Chapter 5 PLACENTAL MAGNETIC RESONANCE IMAGING IN CHRONIC HYPERTENSION: AN OBSERVATIONAL STUDY

5.1 Introduction

Chronic hypertension complicates an estimated 3-5% of all pregnancies (Seely and Ecker 2014) with a rising incidence associated with a global increase in obesity and maternal age. Adverse pregnancy outcomes associated with chronic hypertension include superimposed preeclampsia, preterm delivery, low birthweight, perinatal death and an increased incidence of neonatal admission and caesarean delivery (Bramham et al. 2014), occurring independent of the development of superimposed preeclampsia (Sibai et al. 1998).

Altered placental structure and function may contribute to the pathophysiology of adverse pregnancy outcomes. Histological examination of placentae have demonstrated lesions related to maternal vascular malperfusion to be more prevalent in women with chronic hypertension and preeclampsia compared to those without hypertensive disorders of pregnancy (Kovo et al. 2017; Bustamante Helfrich et al. 2017). In pregnancies complicated by preeclampsia, altered early placental perfusion is hypothesised to lead to placental oxidative stress with cellular damage of fragile villous trees and inflammation. Subsequent ischaemia-reperfusion injury alters the balance of placentally expressed antiangiogenic and angiogenic compounds which can be detected in the maternal circulation (Levine et al. 2004). The clinical manifestation of disease is considered to relate to the interaction between the release of placentally-derived factors and subsequent maternal responses, exacerbated by pre-existing comorbidities characterised by maternal vascular endothelial dysfunction (such as chronic hypertension or renal disease) (Redman and Sargent 2010).

The use of magnetic resonance imaging as a tool to provide *in vivo* assessment of the placenta structure and function is of growing interest. Imaging sequences can be acquired within a clinically acceptable time of 15 minutes to acquire comprehensive assessment including T2* mapping and diffusion MRI (Slator et al. 2019). Resultant measures of interest include the T2* relaxation time (an indicative measure of tissue oxygenation), T1 relaxation (related to oxygen tension) and measures of diffusion (assessing the microstructural properties through the random thermal microscopic translational motion of molecules). Reduced placental T2*(Siauve et al. 2019), mean diffusivity values and reduced mean T1 relaxation times (Ingram et al. 2017)are reported in pregnancies complicated by fetal growth restriction and thus provide a promising indicator of placental dysfunction.

To our knowledge, no studies have assessed the use of magnetic resonance imaging to aid understanding of the heterogeneity of pregnancy outcomes in women with chronic hypertension. The aim of this study was to explore the use of magnetic resonance imaging as a tool to elucidate the placental phenotype in women with chronic hypertension.

5.2 Materials and Methods

5.2.1 Study Design

This prospective observational study was undertaken at St Thomas' Hospital, London, a tertiary level maternity unit. Women with chronic hypertension attending a consultant led specialist antenatal hypertension clinic were approached in person. Women in the control group were recruited at their routine 20-week anomaly scan or self-referred to take part in the study. All women in the study gave written informed consent (Placenta Imaging Project, IRAS 201609). The primary objective of the Placental Imaging Project was to develop a novel magnetic resonance imaging approach to assess growth and development of the human placenta. Women were considered for inclusion in the study if they had a singleton pregnancy, were over 16 years of age, not claustrophobic and had no contraindication for magnetic resonance imaging. Chronic hypertension and preeclampsia were prospectively defined using the international consensus definition (Brown et al. 2018). Clinical management of hypertensive women was according to national guidelines, with responsibility under the attending obstetrician. Follow up was until delivery, with the last woman enrolled delivering in August 2019. Prospective specified data collection included baseline demographic characteristics, maternal and neonatal outcomes.

Women in the control group fulfilled the following criteria: no diagnosis of hypertensive disorder at enrolment and until delivery, no significant past medical history, no pregnancy complications (including gestational diabetes), delivery at term with birthweight between the 3rd and 97th centile (calculated using INTERGROWTH-21st, version 1.3.5) (Villar et al. 2014) thus excluding potential confounders of placental change (Desoye and Hauguel-de Mouzon 2007; Llurba et al. 2014; Salafia et al. 1995). These women were gestation-matched (within a two week gestation range) to women with chronic hypertension, masked to values derived from magnetic resonance imaging, on a 2:1 basis.

No formal sample size was calculated for power of outcome variables as this was an exploratory study describing a novel technique in technology development application. This study was approved by Fulham Research Ethics Committee, REC 16/LO/1573.

5.2.2 Magnetic Resonance Imaging

Magnetic resonance imaging was performed on either a clinical Philips 3T Achieva (60 cm bore) or a Philips 1.5T Ingenia (with a wider 70 cm bore). Parameters were kept constant between women with chronic hypertension and the control group. Women underwent magnetic resonance imaging on up to two occasions, a minimum of two weeks apart and at any time point between their clinically routine anomaly ultrasound scan (at around 18-22 weeks' gestation) and delivery. Imaging was performed supine with padding to support the lower limbs and shoulders, after an initial period of three minutes in left lateral to shift the uterus and minimise potential effects of venocaval compression. Total imaging time did not exceed one hour, and women were offered a break of up to 30 minutes halfway through the scan. Maternal assessments during imaging included continuous maternal heart rate and oxygen saturation monitoring with additional blood pressure measurements every 10 minutes. An obstetrician or midwife was present throughout the scan. No pharmacological sedation was used.

Image based shimming was achieved using an in-house tool, based on a separately acquired B0 map, in order to reduce the effect of inhomogeneities in the magnetic field. To provide anatomical images of the fetus and placenta and their position within the uterus, a T2-weighted single shot turbo spin echo sequence with an echo time (TE) of 180ms of the whole uterus (thereby including placenta) was acquired in coronal and sagittal planes to the woman with repetition time (TR) = 16s, SENSitivity Encoding (SENSE) = 2.5 and partial Fourier 0.625. In-plane resolution was 1.5 mm x 1.5mm, slice thickness 2.5mm with an overlap of 0.5mm. The field of view was 300 x 360 x [100-200] mm (coronal) and 300 x 300 x 340 mm (sagittal) in the foot-head (FH) x right-left (RL) x anterior-posterior (AP) directions respectively.

T2* weighted imaging was acquired using a multi-echo gradient echo, echo planar imaging sequence with free breathing and took less than one minute. For 3T scanning, 5 echo times were used: 13.81ms/ 70.40ms/ 127.00ms/ 183.60ms/ 240.2ms, TR=3s, SENSE=3, halfscan=0.6 at 3mm3 resolution with the whole placenta covered within 60 slices. For 1.5T scanning, 5 echo times were used: 11.376ms / 57.313ms / 103.249ms / 149.186ms / 195.122ms, TR=14s, no SENSE, no halfscan at 2.5mm3 resolution with the whole placenta covered within 90 slices. Echo times result from the chosen Echo Planar Imaging (EPI) train characteristics. The intra-echo spacing was chosen to minimize acoustic noise and the inter-

echo spacing as the minimal possible spacing given chosen resolution and field of view. Data was acquired in the maternal coronal plane.

Given the methods development required during the course of this study, a diffusion prepared spin echo with subsequent gradient echoes was performed in a subset of 31 women, imaged at 3 Tesla, for combined diffusion-relaxometry (Hutter et al. 2018). In another subset of women, a modified inversion-recovery sequence with a global adiabatic inversion pulse and slice shuffling (Ordidge et al. 1990) was also employed with 10 inversion times to produce T1 maps.

An in-house Python script was used to produce T2*, T1 and apparent diffusion coefficient maps by fitting monoexponentially decay curves. The diffusion data were motion corrected using Advanced Normalization Tools, ANTS, a nonrigid template registration (Avants, Johnson, and Tustison 2015). The placenta images were manually segmented by two experienced observers (AH and JH). Further processing steps calculated mean apparent diffusion coefficient values, placental T2*, and kurtosis and skew of T2* histograms, and calculation of mean T1. The acquisition and processing pipeline has been described previously and shown to have good reproducibility with a high Dice coefficient (0.86) between observers who segmented the placenta (Hutter, Jackson, et al. 2019).

As part of this study, anatomical T2-weighted imaging of the fetal brain was performed in three orthogonal planes to the woman suitable for volume reconstruction and clinical reporting (Jiang et al. 2007). Fetal brain images were reported and available to the clinical team. Visual analysis of the placenta was performed and included assessment of signal intensity across the placenta and documentation of the appearance of placental lobules and septa. The signal intensity within lobules was visually assessed for granularity with high granularity defined as the presence of both high and low signal intensity within individual lobules.

5.2.3 Placental growth factor, PlGF

Maternal venepuncture was performed as close to magnetic resonance imaging as feasible, usually on the same day. Six millilitres of blood were drawn into a bottle containing ethylenediamine tetra-acetic acid, transported to the laboratory within 1 hour and underwent centrifugation at 1400 x g (rcf) for 10 minutes at 4˚C. PlGF was quantified using the Triage PlGF Test (Alere, San Diego, CA) according to the manufacturer's instructions while masked to both group and clinical outcome. The clinical team did not receive the result.

5.2.4 Ultrasound

Ultrasound scans were performed on the same day as magnetic resonance imaging wherever possible, or within two weeks. Women with pre-eclampsia had a clinically indicated ultrasound scan performed in line with national guidelines for management of pre-eclampsia (National Institute for Health and Care Excellence 2019). In the control group, ultrasound scans were performed on a Philips EPIQ V7 by sonographers following a clinical protocol. Fetal measurements included biparietal diameter, head circumference, femur length and abdominal circumference which were used to derive an estimated fetal weight using the Hadlock formula [24], umbilical artery Doppler pulsatility index (PI), amniotic fluid index and maternal uterine artery pulsatility index. The presence of fetal growth restriction was established by ultrasonographic assessment using accepted international definitions (Gordijn et al. 2016).

5.2.5 Placental Histology

Following delivery and where available, placentas from women in both groups (chronic hypertension and healthy pregnancies) underwent histological examination according to local protocols at the Cellular Pathology Department, St Thomas' Hospital. Placentas were fixed in 10% buffered formalin and trimmed of both umbilical cord and membranes for placenta weight. The following areas were sampled and then embedded in paraffin: two transverse sections of the umbilical cord, one roll of membranes (including rupture site), two to three full thickness blocks of the placental parenchyma away from the placental edge (including fetal and maternal surfaces). Additional areas were sampled depending on macroscopic findings. Paraffin embedded tissue sections were then cut into four-micron sections, deparaffinized and stained with haemotoxylin and eosin prior to histological examination. A clinical report for all placentas submitted was issued, in accordance with local hospital reporting guidelines. Histological slides were then re-examined by a second experienced histopathologist (masked to first report and to clinical details) specifically for features of maternal vascular malperfusion, fetal vascular malperfusion and acute chorioamnionitis; classified using guidelines from the International Placental Pathology Consensus Meeting, Amsterdam 2014 (Redline et al. 2005; Redline 2015) Any discrepancies between the two reporting histopathologists were re-examined (again masked to the pregnancy outcome) and a consensus opinion was reached.

5.2.6 Statistical methods

In uncomplicated pregnancies, gestation-adjusted reference ranges for placental mean T2* were established using the Stata command xriml, and the 10% to 90% reference range

established. Birthweight centiles were calculated using INTERGROWTH-21st version 1.3.5 (Villar et al. 2014). Statistical analysis was performed using Stata version 15.1 (StataCorp, College Station, Texas).

5.3 Results

129 women underwent placental imaging: 43 women with chronic hypertension were gestation matched to 86 controls (Table 5.1, Supplemental Table S1, Supplemental Figure S1). Of these, 30 women with chronic hypertension and 70 controls were imaged on the 3T Achieva, while 13 women with chronic hypertension and 16 controls were imaged on the 1.5T Ingenia. Maternal PlGF concentrations around time of imaging were lower in women with chronic hypertension (186pg/mL, IQR 109-321) than the control group (341pg/mL, IQR 230-656) (Table 5.1).

There are differences in the demographic findings at booking between the chronic hypertensive group and the control group (Table 5.1). Women had a higher median maternal age of 37 years (IQR 34-41) in the chronic hypertensive group in conjunction with a lower proportion of nulliparity and a higher proportion of black ethnicity women. The median maternal age was 34 years (IQR 32-37) in the control group with a higher proportion of nulliparity. This reflects the risk factors of maternal age and ethnicity in the development of chronic hypertension.

Table 5.1: Characteristics at booking and enrolment.

	Chronic hypertensive pregnancies	**Control pregnancies**
Number of women	43	86
At booking		
Maternal age, y, median (IQR)	37 (34-41)	34 (32-37)
Body mass index, kg/m^2, median (IQR)	26 (24-30)	23 (21-25)
Nulliparous	15 (35)	45 (52)
White ethnicity	25 (58)	75 (87)
Black ethnicity	8 (19)	4 (5)
Other ethnicity	10 (23)	7 (8)
Current smoking	0	1 (1)
Quit smoking before pregnancy	1 (2)	4 (5)
Never smoked	37 (86)	73 (85)
Previous pre-eclampsia	7 (16)	1 (1)
Chronic renal disease	6 (14)	0
Gestational diabetes	2 (5)	0
At enrolment on day of MRI		
Gestational age, wk, median (IQR)	27.7 (23.9-32.1)	28.9 (26.1-32.9)

Table 5.1 (cont)	**Chronic hypertensive pregnancies**	**Control pregnancies**
Aspirin	38 (88)	7 (8)
Ultrasound estimated fetal weight, centile, median (IQR)	48 (27-70)	54 (42-68)
Placental Growth Factor, pg/mL, median (IQR)	187 (109-321)	341 (230-656)
Placental growth factor <100 pg/mL	6 (14)	6 (7)
Placental growth factor <12 pg/mL	1 (2)	0
Systolic blood pressure, mmHg, median (IQR)	125 (115-133)	108 (102-114)
Diastolic blood pressure, mmHg, median (IQR)	79 (71-83)	63 (57-74)
During MRI		
Systolic blood pressure, mmHg, median of individual medians (IQR)	112 (108-115)	99 (95-105)
Diastolic blood pressure, mmHg, median of individual medians (IQR)	69 (63-74)	59 (55-64)

Values given as a number (percentage) unless stated otherwise.

Four out of 43 women (9%) with chronic hypertension developed superimposed preeclampsia (Table 5.2, Supplemental Table S2). Nine (21%) of women with chronic hypertension delivered prematurely compared with no preterm deliveries in the control group (Table 5.2, Supplemental Table S2). 38 (88%) of women with chronic hypertension had a planned delivery (pre-labour caesarean section or induction of labour) compared to 32 (37%) in the control group (Table 5.2, Supplemental Table S2).

68 placentas were examined after delivery (24 from women with chronic hypertension, 44 from controls) (Table 5.2). Five out of six placentae with maternal vascular malperfusion features on histological examination were from women with chronic hypertension (Table 5.2)

Table 5.2: Maternal and neonatal outcomes.

	Chronic hypertensive pregnancies	**Control pregnancies**
Number of women	43	86
Time from MRI to delivery, days, median (IQR)	70 (37-96)	84 (53-99)
Pre-eclampsia	4 (9)	0
Onset of delivery		
Spontaneous	5 (12)	55 (64)
Induction	19 (44)	20 (23)
Pre labour caesarean	19 (44)	12 (14)
Mode of delivery		
Spontaneous vaginal delivery	9 (21)	47 (55)
Assisted vaginal delivery	4 (9)	18 (21)
Elective pre-labour caesarean section	10 (23)	10 (12)
Urgent caesarean section	20 (47)	11 (13)
Primary reason for induction or prelabour caesarean*		
Maternal indication	30 (74)	15 (17)
Fetal indication	8 (19)	16 (19)
Delivery		
Livebirth	43 (100)	86 (100)
Gestational age at delivery, weeks, median, IQR	38.3 (37.5-38.9)	40 (39-41)
Preterm birth <37/40	9 (21)	0

Table 5.2 (cont)	**Chronic hypertensive pregnancies**	**Control pregnancies**
Birthweight, g, median (IQR)	2965 (2520-3362)	3482 (3229-3721)
Birthweight centile, centile, median (IQR)	37 (16-70)	68 (32-83)
Number admitted to neonatal unit for >=48 hours	4 (9)	1 (1)
Prematurity	2 (5)	0
Fetal growth restriction/ small for gestational age	0	0
Respiratory disease	0	1 (1)
Suspected sepsis	0	0
Hypoglycaemia	2 (5)	0
Placental histology findings		
Number of placentae assessed	24	44
Placental weight, g, median (IQR)	384 (310-467)	474 (409-556)
Fetal-placental birthweight ratio, median (IQR)	7.2 (6.0-7.9)	7.3 (6.7-7.9)
Maternal vascular malperfusion features	5 (21)	1 (2)
Fetal vascular malperfusion features	1 (4)	0
Chorioamnionitis features	6 (25)	25 (57)

Values given as a number (percentage) unless stated otherwise. *Full details given in Supplementary Table 1.

Visual analysis of placental images demonstrated that in women with chronic hypertension, appearances were more varied compared to gestation-matched controls (Figure 5.1). Placental images from women with chronic hypertension appeared either appropriate for gestation or advanced for gestation, showing increased lobulation, with wider septa and more marked heterogeneity than expected for age. This was also apparent when visually

assessing the T2* maps. Reflecting this visual analysis, women with chronic hypertension showed a greater range of placental mean T2* values for a given gestation compared to the control group (Figure 5.2).

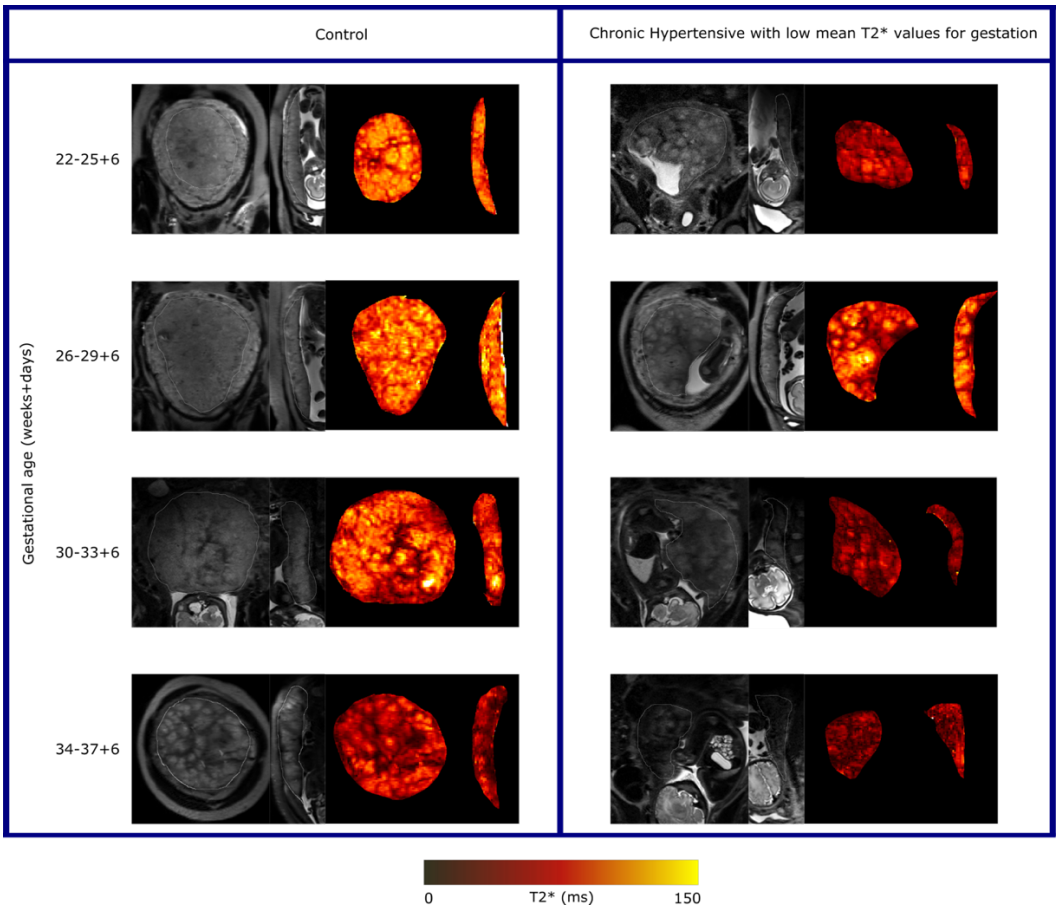

Figure 5.1: Example T2-weighted placental imaging and T2* maps in coronal and sagittal planes across gestation.
On the left, the control panel depicts the following from left to right: T2-weighted imaging in the coronal plane, T2-weighted imaging in the sagittal plane, T2* map in the coronal plane and T2* map in sagittal plane. On the right, the panel depicts images from women with chronic hypertension and a placental mean T2* value below the 10th centile. Within the panel from left to right, images are in the following order: T2-weighted imaging in the coronal plane, T2-weighted imaging in the sagittal plane, T2* map in the coronal plane and T2* map in sagittal plane. Within the T2* maps, darker areas represent low T2* values while brighter orange-yellow areas high T2* values.

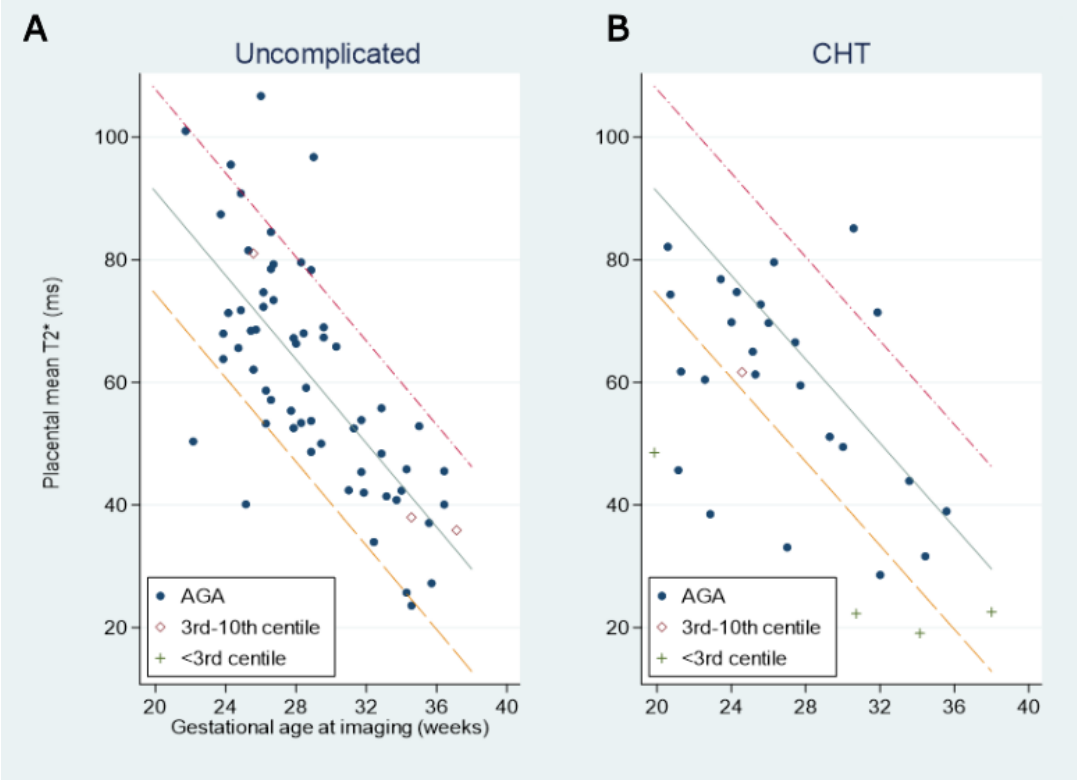

Figure 5.2: Scatterplot of placental mean T2* against gestational age at imaging, subdivided by birthweight centile at subsequent delivery to show appropriate for gestational age (AGA) infants, and those small for gestational age (SGA), divided into 3rd-10th centile, and those <3rd centile (A) in uncomplicated control group and (B) in women with chronic hypertension.

Exemplar histograms of T2* values at 27 weeks' gestation in four different women (Figure 5.3) visually illustrate further analysis of T2* histograms assessing both kurtosis and skewness. This further analysis demonstrated differences in the placenta from those chronic hypertension pregnancies with apparently normal mean T2* placental values. For example, when compared to a T2* placental histogram from a control pregnancy (Figure 5.3A) a lower kurtosis value in the placental signal intensity frequency distribution in a pregnancy with chronic hypertension is demonstrated, despite a mean T2* appropriate for gestational age (Figure 5.3B). A lower mean T2* value corresponds to a left shift in the histogram (for example, in a woman with chronic hypertension (Figure 5.3C). A left shift and higher skewness value (asymmetrical frequency distribution) is seen in a woman with preeclampsia superimposed on chronic hypertension (Figure 5.3D).

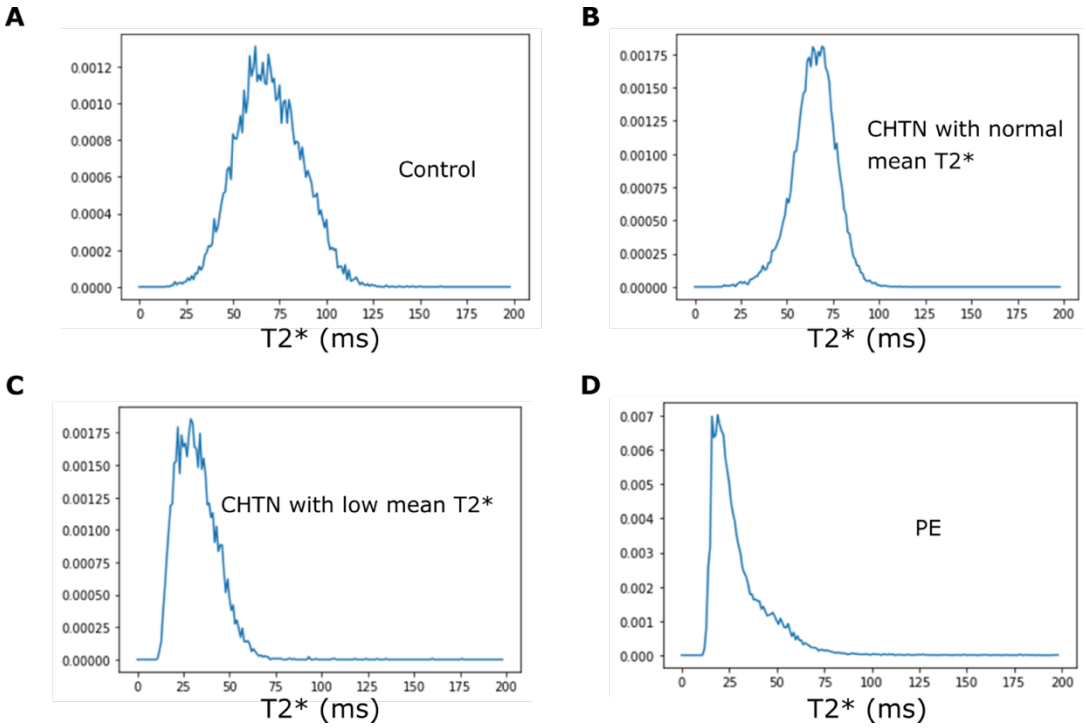

Figure 5.3: Illustrative histogram plot of T2* values at the same gestation (27 weeks' gestation) for one woman from each of the following groups (A) the control group (B) with chronic hypertension (CHTN) and normal placental mean T2* (C) with chronic hypertension and a placental mean T2* less than the 10th centile for gestation (D) CHTN participant who developed superimposed preeclampsia (PE).

Both skewness and kurtosis increased with advancing gestational age at imaging (**Figure 5.4**). Visual inspection showed that some women with chronic hypertension who developed superimposed pre-eclampsia had higher skewness and kurtosis values, compared to the remaining group with chronic hypertension, the majority of whom had values within the range of the control group. The women who developed superimposed preeclampsia on a background of chronic hypertension with skewness and kurtosis values within the range of the control group, delivered at term and of normal birthweight centile. For the presentation of results of skewness and kurtosis values, we have included an additional dataset of women with preeclampsia imaged at 3T in whom we have previously reported enrolment and pregnancy outcome characteristics (Ho et al. 2020). Enrolment and pregnancy outcomes of preeclampsia pregnancies imaged at 1.5T are provided in Supplemental Table S1.

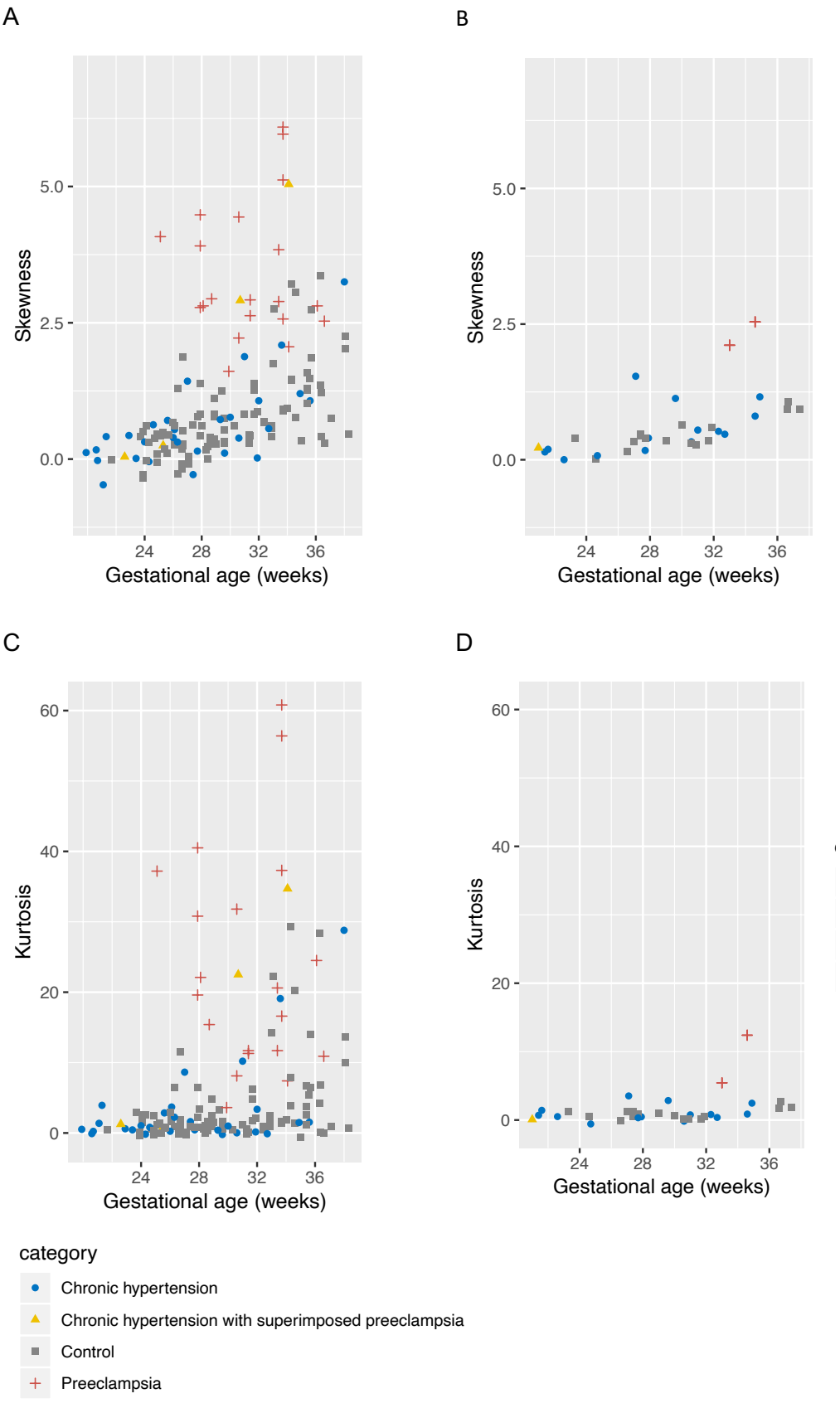

Figure 5.4: Scatterplot of histogram derived measures of (A) skewness at 3T imaging (B) skewness at 1.5T imaging (C) kurtosis at 3T imaging and (D) kurtosis at 1.5T imaging against gestational age at scan with i) chronic hypertension ii) chronic hypertension at

enrolment who subsequently developed superimposed preeclampsia after imaging iii) controls iv) preeclampsia at enrolment.
For the presentation of results, we have included an additional dataset of women with preeclampsia imaged at 3T in whom we have previously reported enrolment and pregnancy outcome characteristics (Ho et al. 2020) and women with preeclampsia imaged at 1.5T in whom enrolment and pregnancy outcome characteristics are provided in Supplemental Table S1 and S2.

When comparing between groups, there was no significant difference in skewness and kurtosis values between the chronic hypertension and control group (geometric mean ratio for skewness values = 0.82, 95% CI 0.67-1.01, geometric mean ratio for kurtosis values = 0.83, 95% CI 0.58-1.19). In contrast, women with preeclampsia had higher skewness and kurtosis values compared to controls (geometric mean ratio for skewness values = 3.15, 95% CI 2.39-4.15, geometric mean ratio for kurtosis values = 7.55, 95% CI 4.53-12.58).

In our subsample, placental apparent diffusion coefficient (ADC) appeared to decline with advancing gestational age (Figure 5.5A). There was a positive correlation between ADC values and placental mean T2* values (Figure 5.5B). Placental mean T1 also declined with advancing gestational age (Figure 5.5C) and positively correlated with mean ADC values (Figure 5.5D). Trends in mean ADC values were consistent with data acquired during the methods development required during the course of this study (Figure 5.6).

A

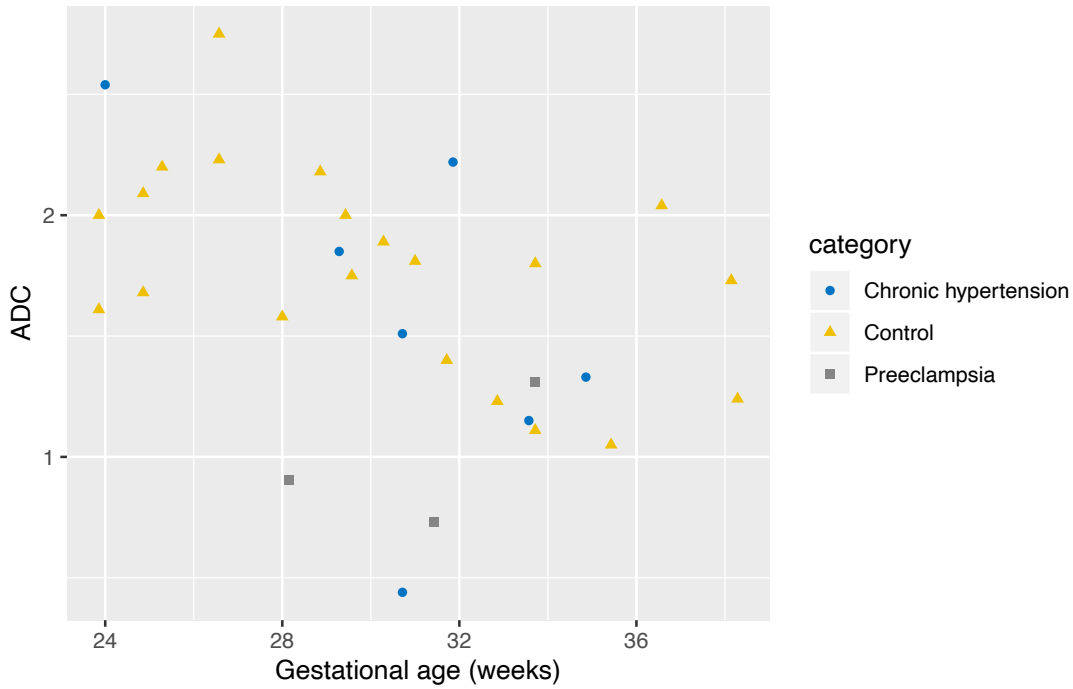

B

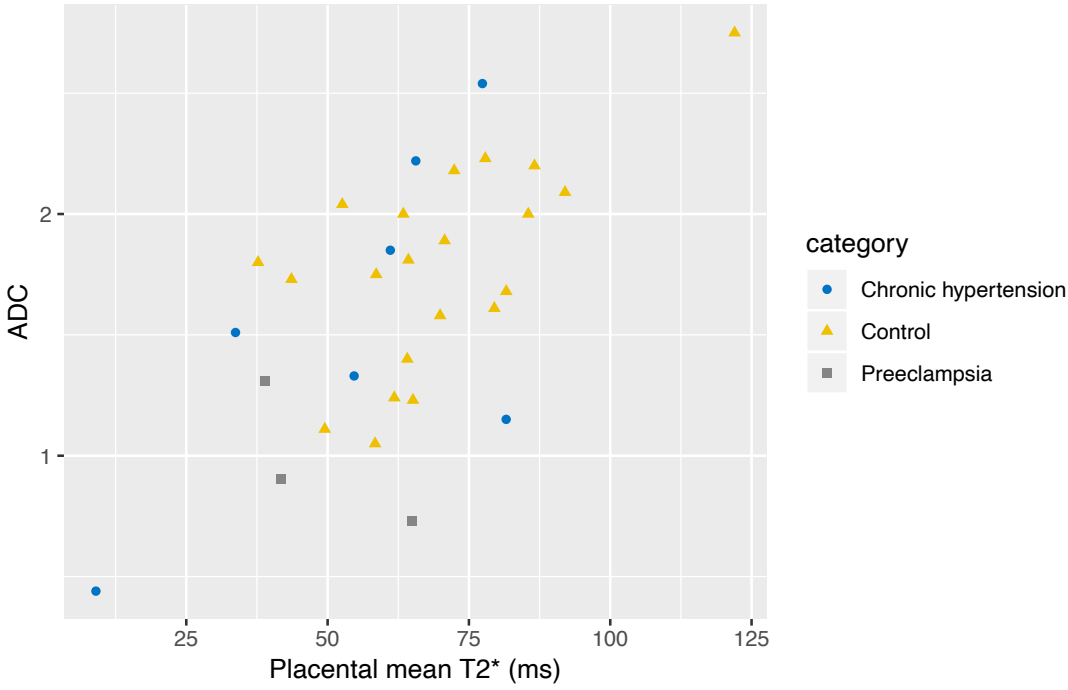
ADC
2
1
25
50
75
100
125
Placental mean T2* (ms)
category
Chronic hypertension
Control
Preeclampsia

C

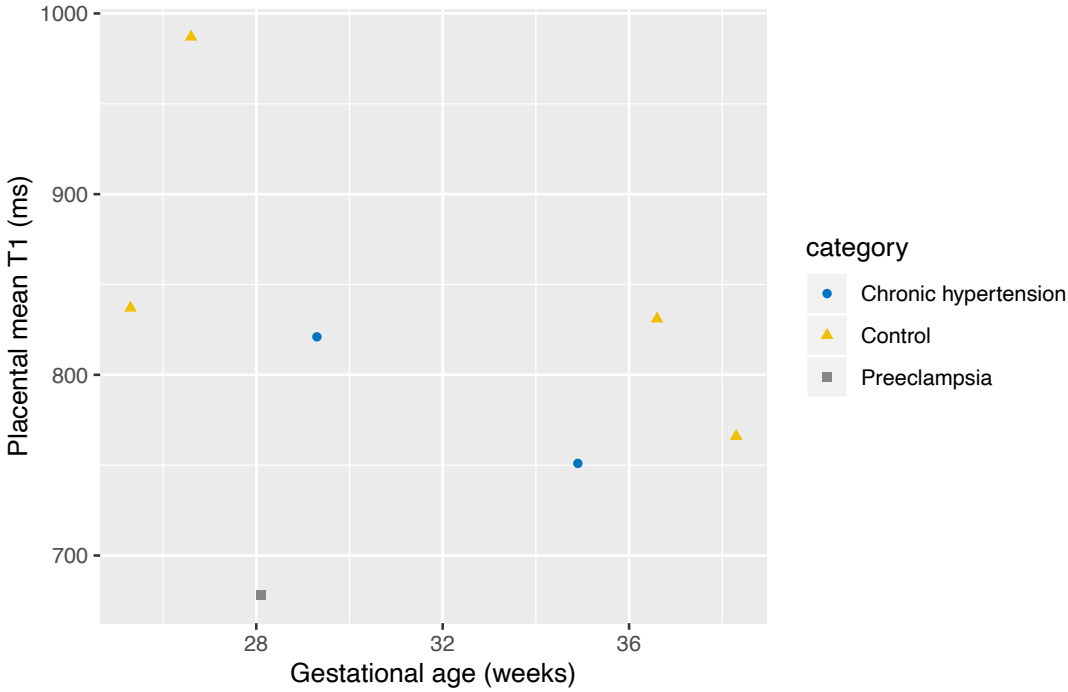
Placental mean T1 (ms)
1000
900
800
700
28
32
36
Gestational age (weeks)
category
Chronic hypertension
Control
Preeclampsia

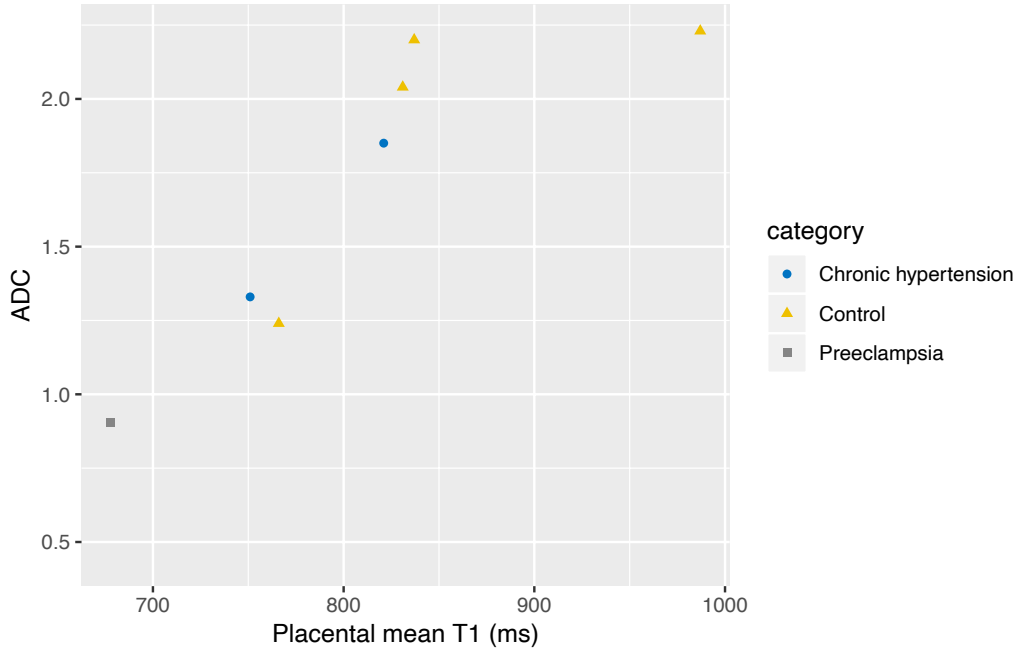

D

Figure 5.5: Scatterplot results from combined diffusion-relaxometry acquisition sequence.
(A) Apparent diffusion coefficient (ADC) against gestational age at imaging (B) ADC against placental mean T2* (C) mean T1 against gestational age at imaging (D) ADC against mean T1.

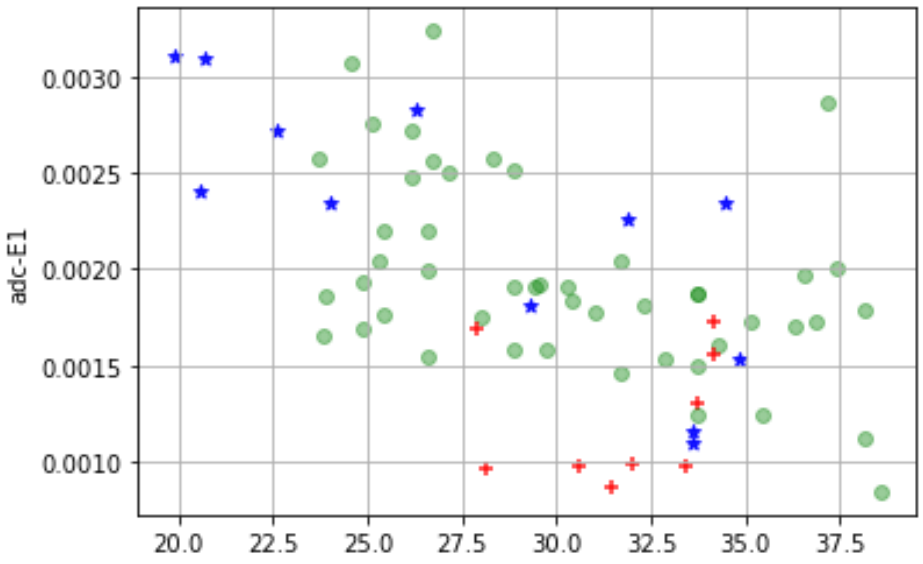

Figure 5.6: Scatterplot results of apparent diffusion coefficient (ADC) against gestational age from a diffusion sequence acquired during the initial methods development phase of the study and thus prior to acquisition of combined diffusion-relaxometry data.
Green circles indicates women with uncomplicated pregnancies, red crosses those with preeclampsia, blue stars those with chronic hypertension.

Placental volume did not differ between the chronic hypertensive group and controls (Figure 5.7).

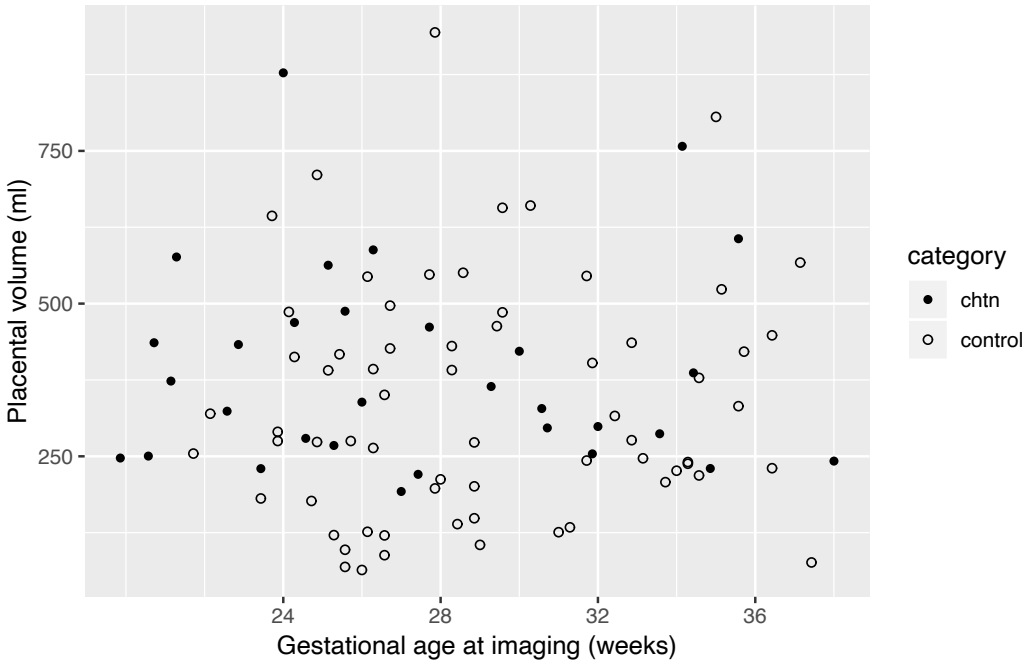

Figure 5.7: Scatterplot of placental volume (from segmentations performed on T2* maps) against gestational age at imaging.

5.4 Discussion

5.4.1 Statement of principal findings

This prospective observational study has used magnetic resonance imaging at both 1.5 and 3 Tesla to acquire T2, T2*, T1 and diffusion weighted imaging of the placenta in a group of women with chronic hypertension and shown a varied visual appearance on images in women with chronic hypertension when compared to controls. T2* values showed expected decrease with gestation in the control groups but a more variable spread of values in chronic hypertension. T2* histogram derived measures of kurtosis and skewness showed an increase in values with advancing gestation and the majority of women with chronic hypertension had values within the range of the control group.

5.4.2 Strengths and weaknesses of the study

A strength of this study is that we have quantitively measured the described visual variation in placental appearance using mean T2* and further probed the characteristics of T2* values across the whole placenta using histogram derived measures of kurtosis and skewness and Apparent Diffusion Coefficient. These histogram derived measures are

independent of magnetic field strength and therefore enable comparisons between groups regardless of the strength of magnetic resonance scanner used to acquire data.

To further investigate both normal and abnormal placental phenotypes we have used in-house optimised sequences combining diffusion-relaxometry which provides regionally matched diffusion and T2* values in a reasonably fast scan time compared to conventional sequences. In the integrated approach, the imaging sequence contains a spin-echo with subsequent gradient echoes. Given T2* values vary with gestation and pregnancy complications, a sequence which can disentangle the molecular motion secondary to T2* values and intrinsic diffusion properties of the placenta is of great benefit when elucidating the underlying mechanisms of placental dysfunction. Secondly, motion correction was achieved post image acquisition. Given diffusion measures the thermal microscopic translational motion of water molecules, any measures which can minimise the effect of macroscopic motion are beneficial. Motion correction was successfully performed on all women in whom the combined diffusion-relaxometry sequence was deployed.

The heterogeneity amongst the chronic hypertensive group with regards to enrolment characteristics and pregnancy outcome reflect the clinical context in which these women are managed. This study additionally demonstrated that imaging was feasible and acceptable in a large group of women across a range of gestations amongst a group which included those with chronic hypertension.

Given the wider clinical phenotype of disease in contrast to women with preeclampsia (whereby there is a close interval between imaging and delivery by clinical nature and a clear placental phenotype previously demonstrated by our group (Ho et al. 2020)), a clear placental phenotype remains challenging in women with chronic hypertension. In addition, the number of women with chronic hypertension who subsequently developed superimposed preeclampsia were small in our study (four women) and the time point at which imaging was performed may not capture potential changes that occur with the development of fetal growth restriction. Given the limitations of using a case-control study in predicting pregnancy outcomes, we have been cautious in our interpretation; however, anticipate that future prospective studies will further address this.

Placental volume did not differ between the chronic hypertensive group and controls, although this must be interpreted with caution due to the varying time interval between imaging and delivery. Additionally, the placental volume was derived from a conservative manual segmentation of the T2* maps to ensure only placental tissue sampled, and

therefore the conservative approach presents a limitation. A more accurate placental volume may be obtained through T2 weighted imaging and 3D reconstruction techniques to further delineate the placental boundaries from surrounding structures.

5.4.3 Strengths and weaknesses in relation to other studies

To our knowledge, there are no studies investigating the use of placental magnetic resonance imaging in women with chronic hypertension. Our group have previously described a placental phenotype in women with preterm preeclampsia, where T2-weighted imaging demonstrated advanced lobulation, varied lobule sizes, high granularity and substantial areas of low signal intensity with reduced entire placental mean T2* values for gestational age (Ho et al. 2020). Other studies have focussed on the prediction of fetal growth restriction (Poulsen et al. 2019) and low mean T2* values have been demonstrated to occur in pregnancies with fetal growth restriction (Sinding, Peters, Frøkjaer, et al. 2016). The use of T2* histogram derived measures of kurtosis and skewness has not been widely described. There is a paucity of literature regarding the use of placental diffusivity measures in hypertensive disorders as studies have mainly focused on pregnancies complicated by fetal growth restriction. Reduced placental ADC values in growth restriction have implicated a phenotype with restricted diffusion (Javor et al. 2013; Bonel et al. 2010). Our results showing a decline in ADC values in the third trimester in uncomplicated pregnancies are consistent with two known studies investigating the relationship between ADC values and gestational age (Siauve et al. 2019; Capuani et al. 2017). The use of a novel combined diffusion-relaxometry sequence has enabled the addition of T2* to ADC values, examined simultaneously for a more accurate evaluation of placental properties. Furthermore, these novel sequences have been deployed in pregnancies complicated by hypertension; a group not extensively studied before using this technique.

5.4.4 Meaning of the study

The placental phenotype in women with chronic hypertension has an overlap with women of uncomplicated pregnancies, as demonstrated by mean T2*, kurtosis, skew and ADC values. However, when more parameters were employed subtle differences found between groups e.g. with variability in histogram measures in the presence of similar T2* value. This potentially reflects the heterogeneity in pregnancy outcomes amongst women with chronic hypertension. The maternal and neonatal outcomes (namely the development of superimposed preeclampsia and birthweight centile) may represent the clinical stability of the women who enrolled, as these women would have fewer clinical appointments compared to those with maternal or fetal complications and thus the additional time

required to take part in research would not be as onerous. The greater range of placental mean T2* values for a given gestation within this group accompanied by skewness, kurtosis and ADC values within the normal range suggests a more complex interaction between the placenta and maternal response determining the development of adverse pregnancy outcomes such as superimposed preeclampsia. This contrasts with a clearer placental phenotype in women with preterm preeclampsia, previously described by our group (Ho et al. 2020). The skewness, kurtosis and mean T2* values within the normal range in women with chronic hypertension who subsequently develop superimposed preeclampsia may be due to the long interval between imaging and preeclampsia diagnosis as these women developed preeclampsia at term, possibly also reflecting varying pathology in term disease.

A reduction in mean T2* and ADC values with advancing gestation in the third trimester perhaps reflects parenchymal changes after initial placental angiogenesis in the first and second trimester, followed by villous maturation, calcium deposition and fibrosis in the third trimester. A further decrease in T2* and ADC values amongst women with superimposed preeclampsia may reflect the histological features seen with hypertensive disorders of pregnancy. These include maternal vascular malperfusion lesions such as increased syncytial knots, villous agglutination, increase intervillous fibrin deposition and villous infarcts.

5.4.5 Unanswered questions and future research

Placental imaging offers a window into the placental contribution and mechanisms potentially accounting for the heterogeneity in pregnancy outcomes of women with chronic hypertension. Future work may focus on evaluating the interaction between the placental dysfunction and the varied maternal response that may elucidate development of the varying adverse pregnancy outcomes. In this study, the interval between imaging and delivery was variable and therefore further large studies would be beneficial in investigating the clinical applicability of magnetic resonance imaging as a potential tool to monitor high risk women (including identification of those at high risk of fetal growth restriction) and aid clinical management decisions around optimal timing of delivery. Further technological developments may enable certain steps in processing to be automated through machine learning algorithms and increase opportunities for implementation in clinical practice.

5.5 Supplemental

Supplemental Table S1: Characteristics at booking and enrolment.

	Chronic hypertensive pregnancies imaged at 3T n=30	**Control pregnancies imaged at 3T n=70**	**Chronic hypertensive pregnancies imaged at 1.5T n=13**	**Control pregnancies imaged at 1.5T n=16**	**Preeclampsia pregnancies imaged at 1.5T n=5**
At booking					
Maternal age, y, median (IQR)	36 (35-40)	34 (32-37)	37 (34-41)	35 (34-37)	3 (30-34)
Gestational age on day of MRI, wk, median (IQR)	27.0 (23.7-31.4)	28.7 (26.0-33.0)	29.6 (24.7-32.7)	29.5 (27.2-31.8)	33.0 (32.7-34.6)
Body mass index, kg/m^2, median (IQR)	24 (22-26)	22 (21-24)	34 (31-34)	27 (24-32)	32 (30-34)
Nulliparous	11 (37)	38 (54)	4 (31)	7 (44)	1 (20)
White ethnicity	20 (67)	62 (89)	5 (38)	13 (81)	1 (20)
Black ethnicity	3 (10)	1 (1)	5 (38)	3 (19)	3 (60)
Other ethnicity	7 (23)	7 (10)	3 (23)	0	1 (5)
Current smoking	0	1 (1)	0	0	0
Quit smoking before pregnancy	0	4 (6)	1 (8)	0	0
Quit in last 6 weeks prior to booking	1 (3)	1 (1)	2 (15)	1 (6)	0
Never smoked	28 (93)	59 (84)	9 (69)	14 (88)	4 (80)
Unknown smoking history	1 (3)	5 (7)	1 (8)	1 (6)	1 (20)
Previous pre-eclampsia	6 (20)	0	1 (8)	1 (6)	3 (60)

Supplemental Table S1 (cont)	**Chronic hypertensive pregnancies imaged at 3T n=30**	**Control pregnancies imaged at 3T n=70**	**Chronic hypertensive pregnancies imaged at 1.5T n=13**	**Control pregnancies imaged at 1.5T n=16**	**Preeclampsia pregnancies imaged at 1.5T n=5**
Chronic renal disease	5 (17)	0	1 (8)	0	0
Gestational diabetes	1 (3)	0	1 (8)	0	1 (20)
At enrolment on day of MRI					
Aspirin	26 (87)	6 (9)	12 (92)	1 (6)	3 (60)
Placental Growth Factor, pg/mL, median (IQR)	195 (111-314)	341 (165-656)	141 (71-259)	329 (274-536)	<12 (<12-<12)
Placental growth factor <100 pg/mL	4 (13)	5 (7)	2 (15)	1 (6)	2/2 (100)
Placental growth factor <12 pg/mL	1 (3)	0	0	0	2/2 (100)
Prior to MRI, on day of MRI					
Systolic blood pressure, mmHg, median (IQR)	121 (115-132.5)	106 (56-72)	130 (118-133)	110 (107-117)	136 (130-136)
Diastolic blood pressure, mmHg, median (IQR)	76 (71-85)	62 (56-72)	80 (76-82)	72 (61-77)	81 (76-85)
Mean Arterial Pressure, mmHg, median (IQR)	91 (86-100)	76 (71-83)	95 (91-100)	84 (77-89)	101 (90-102)

Supplemental Table S1 (cont)	**Chronic hypertensive pregnancies imaged at 3T n=30**	**Control pregnancies imaged at 3T n=70**	**Chronic hypertensive pregnancies imaged at 1.5T n=13**	**Control pregnancies imaged at 1.5T n=16**	**Preeclampsia pregnancies imaged at 1.5T n=5**
During MRI					
Systolic blood pressure, mmHg, median of individual medians (IQR)	112 (108-117)	98 (94-105)	113 (107-115)	103 (101-106)	127(123-132)
Diastolic blood pressure, mmHg, median of individual medians (IQR)	72 (65-77)	59 (54-64)	65 (63-68)	62 (60-64)	80 (78-84)
Mean Arterial Pressure, mmHg, median of individual medians (IQR)	85 (79-89)	73 (68-77)	81 (78-85)	76 (74-78)	95 (93-98)

Supplemental Table S2: Maternal and neonatal outcomes.

	Chronic hypertensive pregnancies imaged at 3T n=30	**Control pregnancies imaged at 3T n=70**	**Chronic hypertensive pregnancies imaged at .5T n=13**	**Control pregnancies imaged at 1.5T n=16**	**Preeclampsia pregnancies imaged at 1.5T n=5**
Time from MRI to delivery, days, median (IQR)	76 (39-95)	84 (51-99)	56 (33-97)	82 (60-91)	7 (6-12)
Onset of delivery					
Spontaneous	3 (10)	45 (64)	2 (15)	10 (63)	0
Induction	14 (47)	16 (23)	5 (38)	4 (25)	1 (20)
Pre labour caesarean	13 (43)	9 (13)	6 (3)	3 (19)	4 (80)
Primary reason for induction or prelabour caesarean*					
Maternal indication	22 (73)	13 (19)	8 (62)	2 (13)	3 (60)
Fetal indication	5 (17)	12 (17)	3 (23)	4 (25)	2(40)
Delivery					
Livebirth	30 (100)	70 (100)	13 (100)	16 (100)	5 (100)
Gestational age at delivery, weeks, median, IQR	38.4 (37.1-39.0)	40.3 (39-41)	38.2 (38.1-38.6)	40.7 (39.3-41.4)	34.7 (33.7-36.4)
Spontaneous vaginal delivery	6 (20)	36 (51)	3 (23)	11 (69)	0
Assisted vaginal delivery	3 (10)	17 (24)	1 (8)	1 (6)	0
Elective pre-labour caesarean section	7 (23)	8 (11)	3 (23)	2 (13)	2 (40)
Urgent caesarean section	14 (47)	9 (13)	6 (46)	2 (13)	3 (60)

Supplemental Table S2 (cont)	**Chronic hypertensive pregnancies imaged at 3T n=30**	**Control pregnancies imaged at 3T n=70**	**Chronic hypertensive pregnancies imaged at .5T n=13**	**Control pregnancies imaged at 1.5T n=16**	**Preeclampsia pregnancies imaged at 1.5T n=5**
Preterm birth <37/40	7 (23)	0	2 (15)	0	4 (80)
Birthweight, g, median (IQR)	2875 (2478-3275)	3482 (3252-3709)	3200 (2670-3400)	3480 (3116-3885)	1750 (1700-1880)
Birthweight centile, centile, median (IQR)	26 (15-64)	68 (32-80)	67 (41-75)	70 (34-84)	3 (2-4)
5 minute Apgar score >/=7	29 (97)	66 (94)	13 (100)	15 (94)	4 (80)
Respiratory support required in delivery room	2 (7)	4 (6)	0	0	2 (40)
Number admitted to neonatal unit for >=48 hours	3 (10)	0	1 (8)	1 (6)	2 (40)
Length of stay in intensive care, day, median, IQR	0 (0-7)	0	0	0	1 (0-1)
Length of stay in high dependency, day, median, IQR	2 (1-14)	0	0	0	6 (3-9)
Length of stay in special care, day, median, IQR	8 (4-19)	0	5 (5-5)	7 (7-7)	16 (13-18)
Primary indication for neonatal unit admission					
Prematurity	2 (7)	0	0	0	0
Fetal growth restriction/ small for gestational age	0	0	0	0	1 (20)

Supplemental Table S2 (cont)	**Chronic hypertensive pregnancies imaged at 3T n=30**	**Control pregnancies imaged at 3T n=70**	**Chronic hypertensive pregnancies imaged at .5T n=13**	**Control pregnancies imaged at 1.5T n=16**	**Preeclampsia pregnancies imaged at 1.5T n=5**
Respiratory disease	0	0	0	1 (6)	1 (20)
Suspected sepsis	0	0	0	0	0
Hypoglycaemia	1 (3)	0	1 (8)	0	0
Maternal outcome from enrolment to post delivery discharge					
Pre-eclampsia	3 (10)	0	1 (8)	0	0
Gestational diabetes	2 (7)	0	2 (15)	0	0
Haemolysis, elevated liver enzymes and low platelet count (HELLP)	0	0	0	0	1 (20)

Values given as a number (percentage) unless stated otherwise.

Supplemental Figure S1: Flow diagram of participants with (A) chronic hypertension (B) healthy pregnancies

A

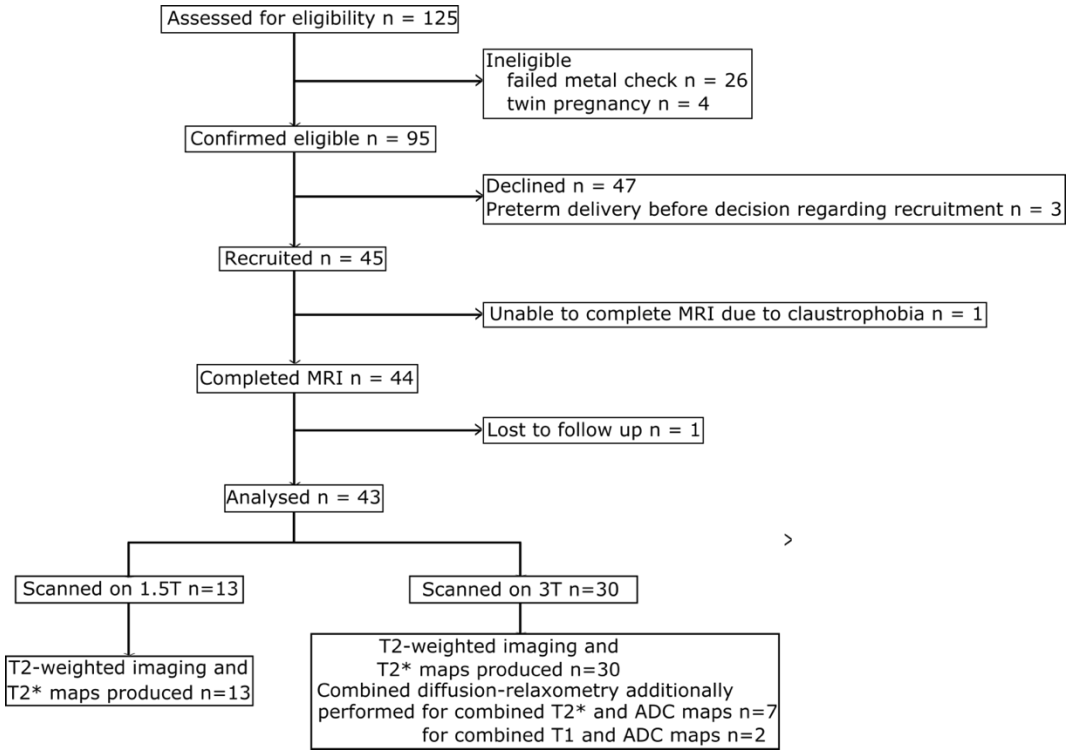

B

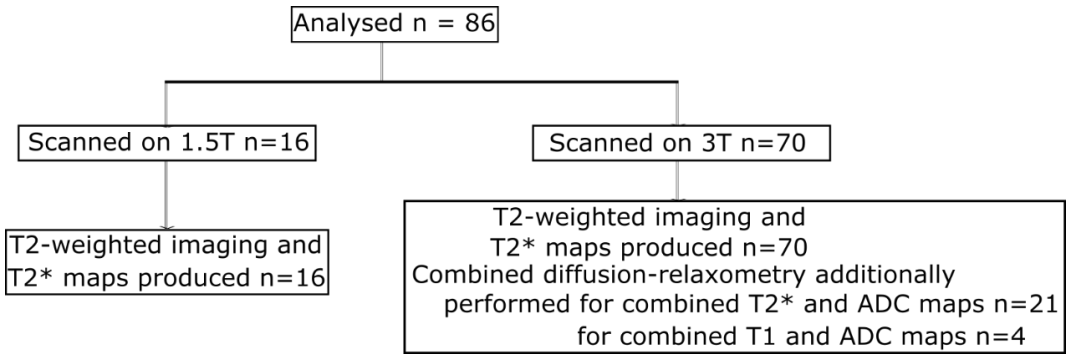

Chapter 6 BIOMARKERS IN CHRONIC HYPERTENSION AND PREECLAMPSIA WITH IMAGING VARIABLES

6.1 Introduction

Placental biomarkers have the potential to aid our understanding of the underlying mechanisms that give rise to clinical features and adverse pregnancy outcomes in hypertensive disorders of pregnancy. Such candidate biomarkers include placental growth factor (PlGF), soluble fms-like-tyrosine kinase 1 (sFlt-1), hyaluronan and vascular cell adhesion molecule-1 (VCAM-1).

PlGF is a proangiogenic factor which, in pregnancy, is predominantly expressed in the vasculosyncytial membrane of villous trophoblast cells (Khaliq et al. 1996). In normal pregnancies, the concentration of PlGF in the maternal circulation rises until 29-32 weeks gestation and subsequently declines until delivery (Romero et al. 2008). Low concentrations of PlGF have been found in women with preeclampsia, including those with a background of chronic hypertension and chronic kidney disease (Bramham et al. 2016; Staff et al. 2013). In women with suspected preeclampsia, low PlGF concentrations have a high sensitivity and negative predictive value for the development of preeclampsia requiring delivery within 14 days (Chappell et al. 2013; Duhig et al. 2019).

The activity of PlGF is influenced by oxygenation and sFlt-1. PlGF production may be down regulated by hypoxia. PlGF exerts its proangiogenic, anticoagulant and vasodilatory activity through binding to fms-like tyrosine kinase 1 receptor on the trophoblast membrane (Shore et al. 1997). sFlt-1 is a soluble form of the receptor; when bound to circulating PlGF the bioavailibility of PlGF binding to flt-1 membrane receptor is reduced. A sFlt-1/PlGF ratio greater than 38 has been found to predict the short term absence of preeclampsia (Zeisler et al. 2016).

The vascular endothelium is lined by a protective endothelial glycocalyx layer. Biomarkers of endothelial dysfunction include VCAM and hyaluronan. Both biomarkers have been found in high concentrations amongst women with preeclampsia (Chaiworapongsa et al. 2002; Wiles et al. 2019). VCAM mediates leukocyte endothelial adhesion and thus high plasma concentrations are thought to signal damage to the endothelial glycocalyx. In comparison, hyaluronan is a component of the endothelial glycocalyx itself, with hyaluronan-hyaluronan complexes stabilising the luminal glycocalyx and mediating cell-cell motility and cell-matrix adhesion (Scott and Heatley 1999).

Advances in magnetic resonance imaging techniques have enabled assessment of the placenta *in vivo*. Recent interest in T2* mapping has developed as it is thought to probe placental oxygenation given the paramagnetic properties of deoxyhaemoglobin can cause magnetic field distortions and faster T2* decay than oxyhaemoglobin. Low placental mean T2* values have been found in women with preeclampsia (Ho et al. 2020); however, the association of T2* values with placental biomarkers have not been extensively explored.

To aid understanding of pathophysiological mechanisms which give rise to the clinical features of preeclampsia and chronic hypertension in pregnancy, the aim of this study is twofold: firstly, to explore placental biomarkers in a group of women with preeclampsia and chronic hypertension; secondly, to investigate the association of these biomarkers with the MRI measure of mean T2*.

6.2 Methods

In this prospective observational study, women with preeclampsia and chronic hypertension were approached antenatally to participate in a study involving MRI scans and blood draws for biomarkers. Preeclampsia and chronic hypertension were defined using international consensus definitions (Brown et al. 2018) and they were considered for inclusion in the study if they had a singleton pregnancy, over 16 years of age and no contraindication for MRI. Women in the control group were approached at their routine 20 week anomaly scan or self referred to take part. They were considered eligible if they had a singleton pregnancy, no diagnosis of a hypertensive disorder at enrolment, no significant past medical history and no pregnancy complications (including gestational diabetes mellitus). Following delivery, women in this group were divided into those with a normal pregnancy outcome (control) and those with an abnormal pregnancy outcome (abnormal control). A normal pregnancy outcome was defined as delivering at term with a birthweight centile between the 3rd and 97th centile (calculated using International Fetal and Newborn Growth Consortium for the 21st Century version 1.3.5 (Villar et al. 2014) with no hypertensive disorder or pregnancy complication (including gestational diabetes mellitus). Those in the abnormal control group either developed a pregnancy complication, delivered preterm or had a birthweight centile less than the 3rd centile or greater than the 97th centile.

All women in this study gave written informed consent to take part in the Placenta Imaging Project (REC 16/LO/1573, IRAS 201609), the primary objective of which was to develop a

novel magnetic resonance imaging approach to assess growth and development of the human placenta. As part of this study, women underwent magnetic resonance imaging and venepuncture blood sampling as close to MRI as feasible.

6.2.1 Assays

Blood samples were transported to the laboratory within one hour of sampling and centrifuged at 1400g (rcf) for 10 minutes at 4°C. The separated supernatant was stored at -80°C until required for assays. All samples were run masked to both group and clinical outcome.

Plasma PlGF concentrations were quantified using the Triage PlGF Test (Quidel, San Diego, CA) according to manufacturer's instructions. Serum PlGF and serum sFlt-1 were quantified using a fully automated electrochemiluminescence immunoassay (Elecsys®, Roche diagnostics). Plasma hyaluronan and plasma VCAM were quantified using enzyme linked immunosorbent assays (Hyaluronan DHYAL0, R&D Systems® and Human sVCAM-1/CD106 DVC00, R&D Systems® respectively) and run in duplicate, with intra-assay precision of <10%.

6.2.2 Magnetic Resonance Imaging

MRI was performed on a clinical Philips 3T Achieva with a 32-channel cardiac coil at any time point between their routine clinical anomaly ultrasound scan and delivery. Following image-based shimming using an in-house tool, a multi-echo gradient echo, echo planar imaging sequence at $3mm^3$ resolution was performed with free breathing. The imaging parameters included 5 echo times 13.81ms/70.40ms/127.00ms/183.60ms/240.2ms with repetition time of 3 seconds, SENSitivity Encoding = 3, halfscan=0.6. An in-house Python script produced T2* maps. The placenta was manually segmented and a further processing step calculated mean placental T2*. Further details can be found in Chapter 3.

6.2.3 Statistical methods

A Mann-Whitney test was used to compare biomarker concentrations between the control group and hypertensive groups (preeclampsia or chronic hypertension). Statistical analysis was performed using R version 3.5.0 (2018).

6.3 Results

A total of 114 women were enrolled in this study: 53 with uncomplicated pregnancies (normal control group), 32 with chronic hypertension and 13 with preeclampsia. 16 women

enrolled in the control group were found to subsequently have an abnormal pregnancy outcome following delivery (abnormal control group). Their details are listed below (Table 6.1).

Table 6.1: Abnormal pregnancy outcome in the abnormal control group.

n	Abnormal pregnancy outcome
3	Gestational diabetes
3	Preterm delivery
2	Gestational diabetes and preterm delivery
2	Birthweight centile above the 97th
2	Birthweight centile below the 3rd
2	Gestational hypertension
1	Obstetric cholestasis
1	Preeclampsia

The median gestational age was higher in the preeclampsia group (33.0 weeks, IQR 28.7-33.7) compared to control (27.9 weeks, IQR 26.0-31.9) and chronic hypertension (26.6 weeks (23.1-30.6) groups (Table 6.2). Both systolic and diastolic blood pressure were higher n the preeclampsia and chronic hypertension groups compared to the controls. A total of 93 out of 114 (82%) underwent an MRI within two weeks of blood sampling, in addition to maternal serum or plasma biomarker analysis. Women who had blood sampling but did not undergo magnetic resonance imaging were those who could not tolerate imaging (secondary to claustrophobia) or it was found to be unsafe to proceed with imaging following enrolment (failed final metal check).

Table 6.2: Characteristics at booking and enrolment.

	Control	Chronic hypertension	Preeclampsia	Abnormal control
Number of women	53	32	13	16
At booking				
Maternal age, y, median (IQR)	34 (32-36)	36 (33-40)	31 (27-35)	32 (31-34)
Body mass index, kg/m^2, median (IQR)	23 (21-24)	25 (24-31)	25 (24-30)	26 (23-27)
Nulliparous	30 (57)	10 (31)	5 (38)	10 (63)
White ethnicity	46 (87)	20 (63)	8 (62)	14 (88)
Black ethnicity	3 (6)	5 (16)	4 (31)	1 (6)
Other ethnicity	4 (8)	7 (22)	1 (8)	1 (6)
Current smoking	1 (2)	0	0	0
Quit smoking before pregnancy	2 (4)	4 (13)	3 (23)	3 (19)
Never smoked	50 (94)	28 (88)	10 (77)	13 (81)
Previous pre-eclampsia	1 (2)	6 (19)	4 (31)	0
Chronic renal disease	0	6 (19)	0	0
Gestational diabetes	0	0	0	0
At enrolment				
Gestational age, wk, median (IQR)	27.9 (26.0-31.9)	26.6 (23.1-30.6)	33.0 (28.7-33.7)	24.6 (23.2-28.4)
Systolic blood pressure, mmHg, median (IQR)	105 (101-109)	122 (115-133)	141 (137-145)	110(110-120)
Diastolic blood pressure, mmHg, median (IQR)	62 (57-69)	78 (70-83)	89 (84-98)	70 (75-90)
Number of women who underwent an MRI	47 (89)	20 (63)	11 (85)	15 (94)

Values given as a number (percentage) unless stated otherwise.

The shortest interval between enrollment to delivery was in the preeclampsia group, with 11 out of 13 women (85%) delivering preterm (Table 6.3). Birthweight centile was highest in the control group (69, IQR 32-82) followed by the chronic hypertensive (45, IQR 19-70), abnormal control (42, IQR 17-71) and preeclampsia (7, IQR 2-18) groups.

Table 6.3: Maternal and neonatal outcomes.

	Control	**Chronic hypertension**	**Preeclampsia**	**Abnormal control**
Number of women	53	32	13	16
Time from venepuncture to delivery, days, median (IQR)	87 (61-101)	79 (46-96)	12 (6-20)	93 (77-110)
Pre-eclampsia	0	4 (13)	13 (100)	1 (6)
Gestational diabetes	0	3 (9)	0	4 (25)
Onset of delivery				
Spontaneous	36 (68)	4 (13)	0	8 (50)
Induction	11 (21)	14 (44)	5 (38)	6 (38)
Pre labour caesarean	6 (11)	14 (44)	8 (62)	2 (13)
Mode of delivery				
Spontaneous vaginal delivery	31 (58)	7 (22)	1 (8)	10 (63)
Assisted vaginal delivery	10 (19)	2 (6)	0	1 (6)
Elective pre-labour caesarean section	6 (11)	7 (22)	0	3 (19)
Urgent caesarean section	6 (11)	16 (50)	12 (92)	2 (13)
Delivery				
Livebirth	53 (100)	32 (100)	13 (100)	16 (100)

Table 6.3 (cont)	**Control**	**Chronic hypertension**	**Preeclampsia**	**Abnormal control**
Gestational age at delivery, weeks, median, IQR	40.4 (39.6-41.3)	38.0 (37.3-39.0)	34.1 (30.7-36.4)	38.7 (36.9-40.2)
Preterm birth <37/40	0	7 (22)	11 (85)	5 (31)
Birthweight, g, median (IQR)	3500 (3260-3725)	2978 (2555-3380)	1700 (1005-2000)	2978 (2559-3570)
Birthweight centile, centile, median (IQR)	69 (32-82)	45 (19-70)	7 (2-18)	42 (17-71)
Number admitted to neonatal unit for ≥48 hours	1 (2)	3 (9)	4 (31)	2 (13)
Prematurity	0	0	0	0
Fetal growth restriction/ small for gestational age	0	0	3 (23)	0
Respiratory disease	0	1 (3)	0	1 (6)
Suspected sepsis	1 (2)	0	1 (8)	1 (6)
Hypoglycaemia	0	2 (6)	0	0

Values given as a number (percentage) unless stated otherwise.

Both the plasma and serum PlGF concentration (measured using Quidel and Roche assays respectively) were lowest in women with preeclampsia compared to controls, while the concentrations in women with chronic hypertension overlapped with the control group (Figure 6.1 and Figure 6.2).

Figure 6.1: Quidel PlGF concentrations in each group (control, chronic hypertension, preeclampsia and abnormal control)

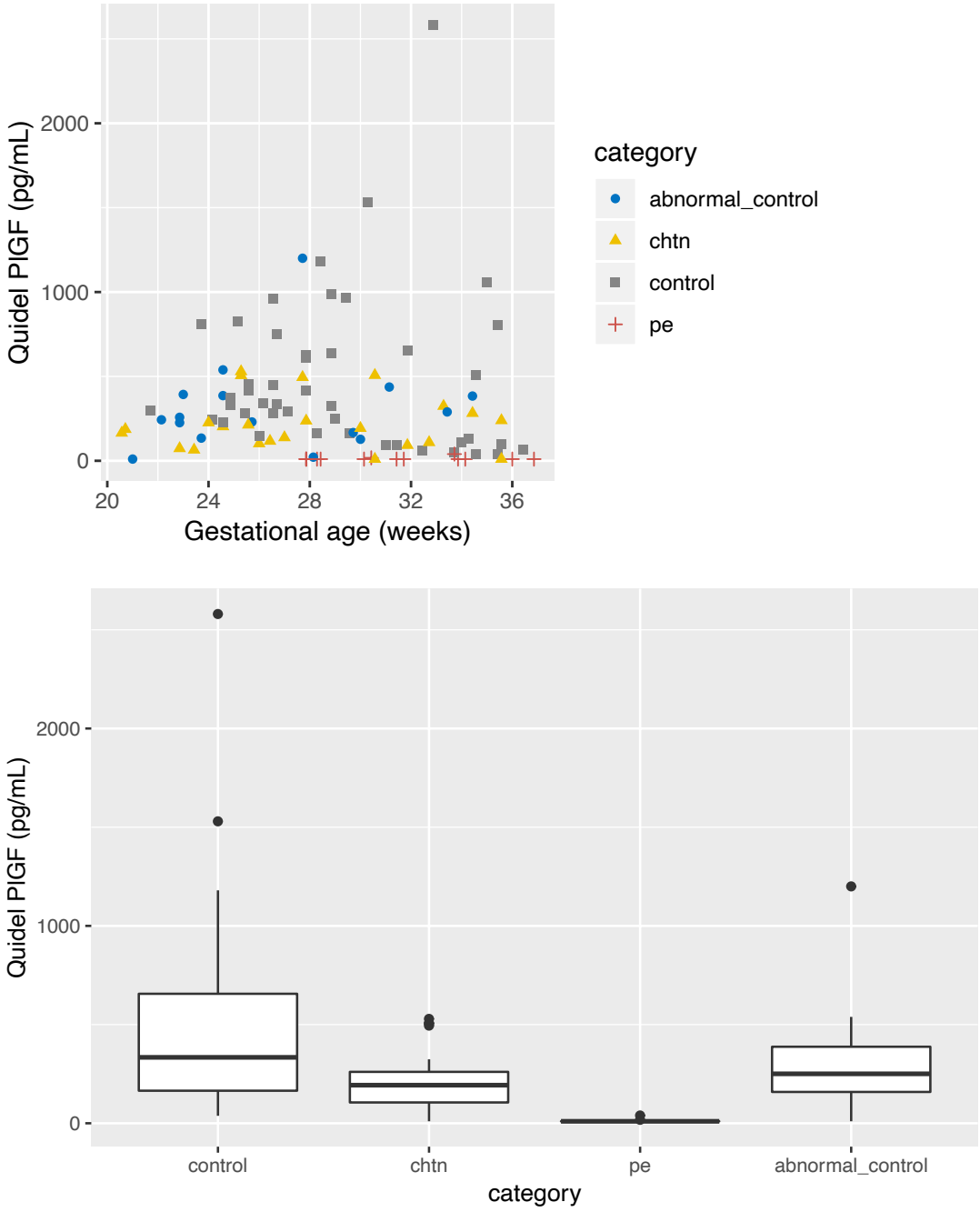

Control versus chronic hypertension p=0.007871

Control versus preeclampsia p=2.031 x 10^{-8}

	Control	Chronic hypertension	Preeclampsia	Abnormal control
Number of samples	41	23	13	16
Quidel PlGF, pg/mL, median (IQR)	334 (165-656)	193 (106-261)	<12(<12-<12)	251 (159-388)

Figure 6.2: Roche PlGF concentrations in each group (control, chronic hypertension, preeclampsia and abnormal control)

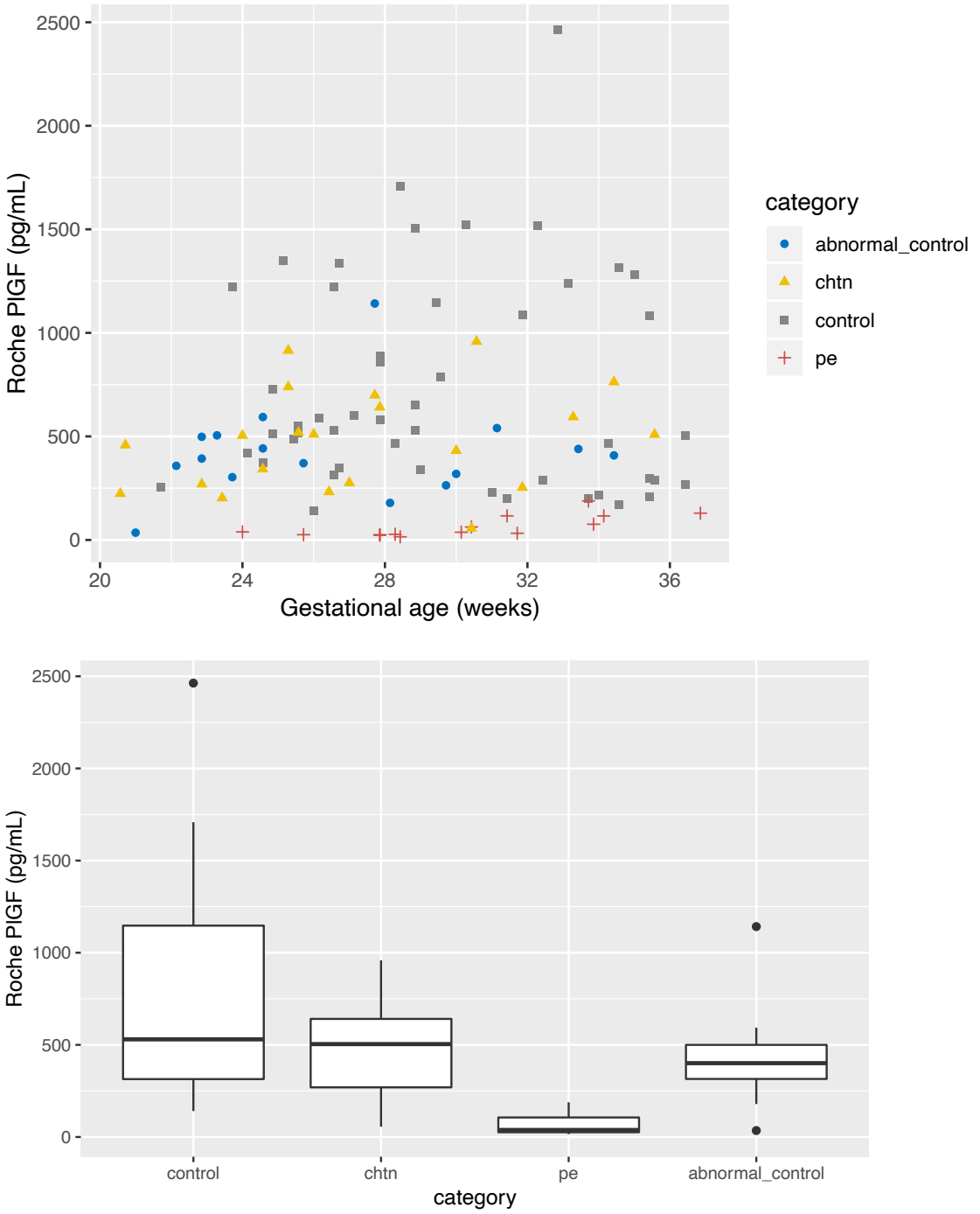

Control versus chronic hypertension p=0.04245

Control versus preeclampsia p=1.369 x 10^{-9}

	Control	Chronic hypertension	Preeclampsia	Abnormal control
Number of samples	49	21	13	16
Roche PlGF, pg/mL, median (IQR)	530 (314-1147)	504 (269-641)	38 (26-106)	400 (315-500)

Overall, higher PlGF concentrations were found when using the Roche assay compared to the Quidel assay. The PlGF concentration measured using two the different assays (Quidel and Roche) were compared in (Figure 6.3). Concentrations measured using Quidel assay were lower than those measured using Roche.

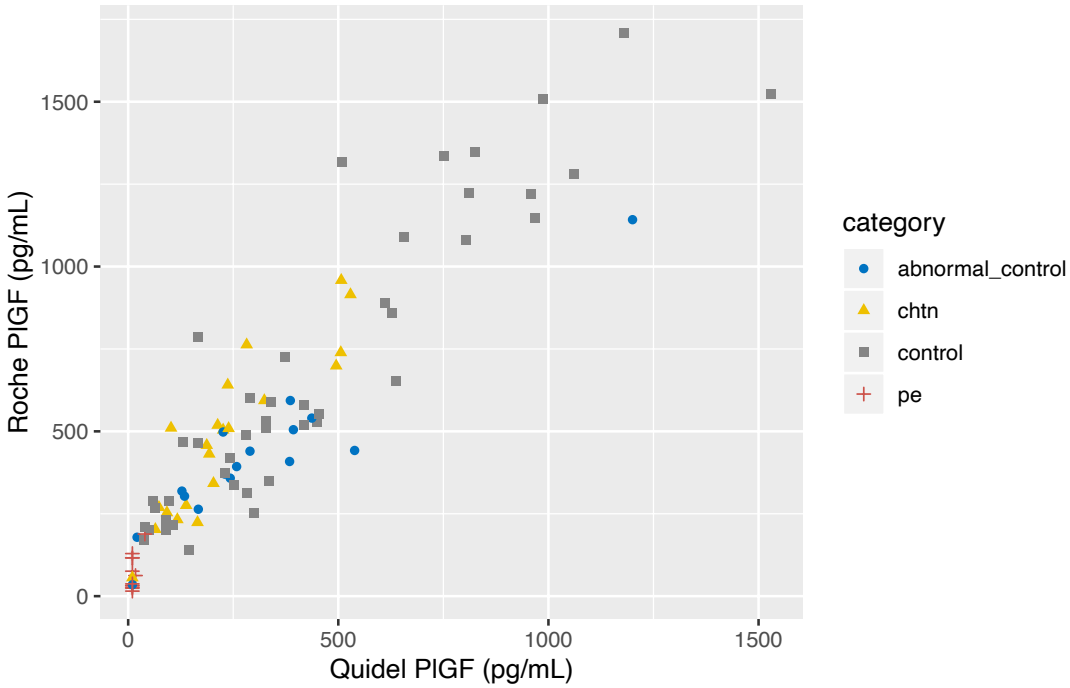

Figure 6.3: Scatterplot of Quidel PlGF concentrations against Roche PlGF concentrations in the same plasma sample.

In women with preeclampsia, the sFlt-1 concentration (Figure 6.4), sFlt-1/PLGF ratio (

Figure **6.5**), hyaluronan (Figure 6.6) and VCAM (Figure 6.7) concentrations were higher than those in the control and chronic hypertension groups. The difference in biomarker concentrations between the preeclampsia and control group was greatest for PlGF compared to all other biomarkers. Both VCAM and hyaluronan did not vary with gestational age (Figure 6.6, Figure 6.7).

Figure 6.4: Roche sFlt-1 concentrations in each group (control, chronic hypertension, preeclampsia and abnormal control)

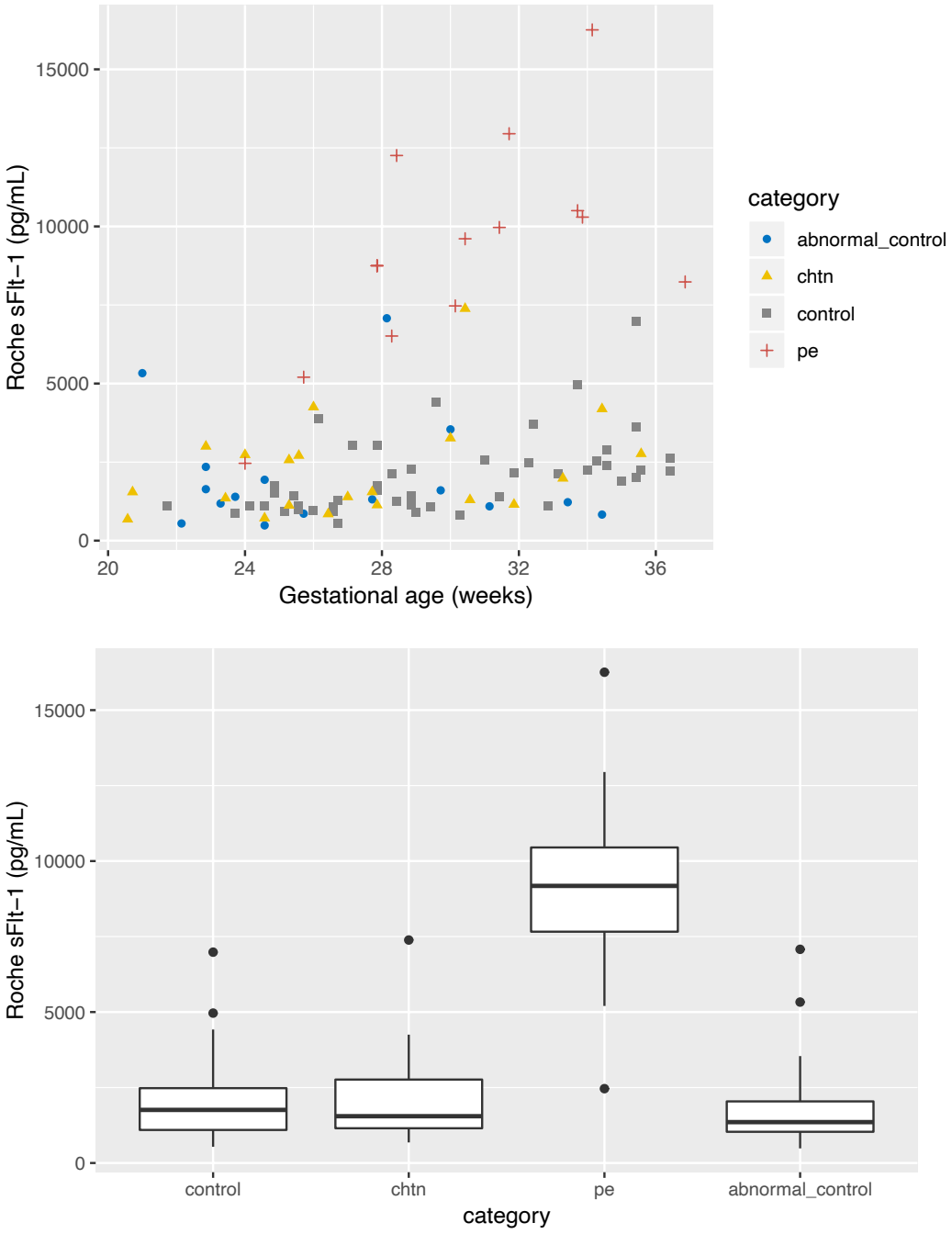

Control versus chronic hypertension p=0.5051

Control versus preeclampsia p=6.147 x 10^{-8}

	Control	Chronic hypertension	Preeclampsia	Abnormal control
Number of samples	49	21	13	16
Roche sFlt-1, pg/mL, median (IQR)	1759 (1095-2479)	1550 (1151-2764)	9178 (7662-10450)	1354 (1034-2040)

Figure 6.5: Roche sFlt-1/PlGF ratio in each group (control, chronic hypertension, preeclampsia and abnormal control)

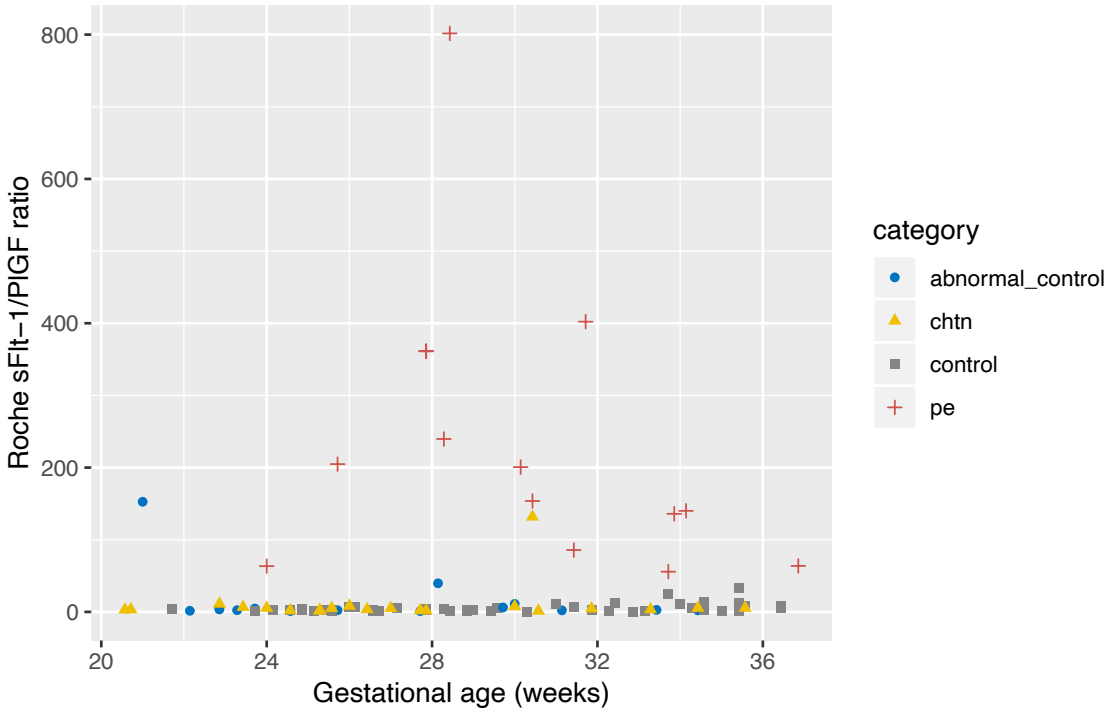

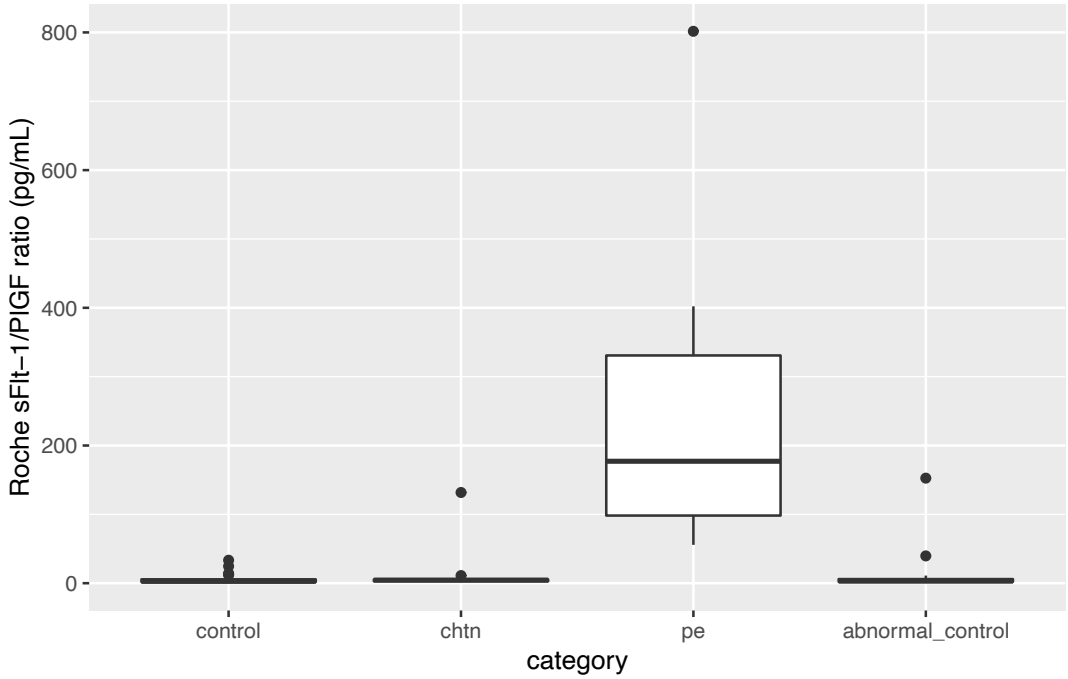

Control versus chronic hypertension p=0.1179

Control versus preeclampsia p=1.492 x 10^{-8}

	Control	Chronic hypertension	Preeclampsia	Abnormal control
Number of samples	49	21	13	16
Roche sFlt-1/PlGF ratio, median (IQR)	2.7 (1.7-5.6)	4.5 (2.8-5.5)	177 (98-331)	3.0 (2.0-6.0)

Figure 6.6: Hyaluronan concentrations in each group (control, chronic hypertension, preeclampsia and abnormal control)

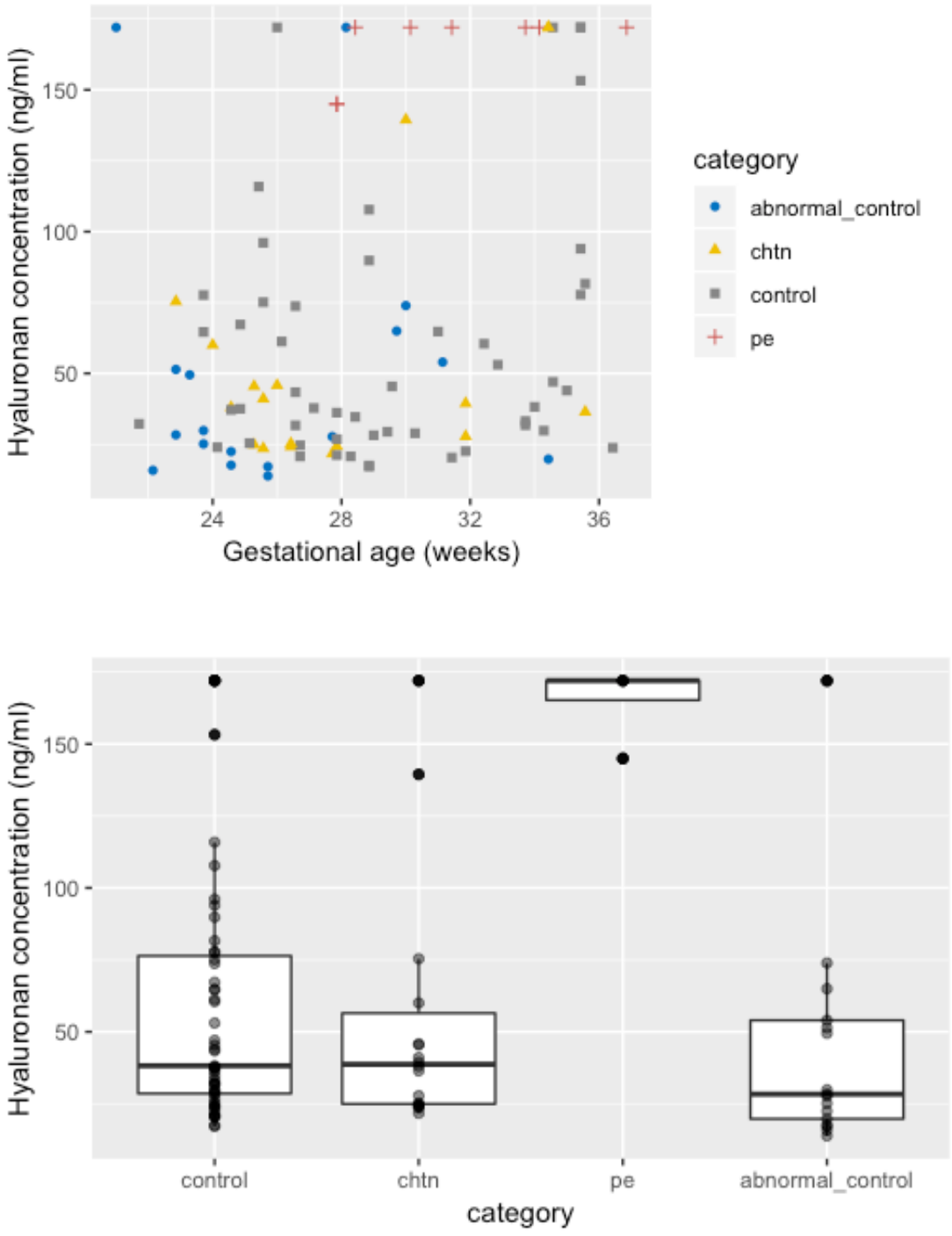

Control versus chronic hypertension p=0.7274

Control versus preeclampsia p=5.619 x 10^{-5}

	Control	Chronic hypertension	Preeclampsia	Abnormal control
Number of samples	51	18	8	16
Hyaluronan concentration ng/ml, median (IQR)	38 (29-76)	39 (25-56)	172 (165-172)	28 (20-54)

Figure 6.7: VCAM concentrations in each group (control, chronic hypertension, preeclampsia and abnormal control)

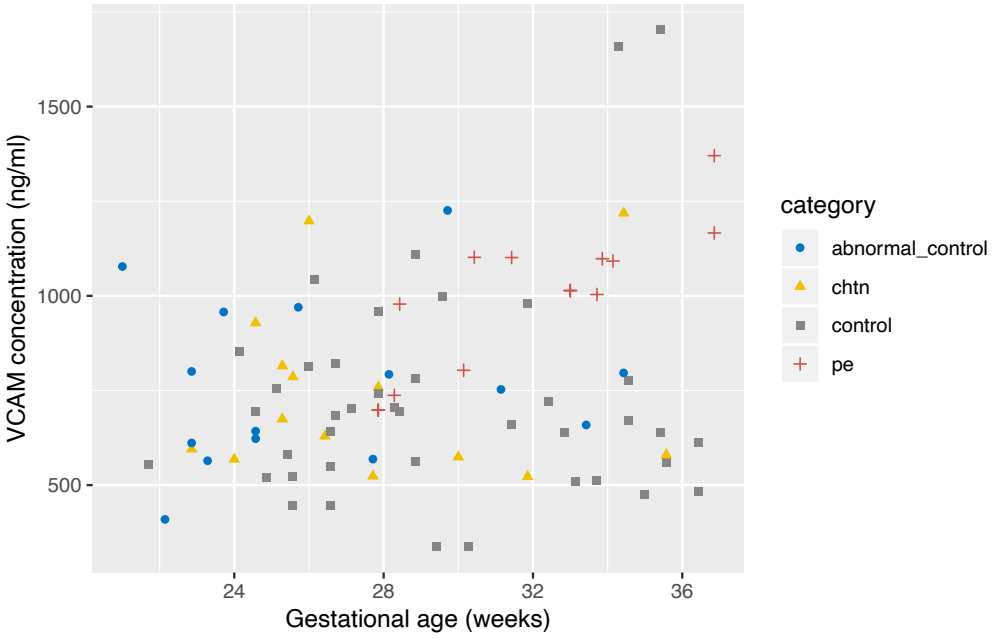

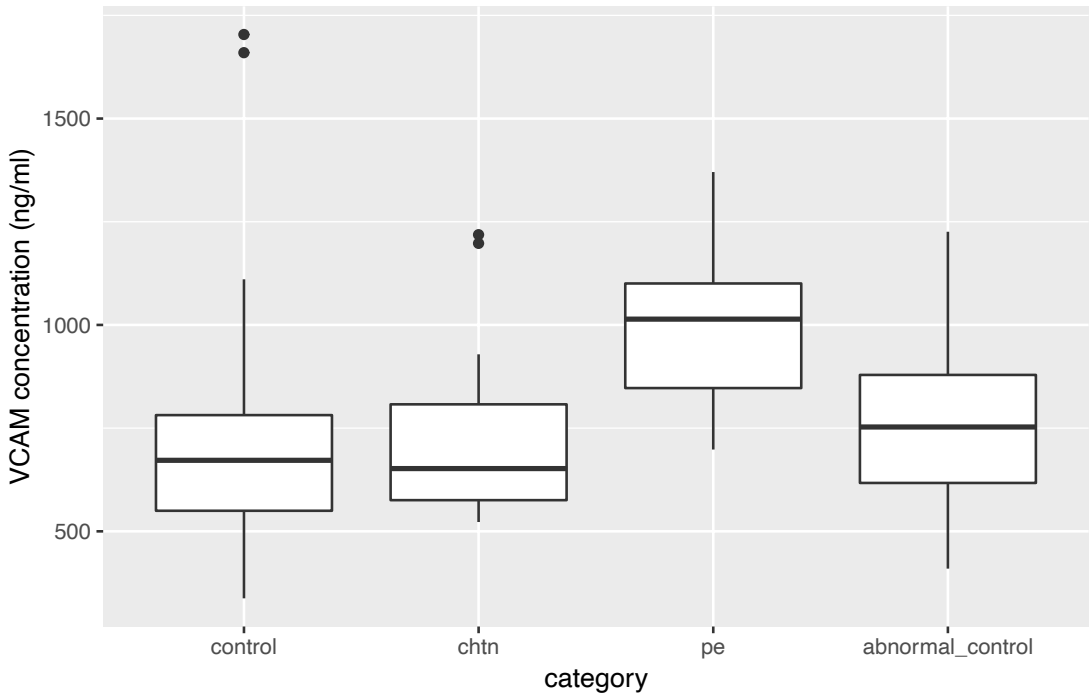

Control versus chronic hypertension p=0.5557

Control versus preeclampsia p=0.0001712

	Control	Chronic hypertension	Preeclampsia	Abnormal control
Number of samples	41	14	13	15
VCAM concentration ng/ml, median (IQR)	672 (550-782)	652 (576-808)	1014 (847-1100)	752 (617-879)

When comparing biomarkers against placental mean T2* values, the preeclampsia group clustered together with low mean T2* values while the chronic hypertensive and abnormal control groups fell within the values of the control group (Figures 6.8-6.11).

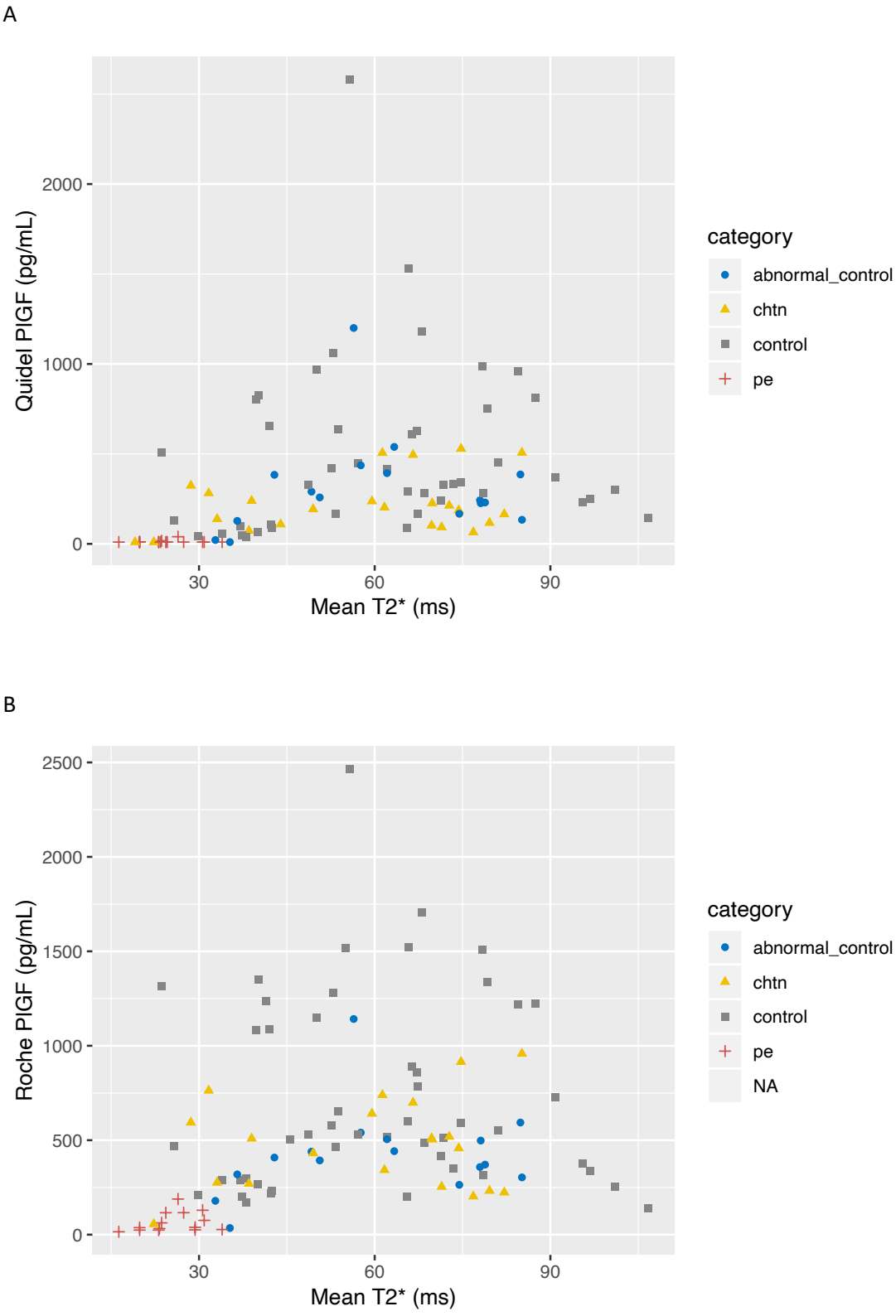

Figure 6.8: Scatterplot of (A) Quidel PlGF and (B) Roche PlGF against mean T2* values

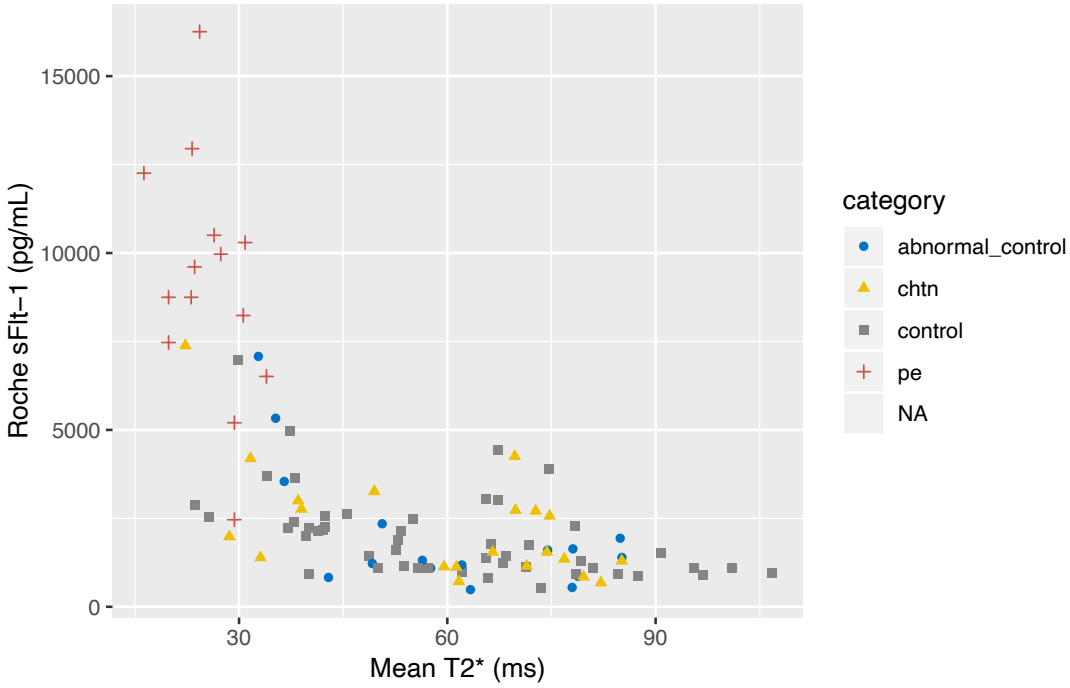

Figure 6.9: Scatterplot of Roche sFlt-1 against mean T2* values

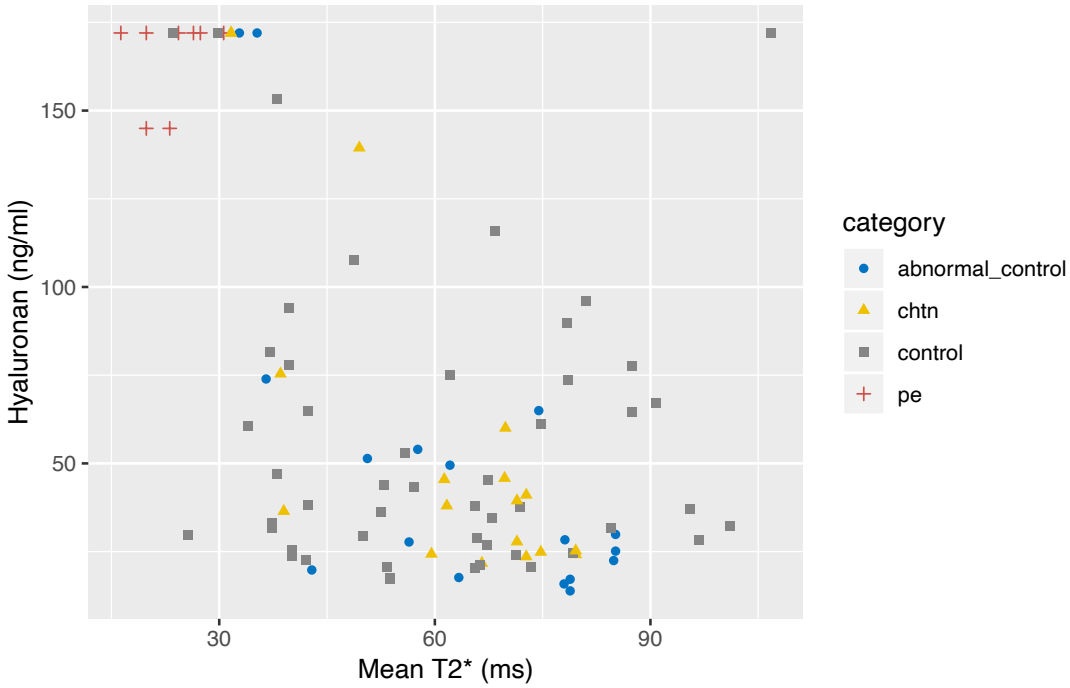

Figure 6.10: Scatterplot of Hyaluronan against mean T2* values

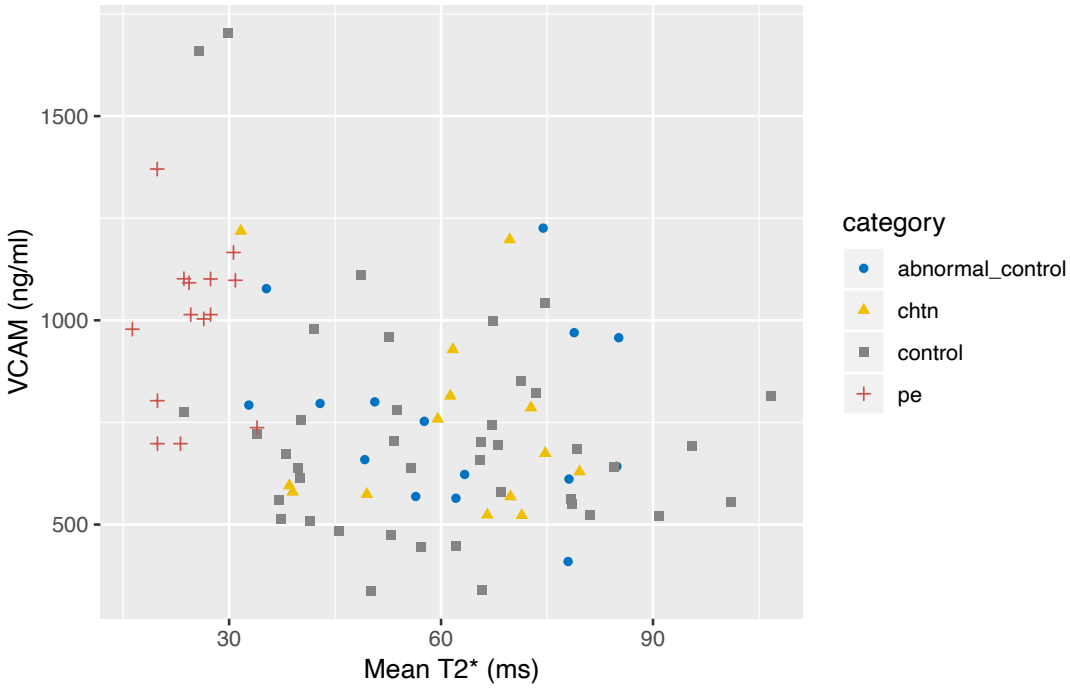

Figure 6.11: Scatterplot of VCAM against mean T2* values

Women with preeclampsia and an estimated fetal weight less than the 10th centile have low PlGF concentrations and high sFlt, VCAM and hyaluronan concentrations (Figures 6.12-6.16). The relationship between biomarkers and estimated fetal weight is less clear for the control, abnormal control and chronic hypertension groups.

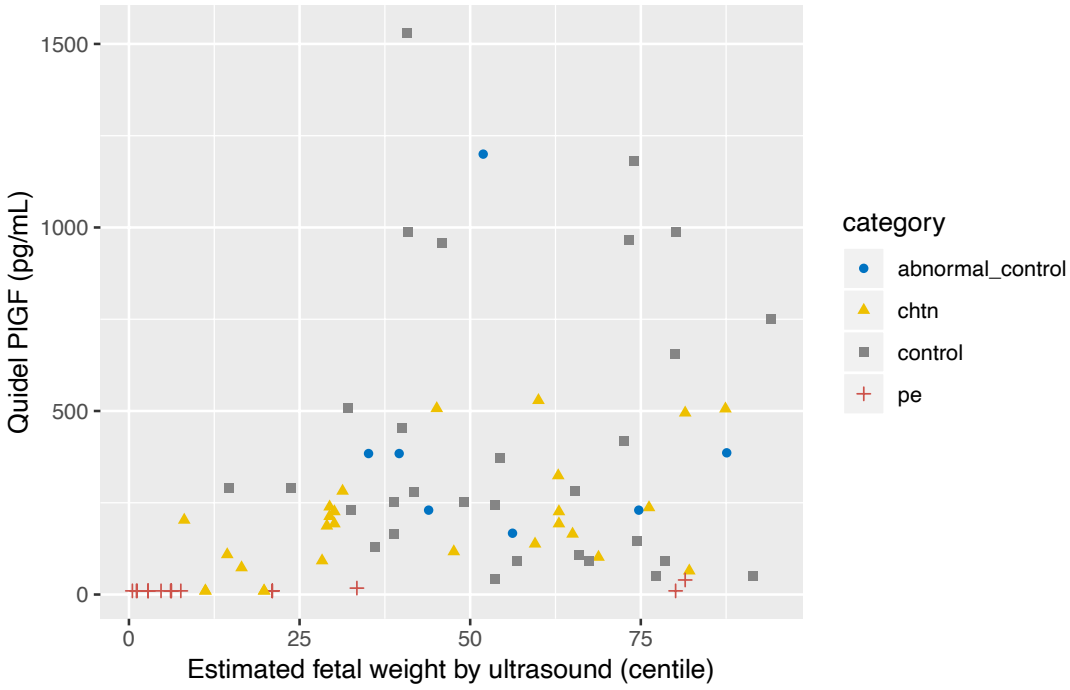

Figure 6.12: Scatterplot of serum PlGF concentration against estimated fetal weight (by ultrasound scan) performed within 2 weeks of blood sample taken.

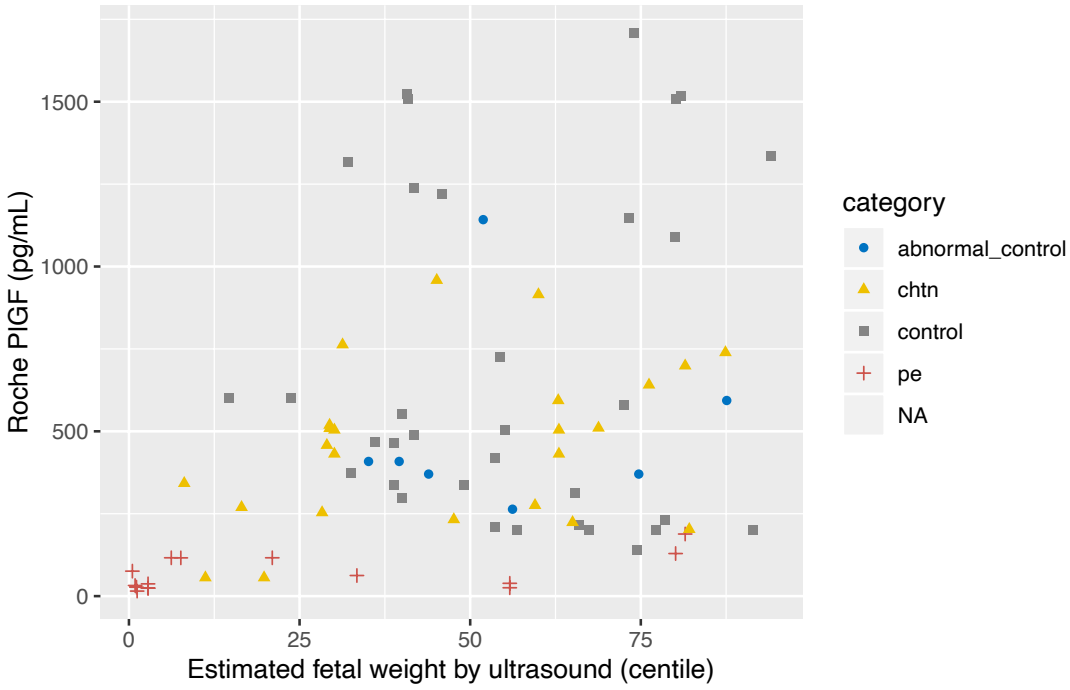

Figure 6.13: Scatterplot of serum PlGF concentration against estimated fetal weight (by ultrasound scan) performed within 2 weeks of blood sample taken.

Figure 6.14: Scatterplot of serum sFlt concentration against estimated fetal weight (by ultrasound scan) performed within 2 weeks of blood sample taken.

Figure 6.15: Scatterplot of serum VCAM concentration against estimated fetal weight (by ultrasound scan) performed within 2 weeks of blood sample taken

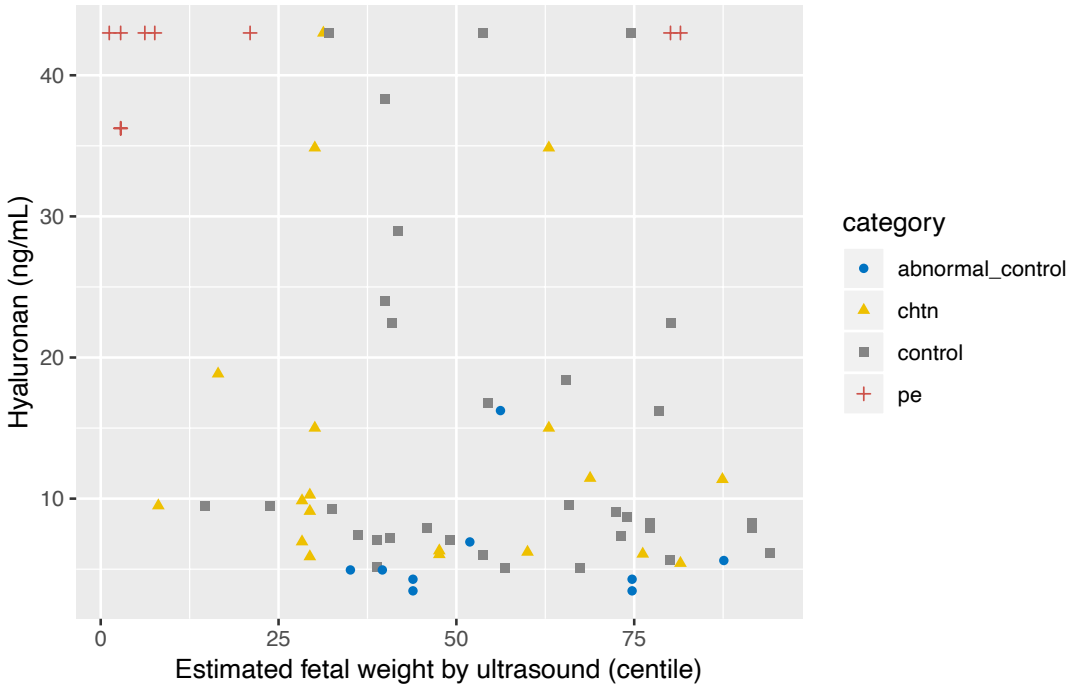

Figure 6.16: Scatterplot of serum hyaluronan concentration against estimated fetal weight (by ultrasound scan) performed within 2 weeks of blood sample taken

The potential use of placental mean T2* in conjunction with placenta growth factor concentrations as a predictor of adverse pregnancy outcomes in women with chronic hypertension was considered. 23 women with chronic hypertension had a blood sample taken within two weeks of their MRI. An abnormal maternal outcome in chronic hypertension was defined as the development of superimposed preeclampsia or delivery due to abnormal maternal biochemical concentrations. An abnormal fetal outcome was defined as preterm delivery and fetal growth restriction.

Figure 6.17 shows that three out of five women with a low mean T2* value had accompanying placenta growth factor concentrations less than 100pg/ml and adverse pregnancy outcomes. In uncomplicated pregnancies, 36 out of 41 women had placenta growth factor concentrations >100pg/ml. 18 women with chronic hypertension had either a normal or high placental mean T2*, six of whom had adverse pregnancy outcomes and a placenta growth factor concentration >100pg/ml; thus a normal placental mean T2* and a high placenta growth factor concentration does not necessarily confer a normal outcome if interval to delivery is prolonged (for example over four weeks). However, the five women with a placental growth factor concentration <100pg/ml and uncomplicated pregnancies had blood drawn between 31 to 37 weeks' gestation, and placental growth factor concentrations are known to fall towards term.

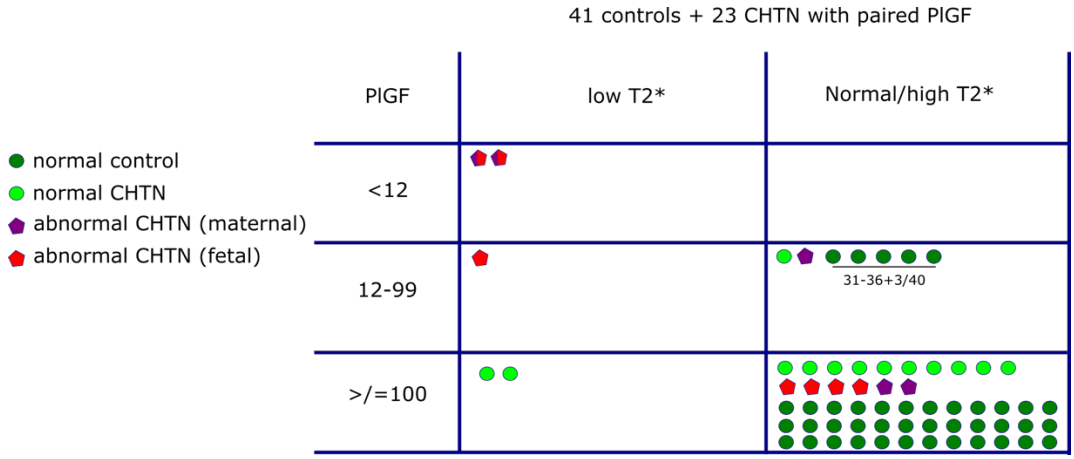

Figure 6.17: Placental growth factor concentrations and placental mean T2* values in uncomplicated pregnancies and those with chronic hypertension, colour coded by pregnancy outcome.

To assess whether there was a particular gestational age window in which pregnancy outcome could be better predicted using placental growth factor concentration and mean T2* values, the same analysis was conducted grouping into gestational age windows of under 24, 24-28, 28-34 and greater than 34 weeks' gestation at imaging Figure 6.18.

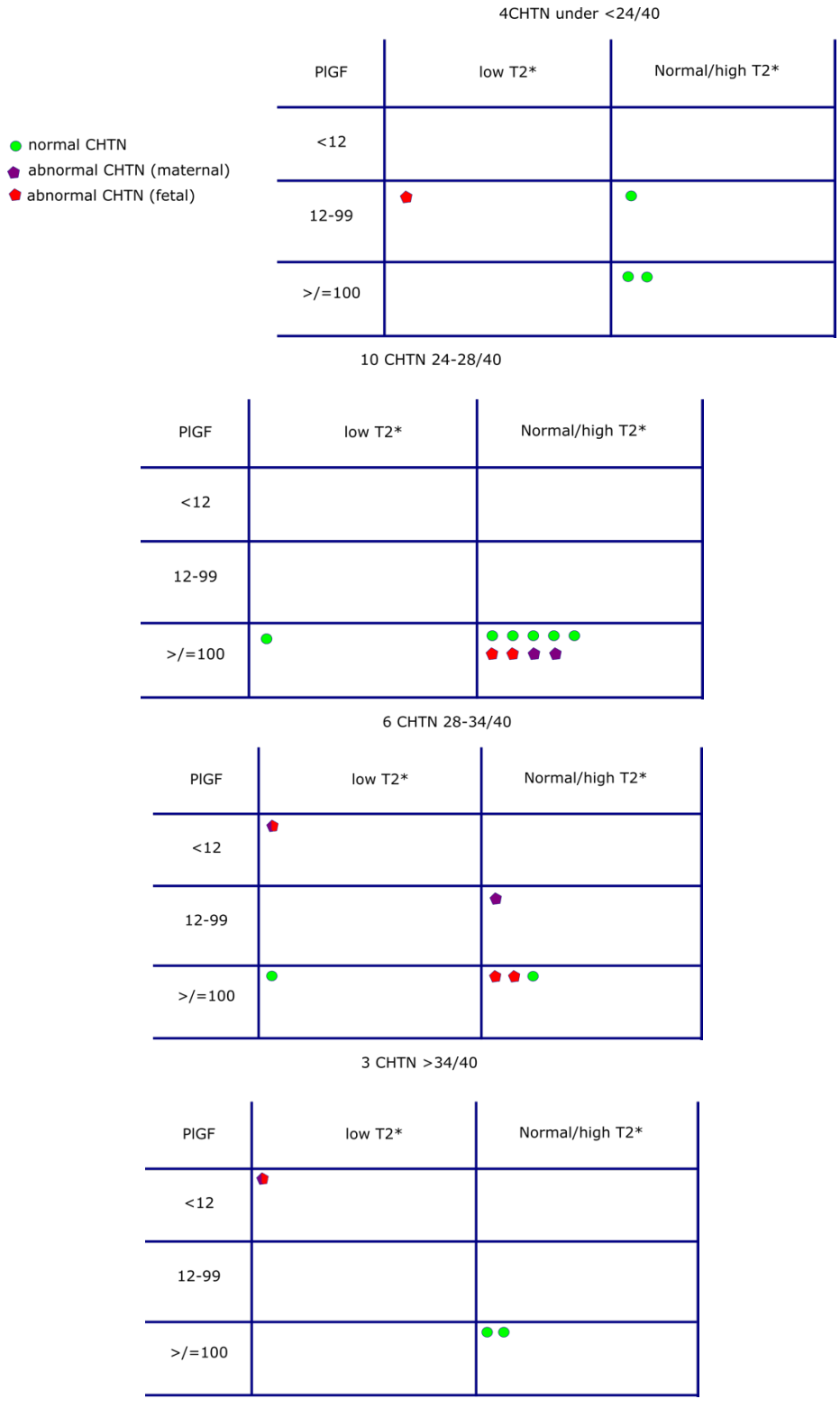

Figure 6.18: Placental growth factor concentrations and placental mean T2* values in pregnancies complicated by chronic hypertension, colour coded by pregnancy outcome and grouped by gestational age at imaging.

Comparing placental growth factor against placental mean T2* as a predictor of adverse outcome was also explored (Figure 6.19). Given the small sample size, these results were interpreted with caution. Following a discussion with a medical statistician, the case control nature of the study was considered inappropriate for prediction of adverse pregnancy outcome as there was a danger of overfitting. Further work, using a cohort study approach, would be advantageous to validate any preliminary data.

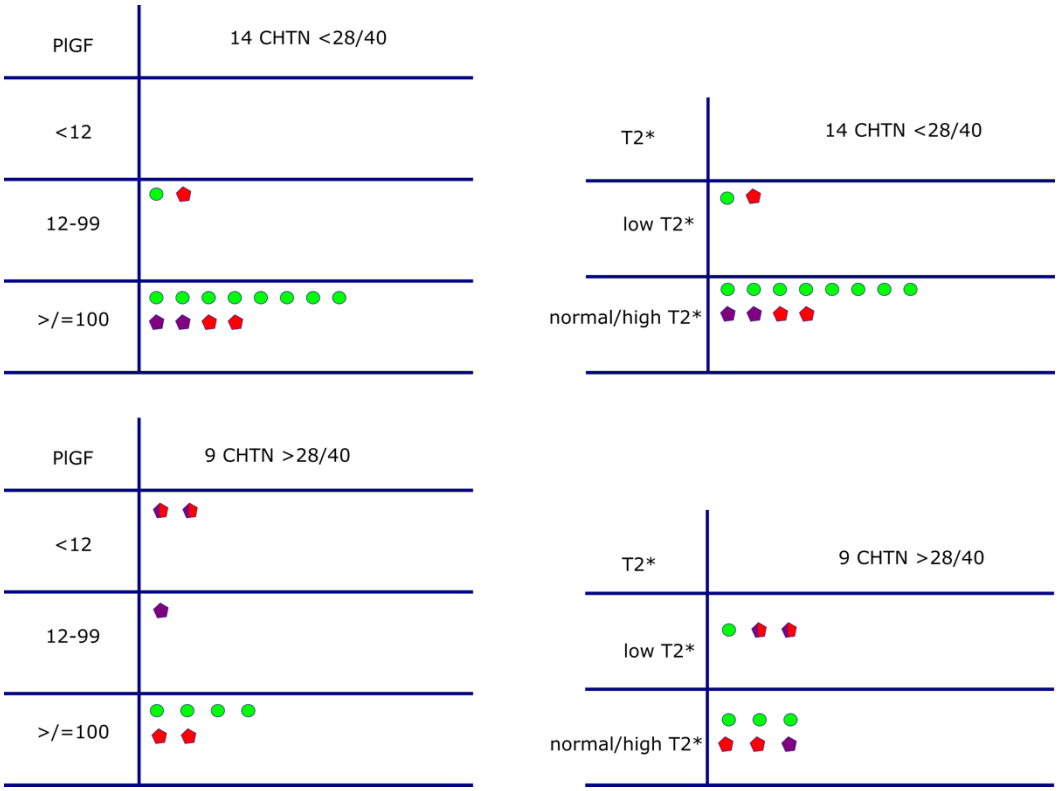

Figure 6.19: Placental growth factor concentration and mean T2* as a predictor of adverse pregnancy outcome, divided into gestational age groups <28 and > 28 weeks' gestation

6.4 Discussion

6.4.1 Statement of principal findings

In this study, we have explored several biomarkers and compared their association with a magnetic resonance imaging parameter of placental mean T2* in a group of women which included those with uncomplicated pregnancies, chronic hypertension and preeclampsia. Women with preeclampsia had low PlGF concentations accompanied by high sFlt-1, sFlt1:PlGF ratio, hyaluronan and VCAM concentrations. Women with chronic hypertension had biomarker concentrations which overlapped with those found in the control group.

When exploring biomarker results with placental mean T2* values, women with preeclampsia were again different to the control group. In comparison, women with chronic hypertension had results that overlapped with the control group.

6.4.2 Strengths and weaknesses of the study

A strength of this study is that we have explored a range of biomarkers in women with chronic hypertension and preeclampsia. Furthermore, PlGF concentrations were measured using two different assays thus allowing for intra-assay comparison. Candidate markers were chosen based on their hypothesised placental role in hypertensive disorders of pregnancy. This has allowed for assessment in conjunction with mean T2* values derived from magnetic resonance imaging to explore placental activity using the two modalities of biomarker concentration and imaging.

Follow up was until delivery, thereby ensuring that women who were in the control group did not develop a pregnancy complication post enrolment. Additionally, this identified women who were low risk clinically at enrolment but subsequently developed a pregnancy complication such as gestational diabetes, gestational hypertension, preeclampsia, fetal growth restriction or delivered preterm (the abnormal control group). Further subdivision of the chronic hypertension and the abnormal control group has not been undertaken in view of the small number of women.

6.4.3 Strengths and weaknesses in relation to other studies

Low PlGF concentrations, high sFlt-1 ratio, high hyaluronan and high VCAM concentrations in women with preeclampsia are consistent with previous studies as discussed in Chapter 1.6). There is paucity in the literature of studies exploring biomarkers in conjunction with magnetic resonance imaging, espcially in women with chronic hypertension. Previous studies have focussed on either fetal growth restriction and preeclampsia, the latter of which has been previously published by our group. To our knowledge, no study has explored the potential use of biomarkers and placental MRI in clinically low risk women to predict adverse pregnancy outcome.

6.4.4 Meaning of the study

Using biomarker analysis, we have confirmed the placental phenotype described in previous chapters whereby women with preterm preeclampsia have a clearer abnormal placental phenotype while women with chronic hypertension have an overlap in measures with women of uncomplicated pregnancies. The two modalities of biomarkers and magnetic resonance imaging provide complementary mechanistic information and an

insight into the pathophysiology of these hypertensive disorders. A larger sample size is needed to explore the clinical utility of these two modalities.

In women with preeclampsia, the low PlGF and high sFlt-1 concentrations suggest altered angiogenesis while high VCAM and hyaluronan concentrations suggest endothelial damage. These results may reflect a mechanistic pathway associated with low placental mean T2* values. Of the biomarkers explored, PlGF is the most discriminatory for preterm preeclampsia suggesting that the disorder is substantially driven by processes that alter PlGF concentrations and its downstream effects. In contrast, the placental phenotype in women with chronic hypertension has an overlap with women of uncomplicated pregnancies, as shown by biomaker concentrations and mean T2* values. This suggests that the maternal response to placental dysfunction may have a key role in determining the development of adverse pregnancy outcomes, but further work is needed to explore this. The lower concentrations of PlGF measured by the Quidel assay compared to the Roche assay may reflect the detection of different PlGF isoforms. However, the two methods of measuring PlGF concentrations have been found to perform similarly when using to predict the need for delivery within 14 days in women with suspected preeclampsia (McCarthy, Ryan, and Chappell 2018).

6.4.5 Unanswered questions and future research

The primary aim of this study was to confirm a placental phenotype rather than for prediction of adverse pregnancy outcome. In order to achieve the latter, future work would include a cohort designed study with a clinically meaningful perinatal outcome. Given the considerable heterogeneity in perinatal outcome (for example umbilical cord pH at delivery may be related to acute intrapartum events rather than an antenatal imaging measure), it may be more realistic to anticipate a surrogate marker such as birthweight centile.

One approach would be to have a large cohort of women with chronic hypertension and examine risk stratification and prediction of adverse pregnancy outcomes with biomarkers and magnetic resonance imaging derived values. Repeated measurements may be more meaningful as many predictive tools have better performance when repeated. Imaging could therefore be performed at fixed time points for the whole cohort, for example at 20, 28 and 36 weeks' gestation in line with their clinical growth ultrasound scans. Alternatively, imaging may be performed at time of suspected disease to further differentiate stratification of care and timing of delivery over and above our existing clinical tools of ultrasound Doppler measurements and computerised cardiotocography. Statistically, a net

reclassification improvement (NRI) index may be used to compare between different predictive models in order to examine the potential additional increments achieved when more data is added, for example biomarker concentrations or different imaging derived measures.

An alternative approach would be to have an unselected cohort that includes women with chronic hypertension, preeclampsia in a previous pregnancy and clinically low risk control women. The challenge in this approach would be the heterogenous incidence of adverse outcomes. Additionally, this approach does not mirror clinical practice.

The complex maternal-placental interaction and its role in influencing pregnancy outcomes has yet to be established. Advanced placental imaging sequences (such as diffusivity measures) may yield further insights into potential placental changes that may occur in association with biomarker concentrations. Future work in a larger group of women may further investigate placental changes (indicated by biomarker and placental T2*) in clinically low risk women who subsequently develop pregnancy complications, and in larger numbers of women with chronic hypertension, thus elucidating the underlying mechanisms that give rise to these complications.

Chapter 7 UNEXPECTED MATERNAL AND FETAL FINDINGS IN ANTENATAL FETAL MAGNETIC RESONANCE IMAGING

7.1 Introduction

Clinical indications for magnetic resonance imaging in pregnancy are increasing. The enhanced image quality compared to obstetric ultrasound is especially advantageous in the context of oligohydramnios and high body mass index while new techniques such as motion-corrected 3D image registration can provide high resolution 3D imaging of fetal vasculature for improved diagnostic capability (Lloyd et al. 2019). Magnetic resonance imaging can further characterise fetal brain, fetal body and placental pathology. Moreover, magnetic resonance imaging in pregnancy may be performed for suspected abdominal or pelvic pathology given the absence of ionising radiation compared to computerized tomography (CT).

Unexpected findings are a known consequence of imaging. The large field of view in obstetric magnetic resonance imaging encompasses several maternal organs including the cervix, renal tract and lumbar spine. The inclusion of these anatomical landmarks aids orientation but also provides a potential source of unexpected findings. Additionally, research studies using magnetic resonance imaging in low risk pregnancies may reveal unexpected fetal anomalies that have developed since an unremarkable routine 20 week anomaly screening ultrasound scan. Unexpected findings can cause anxiety for women, require further investigation and alter management but also, as a consequence, potentially improve clinical outcome for patients.

Current literature and guidelines for unexpected findings focus on non-pregnant adults and paediatric patients. These include splenic (Heller et al. 2013), gallbladder (Sebastian et al. 2013) and adnexal (Patel et al. 2020) unexpected findings when imaging using modalities of magnetic resonance and computerised tomography. Maternal and fetal unexpected findings have previously been reported in a group of 332 women who underwent magnetic resonance imaging for clinical fetal indications (Abdullah, Dietz, and Holm 2016) but there are limited data regarding imaging for research studies.

To aid counselling prior to imaging and inform the design of care pathways following the detection of unexpected findings, the aim of this chapter is to describe the incidence of maternal and fetal unexpected findings in a group of women undergoing obstetric magnetic resonance imaging for either research or clinical indications.

7.2 Methods

This retrospective study was undertaken at St Thomas' Hospital, a tertiary level unit and research centre. The group of women undergoing magnetic resonance imaging as part of the Placenta Imaging Project (and therefore the control, chronic hypertensive and preeclampsia groups in Chapters 3-7) were merged with a larger group to further enrich the study population. This larger group additionally included women imaged for fetal clinical indications and those imaged as part of another magnetic resonance imaging research study (either as a healthy control or with a known fetal or maternal condition). Research studies included the Intelligent Fetal Imaging and Diagnosis project (iFIND, www.ifindproject.com) and the Developing Human Connectome Project (www.developingconnectome.org). All obstetric magnetic resonance imaging occurred between January 2015 until December 2019 (Ethics numbers: 07/H0707/105 16/LO1573 14/LO1169 14/LO1806 17/LO0282 19/SS0032 19/LO0852).

As part of the consent process for each research study, women received a written information sheet highlighting the potential for maternal and fetal unexpected findings. This was then further discussed with them on the day of imaging when written informed consent was obtained. For those women imaged for clinical indications, a signed written consent form was obtained specifying that data could be used for research purposes. In our unit and throughout the course of this study, a standard operating procedure was in place to ensure women were informed of unexpected findings and managed through appropriate clinical pathways.

Imaging was performed at either 1.5 Tesla (Philips or Siemens) or 3 Tesla (Philips). All women had T2-weighted imaging that included the uterus, adnexal structures, sacral and lumbar spine. Depending on gestation, fetal position and maternal habitus, maternal kidneys were additionally captured in the field of view. Images were reviewed by a specialist perinatal radiologist, the majority of which were double reported. All imaging with unexpected findings were double reported.

Maternal unexpected findings were defined as previously unidentified abnormalities of maternal structures (including the maternal cervix) and fetal unexpected findings were defined as previously unidentified abnormalities of the fetus, amniotic fluid volume, placenta or umbilical cord. All unexpected findings were therefore not previously detected on ultrasound imagingTo determine the incidence of fetal unexpected findings, only magnetic resonance imaging from healthy women with normal ultrasound fetal anomly

scans were assessed. This was because in the presence of a known structural fetal abnormality, additional abnormalities could be part of an underlying syndrome rather than a true unexpected unexpected finding.

Unexpected findings were categorized as Level I, II or III in accordance with a previous study (Abdullah, Dietz, and Holm 2016) (Table 7.1). Follow up data were included where available. In women who underwent multiple scans in the same pregnancy, unexpected findings were counted as one instance.

Table 7.1: Unexpected findings categories as listed by Abdullah, Dietz and Holm 2016

Level	Category description
I	Little or no clinical significance, not requiring further evaluation or treatment
II	Unknown clinical significance but considered potentially clinically relevant during pregnancy or require further non-urgent evaluation
III	High clinical significance requiring prompt further evaluation

The classification of unexpected findings was achieved through consensus between a group of experts with extensive relevant clinical experience at St Thomas' Hospital. This included a clinical lecturer with subspecialty training in fetal medicine, an Obstetric consultant, a Neonatal consultant, a fetal medicine consultant and two radiology consultants with a specialist interest in fetal imaging.

7.3 Results

A total of 2569 magnetic resonance imaging scans were included. 28 women were imaged in two separate pregnancies and four women in three separate pregnancies. 1100 magnetic resonance examinations were in healthy volunteers with uncomplicated pregnancies as part of a control group for research (Table 7.2). Reporting was by 14 different experienced clinicians.

Table 7.2: Characteristics of women imaged and indication for imaging

	Number (percentage) unless otherwise stated
Maternal age, years, mean (SD)	32.8 (5.5)
Gestational age, wk, mean (SD)	28.8 (4.6)
1.5 Tesla magnet strength	1388 (54)
3 Tesla magnet strength	1181 (46)
Indication for imaging	
Research healthy control	1100 (43)
Clinical indication (fetal)	
Cardiac anomaly	318 (12.4)
Central nervous system anomaly	607 (23.6)
Thoracic anomaly	28 (1.1)
Gastrointestinal anomaly	35 (1.4)
Unexplained polyhydramnios	3 (0.1)
Congenital infection	28 (1.1)
Urinary tract anomaly	40 (1.6)
Family history/genetic	45 (1.8)
Fetal growth restriction	25 (1.0)
Placental evaluation	36 (1.4)
Multiple system abnormalities	76 (3.0)
MCDA twins post IUD of one twin	35 (1.4)
MCDA twins TTTS/TAPS	26 (1.0)
Post intrauterine transfusion	2 (0.1)
Hydrops	4 (0.2)
Neck/facial mass/micrognathia	17 (0.5)
Musculoskeletal system abnormality	27 (1.0)
Cleft lip/palate	5 (0.2)

Table 7.2 (cont)	Number (percentage) unless otherwise stated
High risk study groups including maternal high risk of preterm birth, ADHD, depression, trisomy 21, hypertension	111 (4.3)
Incomplete ultrasound with suspected abnormality	1 (0.04)

7.3.1 Fetal unexpected findings

146 fetuses had unexpected findings (eight of which had two abnormalities) giving a total of 154 unexpected findings. The fetal unexpected finding rate was 13% in uncomplicated low risk pregnancies (Table 7.3).

Table 7.3: Fetal unexpected findings in uncomplicated low risk pregnancies, imaged as part of research studies.

Unexpected finding	Fetal unexpected findings in uncomplicated low risk pregnancies (n=154)
Neurological	
Level 1	
Asymmetry of ventricles >2mm	15 (9.7)
Cerebellar vermis upward rotation (tegmento-vermian angle >14^{o}) with a normally appearing vermis	2 (1.2)
Prominent cisterna magna (AP) > 10 mm	1 (0.6)
Enlarged CSF space	5 (3.2)
Abnormal signal intensity in the lentiform nuclei (prominent vascular spaces)	1 (0.6)
Level II	
Borderline ventriculomegaly (9-11 mm)	18 (11.7)
Pseudocysts	14 (9.1)
Small transcerebellar diameter (3-5th centile)	2 (1.3)
Prominent venous sinus	1 (0.6)
Head circumference <5th centile	1 (0.6)
Head circumference >97th centile	6 (3.9)
Level III	
Polymicrogyria	1 (0.6)
Germinal matrix haemorrhage	1 (0.6)
Cerebellar haemorrhage	1 (0.6)
Subependymal heterotopia	1 (0.6)
Bilateral ventriculomegaly > 11 mm	1 (0.6)
Genitourinary	
Level 1	
Prominent bladder	1 (0.6)
Level II	
Hydrocele	2 (1.3)
Renal pelvis prominence	15 (9.7)
Level III	-
Thorax	
Level 1	-
Level II	-
Level III	
Congenital Pulmonary Malformation	3 (1.9)
Musculoskeletal	
Level 1	-
Level II	
Talipes	1 (0.6)
Level III	-
Abdomen	
Level 1	-
Level II	
Small stomach	2 (1.3)
Abdominal cyst	2 (1.3)
Ascites	1 (0.6)
Bowel dilatation	1 (0.6)

Table 7.3 (cont)	**Fetal unexpected findings in uncomplicated low risk pregnancies (n=154)**
Level III	-
Umbilical cord/Placenta/Membranes	
Level 1	
Mature placental appearances for gestational age	19 (12.3)
2 vessel umbilical cord	3 (1)
2 loops of umbilical cord around the neck	5 (1.9)
Level II	
Low lying placenta	5 (3.2)
Amniotic band	1 (0.6)
Succenturiate lobe	8 (5.2)
Placental infarction	1 (0.6)
Level III	-
Miscellaneous	
Level 1	
Large for gestation	1 (0.6)
Level II	
Dacrocystocele/nasolacrimal duct cysts	11 (7.1)
Polyhydramnios	1 (0.6)
Level III	-
Total Level 1 findings	53 (34.4)
Total Level II findings	93 (69.3)
Total Level III findings	8 (5.2)

Values given as a number (percentage)

Five Level III neurological fetal unexpected findings were identified. In two of these cases (suspected polymicrogyria and suspected subependymal heterotopia), subsequent second reporting or imaging at a later gestation were reassuringly normal. In the case of grade 1 germinal matrix haemorrhage, there was an uncomplicated neonatal course. The identification of bilateral ventriculomegaly (12mm) prompted follow up ultrasound scans in the fetal medicine unit where the ventricles were noted to not increase any further. Postnatal magnetic resonance imaging showed moderate ventriculomegaly and mild diffuse thinning of the corpus callosum for which a long term follow up plan is in place. No follow up data were available for the fetus with a cerebellar haemorrhage.

Level III thorax fetal unexpected findings identified three cases of Congenital Pulmonary Malformation (CPAM). In all three cases, subsequent imaging (by either antenatal ultrasound scan or postnatal chest X-ray) showed that the lesion was no longer visible. This may represent the natural evolution of the condition.

7.3.2 Maternal unexpected findings

459 women had maternal unexpected findings (62 had two additional findings, one had three and one had four) giving a total of 524 findings. The maternal unexpected finding rate in women undergoing a fetal magnetic resonance imaging was 17% (Table 7.4).

Table 7.4: Maternal unexpected findings

Unexpected finding	Maternal unexpected findings (n=524)
Genitourinary tract	
Level 1	
Fibroids <6cm	35 (6.7)
Nabothian follicles	37 (7.1)
Simple ovarian cyst <5cm	16 (3.1)
Bartholin's cyst	5 (1.0)
Uterine abnormality	4 (0.8)
Polycystic ovaries	2 (0.4)
Fluid in vagina (likely physiological)	1 (0.2)
Possible funneling but long cervix	14 (2.7)
Possible niche at site of C-section scar	3 (0.6)
Dilated vaginal veins	1 (0.2)
Tortuous ovarian vein	1 (0.2)
Small blood clot in the cervix	1 (0.2)
Level II	
Short cervix (< 25 mm)	89 (17.0)
Simple ovarian cyst >5cm	2 (0.4)
Abnormal signal suggestive of adenomyosis	3 (0.6)
Complex ovarian cyst	7 (1.3)
Fibroids >6cm or in uterine lower segment	10 (1.9)
Level III	
Open cervix	5 (1.0)
Cord prolapse	1 (0.2)
Renal Tract	
Level 1	
Mild/moderate hydronephrosis 5-15mm	112 (21.4)
Duplex collecting system	14 (2.7)
Urethral diverticulum	1 (0.2)
Unusual configuration of the bladder	1 (0.2)
Malpositioned kidney	1 (0.2)
Bladder trabeculations	1 (0.2)
Level II	
Severe hydronephrosis >15mm	48 (9.2)
Renal cysts	27 (5.2)
Level III	-
Abdomen	
Level 1	
Abdominal adhesions	1 (0.2)
Mesenteric cyst	2 (0.4)
Small amount of free fluid noted in abdomen	2 (0.4)

Table 7.4 (cont)	**Maternal unexpected findings (n=524)**
Abdomen	
Level II	
Gallstones	2 (0.4)
Liver cyst	6 (1.1)
Splenic cyst	3 (0.6)
Hernia	1 (0.2)
Level III	
Grossly dilated rectum	1 (0.2)
Cutaneous/Musculoskeletal	
Level 1	
Subcutaneous cyst	3 (0.6)
Lipoma	1 (0.2)
Bone islands on femoral heads	4 (0.8)
Cystic lesion femoral head	5 (1.0)
Oedematous sacro-iliac joint	1 (0.2)
Synovitis	1 (0.2)
Perineural cysts	46 (8.8)
Level II	
Degenerative changes in lumbar spine	3 (0.6)
Level III	-
Total Level 1 findings	316 (60.3)
Total Level II findings	201 (38.4)
Total Level III findings	7 (1.3)

A short cervix less than 25mm was the most common Level II maternal finding. In this group of 89 women, the mean gestational age at imaging was 31 weeks (range 20-38) and four were imaged after 37 weeks' gestation. Gestational age at delivery was available for 69 women. The mean gestational age at delivery was 38 weeks (range 26-42) with 48 (70%) delivering at term and 21 (30%) delivering preterm. In those who delivered preterm, five were not considered at risk of preterm delivery at the time of imaging. Iatrogenic delivery also occurred in this group with women delivering due to multi-fetal pregnancies, preeclampsia, fetal growth restriction or elected termination for fetal abnormalities. Delivery information for seven women were not available; however, they were imaged for fetal abnormalities and preterm delivery may therefore have occurred secondary to elective termination.

Level III maternal unexpected findings included five women with an open cervix. Gestational age at imaging ranged from 19-30 weeks' gestation. Two of the five women had preterm premature rupture of membranes prior to imaging and were enrolled in a study investigating women at high risk of preterm birth, one of whom additionally had a cord prolapse reported at imaging who delivered at 24 weeks' gestation for maternal

chorioamnionitis. Three women with an open cervix had magnetic resonance imaging for clinical indications: two had twin pregnancies (one imaged for fetal cardiac rhabdomyomas, the other imaged for fetal ventriculomegaly in one twin) and one underwent fetal cardiac magnetic resonance imaging for left atrial isomerism.

Other Level III maternal unexpected findings included a case of grossly dilated rectum. Imaging was performed for suspected fetal brain anomalies; however, the woman was also experiencing nausea, vomiting and abdominal pain. Emergency review by colorectal surgeons was subsequently organised but symptoms improved spontaneously without further intervention.

7.4 Discussion

7.4.1 Statement of principal findings

This study has characterised unexpected findings in a group of women undergoing fetal magnetic resonance imaging. The maternal unexpected finding rate was 17%. In women with uncomplicated pregnancies undergoing imaging for research studies, there was a fetal unexpected finding rate of 13%.

7.4.2 Strengths and weaknesses of the study

A strength of this study is that the group of women included those with uncomplicated and clinically low risk pregnancies, imaged as part of a research study. Detailed characterisation of both maternal and fetal unexpected findings can assist in the counselling of women prior to fetal magnetic resonance imaging.

In accordance with our local protocols, all incidental findings were reported to the requesting clinician or clinician involved in the relevant research study where imaging was performed for research purposes. This ensured that the women themselves were informed of the result and appropriate clinical follow up was arranged. A limitation of this study is that details of subsequent management and pregnancy outcome were not available and thus future studies may address this to further inform women undergoing antenatal magnetic resonance imaging.

Between January 2015 and December 2019, 14 clinicians reported the scans within this study, three of whom were senior radiologists who signed off all reports. The background and training may influence detection and classification of findings, and thus double reporting was especially beneficial. Classification of abnormal fetal findings could be further strengthened using internationally accepted definitions, such as those proposed by

the Medical Dictionary for Regulatory Activities (MedDRA). During the course of this study, a proposed maternal and fetal adverse event severity grading criteria underwent external review by national and international bodies and we await the formal publication.

In order to confirm the presence of an unexpected finding, all imaging with suspected unexpected findings were reported by two clinicians. This is therefore the final confirmed unexpected findings result. Where available, subsequent imaging at a later gestation was reviewed to investigate whether the unexpected finding persisted. In all three cases of congenital pulmonary malformation, imaging at a later gestation was reassuringly normal; however, this may represent the evolution of the condition.

The field of view of imaging varied depending on indication for imaging. Therefore, only findings within the field of view of imaging could be reported. Unless explicitly mentioned on a referral form for fetal magnetic resonance imaging, it is unclear whether a finding may have been known prior to imaging. The overall unexpected finding rate may therefore be falsely high.

7.4.3 Strengths and weaknesses in relation to other studies

Published studies on fetal unexpected findings are currently lacking. However, maternal unexpected findings have been previously reported. The rate of unexpected maternal findings is lower than a previous study (Abdullah, Dietz, and Holm 2016) in which 79% of 332 pregnancies had maternal unexpected findings: 90.5% Level I, 9.2% Level II and 0.4% Level III. Unlike our study where clinical reports were reviewed at the time of imaging, these authors specifically reviewed images retrospectively for the presence of additional findings.

7.4.4 Meaning of the study

Level I findings may be of limited clinical significance in isolation but become relevant when placed in the wider clinical context. Examples include musculoskeletal findings with pain or placental appearances advanced for gestation in the presence of a small for gestational age fetus later in pregnancy. Some may require follow up postnatally (for example small simple ovarian cysts) and therefore clinicians should inform women of these findings as they may become relevant in the future (Royal College of Obstetricians and Gynaecologists 2011).

Both maternal and fetal unexpected findings may influence pregnancy outcome and management. For example large fibroids may pose a risk of postpartum haemhorrhage and if in the lower segment may also impact on the mode of delivery (Parazzini, Tozzi, and

Bianchi 2016). A maternal unexpected finding of a short cervix may enable monitoring and optimal management for preterm delivery. Further antenatal assessment may be required to ensure conditions are not progressive or associated with additional features. Examples include borderline fetal ventriculomegaly (Tomic et al. 2020), potentially indicating the offer of infection screening or chromosomal testing. Further assessment may also be indicated antenatally if magnetic resonance imaging was unable to obtain optimal views where it was not the focus of the examination (for example prominent fetal renal pelvices). Postnatal follow up may be appropriate for other findings such as fetal hydrocele, or dacrocystocele (Kim et al. 2015). Long-term neurological follow up may be required, for example in the case of bilateral fetal ventriculomegaly confirmed postnatally.

7.4.5 Unanswered questions and future research

Published guidance on unexpected findings during antenatal ultrasound or magnetic resonance imaging are lacking. Neither the International Society of Ultrasound in Obstetrics and Gynecology (ISUOG) nor the Society for Maternal-Fetal medicine have issued a consensus statement or guidelines to aid management. In contrast, the American College of Radiology Incidental Findings Committee have published several white papers that include guidelines and recommendations for management of unexpected findings on CT and MRI in non-pregnant adults and paediatric patients (Heller et al. 2013; Sebastian et al. 2013; Patel et al. 2020). Future work may therefore include building a consensus across the fetal medicine community to develop protocols that define unexpected findings and provide management protocols.

Unexpected findings are an inevitable consequence of fetal magnetic resonance imaging. Women should be fully informed of the possibility of such prior to imaging as part of the consent process. Local protocols, agreed by obstetricians, neonatologists, radiologists and general practitioners are essential in the follow up of unexpected findings. These protocols should include the following:

1. Defining what should be reported as an unexpected finding, agreed by obstetricians, neonatologists and radiologists.
2. Who will interpret the unexpected finding in the clinical context.
3. Who will take responsibility for communicating findings with the woman.
4. Who will arrange appropriate follow up if required.
5. Timeframe for reporting and subsequent management.
6. Where to document adherence to the protocol.

These results have helped to shape our local protocols. With these measures in place, one can potentially optimise both maternal and fetal outcomes.

Chapter 8 CONCLUSIONS AND FUTURE RESEARCH

8.1 Summary of key findings

In this thesis, we have optimised and applied advanced magnetic resonance imaging techniques to provide detailed placental imaging in women with preeclampsia and chronic hypertension. These techniques have enabled qualitative visual assessment and quantitative assessment of placental structure and function. Imaging using these developed sequences was found to be feasible and acceptable to a large group of women across a range of gestations in the second and third trimester.

Optimised T2-weighted imaging sequences have led to the development of a comprehensive approach to visual assessment of the placenta. Features that can be visualised include anatomical landmarks to aid orientation, placental shape, variations in signal intensity, lobularity and granularity. Transient factors shown to affect imaging include fetal movement, gross motion and contractions. Detailed qualitative descriptors for visual assessment of placentae in low risk pregnancies in the second and third trimester at two magnetic field strengths are provided and subsequently used as a reference for assessing women with preeclampsia and chronic hypertension.

Quantitative assessment of the placenta has included the development of T2* mapping and diffusion sequences, culminating in an optimised combined diffusion-relaxometry sequence which provides regionally matched diffusion and T2* values in a reasonably fast and acceptable scan time compared to conventional sequences. Methods assessing placental T2* maps to quantify the visual variation seen are explored and detect variability within such maps. These measures include lacunarity as well as histogram derived measures of kurtosis and skewness, in addition to mean T2*.

These advanced sequences of T2-weighted imaging, T2* mapping and diffusion weighted imaging have been applied to women with preeclampsia and chronic hypertension in order to explore the spectrum of placental phenotypes in these hypertensive disorders of pregnancy. In pregnancies complicated by preeclampsia, T2-weighted imaging showed substantial areas of low signal intensity, advanced lobularity and high granularity within lobules with a reduced entire placental mean T2* for gestational age and higher lacunarity values compared to uncomplicated pregnancies. In pregnancies complicated by chronic hypertension, T2-weighted imaging showed a varied visual appearance compared to gestation matched controls with some showing features similar to those with preeclampsia and some indistinguishable from those in the control group. T2* values decrease with

gestation in both uncomplicated and pregnancies complicated by chronic hypertension; however, the latter group have a more variable spread of values. T2* histogram derived measures of kurtosis and skewness increased with advancing gestation with again a more widespread range of values in women with chronic hypertension compared to uncomplicated pregnancies. Not all women with mean T2* values outside of the normal range developed adverse pregnancy outcomes and conversely not all women with normal mean T2* values had uncomplicated pregnancies. This suggest a more complex interaction between the placenta and maternal or fetal response, while the timing of imaging may be crucial.

Finally, T2* mapping has been explored in conjunction with placental biomarkers of PlGF, sFlt-1, hyaluronan and VCAM to further elucidate mechanisms underlying preeclampsia and chronic hypertension. These biomarkers have been found to provide complementary mechanistic information of placental phenotypes seen with T2* mapping. Low PlGF and high sFlt-1 concentrations suggest altered angiogenesis while high VCAM and hyaluronan concentrations suggest endothelial damage in women with preeclampsia. These results suggest a mechanistic pathway associated with reduced mean T2* values.

8.2 Strengths and limitations of thesis

8.2.1 Imaging in women with preeclampsia and chronic hypertension

A major strength of this thesis is the novelty of magnetic resonance imaging undertaken in women with pregnancies complicated by preeclampsia and chronic hypertension, particularly conducting visual assessment along with measures derived from T2* mapping and diffusion. Furthermore, the addition of placental biomarker analysis has enabled further probing of the differences seen in these quantitative imaging variables. Prior to this study, placental imaging in the literature focussed on fetal growth restriction and screening for placenta accreta spectrum with a paucity in the literature on hypertensive disorders of pregnancy.

8.2.2 Use of 1.5T and 3T imaging

Sequences were optimised on both a 1.5T and a 3T scanner. This has enabled imaging to occur in more women as our 1.5T scanner had a wider magnet bore, thus could accommodate women of a higher body mass index and more advanced gestations comfortably. Comparable T2-weighted imaging using these two magnetic field strengths are shown with multiple imaging examples given the number of women scanned. Histogram derived measures of kurtosis and skewness were developed as they are

independent of magnetic field strength and therefore enable comparisons between groups regardless of the strength of magnetic resonance scanner used to acquire data.

8.2.3 Methods optimisation

Given the paucity in the literature surrounding placental magnetic resonance imaging in hypertensive disorders of pregnancy, the initial challenge was to optimise and adapt imaging techniques to women with pathology. This work required a multidisciplinary approach involving physicists, radiographers and clinicians. Although challenging to achieve within a short time frame, the resultant optimised sequences have ensured a consistent approach to imaging, yielding reproducible results for accurate evaluation of placental properties in a safe and acceptable way for women with pregnancies complicated by preeclampsia and chronic hypertension. Our robust safety approach included blood pressure monitoring with continuous maternal heart rate and oxygen saturation during imaging.

8.3 Meaning and clinical impact

The use of T2-weighted imaging, T2* mapping and apparent diffusion coefficient (ADC) maps in conjunction with biomarker concentrations confirms the placental contribution and mechanisms underlying preeclampsia and chronic hypertension through comparison with uncomplicated pregnancies.

In uncomplicated pregnancies, the low signal intensity areas seen on T2-weighted imaging are consistently between lobules and become more apparent with increasing gestation. These low signal intensity areas are likely to represent normal septae with low oxygenation as they have corresponding low mean T2* values. A reduction in placental mean T2* and apparent diffusion coefficient values with advancing gestation likely reflects parenchymal changes after initial placental angiogenesis in the first and second trimester, followed by villous maturation, calcium deposition and fibrosis as documented in previous histological studies.

In women with pregnancies complicated by preterm preeclampsia, a clear placental phenotype is seen. T2-weighted imaging reveals marked widening of low signal septal areas that extend beyond the normal septae and accelerated maturation of lobules with corresponding short T2* values, suggesting areas of non-functioning or poorly functioning tissue with impaired oxygenation. High lacunarity, skewness and kurtosis values futher support the visual phenotype seen. Low mean apparent diffusion coefficient values suggest a disruption in placental microstructure (such that occurs with fibrosis and calcium

deposition) or an impairment in placental perfusion consistent with maternal vascular malperfusion features seen on histology while low PlGF concentrations, high sFlt-1, VCAM and hyaluronan concentrations further support a distinct preeclampatic placental phenotype in all cases examined in this study.

In women with pregnancies complicated by chronic hypertension, the placental phenotype has an overlap with women of uncomplicated pregnancies, as demonstrated by visual assessment of T2-weighted imaging, quantitatitve T2* and apparent diffusion coefficient (ADC) mapping as well as biomarker analysis. This would be expected given the recognised variablilty in maternal and fetal outcomes in this high risk group. Further probing of T2* maps revealed high skewness and kurtosis values in a small number of women who developed superimposed preeclampsia shortly after imaging. A low mean T2* and/or low placenta growth factor concentration < 100pg/ml did not necessarily confer an adverse pregnancy outcome (defined as development of superimposed preeclampsia, delivery due to abnormal maternal biochemical concentrations, preterm delivery and fetal growth restriction). This potentially reflects the heterogeneity in pregnancy outcomes amongst women with chronic hypertension and a complex interaction between the placenta and maternal response that determines the development of adverse pregnancy outcomes. However, these findings are limited by a small sample size and the time interval between imaging and delivery.

The potential immediate clinical impact lies in the visual placental assessment developed during the course of this study and the ability to perform a T2* protocol with minimal addition to imaging time. Exogenous contrast was not used and therefore placental features described may be applied in cases where magnetic resonance imaging is performed for current clinical indications such as fetal brain or cardiac anomaly; however, this clinical impact warrants further investigation.

8.4 Unanswered questions and future steps

8.4.1 Clinical groups

Optimised magnetic resonance imaging sequences of T2-weighted imaging, T2* mapping and diffusivity measures have demonstrated different phenotypes in subgroups of women with preeclampsia and chronic hypertension, thereby examining potential differing mechanisms that result in additional maternal and fetal morbidity. Further groups that could be assessed in a similar manner including women with and without co-existing fetal growth restriction, gestational diabetes and maternal renal disease. Further work

investigating women with early and late onset preeclampsia would additionally be of interest.

8.4.2 Mechanistic insights

Evaluation of the interaction between placental dysfunction and the varied maternal response may further elucidate the underlying mechanisms that lead to varying adverse pregnancy outcomes. These include biomarkers involved in placental paracrine and endocrine pathways, maternal biochemical parameters and vascular function measures such as central aortic pressure, pulse wave velocity, brachial systolic and diastolic blood pressure.

8.4.3 Clinical application

With the potential identification of placental phenotypes in these hypertensive subgroups, further studies could investigate the clinical utility for magnetic resonance imaging in assisting the triage and monitoring of clinically 'high risk' women such as those with chronic hypertension or gestational hypertension. Magnetic resonance imaging may have a role in prediction of adverse pregnancy outcomes (such as fetal growth restriction, development of superimposed preeclampsia) and thus assist in management decisions such as timing of delivery.

The effectiveness of potential therapies that target underlying placental dysfunction mechanisms may be measured using these optimised imaging sequences. Further technological developments may enable certain steps in processing these sequences to be automated, thereby increasing opportunities for implementation in clicinal practice. The development and application of placental magnetic resonance imaging is an exciting field that has the potential to be a formidable tool in understanding the mechanisms underlying pregnancy complications and assisting the management of pregnancy for improving pregnancy outcomes.

REFERENCES

Abdullah, S. B., K. R. Dietz, and T. L. Holm. 2016. 'Fetal MRI: incidental findings in the mother', *Pediatr Radiol*, 46: 1736-43.

Alfirevic, Z., A. W. Tang, S. L. Collins, S. C. Robson, and J. Palacios-Jaraquemada. 2016. 'Pro forma for ultrasound reporting in suspected abnormally invasive placenta (AIP): an international consensus', *Ultrasound Obstet Gynecol*, 47: 276-8.

Allen, L., E. Jauniaux, S. Hobson, J. Papillon-Smith, and M. A. Belfort. 2018. 'FIGO consensus guidelines on placenta accreta spectrum disorders: Nonconservative surgical management', *Int J Gynaecol Obstet*, 140: 281-90.

American Academy of Pediatrics, . 1997. 'Noise: a hazard for the fetus and newborn. American Academy of Pediatrics. Committee on Environmental Health', *Pediatrics*, 100: 724-7.

Ananth, C. V., G. S. Berkowitz, D. A. Savitz, and R. H. Lapinski. 1999. 'Placental abruption and adverse perinatal outcomes', *Jama*, 282: 1646-51.

Ananth, C. V., M. R. Peltier, W. L. Kinzler, J. C. Smulian, and A. M. Vintzileos. 2007. 'Chronic hypertension and risk of placental abruption: is the association modified by ischemic placental disease?', *Am J Obstet Gynecol*, 197: 273.e1-7.

Andescavage, N., A. duPlessis, M. Metzler, D. Bulas, G. Vezina, M. Jacobs, S. N. Iqbal, A. Baschat, and C. Limperopoulos. 2017. 'In vivo assessment of placental and brain volumes in growth-restricted fetuses with and without fetal Doppler changes using quantitative 3D MRI', *J Perinatol*, 37: 1278-84.

Armstrong, T., D. Liu, T. Martin, R. Masamed, C. Janzen, C. Wong, T. Chanlaw, S. U. Devaskar, K. Sung, and H. H. Wu. 2019. '3D R2* mapping of the placenta during early gestation using free-breathing multiecho stack-of-radial MRI at 3T', *J Magn Reson Imaging*, 49: 291-303.

Aughwane, R., E. Ingram, E. D. Johnstone, L. J. Salomon, A. L. David, and A. Melbourne. 2020. 'Placental MRI and its application to fetal intervention', *Prenat Diagn*, 40: 38-48.

Austgulen, R., E. Lien, G. Vince, and C. W. Redman. 1997. 'Increased maternal plasma levels of soluble adhesion molecules (ICAM-1, VCAM-1, E-selectin) in preeclampsia', *Eur J Obstet Gynecol Reprod Biol*, 71: 53-8.

Avants, B. B., H. J. Johnson, and N. J. Tustison. 2015. 'Neuroinformatics and the The Insight ToolKit', *Front Neuroinform*, 9: 5.

Baker, P. N., I. R. Johnson, P. R. Harvey, P. A. Gowland, and P. Mansfield. 1994. 'A three-year follow-up of children imaged in utero with echo-planar magnetic resonance', *Am J Obstet Gynecol*, 170: 32-3.

Balayla, J., and H. D. Bondarenko. 2013. 'Placenta accreta and the risk of adverse maternal and neonatal outcomes', *J Perinat Med*, 41: 141-9.

Bateman, B. T., P. Bansil, S. Hernandez-Diaz, J. M. Mhyre, W. M. Callaghan, and E. V. Kuklina. 2012. 'Prevalence, trends, and outcomes of chronic hypertension: a nationwide sample of delivery admissions', *Am J Obstet Gynecol*, 206: 134.e1-8.

Baughman, W. C., J. E. Corteville, and R. R. Shah. 2008. 'Placenta accreta: spectrum of US and MR imaging findings', *Radiographics*, 28: 1905-16.

Bellamy, L., J. P. Casas, A. D. Hingorani, and D. J. Williams. 2007. 'Pre-eclampsia and risk of cardiovascular disease and cancer in later life: systematic review and meta-analysis', *Bmj*, 335: 974.

Berg, S. 1997. 'Hyaluronan turnover in relation to infection and sepsis', *J Intern Med*, 242: 73-7.

Berg, S., A. Engman, S. Holmgren, T. Lundahl, and T. C. Laurent. 2001. 'Increased plasma hyaluronan in severe pre-eclampsia and eclampsia', *Scand J Clin Lab Invest*, 61: 131-7.

Blaicher, W., P. C. Brugger, C. Mittermayer, J. Schwindt, J. Deutinger, G. Bernaschek, and D. Prayer. 2006. 'Magnetic resonance imaging of the normal placenta', *Eur J Radiol*, 57: 256-60.

Bonel, H. M., B. Stolz, L. Diedrichsen, K. Frei, B. Saar, B. Tutschek, L. Raio, D. Surbek, S. Srivastav, M. Nelle, J. Slotboom, and R. Wiest. 2010. 'Diffusion-weighted MR imaging of the placenta in fetuses with placental insufficiency', *Radiology*, 257: 810-9.

Bouyssi-Kobar, M., A. J. du Plessis, R. L. Robertson, and C. Limperopoulos. 2015. 'Fetal magnetic resonance imaging: exposure times and functional outcomes at preschool age', *Pediatr Radiol*, 45: 1823-30.

Bramham, K., B. Parnell, C. Nelson-Piercy, P. T. Seed, L. Poston, and L. C. Chappell. 2014. 'Chronic hypertension and pregnancy outcomes: systematic review and meta-analysis', *Bmj*, 348: g2301.

Bramham, K., P. T. Seed, L. Lightstone, C. Nelson-Piercy, C. Gill, P. Webster, L. Poston, and L. C. Chappell. 2016. 'Diagnostic and predictive biomarkers for pre-eclampsia in patients with established hypertension and chronic kidney disease', *Kidney Int*, 89: 874-85.

Brosens, I., I. Derwig, J. Brosens, L. Fusi, G. Benagiano, and R. Pijnenborg. 2010. 'The enigmatic uterine junctional zone: the missing link between reproductive disorders and major obstetrical disorders?', *Hum Reprod*, 25: 569-74.

Brosens, I., R. Pijnenborg, L. Vercruysse, and R. Romero. 2011. 'The "Great Obstetrical Syndromes" are associated with disorders of deep placentation', *Am J Obstet Gynecol*, 204: 193-201.

Brosens, J. J., R. Pijnenborg, and I. A. Brosens. 2002. 'The myometrial junctional zone spiral arteries in normal and abnormal pregnancies: a review of the literature', *Am J Obstet Gynecol*, 187: 1416-23.

Brown, M. A., L. A. Magee, L. C. Kenny, S. A. Karumanchi, F. P. McCarthy, S. Saito, D. R. Hall, C. E. Warren, G. Adoyi, and S. Ishaku. 2018. 'Hypertensive Disorders of Pregnancy: ISSHP Classification, Diagnosis, and Management Recommendations for International Practice', *Hypertension*, 72: 24-43.

Burchell, R. C. 1967. 'Arterial blood flow into the human intervillous space', *Am J Obstet Gynecol*, 98: 303-11.

Burton, G. J., and E. Jauniaux. 2004. 'Placental oxidative stress: from miscarriage to preeclampsia', *J Soc Gynecol Investig*, 11: 342-52.

———. 2015. 'What is the placenta?', *Am J Obstet Gynecol*, 213: S6.e1, S6-8.

———. 2018. 'Pathophysiology of placental-derived fetal growth restriction', *Am J Obstet Gynecol*, 218: S745-s61.

Burton, G. J., E. Jauniaux, and D. S. Charnock-Jones. 2007. 'Human early placental development: potential roles of the endometrial glands', *Placenta*, 28 Suppl A: S64-9.

Burton, G. J., A. W. Woods, E. Jauniaux, and J. C. Kingdom. 2009. 'Rheological and physiological consequences of conversion of the maternal spiral arteries for uteroplacental blood flow during human pregnancy', *Placenta*, 30: 473-82.

Bustamante Helfrich, B., N. Chilukuri, H. He, S. R. Cerda, X. Hong, G. Wang, C. Pearson, I. Burd, and X. Wang. 2017. 'Maternal vascular malperfusion of the placental bed associated with hypertensive disorders in the Boston Birth Cohort', *Placenta*, 52: 106-13.

Cameron, I. L., V. A. Ord, and G. D. Fullerton. 1984. 'Characterization of proton NMR relaxation times in normal and pathological tissues by correlation with other tissue parameters', *Magn Reson Imaging*, 2: 97-106.

Cantwell, R., T. Clutton-Brock, G. Cooper, A. Dawson, J. Drife, D. Garrod, A. Harper, D. Hulbert, S. Lucas, J. McClure, H. Millward-Sadler, J. Neilson, C. Nelson-Piercy, J. Norman, C. O'Herlihy, M. Oates, J. Shakespeare, M. de Swiet, C. Williamson, V. Beale, M. Knight, C. Lennox, A. Miller, D. Parmar, J. Rogers, and A. Springett. 2011. 'Saving Mothers' Lives: Reviewing maternal deaths to make motherhood safer: 2006-2008. The Eighth Report of the Confidential Enquiries into Maternal Deaths in the United Kingdom', *Bjog*, 118 Suppl 1: 1-203.

Capuani, S., M. Guerreri, A. Antonelli, S. Bernardo, M. G. Porpora, A. Giancotti, C. Catalano, and L. Manganaro. 2017. 'Diffusion and perfusion quantified by Magnetic Resonance Imaging are markers of human placenta development in normal pregnancy', *Placenta*, 58: 33-39.

Chaiworapongsa, T., R. Romero, J. Yoshimatsu, J. Espinoza, Y. M. Kim, K. Park, K. Kalache, S. Edwin, E. Bujold, and R. Gomez. 2002. 'Soluble adhesion molecule profile in normal pregnancy and pre-eclampsia', *J Matern Fetal Neonatal Med*, 12: 19-27.

Chalouhi, G. E., and L. J. Salomon. 2014. 'BOLD-MRI to explore the oxygenation of fetal organs and of the placenta', *Bjog*, 121: 1595.

Chappell, L. C., S. Duckworth, P. T. Seed, M. Griffin, J. Myers, L. Mackillop, N. Simpson, J. Waugh, D. Anumba, L. C. Kenny, C. W. Redman, and A. H. Shennan. 2013. 'Diagnostic accuracy of placental growth factor in women with suspected preeclampsia: a prospective multicenter study', *Circulation*, 128: 2121-31.

Chilla, G. S., C. H. Tan, C. Xu, and C. L. Poh. 2015. 'Diffusion weighted magnetic resonance imaging and its recent trend-a survey', *Quant Imaging Med Surg*, 5: 407-22.

Chu, S. Y., S. Y. Kim, J. Lau, C. H. Schmid, P. M. Dietz, W. M. Callaghan, and K. M. Curtis. 2007. 'Maternal obesity and risk of stillbirth: a metaanalysis', *Am J Obstet Gynecol*, 197: 223-8.

Collinot, H., C. Marchiol, I. Lagoutte, F. Lager, N. Siauve, G. Autret, D. Balvay, G. Renault, L. J. Salomon, and D. Vaiman. 2018. 'Preeclampsia induced by STOX1 overexpression in mice induces intrauterine growth restriction, abnormal ultrasonography and BOLD MRI signatures', *J Hypertens*, 36: 1399-406.

Collins, S. L., A. Ashcroft, T. Braun, P. Calda, J. Langhoff-Roos, O. Morel, V. Stefanovic, B. Tutschek, and F. Chantraine. 2016. 'Proposal for standardized ultrasound descriptors of abnormally invasive placenta (AIP)', *Ultrasound Obstet Gynecol*, 47: 271-5.

Conti-Ramsden, F. I., H. L. Nathan, A. De Greeff, D. R. Hall, P. T. Seed, L. C. Chappell, A. H. Shennan, and K. Bramham. 2019. 'Pregnancy-Related Acute Kidney Injury in Preeclampsia: Risk Factors and Renal Outcomes', *Hypertension*, 74: 1144-51.

Couper, S., A. Clark, J. M. D. Thompson, D. Flouri, R. Aughwane, A. L. David, A. Melbourne, A. Mirjalili, and P. R. Stone. 2020. 'The effects of maternal position, in late gestation pregnancy, on placental blood flow and oxygenation: an MRI study', *J Physiol*.

Creanga, A. A., C. Syverson, K. Seed, and W. M. Callaghan. 2017. 'Pregnancy-Related Mortality in the United States, 2011-2013', *Obstet Gynecol*, 130: 366-73.

Cronin, R. S., M. Li, J. M. D. Thompson, A. Gordon, C. H. Raynes-Greenow, A. E. P. Heazell, T. Stacey, V. M. Culling, V. Bowring, N. H. Anderson, L. M. O'Brien, E. A. Mitchell, L. M. Askie, and L. M. E. McCowan. 2019. 'An Individual Participant Data Meta-analysis of Maternal Going-to-Sleep Position, Interactions with Fetal Vulnerability, and the Risk of Late Stillbirth', *EClinicalMedicine*, 10: 49-57.

D'Antonio, F., C. Iacovella, J. Palacios-Jaraquemada, C. H. Bruno, L. Manzoli, and A. Bhide. 2014. 'Prenatal identification of invasive placentation using magnetic resonance

imaging: systematic review and meta-analysis', *Ultrasound Obstet Gynecol*, 44: 8-16.

Dahdouh, S., N. Andescavage, S. Yewale, A. Yarish, D. Lanham, D. Bulas, A. J. du Plessis, and C. Limperopoulos. 2018. 'In vivo placental MRI shape and textural features predict fetal growth restriction and postnatal outcome', *J Magn Reson Imaging*, 47: 449-58.

Damodaram, M., L. Story, E. Eixarch, A. Patel, A. McGuinness, J. Allsop, J. Wyatt-Ashmead, S. Kumar, and M. Rutherford. 2010. 'Placental MRI in intrauterine fetal growth restriction', *Placenta*, 31: 491-8.

David, Tomos W, David P Marshall, and Laure Zanna. 2017. 'The statistical nature of turbulent barotropic ocean jets', *Ocean Modelling*, 113: 34-49.

De Falco, S. 2012. 'The discovery of placenta growth factor and its biological activity', *Exp Mol Med*, 44: 1-9.

De Wilde, J. P., A. W. Rivers, and D. L. Price. 2005. 'A review of the current use of magnetic resonance imaging in pregnancy and safety implications for the fetus', *Prog Biophys Mol Biol*, 87: 335-53.

Dellschaft, N. S., G. Hutchinson, S. Shah, N. W. Jones, C. Bradley, L. Leach, C. Platt, R. Bowtell, and P. A. Gowland. 2020. 'The haemodynamics of the human placenta in utero', *PLoS Biol*, 18: e3000676.

Derwig, I., G. J. Barker, L. Poon, F. Zelaya, P. Gowland, D. J. Lythgoe, and K. Nicolaides. 2013. 'Association of placental T2 relaxation times and uterine artery Doppler ultrasound measures of placental blood flow', *Placenta*, 34: 474-9.

Derwig, I., D. J. Lythgoe, G. J. Barker, L. Poon, P. Gowland, R. Yeung, F. Zelaya, and K. Nicolaides. 2013. 'Association of placental perfusion, as assessed by magnetic resonance imaging and uterine artery Doppler ultrasound, and its relationship to pregnancy outcome', *Placenta*, 34: 885-91.

Desoye, G., and S. Hauguel-de Mouzon. 2007. 'The human placenta in gestational diabetes mellitus. The insulin and cytokine network', *Diabetes Care*, 30 Suppl 2: S120-6.

Dill, T. 2008. 'Contraindications to magnetic resonance imaging: non-invasive imaging', *Heart*, 94: 943-8.

Duckworth, S., M. Griffin, P. T. Seed, R. North, J. Myers, L. Mackillop, N. Simpson, J. Waugh, D. Anumba, L. C. Kenny, C. W. Redman, A. H. Shennan, and L. C. Chappell. 2016. 'Diagnostic Biomarkers in Women With Suspected Preeclampsia in a Prospective Multicenter Study', *Obstet Gynecol*, 128: 245-52.

Duhig, K. E., J. Myers, P. T. Seed, J. Sparkes, J. Lowe, R. M. Hunter, A. H. Shennan, and L. C. Chappell. 2019. 'Placental growth factor testing to assess women with suspected pre-eclampsia: a multicentre, pragmatic, stepped-wedge cluster-randomised controlled trial', *Lancet*, 393: 1807-18.

Duley, L. 2009. 'The global impact of pre-eclampsia and eclampsia', *Semin Perinatol*, 33: 130-7.

Edwards, M. J., R. D. Saunders, and K. Shiota. 2003. 'Effects of heat on embryos and foetuses', *Int J Hyperthermia*, 19: 295-324.

Falco, M. L., J. Sivanathan, A. Laoreti, B. Thilaganathan, and A. Khalil. 2017. 'Placental histopathology associated with pre-eclampsia: systematic review and meta-analysis', *Ultrasound Obstet Gynecol*, 50: 295-301.

Farquhar, C. M., Z. Li, S. Lensen, C. McLintock, W. Pollock, M. J. Peek, D. Ellwood, M. Knight, C. S. Homer, G. Vaughan, A. Wang, and E. Sullivan. 2017. 'Incidence, risk factors and perinatal outcomes for placenta accreta in Australia and New Zealand: a case-control study', *BMJ Open*, 7: e017713.

Gélat, P., A. L. David, S. R. Haqhenas, J. Henriques, A. Thibaut de Maisieres, T. White, and E. Jauniaux. 2019. 'Evaluation of fetal exposure to external loud noise using a sheep

model: quantification of in utero acoustic transmission across the human audio range', *Am J Obstet Gynecol*, 221: 343.e1-43.e11.

Glover, P., J. Hykin, P. Gowland, J. Wright, I. Johnson, and P. Mansfield. 1995. 'An assessment of the intrauterine sound intensity level during obstetric echo-planar magnetic resonance imaging', *Br J Radiol*, 68: 1090-4.

Gordijn, S. J., I. M. Beune, B. Thilaganathan, A. Papageorghiou, A. A. Baschat, P. N. Baker, R. M. Silver, K. Wynia, and W. Ganzevoort. 2016. 'Consensus definition of fetal growth restriction: a Delphi procedure', *Ultrasound Obstet Gynecol*, 48: 333-9.

Gordon, A., C. Raynes-Greenow, D. Bond, J. Morris, W. Rawlinson, and H. Jeffery. 2015. 'Sleep position, fetal growth restriction, and late-pregnancy stillbirth: the Sydney stillbirth study', *Obstet Gynecol*, 125: 347-55.

Gowland, P. 2005. 'Placental MRI', *Semin Fetal Neonatal Med*, 10: 485-90.

Gowland, P. A., A. Freeman, B. Issa, P. Boulby, K. R. Duncan, R. J. Moore, P. N. Baker, R. W. Bowtell, I. R. Johnson, and B. S. Worthington. 1998. 'In vivo relaxation time measurements in the human placenta using echo planar imaging at 0.5 T', *Magn Reson Imaging*, 16: 241-7.

Grannum, P. A., R. L. Berkowitz, and J. C. Hobbins. 1979. 'The ultrasonic changes in the maturing placenta and their relation to fetal pulmonic maturity', *Am J Obstet Gynecol*, 133: 915-22.

Hand, J. W., Y. Li, E. L. Thomas, M. A. Rutherford, and J. V. Hajnal. 2006. 'Prediction of specific absorption rate in mother and fetus associated with MRI examinations during pregnancy', *Magn Reson Med*, 55: 883-93.

Harris, John W. S., and Elizabeth Mapelsden Ramsey. 1966. *The morphology of human uteroplacental vasculature*.

Hazelgrove, J. F., C. Price, V. J. Pappachan, and G. B. Smith. 2001. 'Multicenter study of obstetric admissions to 14 intensive care units in southern England', *Crit Care Med*, 29: 770-5.

Heazell, A., M. Li, J. Budd, J. Thompson, T. Stacey, R. S. Cronin, B. Martin, D. Roberts, E. A. Mitchell, and L. McCowan. 2018. 'Association between maternal sleep practices and late stillbirth - findings from a stillbirth case-control study', *Bjog*, 125: 254-62.

Heller, M. T., M. Harisinghani, J. D. Neitlich, P. Yeghiayan, and L. L. Berland. 2013. 'Managing incidental findings on abdominal and pelvic CT and MRI, part 3: white paper of the ACR Incidental Findings Committee II on splenic and nodal findings', *J Am Coll Radiol*, 10: 833-9.

Hempstock, J., Y. P. Bao, M. Bar-Issac, N. Segaren, A. L. Watson, D. S. Charnock-Jones, E. Jauniaux, and G. J. Burton. 2003. 'Intralobular differences in antioxidant enzyme expression and activity reflect the pattern of maternal arterial bloodflow within the human placenta', *Placenta*, 24: 517-23.

Herman, H. G., L. Tamayev, O. Feldstein, M. Bustan, Z. Rachmiel, L. Schreiber, A. Raziel, J. Bar, and M. Kovo. 2020. 'Placental-related disorders of pregnancy and IVF: does placental histological examination explain the excess risk?', *Reprod Biomed Online*, 41: 81-87.

Hertig, A., N. Berkane, G. Lefevre, K. Toumi, H. P. Marti, J. Capeau, S. Uzan, and E. Rondeau. 2004. 'Maternal serum sFlt1 concentration is an early and reliable predictive marker of preeclampsia', *Clin Chem*, 50: 1702-3.

Heslehurst, N., L. J. Ells, H. Simpson, A. Batterham, J. Wilkinson, and C. D. Summerbell. 2007. 'Trends in maternal obesity incidence rates, demographic predictors, and health inequalities in 36,821 women over a 15-year period', *Bjog*, 114: 187-94.

Higuchi, H., S. Takagi, K. Zhang, I. Furui, and M. Ozaki. 2015. 'Effect of lateral tilt angle on the volume of the abdominal aorta and inferior vena cava in pregnant and

nonpregnant women determined by magnetic resonance imaging', *Anesthesiology*, 122: 286-93.

Ho, A. E. P., J. Hutter, L. H. Jackson, P. T. Seed, L. McCabe, M. Al-Adnani, A. Marnerides, S. George, L. Story, J. V. Hajnal, M. A. Rutherford, and L. C. Chappell. 2020. 'T2* Placental Magnetic Resonance Imaging in Preterm Preeclampsia: An Observational Cohort Study', *Hypertension*, 75: 1523-31.

Hod, T., A. S. Cerdeira, and S. A. Karumanchi. 2015. 'Molecular Mechanisms of Preeclampsia', *Cold Spring Harb Perspect Med*, 5.

Huen, I., D. M. Morris, C. Wright, G. J. Parker, C. P. Sibley, E. D. Johnstone, and J. H. Naish. 2013. 'R1 and R2 * changes in the human placenta in response to maternal oxygen challenge', *Magn Reson Med*, 70: 1427-33.

Hughes, E. J., A. N. Price, L. McCabe, S. Hiscocks, L. Waite, E. Green, J. Hutter, K. Pegoretti, L. Cordero-Grande, A. D. Edwards, J. V. Hajnal, and M. A. Rutherford. 2021. 'The effect of maternal position on venous return for pregnant women during MRI', *NMR Biomed*, 34: e4475.

Hughes, E.J., A. Price, L. McCabe, K. Pegoretti Baruteau, J. Hutter, O Carney, A. Gaspar, J. V. Hajnal, and M. A. Rutherford. 2016. 'Magnetic Resonance Imaging quantification of venous return in pregnant women: A comparison between supine and left lateral tilt position', *ISMRM 24th Annual Meeting & Exhibition*.

Humphries, A., S. A. Mirjalili, G. P. Tarr, J. M. D. Thompson, and P. Stone. 2019. 'The effect of supine positioning on maternal hemodynamics during late pregnancy', *J Matern Fetal Neonatal Med*, 32: 3923-30.

Humphries, A., P. Stone, and S. A. Mirjalili. 2017. 'The collateral venous system in late pregnancy: A systematic review of the literature', *Clin Anat*, 30: 1087-95.

Hung, T. H., J. N. Skepper, D. S. Charnock-Jones, and G. J. Burton. 2002. 'Hypoxia-reoxygenation: a potent inducer of apoptotic changes in the human placenta and possible etiological factor in preeclampsia', *Circ Res*, 90: 1274-81.

Hutcheon, J. A., S. Lisonkova, and K. S. Joseph. 2011. 'Epidemiology of pre-eclampsia and the other hypertensive disorders of pregnancy', *Best Pract Res Clin Obstet Gynaecol*, 25: 391-403.

Hutter, J, L Jackson, A Ho, M Pietsch, L Story, LC Chappell, JV Hajnal, and M Rutherford. 2019. 'T2* relaxometry to characterize normal placental development over gestation in-vivo at 3T [version 1; peer review: 1 approved, 1 approved with reservations]', *Wellcome Open Research*, 4.

Hutter, J., P. J. Slator, D. Christiaens, Rpag Teixeira, T. Roberts, L. Jackson, A. N. Price, S. Malik, and J. V. Hajnal. 2018. 'Integrated and efficient diffusion-relaxometry using ZEBRA', *Sci Rep*, 8: 15138.

Hutter, J., P. J. Slator, L. Jackson, A. D. S. Gomes, A. Ho, L. Story, J. O'Muircheartaigh, Rpag Teixeira, L. C. Chappell, D. C. Alexander, M. A. Rutherford, and J. V. Hajnal. 2019. 'Multi-modal functional MRI to explore placental function over gestation', *Magn Reson Med*, 81: 1191-204.

Ingram, E., D. Morris, J. Naish, J. Myers, and E. Johnstone. 2017. 'MR Imaging Measurements of Altered Placental Oxygenation in Pregnancies Complicated by Fetal Growth Restriction', *Radiology*, 285: 953-60.

Irgens, H. U., L. Reisaeter, L. M. Irgens, and R. T. Lie. 2001. 'Long term mortality of mothers and fathers after pre-eclampsia: population based cohort study', *Bmj*, 323: 1213-7.

Jaimes, C., J. Delgado, M. B. Cunnane, H. L. Hedrick, N. S. Adzick, M. S. Gee, and T. Victoria. 2019. 'Does 3-T fetal MRI induce adverse acoustic effects in the neonate? A preliminary study comparing postnatal auditory test performance of fetuses scanned at 1.5 and 3 T', *Pediatr Radiol*, 49: 37-45.

Jain, C. 2019. 'ACOG Committee Opinion No. 723: Guidelines for Diagnostic Imaging During Pregnancy and Lactation', *Obstet Gynecol*, 133: 186.

Jauniaux, E., Z. Alfirevic, A. G. Bhide, M. A. Belfort, G. J. Burton, S. L. Collins, S. Dornan, D. Jurkovic, G. Kayem, J. Kingdom, R. Silver, and L. Sentilhes. 2019. 'Placenta Praevia and Placenta Accreta: Diagnosis and Management: Green-top Guideline No. 27a', *Bjog*, 126: e1-e48.

Jauniaux, E., and A. Bhide. 2017. 'Prenatal ultrasound diagnosis and outcome of placenta previa accreta after cesarean delivery: a systematic review and meta-analysis', *Am J Obstet Gynecol*, 217: 27-36.

Javor, D., C. Nasel, T. Schweim, S. Dekan, K. Chalubinski, and D. Prayer. 2013. 'In vivo assessment of putative functional placental tissue volume in placental intrauterine growth restriction (IUGR) in human fetuses using diffusion tensor magnetic resonance imaging', *Placenta*, 34: 676-80.

Jiang, S., H. Xue, A. Glover, M. Rutherford, D. Rueckert, and J. V. Hajnal. 2007. 'MRI of moving subjects using multislice snapshot images with volume reconstruction (SVR): application to fetal, neonatal, and adult brain studies', *IEEE Trans Med Imaging*, 26: 967-80.

Kajantie, E., J. G. Eriksson, C. Osmond, K. Thornburg, and D. J. Barker. 2009. 'Pre-eclampsia is associated with increased risk of stroke in the adult offspring: the Helsinki birth cohort study', *Stroke*, 40: 1176-80.

Kalafat, E., I. Mir, H. Perry, B. Thilaganathan, and A. Khalil. 2018. 'Is home blood-pressure monitoring in hypertensive disorders of pregnancy consistent with clinic recordings?', *Ultrasound Obstet Gynecol*, 52: 515-21.

Kanal, E., J. Gillen, J. A. Evans, D. A. Savitz, and F. G. Shellock. 1993. 'Survey of reproductive health among female MR workers', *Radiology*, 187: 395-9.

Kario, Kazuomi, Jinho Shin, Chen-Huan Chen, Peera Buranakitjaroen, Yook-Chin Chia, Romeo Divinagracia, Jennifer Nailes, Satoshi Hoshide, Saulat Siddique, Jorge Sison, Arieska Ann Soenarta, Guru Prasad Sogunuru, Jam Chin Tay, Boon Wee Teo, Yuda Turana, Yuqing Zhang, Sungha Park, Huynh Van Minh, and Ji-Guang Wang. 2019. 'Expert panel consensus recommendations for ambulatory blood pressure monitoring in Asia: The HOPE Asia Network', *The Journal of Clinical Hypertension*, 21: 1250-83.

Karperien, A. L., and H. F. Jelinek. 2015. 'Fractal, multifractal, and lacunarity analysis of microglia in tissue engineering', *Front Bioeng Biotechnol*, 3: 51.

Karumanchi, S. A., S. E. Maynard, I. E. Stillman, F. H. Epstein, and V. P. Sukhatme. 2005. 'Preeclampsia: a renal perspective', *Kidney Int*, 67: 2101-13.

Khaliq, A., X. F. Li, M. Shams, P. Sisi, C. A. Acevedo, M. J. Whittle, H. Weich, and A. Ahmed. 1996. 'Localisation of placenta growth factor (PIGF) in human term placenta', *Growth Factors*, 13: 243-50,color plates I-II,pre.bk cov.

Kim, S. Y., H. M. Ryu, J. H. Yang, M. Y. Kim, H. K. Ahn, H. J. Lim, J. S. Shin, H. J. Woo, S. Y. Park, Y. M. Kim, J. W. Kim, and E. H. Cho. 2004. 'Maternal serum levels of VCAM-1, ICAM-1 and E-selectin in preeclampsia', *J Korean Med Sci*, 19: 688-92.

Kim, Y. H., Y. J. Lee, M. J. Song, B. H. Han, Y. H. Lee, and K. S. Lee. 2015. 'Dacryocystocele on prenatal ultrasonography: diagnosis and postnatal outcomes', *Ultrasonography*, 34: 51-7.

Kingdom, J. C., M. C. Audette, S. R. Hobson, R. C. Windrim, and E. Morgen. 2018. 'A placenta clinic approach to the diagnosis and management of fetal growth restriction', *Am J Obstet Gynecol*, 218: S803-s17.

Kinsella, S. M., and G. Lohmann. 1994. 'Supine hypotensive syndrome', *Obstet Gynecol*, 83: 774-88.

Knight, M., K. Bunch, D. Tuffnell, J. Shakespear, R. Kotnis, S. Kenyon, J. J. Kurinczuk, and on behalf of MBRRACE-UK. 2019. 'Saving Lives, Improving Mothers' Care - Lessons learned to inform maternity care from the UK and Ireland Confidential Enquiries into Maternal Deaths and Morbidity 2015-17', *Oxford: National Perinatal Epidemiology Unit*.

Koh, D. M., and D. J. Collins. 2007. 'Diffusion-weighted MRI in the body: applications and challenges in oncology', *AJR Am J Roentgenol*, 188: 1622-35.

Kornacki, J., P. Wirstlein, and E. Wender-Ozegowska. 2019. 'Levels of syndecan-1 and hyaluronan in early- and late-onset preeclampsia', *Pregnancy Hypertens*, 18: 108-11.

Kovo, M., J. Bar, L. Schreiber, and M. Shargorodsky. 2017. 'The relationship between hypertensive disorders in pregnancy and placental maternal and fetal vascular circulation', *J Am Soc Hypertens*, 11: 724-29.

Krauss, T., W. Kuhn, C. Lakoma, and H. G. Augustin. 1997. 'Circulating endothelial cell adhesion molecules as diagnostic markers for the early identification of pregnant women at risk for development of preeclampsia', *Am J Obstet Gynecol*, 177: 443-9.

Kuklisova-Murgasova, M., G. Quaghebeur, M. A. Rutherford, J. V. Hajnal, and J. A. Schnabel. 2012. 'Reconstruction of fetal brain MRI with intensity matching and complete outlier removal', *Med Image Anal*, 16: 1550-64.

Langhoff, L., L. Grønbeck, S. von Huth, A. Axelsson, C. Jørgensen, C. Thomsen, and N. Vejlstrup. 2017. 'Placental Growth during Normal Pregnancy - A Magnetic Resonance Imaging Study', *Gynecol Obstet Invest*, 82: 462-67.

Lax, A., M. R. Prince, K. W. Mennitt, J. R. Schwebach, and N. E. Budorick. 2007. 'The value of specific MRI features in the evaluation of suspected placental invasion', *Magn Reson Imaging*, 25: 87-93.

Lees, C. C., N. Marlow, A. van Wassenaer-Leemhuis, B. Arabin, C. M. Bilardo, C. Brezinka, S. Calvert, J. B. Derks, A. Diemert, J. J. Duvekot, E. Ferrazzi, T. Frusca, W. Ganzevoort, K. Hecher, P. Martinelli, E. Ostermayer, A. T. Papageorghiou, D. Schlembach, K. T. Schneider, B. Thilaganathan, T. Todros, A. Valcamonico, G. H. Visser, and H. Wolf. 2015. '2 year neurodevelopmental and intermediate perinatal outcomes in infants with very preterm fetal growth restriction (TRUFFLE): a randomised trial', *Lancet*, 385: 2162-72.

Lees, M. M., D. B. Scott, M. G. Kerr, and S. H. Taylor. 1967. 'The circulatory effects of recumbent postural change in late pregnancy', *Clin Sci*, 32: 453-65.

Levine, R. J., S. E. Maynard, C. Qian, K. H. Lim, L. J. England, K. F. Yu, E. F. Schisterman, R. Thadhani, B. P. Sachs, F. H. Epstein, B. M. Sibai, V. P. Sukhatme, and S. A. Karumanchi. 2004. 'Circulating angiogenic factors and the risk of preeclampsia', *N Engl J Med*, 350: 672-83.

Linduska, N., S. Dekan, A. Messerschmidt, G. Kasprian, P. C. Brugger, K. Chalubinski, M. Weber, and D. Prayer. 2009. 'Placental pathologies in fetal MRI with pathohistological correlation', *Placenta*, 30: 555-9.

Livingston, J. C., R. Chin, B. Haddad, E. T. McKinney, R. Ahokas, and B. M. Sibai. 2000. 'Reductions of vascular endothelial growth factor and placental growth factor concentrations in severe preeclampsia', *Am J Obstet Gynecol*, 183: 1554-7.

Lloyd, D. F. A., K. Pushparajah, J. M. Simpson, J. F. P. van Amerom, M. P. M. van Poppel, A. Schulz, B. Kainz, M. Deprez, M. Lohezic, J. Allsop, S. Mathur, H. Bellsham-Revell, T. Vigneswaran, M. Charakida, O. Miller, V. Zidere, G. Sharland, M. Rutherford, J. V. Hajnal, and R. Razavi. 2019. 'Three-dimensional visualisation of the fetal heart using prenatal MRI with motion-corrected slice-volume registration: a prospective, single-centre cohort study', *Lancet*, 393: 1619-27.

Llurba, E., O. Sánchez, Q. Ferrer, K. H. Nicolaides, A. Ruíz, C. Domínguez, J. Sánchez-de-Toledo, B. García-García, G. Soro, S. Arévalo, M. Goya, A. Suy, S. Pérez-Hoyos, J. Alijotas-Reig, E. Carreras, and L. Cabero. 2014. 'Maternal and foetal angiogenic imbalance in congenital heart defects', *Eur Heart J*, 35: 701-7.

Lo, J. O., V. H. J. Roberts, M. C. Schabel, X. Wang, T. K. Morgan, Z. Liu, C. Studholme, C. D. Kroenke, and A. E. Frias. 2018. 'Novel Detection of Placental Insufficiency by Magnetic Resonance Imaging in the Nonhuman Primate', *Reprod Sci*, 25: 64-73.

Luo, J., E. Abaci Turk, C. Bibbo, B. Gagoski, D. J. Roberts, M. Vangel, C. M. Tempany-Afdhal, C. Barnewolt, J. Estroff, A. Palanisamy, W. H. Barth, C. Zera, N. Malpica, P. Golland, E. Adalsteinsson, J. N. Robinson, and P. E. Grant. 2017. 'In Vivo Quantification of Placental Insufficiency by BOLD MRI: A Human Study', *Sci Rep*, 7: 3713.

Magin, R. L., J. K. Lee, A. Klintsova, K. I. Carnes, and F. Dunn. 2000. 'Biological effects of long-duration, high-field (4 T) MRI on growth and development in the mouse', *J Magn Reson Imaging*, 12: 140-9.

Maglione, D., V. Guerriero, G. Viglietto, M. G. Ferraro, O. Aprelikova, K. Alitalo, S. Del Vecchio, K. J. Lei, J. Y. Chou, and M. G. Persico. 1993. 'Two alternative mRNAs coding for the angiogenic factor, placenta growth factor (PlGF), are transcribed from a single gene of chromosome 14', *Oncogene*, 8: 925-31.

Marzioni, D., C. Crescimanno, D. Zaccheo, R. Coppari, C. B. Underhill, and M. Castellucci. 2001. 'Hyaluronate and CD44 expression patterns in the human placenta throughout pregnancy', *Eur J Histochem*, 45: 131-40.

Matejevic, D., S. Bussen, T. Steck, T. Müller, and J. Dietl. 1999. '[Hyaluronan and CD44 in maternal serum in pre-eclampsia]', *Z Geburtshilfe Neonatol*, 203: 246-9.

Mattar, F., and B. M. Sibai. 2000. 'Eclampsia. VIII. Risk factors for maternal morbidity', *Am J Obstet Gynecol*, 182: 307-12.

Maynard, S. E., J. Y. Min, J. Merchan, K. H. Lim, J. Li, S. Mondal, T. A. Libermann, J. P. Morgan, F. W. Sellke, I. E. Stillman, F. H. Epstein, V. P. Sukhatme, and S. A. Karumanchi. 2003. 'Excess placental soluble fms-like tyrosine kinase 1 (sFlt1) may contribute to endothelial dysfunction, hypertension, and proteinuria in preeclampsia', *J Clin Invest*, 111: 649-58.

McCarthy, F. P., R. M. Ryan, and L. C. Chappell. 2018. 'Prospective biomarkers in preterm preeclampsia: A review', *Pregnancy Hypertens*, 14: 72-78.

Melbourne, A., R. Aughwane, M. Sokolska, D. Owen, G. Kendall, D. Flouri, A. Bainbridge, D. Atkinson, J. Deprest, T. Vercauteren, A. David, and S. Ourselin. 2019. 'Separating fetal and maternal placenta circulations using multiparametric MRI', *Magn Reson Med*, 81: 350-61.

Meng, X., L. Xie, and W. Song. 2013. 'Comparing the diagnostic value of ultrasound and magnetic resonance imaging for placenta accreta: a systematic review and meta-analysis', *Ultrasound Med Biol*, 39: 1958-65.

Michel, S. C., A. Rake, T. M. Keller, R. Huch, V. König, B. Seifert, B. Marincek, and R. A. Kubik-Huch. 2003. 'Original report. Fetal cardiographic monitoring during 1.5-T MR imaging', *AJR Am J Roentgenol*, 180: 1159-64.

Millischer, A. E., L. J. Salomon, R. Porcher, M. Brasseur-Daudruy, A. L. Gourdier, P. Hornoy, S. Silvera, D. Loisel, V. Tsatsaris, B. Delorme, N. Boddaert, Y. Ville, and L. Sentilhes. 2017. 'Magnetic resonance imaging for abnormally invasive placenta: the added value of intravenous gadolinium injection', *Bjog*, 124: 88-95.

Miyakoshi, J. 2005. 'Effects of static magnetic fields at the cellular level', *Prog Biophys Mol Biol*, 87: 213-23.

Moore, R. J., S. S. Ong, D. J. Tyler, R. Duckett, P. N. Baker, W. R. Dunn, I. R. Johnson, and P. A. Gowland. 2008. 'Spiral artery blood volume in normal pregnancies and those compromised by pre-eclampsia', *NMR Biomed*, 21: 376-80.

Moore, R. J., B. K. Strachan, D. J. Tyler, K. R. Duncan, P. N. Baker, B. S. Worthington, I. R. Johnson, and P. A. Gowland. 2000. 'In utero perfusing fraction maps in normal and growth restricted pregnancy measured using IVIM echo-planar MRI', *Placenta*, 21: 726-32.

Murphy, K. J., and J. A. Brunberg. 1997. 'Adult claustrophobia, anxiety and sedation in MRI', *Magn Reson Imaging*, 15: 51-4.

Myers, C., K. R. Duncan, P. A. Gowland, I. R. Johnson, and P. N. Baker. 1998. 'Failure to detect intrauterine growth restriction following in utero exposure to MRI', *Br J Radiol*, 71: 549-51.

Myint, Soe Win, and Nina Lam. 2005. 'A study of lacunarity-based texture analysis approaches to improve urban image classification', *Computers, Environment and Urban Systems*, 29: 501-23.

Nandi, A., P. Estess, and M. H. Siegelman. 2000. 'Hyaluronan anchoring and regulation on the surface of vascular endothelial cells is mediated through the functionally active form of CD44', *J Biol Chem*, 275: 14939-48.

National Institute for Health and Care Excellence, . 2019. 'Hypertension in pregnancy: diagnosis and management', *NICE guideline*.

Neil, J. J. 2008. 'Diffusion imaging concepts for clinicians', *J Magn Reson Imaging*, 27: 1-7.

Nelson, D. B., M. S. Ziadie, D. D. McIntire, B. B. Rogers, and K. J. Leveno. 2014. 'Placental pathology suggesting that preeclampsia is more than one disease', *Am J Obstet Gynecol*, 210: 66.e1-7.

Obstetricians, American College of, and Gynecologists. 2013. 'Hypertension in pregnancy. Report of the American College of Obstetricians and Gynecologists' task force on hypertension in pregnancy', *Obstetrics and gynecology*, 122: 1122.

Ohgiya, Y., H. Nobusawa, N. Seino, O. Miyagami, N. Yagi, S. Hiroto, J. Munechika, M. Hirose, N. Takeyama, N. Ohike, R. Matsuoka, A. Sekizawa, and T. Gokan. 2016. 'MR Imaging of Fetuses to Evaluate Placental Insufficiency', *Magn Reson Med Sci*, 15: 212-9.

Ordidge, R. J., P. Gibbs, B. Chapman, M. K. Stehling, and P. Mansfield. 1990. 'High-speed multislice T1 mapping using inversion-recovery echo-planar imaging', *Magn Reson Med*, 16: 238-45.

Osmers, R. G., E. Schütz, F. Diedrich, B. Wehry, T. Krauss, M. Oellerich, and W. Kuhn. 1998. 'Increased serum levels of hyaluronic acid in pregnancies complicated by preeclampsia or hemolysis, elevated liver enzymes, and low platelets syndrome', *Am J Obstet Gynecol*, 178: 341-5.

Parati, Gianfranco, George S Stergiou, Roland Asmar, Grzegorz Bilo, Peter De Leeuw, Yutaka Imai, Kazuomi Kario, Empar Lurbe, Athanasios Manolis, and Thomas Mengden. 2008. 'European Society of Hypertension guidelines for blood pressure monitoring at home: a summary report of the Second International Consensus Conference on Home Blood Pressure Monitoring', *Journal of hypertension*, 26: 1505-26.

Parazzini, F., L. Tozzi, and S. Bianchi. 2016. 'Pregnancy outcome and uterine fibroids', *Best Pract Res Clin Obstet Gynaecol*, 34: 74-84.

Patel, M. D., S. M. Ascher, M. M. Horrow, P. J. Pickhardt, L. Poder, M. Goldman, L. L. Berland, P. V. Pandharipande, and K. E. Maturen. 2020. 'Management of Incidental Adnexal Findings on CT and MRI: A White Paper of the ACR Incidental Findings Committee', *J Am Coll Radiol*, 17: 248-54.

Patenaude, Y., D. Pugash, K. Lim, L. Morin, K. Lim, S. Bly, K. Butt, Y. Cargill, G. Davies, N. Denis, G. Hazlitt, L. Morin, K. Naud, A. Ouellet, and S. Salem. 2014. 'The use of magnetic resonance imaging in the obstetric patient', *J Obstet Gynaecol Can*, 36: 349-63.

Persico, M. G., V. Vincenti, and T. DiPalma. 1999. 'Structure, expression and receptor-binding properties of placenta growth factor (PlGF)', *Curr Top Microbiol Immunol*, 237: 31-40.

Pijnenborg, R., J. Anthony, D. A. Davey, A. Rees, A. Tiltman, L. Vercruysse, and A. van Assche. 1991. 'Placental bed spiral arteries in the hypertensive disorders of pregnancy', *Br J Obstet Gynaecol*, 98: 648-55.

Pijnenborg, R., L. Vercruysse, and M. Hanssens. 2006. 'The uterine spiral arteries in human pregnancy: facts and controversies', *Placenta*, 27: 939-58.

Poulsen, S. S., M. Sinding, D. N. Hansen, D. A. Peters, J. B. Frøkjær, and A. Sørensen. 2019. 'Placental T2* estimated by magnetic resonance imaging and fetal weight estimated by ultrasound in the prediction of birthweight differences in dichorionic twin pairs', *Placenta*, 78: 18-22.

Poutamo, J., K. Partanen, R. Vanninen, P. Vainio, and P. Kirkinen. 1998. 'MRI does not change fetal cardiotocographic parameters', *Prenat Diagn*, 18: 1149-54.

Prato, F. S., M. Kavaliers, K. P. Ossenkopp, J. J. Carson, D. J. Drost, and J. R. Frappier. 1992. 'Extremely low frequency magnetic field exposure from MRI/MRS procedures. Implications for patients (acute exposures) and operational personnel (chronic exposures)', *Ann N Y Acad Sci*, 649: 44-58.

Public Health England, . 2018. 'NHS Fetal Anomaly Screening Programme Handbook'.

Rana, S., C. E. Powe, S. Salahuddin, S. Verlohren, F. H. Perschel, R. J. Levine, K. H. Lim, J. B. Wenger, R. Thadhani, and S. A. Karumanchi. 2012. 'Angiogenic factors and the risk of adverse outcomes in women with suspected preeclampsia', *Circulation*, 125: 911-9.

Ray, J. G., M. J. Vermeulen, A. Bharatha, W. J. Montanera, and A. L. Park. 2016. 'Association Between MRI Exposure During Pregnancy and Fetal and Childhood Outcomes', *Jama*, 316: 952-61.

Redline, R. W. 2015. 'Classification of placental lesions', *Am J Obstet Gynecol*, 213: S21-8.

Redline, R. W., D. Heller, S. Keating, and J. Kingdom. 2005. 'Placental diagnostic criteria and clinical correlation--a workshop report', *Placenta*, 26 Suppl A: S114-7.

Redman, C. W., and I. L. Sargent. 2010. 'Immunology of pre-eclampsia', *Am J Reprod Immunol*, 63: 534-43.

Reece, E. A., A. Wiznitzer, E. Le, C. J. Homko, H. Behrman, and E. M. Spencer. 1994. 'The relation between human fetal growth and fetal blood levels of insulin-like growth factors I and II, their binding proteins, and receptors', *Obstet Gynecol*, 84: 88-95.

Reeves, M. J., M. Brandreth, E. H. Whitby, A. R. Hart, M. N. Paley, P. D. Griffiths, and J. C. Stevens. 2010. 'Neonatal cochlear function: measurement after exposure to acoustic noise during in utero MR imaging', *Radiology*, 257: 802-9.

Reitsma, S., D. W. Slaaf, H. Vink, M. A. van Zandvoort, and M. G. oude Egbrink. 2007. 'The endothelial glycocalyx: composition, functions, and visualization', *Pflugers Arch*, 454: 345-59.

Riteau, A. S., M. Tassin, G. Chambon, C. Le Vaillant, J. de Laveaucoupet, M. P. Quéré, M. Joubert, S. Prevot, H. J. Philippe, and A. Benachi. 2014. 'Accuracy of ultrasonography and magnetic resonance imaging in the diagnosis of placenta accreta', *PLoS One*, 9: e94866.

Roberts, C. L., J. C. Bell, J. B. Ford, R. M. Hadfield, C. S. Algert, and J. M. Morris. 2008. 'The accuracy of reporting of the hypertensive disorders of pregnancy in population health data', *Hypertens Pregnancy*, 27: 285-97.

Roberts, C. L., J. B. Ford, C. S. Algert, S. Antonsen, J. Chalmers, S. Cnattingius, M. Gokhale, M. Kotelchuck, K. K. Melve, A. Langridge, C. Morris, J. M. Morris, N. Nassar, J. E. Norman, J. Norrie, H. T. Sørensen, R. Walker, and C. J. Weir. 2011. 'Population-

based trends in pregnancy hypertension and pre-eclampsia: an international comparative study', *BMJ Open*, 1: e000101.

Roberts, V. H. J., T. K. Morgan, P. Bednarek, M. Morita, G. J. Burton, J. O. Lo, and A. E. Frias. 2017. 'Early first trimester uteroplacental flow and the progressive disintegration of spiral artery plugs: new insights from contrast-enhanced ultrasound and tissue histopathology', *Hum Reprod*, 32: 2382-93.

Romão, M., I. C. Weel, S. J. Lifshitz, and M. T. Peraçoli. 2014. 'Elevated hyaluronan and extracellular matrix metalloproteinase inducer levels in women with preeclampsia', *Arch Gynecol Obstet*, 289: 575-9.

Romero, R., J. K. Nien, J. Espinoza, D. Todem, W. Fu, H. Chung, J. P. Kusanovic, F. Gotsch, O. Erez, S. Mazaki-Tovi, R. Gomez, S. Edwin, T. Chaiworapongsa, R. J. Levine, and S. A. Karumanchi. 2008. 'A longitudinal study of angiogenic (placental growth factor) and anti-angiogenic (soluble endoglin and soluble vascular endothelial growth factor receptor-1) factors in normal pregnancy and patients destined to develop preeclampsia and deliver a small for gestational age neonate', *J Matern Fetal Neonatal Med*, 21: 9-23.

Royal College of Obstetricians and Gynaecologists, . 2011. 'Management of Suspected Ovarian Masses in Premenopausal Women', *Green-top Guideline No. 62*.

Saffer, C., G. Olson, K. A. Boggess, R. Beyerlein, C. Eubank, and B. M. Sibai. 2013. 'Determination of placental growth factor (PlGF) levels in healthy pregnant women without signs or symptoms of preeclampsia', *Pregnancy Hypertens*, 3: 124-32.

Salafia, C. M., V. K. Minior, J. C. Pezzullo, E. J. Popek, T. S. Rosenkrantz, and A. M. Vintzileos. 1995. 'Intrauterine growth restriction in infants of less than thirty-two weeks' gestation: associated placental pathologic features', *Am J Obstet Gynecol*, 173: 1049-57.

Sau, A., P. Seed, and K. Langford. 2004. 'Intraobserver and interobserver variation in the sonographic grading of placental maturity', *Ultrasound Obstet Gynecol*, 23: 374-7.

Say, Lale, Doris Chou, Alison Gemmill, Özge Tunçalp, Ann-Beth Moller, Jane Daniels, A. Metin Gülmezoglu, Marleen Temmerman, and Leontine Alkema. 2014. 'Global causes of maternal death: a WHO systematic analysis', *The Lancet Global Health*, 2: e323-e33.

Schabel, M. C., V. H. J. Roberts, J. O. Lo, S. Platt, K. A. Grant, A. E. Frias, and C. D. Kroenke. 2016. 'Functional imaging of the nonhuman primate Placenta with endogenous blood oxygen level-dependent contrast', *Magn Reson Med*, 76: 1551-62.

Scott, J. E., and F. Heatley. 1999. 'Hyaluronan forms specific stable tertiary structures in aqueous solution: a 13C NMR study', *Proc Natl Acad Sci U S A*, 96: 4850-5.

Sebastian, S., C. Araujo, J. D. Neitlich, and L. L. Berland. 2013. 'Managing incidental findings on abdominal and pelvic CT and MRI, Part 4: white paper of the ACR Incidental Findings Committee II on gallbladder and biliary findings', *J Am Coll Radiol*, 10: 953-6.

Seely, E. W., and J. Ecker. 2014. 'Chronic hypertension in pregnancy', *Circulation*, 129: 1254-61.

Shamshirsaz, A. A., K. A. Fox, B. Salmanian, C. R. Diaz-Arrastia, W. Lee, B. W. Baker, J. Ballas, Q. Chen, T. R. Van Veen, P. Javadian, H. Sangi-Haghpeykar, N. Zacharias, S. Welty, C. I. Cassady, A. Moaddab, E. J. Popek, S. K. Hui, J. Teruya, V. Bandi, M. Coburn, T. Cunningham, S. R. Martin, and M. A. Belfort. 2015. 'Maternal morbidity in patients with morbidly adherent placenta treated with and without a standardized multidisciplinary approach', *Am J Obstet Gynecol*, 212: 218.e1-9.

Shawkat, E., H. Mistry, C. Chmiel, L. Webster, L. Chappell, E. D. Johnstone, and J. E. Myers. 2018. 'The effect of labetalol and nifedipine MR on blood pressure in women with chronic hypertension in pregnancy', *Pregnancy Hypertens*, 11: 92-98.

Shore, V. H., T. H. Wang, C. L. Wang, R. J. Torry, M. R. Caudle, and D. S. Torry. 1997. 'Vascular endothelial growth factor, placenta growth factor and their receptors in isolated human trophoblast', *Placenta*, 18: 657-65.

Siauve, N., P. H. Hayot, B. Deloison, G. E. Chalouhi, M. Alison, D. Balvay, L. Bussières, O. Clément, and L. J. Salomon. 2019. 'Assessment of human placental perfusion by intravoxel incoherent motion MR imaging', *J Matern Fetal Neonatal Med*, 32: 293-300.

Sibai, B. M., M. Lindheimer, J. Hauth, S. Caritis, P. VanDorsten, M. Klebanoff, C. MacPherson, M. Landon, M. Miodovnik, R. Paul, P. Meis, and M. Dombrowski. 1998. 'Risk factors for preeclampsia, abruptio placentae, and adverse neonatal outcomes among women with chronic hypertension. National Institute of Child Health and Human Development Network of Maternal-Fetal Medicine Units', *N Engl J Med*, 339: 667-71.

Sinding, M., D. A. Peters, J. B. Frøkjaer, O. B. Christiansen, A. Petersen, N. Uldbjerg, and A. Sørensen. 2016. 'Placental magnetic resonance imaging T2* measurements in normal pregnancies and in those complicated by fetal growth restriction', *Ultrasound Obstet Gynecol*, 47: 748-54.

Sinding, M., D. A. Peters, J. B. Frøkjær, O. B. Christiansen, A. Petersen, N. Uldbjerg, and A. Sørensen. 2017. 'Prediction of low birth weight: Comparison of placental T2* estimated by MRI and uterine artery pulsatility index', *Placenta*, 49: 48-54.

Sinding, M., D. A. Peters, J. B. Frøkjær, O. B. Christiansen, N. Uldbjerg, and A. Sørensen. 2016. 'Reduced placental oxygenation during subclinical uterine contractions as assessed by BOLD MRI', *Placenta*, 39: 16-20.

Sinding, M., D. A. Peters, S. S. Poulsen, J. B. Frøkjær, O. B. Christiansen, A. Petersen, N. Uldbjerg, and A. Sørensen. 2018. 'Placental baseline conditions modulate the hyperoxic BOLD-MRI response', *Placenta*, 61: 17-23.

Slator, P. J., J. Hutter, M. Palombo, L. H. Jackson, A. Ho, E. Panagiotaki, L. C. Chappell, M. A. Rutherford, J. V. Hajnal, and D. C. Alexander. 2019. 'Combined diffusion-relaxometry MRI to identify dysfunction in the human placenta', *Magn Reson Med*, 82: 95-106.

Śliwińska-Kowalska, M., and K. Zaborowski. 2017. 'WHO Environmental Noise Guidelines for the European Region: A Systematic Review on Environmental Noise and Permanent Hearing Loss and Tinnitus', *Int J Environ Res Public Health*, 14.

Sohlberg, S., A. Mulic-Lutvica, P. Lindgren, F. Ortiz-Nieto, A. K. Wikström, and J. Wikström. 2014. 'Placental perfusion in normal pregnancy and early and late preeclampsia: a magnetic resonance imaging study', *Placenta*, 35: 202-6.

Sohlberg, S., A. Mulic-Lutvica, M. Olovsson, J. Weis, O. Axelsson, J. Wikström, and A. K. Wikström. 2015. 'Magnetic resonance imaging-estimated placental perfusion in fetal growth assessment', *Ultrasound Obstet Gynecol*, 46: 700-5.

Sørensen, A., J. Hutter, M. Seed, P. E. Grant, and P. Gowland. 2020. 'T2*-weighted placental MRI: basic research tool or emerging clinical test for placental dysfunction?', *Ultrasound Obstet Gynecol*, 55: 293-302.

Sørensen, A., D. Peters, E. Fründ, G. Lingman, O. Christiansen, and N. Uldbjerg. 2013. 'Changes in human placental oxygenation during maternal hyperoxia estimated by blood oxygen level-dependent magnetic resonance imaging (BOLD MRI)', *Ultrasound Obstet Gynecol*, 42: 310-4.

Srinivas, S. K., A. G. Edlow, P. M. Neff, M. D. Sammel, C. M. Andrela, and M. A. Elovitz. 2009. 'Rethinking IUGR in preeclampsia: dependent or independent of maternal hypertension?', *J Perinatol*, 29: 680-4.

Staff, A. C., S. J. Benton, P. von Dadelszen, J. M. Roberts, R. N. Taylor, R. W. Powers, D. S. Charnock-Jones, and C. W. Redman. 2013. 'Redefining preeclampsia using placenta-derived biomarkers', *Hypertension*, 61: 932-42.

Stone, P. R., W. Burgess, J. P. McIntyre, A. J. Gunn, C. A. Lear, L. Bennet, E. A. Mitchell, and J. M. Thompson. 2017. 'Effect of maternal position on fetal behavioural state and heart rate variability in healthy late gestation pregnancy', *J Physiol*, 595: 1213-21.

Sweetland, J., A. Kertesz, F. S. Prato, and K. Nantau. 1987. 'The effect of magnetic resonance imaging on human cognition', *Magn Reson Imaging*, 5: 129-35.

Tan, M. Y., A. Syngelaki, L. C. Poon, D. L. Rolnik, N. O'Gorman, J. L. Delgado, R. Akolekar, L. Konstantinidou, M. Tsavdaridou, S. Galeva, U. Ajdacka, F. S. Molina, N. Persico, J. C. Jani, W. Plasencia, E. Greco, G. Papaioannou, A. Wright, D. Wright, and K. H. Nicolaides. 2018. 'Screening for pre-eclampsia by maternal factors and biomarkers at 11-13 weeks' gestation', *Ultrasound Obstet Gynecol*, 52: 186-95.

Tenhola, S., E. Rahiala, P. Halonen, E. Vanninen, and R. Voutilainen. 2006. 'Maternal preeclampsia predicts elevated blood pressure in 12-year-old children: evaluation by ambulatory blood pressure monitoring', *Pediatr Res*, 59: 320-4.

Toivonen, S., S. Heinonen, M. Anttila, V. M. Kosma, and S. Saarikoski. 2002. 'Reproductive risk factors, Doppler findings, and outcome of affected births in placental abruption: a population-based analysis', *Am J Perinatol*, 19: 451-60.

Tomic, K., H. Schonberger, P. Weber, O. Lapaire, and G. Manegold-Brauer. 2020. 'Significance of isolated borderline ventriculomegaly', *Childs Nerv Syst*, 36: 393-99.

Vadeyar, S. H., R. J. Moore, B. K. Strachan, P. A. Gowland, S. A. Shakespeare, D. K. James, I. R. Johnson, and P. N. Baker. 2000. 'Effect of fetal magnetic resonance imaging on fetal heart rate patterns', *Am J Obstet Gynecol*, 182: 666-9.

Veerbeek, J. H., L. Brouwers, M. P. Koster, S. V. Koenen, E. O. van Vliet, P. G. Nikkels, A. Franx, and B. B. van Rijn. 2016. 'Spiral artery remodeling and maternal cardiovascular risk: the spiral artery remodeling (SPAR) study', *J Hypertens*, 34: 1570-7.

Viglietto, G., D. Maglione, M. Rambaldi, J. Cerutti, A. Romano, F. Trapasso, M. Fedele, P. Ippolito, G. Chiappetta, G. Botti, and et al. 1995. 'Upregulation of vascular endothelial growth factor (VEGF) and downregulation of placenta growth factor (PlGF) associated with malignancy in human thyroid tumors and cell lines', *Oncogene*, 11: 1569-79.

Villar, J., L. Cheikh Ismail, C. G. Victora, E. O. Ohuma, E. Bertino, D. G. Altman, A. Lambert, A. T. Papageorghiou, M. Carvalho, Y. A. Jaffer, M. G. Gravett, M. Purwar, I. O. Frederick, A. J. Noble, R. Pang, F. C. Barros, C. Chumlea, Z. A. Bhutta, and S. H. Kennedy. 2014. 'International standards for newborn weight, length, and head circumference by gestational age and sex: the Newborn Cross-Sectional Study of the INTERGROWTH-21st Project', *Lancet*, 384: 857-68.

Voros, G., E. Maquoi, D. Demeulemeester, N. Clerx, D. Collen, and H. R. Lijnen. 2005. 'Modulation of angiogenesis during adipose tissue development in murine models of obesity', *Endocrinology*, 146: 4545-54.

Wang, G., M. A. Zuluaga, W. Li, R. Pratt, P. A. Patel, M. Aertsen, T. Doel, A. L. David, J. Deprest, S. Ourselin, and T. Vercauteren. 2019. 'DeepIGeoS: A Deep Interactive Geodesic Framework for Medical Image Segmentation', *IEEE Trans Pattern Anal Mach Intell*, 41: 1559-72.

Wang, G., M. A. Zuluaga, R. Pratt, M. Aertsen, T. Doel, M. Klusmann, A. L. David, J. Deprest, T. Vercauteren, and S. Ourselin. 2016. 'Slic-Seg: A minimally interactive segmentation of the placenta from sparse and motion-corrupted fetal MRI in multiple views', *Med Image Anal*, 34: 137-47.

Wikström, A. K., A. Larsson, U. J. Eriksson, P. Nash, S. Nordén-Lindeberg, and M. Olovsson. 2007. 'Placental growth factor and soluble FMS-like tyrosine kinase-1 in early-onset and late-onset preeclampsia', *Obstet Gynecol*, 109: 1368-74.

Wiles, K., K. Bramham, P. T. Seed, L. O. Kurlak, H. D. Mistry, C. Nelson-Piercy, L. Lightstone, and L. C. Chappell. 2019. 'Diagnostic Indicators of Superimposed Preeclampsia in Women With CKD', *Kidney Int Rep*, 4: 842-53.

Wiskirchen, J., E. F. Groenewaeller, R. Kehlbach, F. Heinzelmann, M. Wittau, H. P. Rodemann, C. D. Claussen, and S. H. Duda. 1999. 'Long-term effects of repetitive exposure to a static magnetic field (1.5 T) on proliferation of human fetal lung fibroblasts', *Magn Reson Med*, 41: 464-8.

World Health Organisation, . 2011. *WHO recommendations for prevention and treatment of pre-eclampsia and eclampsia*.

Wright, C., D. M. Morris, P. N. Baker, I. P. Crocker, P. A. Gowland, G. J. Parker, and C. P. Sibley. 2011. 'Magnetic resonance imaging relaxation time measurements of the placenta at 1.5 T', *Placenta*, 32: 1010-5.

Wright, E., and P. Royston. 1996. 'Age-specific reference intervals (‘normal ranges’)', *Stata Technical Bulletin*: 24-34.

Yang, W., H. Ahn, M. Hinrichs, R. J. Torry, and D. S. Torry. 2003. 'Evidence of a novel isoform of placenta growth factor (PlGF-4) expressed in human trophoblast and endothelial cells', *J Reprod Immunol*, 60: 53-60.

Yip, Y. P., C. Capriotti, S. L. Talagala, and J. W. Yip. 1994. 'Effects of MR exposure at 1.5 T on early embryonic development of the chick', *J Magn Reson Imaging*, 4: 742-8.

Zeisler, H., E. Llurba, F. Chantraine, M. Vatish, A. C. Staff, M. Sennström, M. Olovsson, S. P. Brennecke, H. Stepan, D. Allegranza, P. Dilba, M. Schoedl, M. Hund, and S. Verlohren. 2016. 'Predictive Value of the sFlt-1:PlGF Ratio in Women with Suspected Preeclampsia', *N Engl J Med*, 374: 13-22.

Zetterström, K., S. N. Lindeberg, B. Haglund, and U. Hanson. 2008. 'The association of maternal chronic hypertension with perinatal death in male and female offspring: a record linkage study of 866,188 women', *Bjog*, 115: 1436-42.

Zun, Z., G. Zaharchuk, N. N. Andescavage, M. T. Donofrio, and C. Limperopoulos. 2017. 'Non-Invasive Placental Perfusion Imaging in Pregnancies Complicated by Fetal Heart Disease Using Velocity-Selective Arterial Spin Labeled MRI', *Sci Rep*, 7: 16126.

Appendix

Placenta 104 (2021) 138–145

Contents lists available at ScienceDirect

Placenta

journal homepage: http://www.elsevier.com/locate/placenta

Placental magnetic resonance imaging in chronic hypertension: A case-control study

Alison Ho [a,*], Jana Hutter [b,c], Paddy Slator [d], Laurence Jackson [b,c], Paul T. Seed [a], Laura Mccabe [b], Mudher Al-Adnani [e], Andreas Marnerides [e], Simi George [e], Lisa Story [a], Joseph V. Hajnal [b,c], Mary Rutherford [b,1], Lucy C. Chappell [a,1]

[a] Department of Women and Children's Health, School of Life Course Sciences, King's College London, London, United Kingdom
[b] Centre for the Developing Brain, King's College London, London, United Kingdom
[c] Biomedical Engineering Department, King's College London, London, United Kingdom
[d] Centre for Medical Image Computing and Department of Computer Science, University College London, London, United Kingdom
[e] Department of Cellular Pathology, Guy's and St Thomas' Hospital, London, United Kingdom

ARTICLE INFO

Keywords:
Chronic hypertension
Placenta
Magnetic resonance imaging (MRI)

ABSTRACT

Introduction: We aimed to explore the use of magnetic resonance imaging (MRI) *in vivo* as a tool to elucidate the placental phenotype in women with chronic hypertension.
Methods: In case-control study, women with chronic hypertension and those with uncomplicated pregnancies were imaged using either a 3T Achieva or 1.5T Ingenia scanner. T2-weighted images, diffusion weighted and T1/T2* relaxometry data was acquired. Placental T2*, T1 and apparent diffusion coefficient (ADC) maps were calculated.
Results: 129 women (43 with chronic hypertension and 86 uncomplicated pregnancies) were imaged at a median of 27.7 weeks' gestation (interquartile range (IQR) 23.9–32.1) and 28.9 (IQR 26.1–32.9) respectively. Visual analysis of T2-weighted imaging demonstrated placentae to be either appropriate for gestation or to have advanced lobulation in women with chronic hypertension, resulting in a greater range of placental mean T2* values for a given gestation, compared to gestation-matched controls. Both skew and kurtosis (derived from histograms of T2* values across the whole placenta) increased with advancing gestational age at imaging in healthy pregnancies; women with chronic hypertension had values overlapping those in the control group range. Upon visual assessment, the mean ADC declined in the third trimester, with a corresponding decline in placental mean T2* values and showed an overlap of values between women with chronic hypertension and the control group.
Discussion: A combined placental MR examination including T2 weighted imaging, T2*, T1 mapping and diffusion imaging demonstrates varying placental phenotypes in a cohort of women with chronic hypertension, showing overlap with the control group.

1. Introduction

Chronic hypertension complicates an estimated 3–5% of all pregnancies [1] with a rising incidence associated with a global increase in obesity and maternal age. Adverse pregnancy outcomes associated with chronic hypertension include superimposed preeclampsia, preterm delivery, low birthweight, perinatal death and an increased incidence of neonatal admission and caesarean delivery [2], occurring independent of the development of superimposed preeclampsia [3].

Altered placental structure and function may contribute to the pathophysiology of adverse pregnancy outcomes. Histological examination of placentae have demonstrated lesions related to maternal vascular malperfusion to be more prevalent in women with chronic hypertension and preeclampsia compared to those without hypertensive

* Corresponding author. Department of Women and Children's Health, School of Life Course Sciences, King's College London, 10th Floor, North Wing, St Thomas' Hospital, Westminster Bridge Road, Lambeth, London, SE1 7EH.
E-mail address: alison.ho@kcl.ac.uk (A. Ho).
[1] joint senior authors.

https://doi.org/10.1016/j.placenta.2020.12.006
Received 20 July 2020; Received in revised form 28 November 2020; Accepted 9 December 2020
Available online 13 December 2020

disorders of pregnancy [4,5]. In pregnancies complicated by pre-eclampsia, altered early placental perfusion is hypothesised to lead to placental oxidative stress with cellular damage of fragile villous trees and inflammation. Subsequent ischaemia-reperfusion injury alters the balance of placentally expressed antiangiogenic and angiogenic compounds which can be detected in the maternal circulation [6]. The clinical manifestation of disease is considered to relate to the interaction between the release of placentally-derived factors and subsequent maternal responses, exacerbated by pre-existing comorbidities characterised by maternal vascular endothelial dysfunction (such as chronic hypertension or renal disease) [7].

The use of magnetic resonance imaging as a tool to provide *in vivo* assessment of the placenta structure and function is of growing interest. Imaging sequences can be acquired within a clinically acceptable time of 15 min to acquire comprehensive assessment including T2* mapping and diffusion MRI [8]. Resultant measures of interest include the T2* relaxation time (an indicative measure of tissue oxygenation), T1 relaxation (related to oxygen tension) and measures of diffusion (assessing the microstructural properties through the random thermal microscopic translational motion of molecules). Reduced placental T2* [9], mean diffusivity values [10] and reduced mean T1 relaxation times [10] are reported in pregnancies complicated by fetal growth restriction and thus provide a promising indicator of placental dysfunction.

To our knowledge, no studies have assessed the use of magnetic resonance imaging to aid understanding of the heterogeneity of pregnancy outcomes in women with chronic hypertension. The aim of this study was to explore the use of magnetic resonance imaging as a tool to elucidate the placental phenotype in women with chronic hypertension.

2. Materials and methods

2.1. Study design

This case-control study was undertaken at St Thomas' Hospital, London, a tertiary level maternity unit. Women with chronic hypertension attending a consultant led specialist antenatal hypertension clinic were approached in person. Women in the control group were recruited at their routine 20-week anomaly scan or self-referred to take part in the study. All women in the study (both the hypertensive and control group) gave written informed consent for this specific project (Placenta Imaging Project, IRAS 201609). This study was part of a larger body of work (Placenta Imaging Project, IRAS 201609) that aimed to optimise and develop novel magnetic resonance imaging protocols for placental assessment. Standard core protocols of imaging in our unit were adhered to that included patient positioning, monitoring during imaging, imaging time and anatomical T2-weighted imaging of the fetal brain in three orthogonal planes to the woman, suitable for volume reconstruction and clinical reporting [22].

Women were considered for inclusion in the study if they had a singleton pregnancy, were over 16 years of age, not claustrophobic and had no contraindication for magnetic resonance imaging. Chronic hypertension and preeclampsia were prospectively defined using the international consensus definition [11]. Clinical management of hypertensive women were according to national guidelines, with responsibility under the attending obstetrician. Follow up was until delivery, with the last woman enrolled delivering in August 2019. Prospective specified data collection included baseline demographic characteristics, maternal and neonatal outcomes.

Women in the chronic hypertension and the control group were prospectively recruited, all of whom were enrolled in a larger body of work (Placenta Imaging Project, IRAS 201609, REC16/LO/1573), that aimed to optimise and develop novel magnetic resonance imaging protocols for placental assessment. Women in the control group fulfilled the following prespecified criteria based on pregnancy outcome: no diagnosis of hypertensive disorder at enrolment and until delivery, no significant past medical history, no pregnancy complications (including gestational diabetes), delivery at term with birthweight between the 3rd and 97th centile (calculated using INTERGROWTH-21st, version 1.3.5) [12] thus excluding potential confounders of placental change [13–16]. The definition was prospectively defined as including women with term delivery only, as preterm delivery is typically considered pathological, whether occurring spontaneously or for iatrogenic reasons. In order to enable meaningful comparisons to be made, women in the control group were identified as meeting these criteria after delivery and subsequently gestation-matched (within a two week gestation range) to women with chronic hypertension, masked to values derived from magnetic resonance imaging, on a 2:1 basis.

No formal sample size was calculated for power of outcome variables as this was an exploratory study describing a novel technique in technology development application. This study was approved by Fulham Research Ethics Committee, REC 16/LO/1573.

2.2. Magnetic resonance imaging

Magnetic resonance imaging was performed on either a clinical Philips 3T Achieva (60 cm bore) or a Philips 1.5T Ingenia (with a wider 70 cm bore). Parameters were kept constant between women with chronic hypertension and the control group. Women underwent magnetic resonance imaging on up to two occasions, a minimum of two weeks apart and at any time point between their clinically routine anomaly ultrasound scan (at around 18–22 weeks' gestation) and delivery. Imaging was performed supine with padding to support the lower limbs and shoulders, after an initial period of 3 min in left lateral to shift the uterus and minimise potential effects of venocaval compression. Total imaging time did not exceed 1 h, and women were offered a break of up to 30 min halfway through the scan. Maternal assessments during imaging included continuous maternal heart rate and oxygen saturation monitoring with additional blood pressure measurements every 10 min. An obstetrician or midwife was present throughout the scan. No pharmacological sedation was used.

Image based shimming was achieved using an in-house tool, based on a separately acquired B0 map, in order to reduce the effect of inhomogeneities in the magnetic field. To provide anatomical images of the fetus and placenta and their position within the uterus, a T2-weighted single shot turbo spin echo sequence with an echo time (TE) of 180 ms of the whole uterus (thereby including placenta) was acquired in coronal and sagittal planes to the mother with repetition time (TR) = 16s, SENSitivity Encoding (SENSE) = 2.5 and partial Fourier 0.625. In-plane resolution was 1.5 mm × 1.5 mm, slice thickness 2.5 mm with an overlap of 0.5 mm. The field of view was 300 × 360 x [100−200] mm (coronal) and 300 × 300 × 340 mm (sagittal) in the foot-head (FH) x right-left (RL) x anterior-posterior (AP) directions respectively.

T2* weighted imaging was acquired using a multi-echo gradient echo, echo planar imaging sequence with free breathing and took less than 1 min. For 3T scanning, 5 echo times were used: 13.81 ms/70.40 ms/127.00 ms/183.60 ms/240.2 ms, TR = 3s, SENSE = 3, halfscan = 0.6 at 3mm3 resolution with the whole placenta covered within 60 slices. For 1.5T scanning, 5 echo times were used: 11.376 ms/57.313 ms/103.249 ms/149.186 ms/195.122 ms, TR = 14s, no SENSE, no halfscan at 2.5mm3 resolution with the whole placenta covered within 90 slices. Echo times result from the chosen Echo Planar Imaging (EPI) train characteristics. The intra-echo spacing was chosen to minimise acoustic noise and the inter-echo spacing as the minimal possible spacing given chosen resolution and field of view. Data was acquired in the maternal coronal plane.

Given the methods development required during the course of this study, a diffusion prepared spin echo with subsequent gradient echoes was performed in a subset of 31 women, imaged at only 3 T, for combined diffusion-relaxometry [17]. In another subset of women, a modified inversion-recovery sequence with a global adiabatic inversion pulse and slice shuffling [17,18] was also employed with 10 inversion times to produce T1 maps.

An in-house Python script was used to produce T2*, T1 and apparent diffusion coefficient maps by fitting monoexponentially decay curves. The diffusion data were motion corrected using Advanced Normalization Tools, ANTS, a nonrigid template registration [19]. The placenta images were manually segmented by two experienced observers (AH and JH). Further processing steps calculated mean apparent diffusion coefficient values, placental T2*, and kurtosis and skew of T2* histograms, and calculation of mean T1. The acquisition and processing pipeline has been described previously and shown to have good reproducibility with a high Dice coefficient (0.86) between observers who segmented the placenta [20,21].

As part of this study, anatomical T2-weighted imaging of the fetal brain was performed in three orthogonal planes to the woman suitable for volume reconstruction and clinical reporting [22]. ~~Fetal brain images were reported and available to the clinical team.~~ Visual analysis of the placenta was performed and included assessment of signal intensity across the placenta and documentation of the appearance of placental lobules and septa. The signal intensity within lobules was visually assessed for granularity with high granularity defined as the presence of both high and low signal intensity within individual lobules.

Maternal venepuncture was performed as close to magnetic resonance imaging as feasible, usually on the same day. Six millilitres of blood were drawn into a bottle containing ethylenediamine tetra-acetic acid, transported to the laboratory within 1 h and underwent centrifugation at 1400×*g* (rcf) for 10 min at 4 °C. PlGF was quantified using the Triage PlGF Test (Alere, San Diego, CA) according to the manufacturer's instructions while masked to both cohort and clinical outcome. The clinical team did not receive the result.

2.3. Ultrasound

Ultrasound scans were performed on the same day as magnetic resonance imaging wherever possible, or within two weeks. Women with pre-eclampsia had a clinically indicated ultrasound scan performed in line with national guidelines for management of pre-eclampsia [23]. In the control group, ultrasound scans were performed on a Philips EPIQ V7 by sonographers following a clinical protocol. Fetal measurements included biparietal diameter, head circumference, femur length and abdominal circumference which were used to derive an estimated fetal weight using the Hadlock formula [24], umbilical artery Doppler pulsatility index (PI), amniotic fluid index and maternal uterine artery pulsatility index. The presence of fetal growth restriction was established by ultrasonographic assessment using accepted international definitions [25].

2.4. Placental histology

Following delivery and where available, placentas from women in both groups (chronic hypertension and healthy pregnancies) underwent histological examination according to local protocols at the Cellular Pathology Department, St Thomas' Hospital. Placentas were fixed in 10% buffered formalin and trimmed of both umbilical cord and membranes for placenta weight. The following areas were sampled and then embedded in paraffin: two transverse sections of the umbilical cord, one roll of membranes (including rupture site), two to three full thickness blocks of the placental parenchyma away from the placental edge (including fetal and maternal surfaces). Additional areas were sampled depending on macroscopic findings. Paraffin embedded tissue sections were then cut into four-micron sections, deparaffinized and stained with haemotoxylin and eosin prior to histological examination. A clinical report for all placentas submitted was issued, in accordance with local hospital reporting guidelines. Histological slides were then re-examined by a second experienced histopathologist (masked to first report and to clinical details aside from gestational age at delivery) specifically for features of maternal vascular malperfusion, fetal vascular malperfusion and acute chorioamnionitis; classified using guidelines from the International Placental Pathology Consensus Meeting, Amsterdam 2014 [26]. Any discrepancies between the two reporting histopathologists were re-examined (again masked to the pregnancy outcome) and a consensus opinion was reached.

2.5. Statistical methods

In uncomplicated pregnancies, gestation-adjusted reference ranges for placental mean T2* were established using the Stata command xriml, and the 10%–90% reference range established. Birthweight centiles were calculated using INTERGROWTH-21st version 1.3.5 [12]. Statistical analysis was performed using Stata version 15.1 (StataCorp, College Station, Texas). Results were visually assessed between groups after plotting imaging derived measures against gestational age at imaging. A two sample *t*-test was used to compare placental mean T2* values (z scores) between women with chronic hypertension and controls. The imaging derived values of skewness and kurtosis were transformed (a constant added and the value subsequently logged) ensuring that the skewness of the data remained the same in order to compare groups by geometric mean ratio with adjustment for gestation.

3. Results

129 women underwent placental imaging: 43 women with chronic hypertension were gestation matched to 86 controls (Table 1, Supplemental Table S1, Supplemental Fig. S1). Of these, 30 women with chronic hypertension and 70 controls were imaged on the 3T Achieva, while 13 women with chronic hypertension and 16 controls were imaged on the 1.5T Ingenia. Maternal PlGF concentrations around time of imaging were lower in women with chronic hypertension (186 pg/mL, IQR 109–321) than the control group (341 pg/mL, IQR 230–656)

Table 1
Characteristics at booking and enrolment.

	Chronic hypertensive pregnancies	Control pregnancies
Number of women	43	86
At booking		
Maternal age, y, median (IQR)	37 (34–41)	34 (32–37)
Body mass index, kg/m^2, median (IQR)	26 (24–30)	23 (21–25)
Nulliparous	15 (35)	45 (52)
White ethnicity	25 (58)	75 (87)
Black ethnicity	8 (19)	4 (5)
Other ethnicity	10 (23)	7 (8)
Current smoking	0	1 (1)
Quit smoking before pregnancy	1 (2)	4 (5)
Never smoked	37 (86)	73 (8)
Previous pre-eclampsia	7 (16)	1 (1)
Chronic renal disease	6 (14)	0
Gestational diabetes	2 (5)	0
At enrolment on day of MRI		
Gestational age, wk, median (IQR)	27.7 (23.9–32.1)	28.9 (26.1–32.9)
Aspirin	38 (88)	7 (8)
Ultrasound estimated fetal weight, centile, median (IQR)	48 (27–70)	54 (42–68)
Placental Growth Factor, pg/mL, median (IQR)	187 (109–321)	341 (230–656)
Placental growth factor <100 pg/mL	6 (14)	6 (7)
Placental growth factor <12 pg/mL	1 (2)	0
Systolic blood pressure, mmHg, median (IQR)	125 (115–133)	108 (102–114)
Diastolic blood pressure, mmHg, median (IQR)	79 (71–83)	63 (57–74)
During MRI		
Systolic blood pressure, mmHg, median of individual medians (IQR)	112 (108–115)	99 (95–105)
Diastolic blood pressure, mmHg, median of individual medians (IQR)	69 (63–74)	59 (55–64)

Values given as a number (percentage) unless stated otherwise.

(Table 1).

Four out of 43 women (9%) with chronic hypertension developed superimposed preeclampsia (Table 2, Supplemental Table S2). Nine (21%) of women with chronic hypertension delivered prematurely compared with no preterm deliveries in the control group (Table 2, Supplemental Table S2). 38 (88%) of women with chronic hypertension had a planned delivery (pre-labour caesarean section or induction of labour) compared to 32 (37%) in the control group (Table 2, Supplemental Table S2).

68 placentas were examined after delivery (24 from women with chronic hypertension, 44 from controls) (Table 2). Five out of six placentae with maternal vascular malperfusion features on histological examination were from women with chronic hypertension (Table 2). Out of the six cases that had maternal vascular malperfusion features on histology, three had low mean T2* values and one had high skewness and kurtosis values when compared to the control group. Median interval from imaging to delivery in cases of maternal vascular malperfusion was 40 days (interquartile range 26–79).

3.1. Magnetic resonance imaging analysis

Visual analysis of placental images demonstrated that in women with chronic hypertension, appearances were more varied compared to gestation-matched controls (Fig. 1). Placental images from women with chronic hypertension appeared either appropriate for gestation or advanced for gestation showing with increased lobulation, with wider septa and more marked heterogeneity than expected for age. This was also apparent when visually assessing the T2* maps. Reflecting this visual analysis, women with chronic hypertension showed a greater range of placental mean T2* values for a given gestation compared to the control group (Fig. 2, Supplemental Fig. S2). Women with chronic hypertension had lower placental mean T2* values compared to controls (gestation adjusted z score mean = −0.830, standard deviation 1.3), that was substantially different (two sample *t*-test, t = 3.11, p = 0.0031).

Exemplar histograms of T2* values at 27 weeks' gestation in four different women (Fig. 3) visually illustrate further analysis of T2* histograms assessing both kurtosis and skewness. This further analysis demonstrated differences in the placenta from those chronic hypertension pregnancies with apparently normal mean T2* placental values. For example, when compared to a T2* placental histogram from a control pregnancy (Fig. 3A) a lower kurtosis value in the placental signal intensity frequency distribution in a pregnancy with chronic hypertension is demonstrated, despite a mean T2* appropriate for gestational age (Fig. 3B). A lower mean T2* value corresponds to a left shift in the histogram (for example, in a woman with chronic hypertension (Fig. 3C). A left shift and higher skewness value (asymmetrical frequency distribution) is seen in a woman with preeclampsia superimposed on chronic hypertension (Fig. 3D). Both skewness and kurtosis increased with advancing gestational age at imaging (Fig. 4); visual inspection showed that some women with chronic hypertension who developed superimposed pre-eclampsia had higher skewness and kurtosis values, compared to the remaining group with chronic hypertension, the majority of whom had values within the range of the control group. The women who developed superimposed preeclampsia on a background of chronic hypertension with skewness and kurtosis values within the range of the control group, delivered at term and of normal birthweight centile. For the presentation of results of skewness and kurtosis values, we have included an additional dataset of women with preeclampsia imaged at 3T in whom we have previously reported enrolment and pregnancy outcome characteristics [27]. The new histogram derived measures of skewness and kurtosis in this group of women with preeclampsia have not previously been reported. Enrolment and pregnancy outcomes of preeclampsia pregnancies imaged at 1.5T are provided in Supplemental Table S1 and Supplemental Table S2. When comparing between groups, there was no significant difference in skewness and kurtosis values between the chronic hypertension and control group (geometric mean ratio for skewness values = 0.82, 95% CI 0.67–1.01, geometric mean ratio for kurtosis values = 0.83, 95% CI 0.58–1.19). In contrast, women with preeclampsia had higher skewness and kurtosis values compared to controls (geometric mean ratio for skewness values = 3.15, 95% CI 2.39–4.15, geometric mean ratio for kurtosis values = 7.55, 95% CI 4.53–12.58). Actual placental mean T2*, skewness and kurtosis values are provided in Supplemental Table S3.

In our subsample, placental apparent diffusion coefficient (ADC) appeared to decline with advancing gestational age (Supplemental Fig. S3A). There was a positive correlation between ADC values and placental mean T2* values (Supplemental Fig. S3B). Placental mean T1 also declined with advancing gestational age (Supplemental Fig. S3C) and positively correlated with mean ADC values (Supplemental Fig. S3D). Trends in mean ADC values were consistent with data acquired during the methods development required during the course of this study (Supplemental Fig. S4).

Table 2
Maternal and neonatal outcomes.

	Chronic hypertensive pregnancies	Control pregnancies
Number of women	43	86
Time from MRI to delivery, days, median (IQR)	70 (37–96)	84 (53–99)
Pre-eclampsia	4 (9)	0
Onset of delivery		
Spontaneous	5 (12)	55 (64)
Induction	19 (44)	20 (23)
Pre labour caesarean	19 (44)	12 (14)
Mode of delivery		
Spontaneous vaginal delivery	9 (21)	47 (55)
Assisted vaginal delivery	4 (9)	18 (21)
Elective pre-labour caesarean section	10 (23)	10 (12)
Urgent caesarean section	20 (47)	11 (13)
Primary reason for induction or prelabour caesarean*		
Maternal indication	30 (74)	15 (17)
Fetal indication	8 (19)	16 (19)
Delivery		
Livebirth	43 (100)	86 (100)
Gestational age at delivery, weeks, median, IQR	38.3 (37.5–38.9)	40 (39–41)
Preterm birth <37/40	9 (21)	0
Birthweight, g, median (IQR)	2965 (2520–3362)	3482 (3229–3721)
Birthweight centile, centile, median (IQR)	37 (16–70)	68 (32–83)
Number admitted to neonatal unit for ≥ 48 h	4 (9)	1 (1)
Prematurity	2 (5)	0
Fetal growth restriction/small for gestational age	0	0
Respiratory disease	0	1 (1)
Suspected sepsis	0	0
Hypoglycaemia	2 (5)	0
Placental histology findings		
Number of placentae assessed	24	44
Placental weight, g, median (IQR)	384 (310–467)	474 (409–556)
Fetal-placental birthweight ratio, median (IQR)	7.2 (6.0–7.9)	7.3 (6.7–7.9)
Maternal vascular malperfusion features	5 (21)	1 (2)
Fetal vascular malperfusion features	1 (4)	0
Chorioamnionitis features	6 (25)	25 (57)

Values given as a number (percentage) unless stated otherwise. *Full details given in Supplementary Table 1.

4. Discussion

This case-control study has used magnetic resonance imaging at both 1.5 and 3 T to acquire T2, T2*, T1 and diffusion weighted imaging of the placenta in a group of women with chronic hypertension and shown a

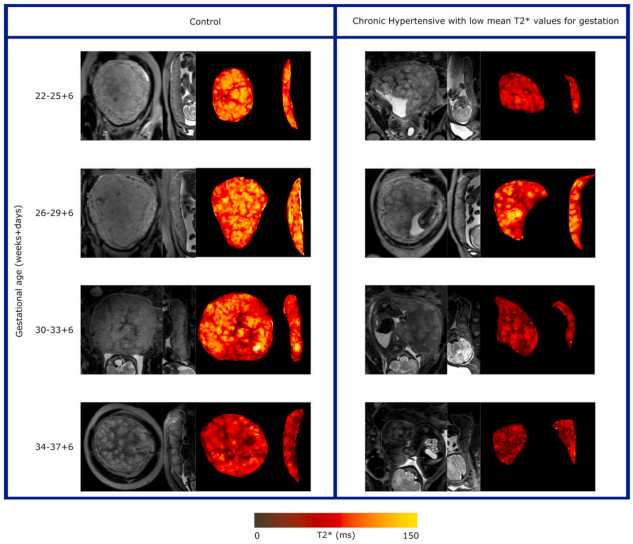

Fig. 1. Example T2 weighted imaging and T2* maps in coronal and sagittal planes across gestation. On the left, the control panel depicts the following from left to right: T2-weighted imaging in the coronal plane, T2-weighted imaging in the sagittal plane, T2* map in the coronal plane and T2* map in sagittal plane. On the right, the panel depicts images from women with chronic hypertension and a placental mean T2* value below the 10th centile. Within the panel from left to right, images are in the following order: T2-weighted imaging in the coronal plane, T2 weighted imaging in the sagittal plane, T2* map in the coronal plane and T2* map in sagittal plane. Within the T2* maps, darker areas represent low T2* values while brighter orange-yellow areas high T2* values.

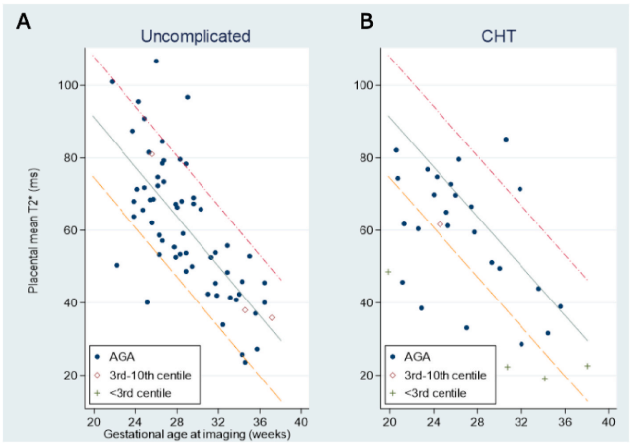

Fig. 2. Scatterplot of placental mean T2* at 3 T against gestational age at imaging, subdivided by birthweight centile at subsequent delivery to show Appropriate for Gestational Age (AGA) infants, and those Small for Gestational Age, divided into 3rd-10th centile, and those <3rd centile (A) in uncomplicated control group and (B) in women with chronic hypertension.

varied visual appearance on images in women with chronic hypertension when compared to controls. T2* values showed expected decrease with gestation in the control group (consistent with previously reported values in the literature (Sorenson et al., 2019) but a more variable spread of values in chronic hypertension. T2* histogram derived measures of kurtosis and skewness showed an increase in values with advancing gestation and the majority of women with chronic hypertension had values within the range of the control group. We found no direct correlation between placental histology findings and imaging derived measures. However, these results may be a feature of the time interval between imaging and delivery.

A strength of this study is that we have quantitively measured the described visual variation in placental appearance using mean T2* and further probed the characteristics of T2* values across the whole

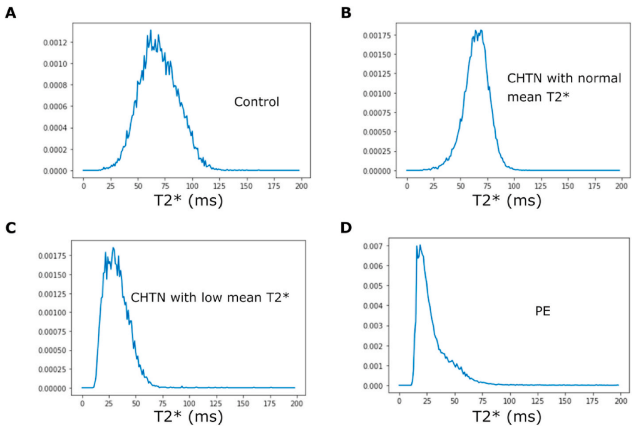

Fig. 3. Illustrative histogram plot of T2* values at the same gestation (27 weeks' gestation) for one woman from each of the following groups (A) the control group (B) with chronic hypertension (CHTN) and normal placental mean T2* (C) with chronic hypertension and a placental mean T2* less than the 10th centile for gestation (D) CHTN participant who developed superimposed preeclampsia (PE).

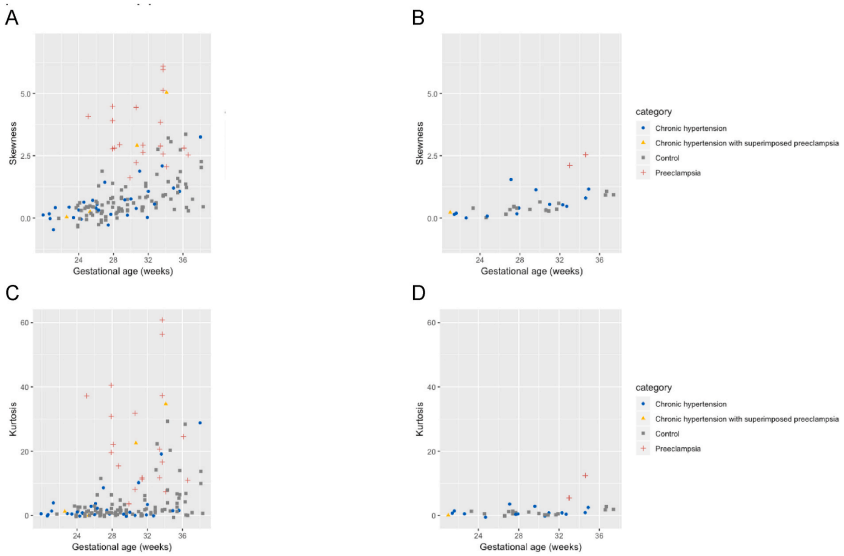

Fig. 4. Scatterplot of histogram derived measures of (A) skewness at 3T imaging, (B) skewness at 1.5T imaging, (C) kurtosis at 3T imaging and (D) kurtosis at 1.5T imaging against gestational age at scan with i) chronic hypertension ii) chronic hypertension at enrolment who subsequently developed superimposed preeclampsia after imaging iii) controls iv) preeclampsia at enrolment. For the presentation of results, we have included an additional dataset of women with preeclampsia imaged at 3T in whom we have previously reported enrolment and pregnancy outcome characteristics [27] and women with preeclampsia imaged at 1.5T in whom enrolment and pregnancy outcome characteristics are provided in Supplemental Tables S1 and S2.

placenta using histogram derived measures of kurtosis and skewness and Apparent Diffusion Coefficient. These histogram derived measures are independent of magnetic field strength and therefore enable comparisons between groups regardless of the strength of MR scanner used to acquire data. Imaging in women with chronic hypertension has not (to our knowledge) been previously published. The extent of the

diverse phenotype seen was therefore uncertain prior to conducting the study.

To further investigate both normal and abnormal placental phenotypes we have used in-house optimised sequences combining diffusion-relaxometry which provides regionally matched diffusion and T2* values in a reasonably fast scan time compared to conventional sequences. In the integrated approach, the imaging sequence contains a spin-echo with subsequent gradient echoes. Given T2* values vary with gestation and pregnancy complications, a sequence which can disentangle the molecular motion secondary to T2* values and intrinsic diffusion properties of the placenta is of great benefit when elucidating the underlying mechanisms of placental dysfunction. Secondly, motion correction was achieved post image acquisition. Given diffusion measures the thermal microscopic translational motion of water molecules, any measures which can minimise the effect of macroscopic motion are beneficial. Motion correction was successfully performed on all women in whom the combined diffusion-relaxometry sequence was deployed.

The heterogeneity amongst the chronic hypertensive group with regards to enrolment characteristics and pregnancy outcome reflect the clinical context in which these women are managed. This study was inclusive in order to lay the foundation for assessment as a potential tool in a clinical setting. The use of scanners at two magnetic field strengths (1.5 T and 3 T) further increases clinical applicability given their use in different hospital centres and the wider bore of our 1.5 T scanner enabled women of a greater abdominal girth and body mass index to be imaged. The addition of combined diffusion relaxometry examination protocols in women enrolled later in the study reflects the imaging methods development required during the course of this study. This study additionally demonstrated that imaging was feasible and acceptable in a large cohort of women across a range of gestations amongst a group which included those with chronic hypertension. Given the wider clinical phenotype of disease in contrast to women with preeclampsia (whereby there is a close interval between imaging and delivery by clinical nature and a clear placental phenotype previously demonstrated by our group (Ho et al., 2020), a clear placental phenotype remains challenging in women with chronic hypertension.

To our knowledge, there are no studies investigating the use of placental magnetic resonance imaging in women with chronic hypertension. Our group have previously described a placental phenotype in women with preterm preeclampsia, where T2-weighted imaging demonstrated advanced lobulation, varied lobule sizes, high granularity and substantial areas of low signal intensity with reduced entire placental mean T2* values for gestational age [27]. Other studies have focussed on the prediction of fetal growth restriction [28] and low mean T2* values have been demonstrated to occur in pregnancies with fetal growth restriction [29]. The use of T2* histogram derived measures of kurtosis and skewness has not been widely described. There is a paucity of literature regarding the use of placental diffusivity measures in hypertensive disorders as studies have mainly focused on pregnancies complicated by fetal growth restriction. Reduced placental ADC values in growth restriction have implicated a phenotype with restricted diffusion [30,31]. Our results showing a decline in ADC values in the third trimester in uncomplicated pregnancies are consistent with two known studies investigating the relationship between ADC values and gestational age [9,32]. However, there is a paucity in the literature for these measures at 3 T. The use of a novel combined diffusion-relaxometry sequence has enabled the addition of T2* to ADC values, examined simultaneously for a more accurate evaluation of placental properties. Furthermore, these novel sequences have been deployed in pregnancies complicated by hypertension; a group not extensively studied before using this technique.

The placental phenotype in women with chronic hypertension has an overlap with women of uncomplicated pregnancies, as demonstrated by mean T2*, kurtosis, skew and ADC values. However, when more parameters were employed subtle differences found between groups e.g. with histogram measures in the presence of same T2* value. This potentially reflects the heterogeneity in pregnancy outcomes amongst women with chronic hypertension. The greater range of placental mean T2* values for a given gestation within this group accompanied by skewness, kurtosis and ADC values within the normal range suggests a more complex interaction between the placenta and maternal response determining the development of adverse pregnancy outcomes such as superimposed preeclampsia. This contrasts with a clearer placental phenotype in women with preterm preeclampsia, previously described by our group [27]. The skewness, kurtosis and mean T2* values within the normal range in women with chronic hypertension who develop superimposed preeclampsia may be due to the long interval between imaging and preeclampsia diagnosis as these women developed preeclampsia at term. We evaluated new measures (skewness and kurtosis) in women with preeclampsia, that had not previously been reported to enable the chronic hypertensive group results to be interpreted in context. In addition, the number of women with chronic hypertension who subsequently developed superimposed preeclampsia were small in our study (four women). Given the limitations of using a case-control study in predicting pregnancy outcomes, we have been cautious in our interpretation; however, anticipate that future prospective studies will further address this.

A reduction in mean T2* and ADC values with advancing gestation in the third trimester perhaps reflects parenchymal changes after initial placental angiogenesis in the first and second trimester, followed by villous maturation, calcium deposition and fibrosis in the third trimester. Decreased T2* and ADC values amongst women with preeclampsia may reflect the histological features seen with hypertensive disorders of pregnancy. These include maternal vascular malperfusion lesions such as increased syncytial knots, villous agglutination, increase intervillous fibrin deposition and villous infarcts.

Given the exploratory nature of the study, describing a novel technique in technology development application, visual assessment of results was carried out. This is (to our knowledge) the first study of magnetic resonance imaging in women with pregnancies complicated by chronic hypertension and therefore anticipate that this study will usefully define further research directions. A larger data set imaging woman with uncomplicated pregnancies would enable robust derivation of normal ranges over gestation for comparison against groups of interest. Future work may focus on deriving gestation adjusted normal ranges for each imaging measure. This would assist in calculating multiple of median (MoM) values in order for group comparisons. Although this is one of the largest magnetic resonance imaging studies in the literature, we have been cautious in direct group comparisons to avoid being potentially misleading. Typically, a minimum of over 200 measurements (Saffer et al., 2013) equally spaced across 20–40 weeks' gestational age are required to robustly derive normal ranges. In addition, women enrolled as control pregnancies would require confirmation of a normal pregnancy outcome and a non-linear trend of imaging derived values with gestational age would further complicate this.

Placental imaging offers a window into the placental contribution and mechanisms potentially accounting for the heterogeneity in pregnancy outcomes of women with chronic hypertension. Future work may focus on evaluating the interaction between the placental dysfunction and the varied maternal response that may elucidate development of the varying adverse pregnancy outcomes. In this study, the interval between imaging and delivery was variable and therefore further large studies would be beneficial in investigating the clinical applicability of magnetic resonance imaging as a potential tool to monitor high risk women and aid clinical management decisions around optimal timing of delivery. Further technological developments may enable certain steps in processing to be automated through machine learning algorithms and increase opportunities for implementation in clinical practice.

Contributors

AH, JH, JVH, MR and LCC were involved in study conception,

design, data acquisition and analysis. PS and PTS were involved in data analysis. LJ, LM, MA, AM, SG and LS contributed to data acquisition. All co-authors made substantial contribution to data interpretation, manuscript drafting, revision and have all approved the final version.

Sources of funding

This work is funded by the NIH Human Placenta Project grant 1U01HD087202-01, the National Institute for Health Research (NIHR) Research Professorship (Chappell; RP-2014-05-019), Tommy's (Registered charity no. 1060508) and Holbeck Charitable Trust with support from the Wellcome EPSRC Centre for Medical Engineering at Kings College London (WT 203148/Z/16/Z) and by the National Institute for Health Research Biomedical Research Centre based at Guy's and St Thomas' NHS Foundation Trust and King's College London. PTS is partly funded by King's Health Partners Institute of Women and Children's Health, Tommy's (Registered charity no. 1060508) and by ARC South London (NIHR). JH is funded by the Wellcome Trust through a Sir Henry Wellcome Fellowship (201,374).

Declaration of competing interest

The views expressed are those of the authors and not necessarily those of the UK National Health Service, the National Institute for Health Research, or the Department of Health and Social Care.

Acknowledgements

We thank all the women who participated in the study, their midwives and obstetricians involved in study recruitment. We thank Alexia Egloff for clinical reporting and the research radiographers.

Appendix A. Supplementary data

Supplementary data to this article can be found online at https://doi.org/10.1016/j.placenta.2020.12.006.

References

[1] E.W. Seely, J. Ecker, Circulation 129 (2014) 1254–1261.
[2] K. Bramham, B. Parnell, C. Nelson-Piercy, P.T. Seed, L. Poston, L.C. Chappell, BMJ 348 (2014) g2301–g2301.
[3] B.M. Sibai, M. Lindheimer, J. Hauth, S. Caritis, P. VanDorsten, M. Klebanoff, C. MacPherson, M. Landon, M. Miodovnik, R. Paul, N. Engl. J. Med. 339 (1998) 667–671.
[4] M. Kovo, J. Bar, L. Schreiber, M. Shargorodsky, The relationship between hypertensive disorders in pregnancy and placental maternal and fetal vascular circulation, J. Am. Soc. Hypertens. 11 (2017), 724-29.
[5] B. Bustamante Helfrich, N. Chilukuri, H. He, S.R. Cerda, X. Hong, G. Wang, C. Pearson, I. Burd, X. Wang, Placenta 52 (2017) 106–113.
[6] R.J. Levine, K.-H. Lim, E.F. Schisterman, B.P. Sachs, B.M. Sibai, S.A. Karumanchi, N. Engl. J. Med. (2004) 12.
[7] C.W.G. Redman, I.L. Sargent, Am. J. Reprod. Immunol. 63 (2010) 534–543.
[8] P.J. Slator, J. Hutter, M. Palombo, L.H. Jackson, A. Ho, E. Panagiotaki, L. C. Chappell, M.A. Rutherford, J.V. Hajnal, D.C. Alexander, Magn. Reson. Med. (2019) 27733, mrm.
[9] N. Siauve, P.H. Hayot, B. Deloison, G.E. Chalouhi, M. Alison, D. Balvay, L. Bussières, O. Clément, L.J. Salomon, J. Matern.-Fetal Neonatal Med. Off. J. Eur. Assoc. Perinat. Med. Fed. Asia Ocean. Perinat. Soc. Int. Soc. Perinat. Obstet. 32 (2019) 293–300.
[10] E. Ingram, D. Morris, J. Naish, J. Myers, E. Johnstone, Radiology 285 (2017) 953–960.
[11] M.A. Brown, L.A. Magee, L.C. Kenny, S.A. Karumanchi, F.P. McCarthy, S. Saito, D. R. Hall, C.E. Warren, G. Adoyi, S. Ishaku, International society for the study of hypertension in pregnancy (ISSHP), Pregnancy Hypertens 13 (2018) 291–310.
[12] J. Villar, L.C. Ismail, C.G. Victora, E.O. Ohuma, E. Bertino, D.G. Altman, A. Lambert, A.T. Papageorghiou, M. Carvalho, Y.A. Jaffer, M.G. Gravett, M. Purwar, I.O. Frederick, A.J. Noble, R. Pang, F.C. Barros, C. Chumlea, Z. A. Bhutta, S.H. Kennedy, Lancet 384 (2014) 857–868.
[13] G. Desoye, S. Hauguel-de Mouzon, Diabetes Care 30 (2007) S120–S126.
[14] E. Llurba, O. Sanchez, Q. Ferrer, K.H. Nicolaides, A. Ruiz, C. Dominguez, J. Sanchez-de-Toledo, B. Garcia-Garcia, G. Soro, S. Arevalo, M. Goya, A. Suy, S. Perez-Hoyos, J. Alijotas-Reig, E. Carreras, L. Cabero, Eur. Heart J. 35 (2014) 701–707.
[15] C.M. Salafia, V.K. Minior, J.C. Pezzullo, E.J. Popek, T.S. Rosenkrantz, A. M. Vintzileos, Am. J. Obstet. Gynecol. 173 (1995) 1049–1057.
[16] C.M. Salafia, C.A. Vogel, A.M. Vintzileos, K.F. Bantham, J. Pezzullo, L. Silberman, Am. J. Obstet. Gynecol. 165 (1991) 934–938.
[17] J. Hutter, P.J. Slator, D. Christiaens, R.P.A.G. Teixeira, T. Roberts, L. Jackson, A. N. Price, S. Malik, J.V. Hajnal, Sci. Rep. 8 (2018) 15138.
[18] R.J. Ordidge, P. Gibbs, B. Chapman, M.K. Stehling, P. Mansfield, Magn. Reson. Med. 16 (1990) 238–245.
[19] B.B. Avants, N. Tustison, H. Johnson, (n.d.) 41.
[20] J. Hutter, P.J. Slator, L. Jackson, A.D.S. Gomes, A. Ho, L. Story, J. O'Muircheartaigh, R.P.A.G. Teixeira, L.C. Chappell, D.C. Alexander, M. A. Rutherford, J.V. Hajnal, Magn. Reson. Med. 81 (2019) 1191–1204.
[21] J. Hutter, L. Jackson, A. Ho, M. Pietsch, L. Story, L.C. Chappell, J.V. Hajnal, M. Rutherford, Wellcome Open Res 4 (2019) 166.
[22] Shuzhou Jiang, Hui Xue, A. Glover, M. Rutherford, D. Rueckert, J.V. Hajnal, IEEE Trans. Med. Imag. 26 (2007) 967–980.
[23] National Institute for Clinical Excellence, 2009.
[24] F.P. Hadlock, R.B. Harrist, R.S. Sharman, R.L. Deter, S.K. Park, Am. J. Obstet. Gynecol. 151 (1985) 333–337.
[25] S.J. Gordijn, I.M. Beune, B. Thilaganathan, A. Papageorghiou, A.A. Baschat, P. N. Baker, R.M. Silver, K. Wynia, W. Ganzevoort, Ultrasound obstet, Gynecol 48 (2016) 333–339.
[26] R.W. Redline, Am. J. Obstet. Gynecol. 213 (2015) S21–S28.
[27] A.E.P. Ho, J. Hutter, L.H. Jackson, P.T. Seed, L. McCabe, M. Al-Adnani, A. Marnerides, S. George, L. Story, J.V. Hajnal, M.A. Rutherford, L.C. Chappell, T2* placental magnetic resonance imaging in preterm PPreeclampsia: an observational cohort study, Hypertension 75 (2020), 1523-31.
[28] S.S. Poulsen, M. Sinding, D.N. Hansen, D.A. Peters, J.B. Frøkjær, A. Sørensen, Placenta 78 (2019) 18–22.
[29] M. Sinding, D.A. Peters, J.B. Frøkjær, O.B. Christiansen, A. Petersen, N. Uldbjerg, A. Sørensen, Ultrasound obstet, Gynecol 47 (2016) 748–754.
[30] D. Javor, C. Nasel, T. Schweim, S. Dekan, K. Chalubinski, D. Prayer, Placenta 34 (2013) 676–680.
[31] H.M. Bonel, B. Stolz, L. Diedrichsen, K. Frei, B. Saar, B. Tutschek, L. Raio, D. Surbek, S. Srivastav, M. Nelle, J. Slotboom, R. Wiest, Radiology 257 (2010) 810–819.
[32] S. Capuani, M. Guerreri, A. Antonelli, S. Bernardo, M.G. Porpora, A. Giancotti, C. Catalano, L. Manganaro, Placenta 58 (2017) 33–39.